Identification of DLK1-positive cell clusters in the human adrenal cortex and their potential involvement in adrenocortical carcinoma.

Irene Hadjidemetriou

Thesis submitted to Queen Mary University of London
for the Degree of Doctor of Philosophy (PhD)

Centre for Endocrinology
William Harvey Research Institute
Barts and the London School of Medicine and Dentistry
Queen Mary University of London

Statement of originality

I, Irene Hadjidemetriou, confirm that the research included within this thesis is my own work or that where it has been carried out in collaboration with, or supported by others, that this is duly acknowledged below and my contribution indicated. Previously published material is also acknowledged below.

I attest that I have exercised reasonable care to ensure that the work is original, and does not to the best of my knowledge break any UK law, infringe any third party's copyright or other Intellectual Property Right, or contain any confidential material.

I accept that the College has the right to use plagiarism detection software to check the electronic version of the thesis.

I confirm that this thesis has not been previously submitted for the award of a degree by this or any other university.

Signature:

Date:

Details of collaboration and publications:

1. Guasti L., New S., **Hadjidemetriou I.**, Palmiero M., Ferretti P. (Pasticity of human adipose-derived stem cells- relevance to tissue repair. International journal of developmental biology. In press.

2. Ruiz-Babot, G., Balyura, M., **Hadjidemetriou, I**., Ajodha, S.J., Taylor, D.R., Ghataore, L., Taylor, N.F., Schubert, U., Ziegler, C.G., Storr, H.L. and Druce, M.R., 2018. Modeling Congenital Adrenal Hyperplasia and Testing Interventions for Adrenal Insufficiency Using Donor-Specific Reprogrammed Cells. *Cell reports*, *22*(5), pp.1236-1249.

3. Prasad, R., **Hadjidemetriou, I**., Maharaj, A., Meimaridou, E., Buonocore, F., Saleem, M., Hurcombe, J., Bierzynska, A., Barbagelata, E., Bergadá, I. and Cassinelli, H., 2017. Sphingosine-1-phosphate lyase mutations cause primary adrenal insufficiency and steroid-resistant nephrotic syndrome. *The Journal of clinical investigation*, *127*(3), pp.942-953.

4. Tufton, N., Roncaroli, F., **Hadjidemetriou, I.**, Dang, M.N., Dénes, J., Guasti, L., Thom, M., Powell, M., Baldeweg, S.E., Fersht, N. and Korbonits, M., 2017. Pituitary carcinoma in a patient with an SDHB mutation. *Endocrine pathology*, *28*(4), pp.320-325.

5. Ruiz-Babot, G., **Hadjidemetriou, I**., King, P.J. and Guasti, L., 2015. New directions for the treatment of adrenal insufficiency. *Frontiers in endocrinology*, *6*, p.70.

Abstract

The adrenal glands are vital endocrine organs responsible for the synthesis and secretion of multiple steroids and hormones. They are composed of an inner adrenal medulla and an outer adrenal cortex. The human adrenal cortex is further subdivided into three distinct zones that differ both morphologically and functionally: the Zona Glomerulosa (ZG), the Zona Fasciculata (ZF), and the Zona Reticularis (ZR). In rats, another zone has been identified between the ZG and the ZF, termed the undifferentiated zone (ZU). This zone has been shown to consist of adrenocortical progenitor cells, expressing Sonic Hedgehog and Delta like homologue 1 (Dlk1). The presence and function of the ZU in human adrenals is not known. In this project I studied the expression of stem/progenitor and steroidogenic markers in the human adrenal cortex and identified a novel cell population in the subcapsular region, which is hypothesised to be similar to the ZU in rats. This cell population expressed the atypical Notch ligand Delta-like homologue 1 (DLK1) but not steroidogenic markers (similar to the rat model), and we termed this as DLK1-cell clusters (DCCs).

Following assessment of DLK1 expression across normal adrenals from foetuses to ageing adults, DCCs appear to be of layered continuous appearance in foetuses and in younger individuals and become clustered later in life. However, these were found to be different entities to aldosterone producing cell clusters (APCCs), which are precursors of aldosterone producing adenomas (APAs). Since DLK1 has shown involvement in carcinogenesis, I assessed whether it is involved in DLK1 in adrenocortical carcinomas (ACCs). DLK1 was significantly upregulated in all ACC samples analysed compared to normal adrenals. Further *in vitro* experiments using human adrenocortical cell line H295R, showed that DLK1-expressing cells possess cancer stem cell characteristics. Collectively, these results indicate that DLK1 could be a novel marker of cancer stem cells in adrenocortical carcinoma, which could potentially be used as a biomarker for identification and treatment.

Acknowledgements

I would like to thank my supervisor Leonardo Guasti for giving me the opportunity to work on this PhD project and be part of his team. I would also like to thank group members Gerard Ruiz-Babot and Sharon Ajodha for their help in the lab over the years.

In addition, I would like to express my gratitude to colleagues in the Centre for Endocrinology who were helpful, particularly Nikolina Kyprianou and Antonia Solomou for making my time in the lab more enjoyable. I would also like to take this opportunity to thank the Medical Research Council, Queen Mary University School of Medicine and Dentistry and Rosetrees Trust for funding this work.

I would also like to thank my parents, Andreas and Stella Hadjidemetriou and grandparents, Pantelis and Kalliroi Georgiou for their continuous support, encouragement and love.

Finally, I would like to thank my partner, Jorrit Schafer for all his help and the useful suggestions he had regarding this project, and most importantly for always being so loving and supportive.

I would like to dedicate this thesis to my parents who have supported me throughout my life, helped me succeed in life and raised me into the kind and virtuous person I am today. I hope I have and will continue to make you proud.

Table of Contents

List of Figures

List of Tables

List of Abbreviations

3βHSD	3β-hydroxysteroid dehydrogenase
ACA	Adrenocortical adenoma
ACC	Adrenocortical carcinoma
AGP	Adrenogonadal primordium
AHC	Adrenal hypoplasia congenital
AP	Adrenal primordium
APCC	Aldosterone producing cell clusters
ATP	Adenosine triphosphate
Boc	Brother of Cdo/bioregional Cdon-binding protein
BWS	Beckwith-Wiedemann syndrome
cAMP	Cyclic adenosine monophosphate
C/EBPβ	CCAAT-enhancer binding protein β
C/EBPδ	CCAAT-enhancer binding protein δ
Cdo	cell adhesion molecule-related/downregulated by oncogenes
Cited2	Glu/Asp-Rich carboxy-terminal domain 2
CT	Computer tomography
CYP11B1	11β-hydroxylase
CYP11B2	Aldosterone synthase
DAX1	Dosage-sensitive sex-reversal, adrenal hypoplasia congenital, X chromosome; NR0B1
DCC	DLK1 cell clusters
DHEA	Dehydroepiandrosterone
DHEAS	Dehydroepiandrosterone sulfate
DHH	Desert hedgehog
DLK1	Delta-like homologue 1
dpc	Days post conception
DSL	Delta, Serrate and LAG-2
DSS	Dosage-sensitive XY sex-reversal
DZ	Definitive zone
e	Embryonic day

ECM	Extracellular matrix
EGF	Epidermal growth factor
FAdE	Fetal adrenal enhancer
FGF	Fibroblast growth factor
FGFβ	Fibroblast growth factor beta
FH-I/II/III	Familial Hyperaldosteronism Type I/II/III
FZ	Fetal zone
Gas1	Growth arrest specific 1
GP	Gonadal primordium
Hox9b	Homeobox gene 9b
HPA	Hypothalamic pituitary adrenal
IGF1	Insulin growth factor 1
IGF-1R	Insulin growth factor receptor 1
IGF2	Insulin growth factor 2
IHH	Indian Hedgehog
KO	Knockout
MC2R	Mineralocorticoid 2 receptor
MRAP	Melanocortin 2 receptor accessory protein
MRI	Magnetic resonance imaging
PAI	Primary adrenal insufficiency
Pbx1	Pre B-cell leukemia factor 1
PEI	Polyethylenimine
PET	Positron emission tomography
PKA	Protein kinase A
POMC	Proopiomelanocortin
Prep1	Homeobox protein PKNOX1
Ptch1	Patched 1 transmembrane binding protein
RAAS	Renin angiotensin aldosterone system
Rspo	R-spondin
SF1	Steroidogenic factor 1
SGPL1	Sphingosine-1-phosphate lyase
SHH	Sonic Hedgehog

Smo	Smoothened
StAR	Steroidogenic acute regulatory protein
Sufu	Suppressed or fused
TACE	TNF-α-converting enzyme
TCF21	Transcription factor 21
TCF/LEF	T-cell factor/lymphoid enhancer binding factor
TGF-α	Transforming growth factor-α
VEGF	Vascular endothelial growth factor
WT	Wild type
Wt1	Wilm's tumour 1
ZF	Zona Fasciculata
ZG	Zona Glomerulosa
ZR	Zona Reticularis
ZU	Undifferentiated zone

Chapter 1: Introduction

1.1 Adrenal gland: Structure and Function

The adrenal glands are vital endocrine organs responsible for the synthesis and secretion of multiple hormones and steroids, including adrenaline, aldosterone and cortisol. The two adrenal glands differ in size and shape with the left adrenal gland being larger and crescent-shaped and the right being smaller in size and pyramidal in shape[1]. Each adrenal gland is located on top of each of the kidneys and is composed of two distinct organs. These include the adrenal cortex and the adrenal medulla (Figure 1.1a)[2, 3]. A thin fibrous tissue composed of mesenchymal cells encapsulates the adrenal gland, which serves both as a support structure and, at least in rodents, as a stem cell niche able to generate new functional steroidogenic cells during embryological development and throughout life [4].

1.1.1 Adrenocortical zonation

The adrenal cortex, found directly under the capsule, is further subdivided into at least three concentric zones; the Zona Glomerulosa (ZG), the Zona Fasciculata (ZF), and the Zona Reticularis (ZR). These zones differ both morphologically and functionally and are responsible for the production of mineralocorticoids, glucocorticoids or androgens.

The ZG is the outermost zone of the adrenal cortex, lying just beneath the capsule and accounts for approximately 15% of the adrenal cortex. It consists of cells arranged in circular clusters (rosettes) throughout the subcapsular region. These cells have a highly basophilic cytoplasm, containing small lipid droplets[1]. The ZF is the thickest layer of the adrenal cortex and resides between the ZG and the ZR. It is comprised of larger polygonal epithelial cells with a high lipid content, arranged in radial columns along the width of the zone. The innermost layer of the adrenal cortex is the ZR, which is found between the ZF and the adrenal medulla. This is composed of polyhedral cells that are arranged in cords, projecting into different directions, giving a mesh-like appearance (Figure 1.1b).

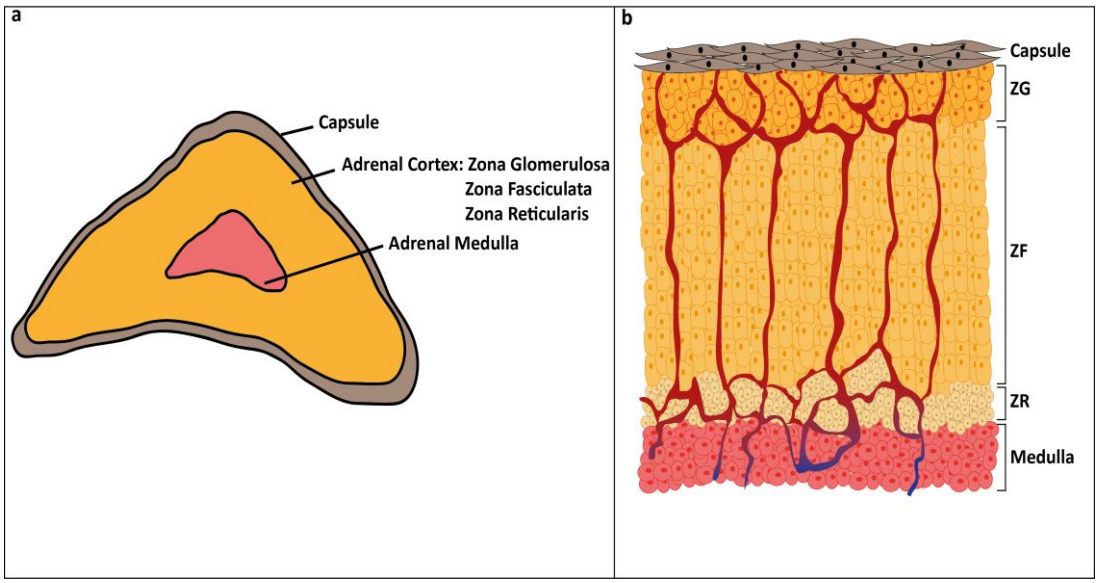

Figure 1.1 – Adrenal gland structure. Schematic diagram of the adrenal gland illustrating the shape (a) and cell structure and organisation (b) of the adrenal gland. ZG=Zona Glomerulosa; ZF=Zona Fasciculata; ZR=Zona Reticularis.

However, different species have different zonation patterns as illustrated in Figure 1.2. The adrenal glands of mice and rats lack the ZR that is normally present in the human adrenal. Instead, in the mouse an X-zone is present, the function of which remains unclear, with some studies suggesting that it is involved in progesterone inactivation[5]. This zone is known to disappear at puberty in male mice and after the first pregnancy in females[6]. Although both human and rodent adrenal glands consist of a ZG and ZF, there still are some differences in cell organisation of these two zones. In the case of the humans, cells from the two zones are more intermixed at the ZG-ZF border, whereas in rodents there is a clear separation between the two zones.

Finally, recent studies in rats have supported the presence of a new zone, namely the ZU, between the ZG and the ZF that is hypothesized to contain adrenocortical stem/progenitor cells. In the rat the ZU is further subdivided into the outer and the inner ZU, with cells of the outer ZU expressing markers such as Sonic hedgehog (Shh) and Dlk1[7, 8]. The subcapsular region of humans is less characterized and considered to be more complex than that of rodents[9].

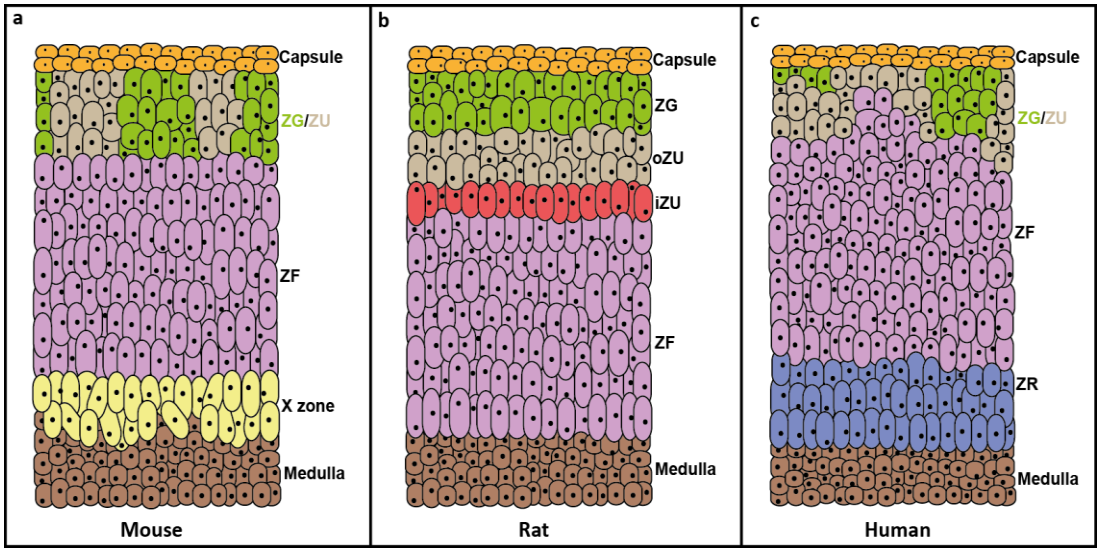

Figure 1.2 – Adrenocortical zonation in humans and rodents. Schematic diagram illustrating the structural and cellular organisation of the adrenal cortex in the mouse (a), rat (b) and human (c).

1.1.2 Steroid synthesis

Steroid synthesis in the adrenal glands is a tightly regulated process (Figure 1.3), initiated by the transport of free cholesterol into the cells via the low density lipoprotein receptor in humans and the SR-B1 selective transporter in rodents[10, 11]. Cholesterol is initially cleaved by cholesteryl ester hydrolase and translocated from the outer to the inner mitochondrial membrane with the aid of transporter enzyme steroidogenic acute regulatory protein (StAR)[12-14]. Initial conversion to pregnenolone by side-chain cleavage (encoded by *CYP11A1*) takes place, followed by transport to the smooth endoplasmic reticulum where it is converted to 17OH-pregnenolone by CYP17 in the ZF and ZR but not the ZG. Furthermore, 3β-hydroxysteroid dehydrogenase (3βHSD) converts 17OH-pregnenalone to 17OH-progesterone in the ZF and ZR and pregnenolone to progesterone in the ZG. CYP21 then converts progesterone to 11-deoxycorticosterone in the ZG, and 17OH progesterone to 11-deoxycortisol in the ZF. These are transported back to the inner mitochondrial membrane, where 11β-hydroxylase (CYP11B1) in the ZF converts 11-deoxycortisol to cortisol in humans. Similarly, in the ZG aldosterone synthase (CYP11B2) converts 11-deoxycorticosterone to aldosterone. In the ZR, CYP17 along with cytochrome b5 lead to conversion of 17OH-pregnenolone to dehydroepiandrosterone (DHEA), which can then be converted to DHEA sulfate

(DHEAS) or androsteneidone by sulfotransferase 2A1 (SULT2A1) and 3βHSD, respectively. *Cyp17* is epigenetically silenced in rodents postnatally [15], hence 11-deoxycorticosterone is the substrate of *Cyp11B1* instead, leading to synthesis and production of corticosterone, rather than cortisol. In addition they do not synthesize adrenal androgens therefore the ZR does not exist in rodents[1, 16-18].

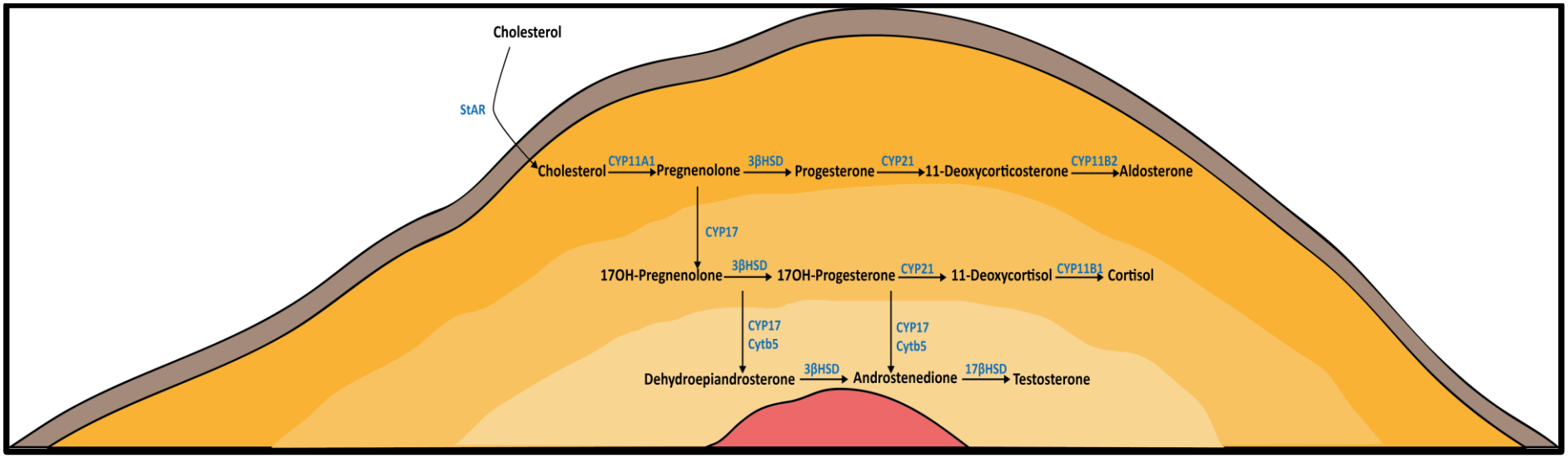

Figure 1.3- Steroid synthesis in the human adrenal cortex. Free cholesterol is transported into the adrenocortical cells, where it is initially cleaved and then translocated from the outer to the inner mitochondrial membrane by StAR. Following initial conversion to pregnenolone by CYP11A1, subsequent action of multiple enzymes (CYP17, 3βHSD and CYP21) are responsible for further processing. Finally, zonal specific enzymes in the ZG (CYP11B2) and ZF (CYP11B1) act on the steroid/hormone precursors to give rise to aldosterone and cortisol, respectively. The ZR is only present in humans and is responsible for androgen production, including testosterone. C=Capsule; ZG=Zona Glomerulosa; ZF=Zona Fasciculats; ZR=Zona Reticularis; M=Medulla.

1.1.3 Zonal specific and medullary functions

The ZG secretes the mineralocorticoid aldosterone, under the influence of the renin-angiotensin-aldosterone system (RAAS)(Figure 1.4a)[16].This occurs when secretion of the serine-protease renin from the juxtaglomerular cells in the kidneys is triggered, either following sympathetic nerve activation, catecholamine accumulation, renal artery hypotension or decreased sodium delivery to the distal tubules [19, 20]. Renin cleaves angiotensinogen released by the liver into angiotensin I, which is subsequently converted to angiotensin II by angiotensin converting enzyme, mainly located in the capillaries of the lung[21, 22]. Angiotensin II has a direct effect on multiple organs, including the adrenal gland, and acts by binding to its receptor Angiotensin I receptor to produce a synergistic effect resulting in an increase in blood volume and hence blood pressure. In the adrenal gland, binding of angiotensin II to its receptor causes the generation of inositol 1,4,5-trisphosphate and 1,2-diacylglycerol. This results in activation of a series of cascades and phosphorylation events leading to an increase in aldosterone production by the ZG in the adrenal cortex[23, 24].

Aldosterone acts to increase sodium reabsorption and water retention by the kidneys, through binding to the mineralocorticoid receptor, thus having a direct effect in regulating blood volume and systemic vascular resistance; hence controlling blood pressure[21]. Dysregulation of RAAS leading to excess aldosterone secretion causes electrolyte imbalance and hypertension. In addition, it has an effect on other tissues and can have severe cardiometabolic implications, such as cardiac fibrosis, decreased insulin sensitivity and increased adipogenesis[25-27].

The ZF is responsible for glucocorticoid secretion, mainly cortisol in humans (or corticosterone in rodents), under the control of the hypothalamic pituitary adrenal axis (HPA axis) as shown in Figure 1.4b. Biological stress, low blood glucose concentration or low blood cortisol levels activate the HPA axis and stimulate the paraventricular nucleus of the hypothalamus to secrete corticotrophin releasing hormone (CRH). This in turn promotes the release of adrenocorticotropic hormone

(ACTH) by the anterior pituitary that binds to the melanocortin 2 receptor (MC2R), which along with melanocortin 2 receptor accessory protein (MRAP), is almost exclusively expressed in the ZF. MC2R being a G-protein coupled receptor, converts adenosine triphosphate (ATP) into cyclic adenosine monophosphate (cAMP); the function of which is two-fold. It initiates transcription of StAR, CYP11A1 and CYP17A1 thus favouring cortisol production and activates cAMP-dependent protein kinase (PKA), which in turn phosphorylates cholesterlyl ester hydrolases and StAR; thus increasing transport of cholesterol to the inner mitochondrial membrane[28-30].

Cortisol is the main glucocorticoid released by the ZF and has very important and widespread multi-organ effects, including metabolic and cardiovascular regulation as well as vital anti-inflammatory effects through immune system regulation. Elevated cortisol levels lead to an increase in gluconeogenesis in the liver. As a result, there is an increase in lipolysis of fat stores to release fatty acids and glycerol, and sometimes proteolysis of muscle tissue, in order to provide sufficient amounts of substrates for increased glucose synthesis [1, 16]. Both an increase in cortisol levels, as well as an increase in glucose and fatty acid formation, exerts a negative feedback effect on the HPA axis resulting in an inhibition of CRH and/or ACTH; hence preventing over-secretion of cortisol. In situations where cortisol is chronically high (ie: during periods of chronic stress or in patients with Cushing's syndrome), metabolic abnormalities can occur, as well as altered body fat distribution and increased visceral obesity[31, 32]. Apart from metabolic regulation, cortisol can have anti-inflammatory properties by inhibiting the synthesis and release of specific cytokines including Interleukin-12 and Interferon gamma and other inflammatory mediators such as histamine, thus playing a role in immune system regulation[33]. This regulation can be vital to prevent organ damage in situations of excessive inflammation. In addition cortisol can have an effect on the cardiovascular system, by regulating blood pressure, tone of the heart and contractility[34].

The innermost layer of the adrenal cortex, the ZR, appears later in life at around 6-8 years of age in females and 7-9 years in males in a process called adrenarche. It secretes androgen precursors such as, DHEA and DHEA sulfate (DHEAS)[2, 35]. Finally,

the adrenal medulla is found in the inner portion of the adrenal gland. It consists of polygonal epithelial cells, which are grouped around blood vessels and is responsible for the synthesis and secretion of the catecholamines, mainly adrenaline and noradrenaline. It is connected to the sympathetic nervous system and therefore it controls the body's 'fight or flight' response.

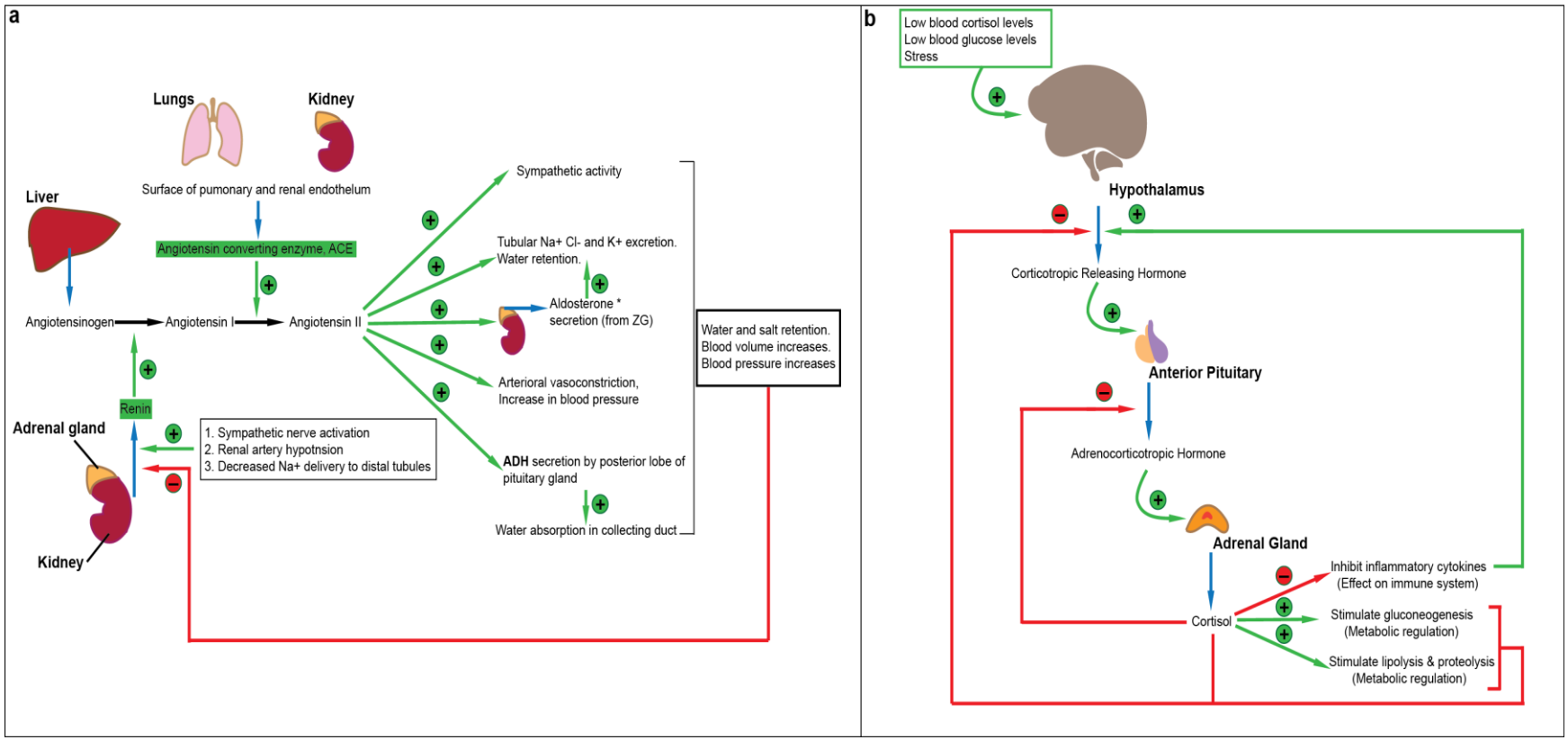

Figure 1.4 - Schematic diagram of the Renin-angiotensin-aldosterone system (a) and the hypothalamic pituitary adrenal axis (b) and their effects. The RAAS is the main regulator of aldosterone secretion in the adrenal gland. Renin secretion by the kidneys, following either sympathetic nerve activation, renal artery hypotension or decreased [Na^+] in distal tubules, converts angiotensinogen into angiotensin I. This is further processed to Angiotensin II via the action of angiotensin converting enzyme secreted by the pulmonary and renal endothelium.

Angiotensin II exerts its effects on a wide range of tissues including the adrenal cortex, where it stimulates aldosterone secretion. Collectively the tissues stimulated by Angiotensin II have a synergistic role in regulating blood volume and pressure. The HPA is the main regulator of cortisol secretion in the ZF. CRH release by the hypothalamus following a drop in blood cortisol/glucose concentrations or during periods of stress stimulates ACTH release by the anterior pituitary, which in turn stimulates the adrenal gland to secrete cortisol.

1.2 Adrenal Gland Development

Developmentally, the adrenal gland originates from two distinct embryological organs; the intermediate mesoderm which gives rise to the adrenal cortex and the neurectoderm which forms the adrenal medulla[36]. Development of the adrenal gland commences with the expression of steroidogenic factor 1 (Sf1), leading to mesoderm-derived cells of the coelomic epithelium and the underlying mesonephros to coalesce and form the adrenogonadal primordium (AGP). This event occurs at 28 days post conception (dpc) in humans and embryonic day (e) 9.0 in mice (Figure 1.5).

Each AGP forms between the urogenital ridge and the dorsal mesentery and consists of both adrenocortical and gonadal progenitor cells. At 8 weeks of gestation in humans and e10.5 in mice, combinations of transcription factors act upon the undifferentiated primordial cells and force them to commit towards distinct lineages[1, 7, 36, 37]. The majority of these cells will migrate dorsolaterally to form the gonadal primordial (GP) which will give rise to the gonads, while those with the highest expression of Sf1 will migrate dorsomedially to form the adrenal primordial (AP)[38]. Following formation of the AP, at around 48dpc in humans and at e11.5-e12.5 in mice, the fetal adrenal is invaded by neural crest cells that have migrated from the neurectoderm. These neural crest cells will eventually differentiate into catecholamine-producing cells to form the adrenal medulla and will have no contribution to the adult adrenal cortex[39, 40]. At the same time the fetal adrenal becomes encapsulated by a fibrous layer, which forms the adrenal capsule by 52dpc in humans and e12.5-e14.5 in mice[41].

Following encapsulation, the embryonic adrenal cortex continuous to expand rapidly. By e14.5 in mice the emergence of a new zone occurs between the capsule and the fetal zone (FZ), known as the definitive zone (DZ). This will later become the adult adrenal cortex. As the development of the adrenal continues, the DZ grows while the FZ regresses. The timing of FZ regression is species-specific; in humans it regresses perinatally, while in mice it persists until puberty in males and the first pregnancy in females (also known as X-zone in adult mice)[1, 36, 42]. In the last months of

gestation in humans adrenocortical cells of the DZ expand and start producing cortisol marking the appearance of the ZF of the adrenal cortex.

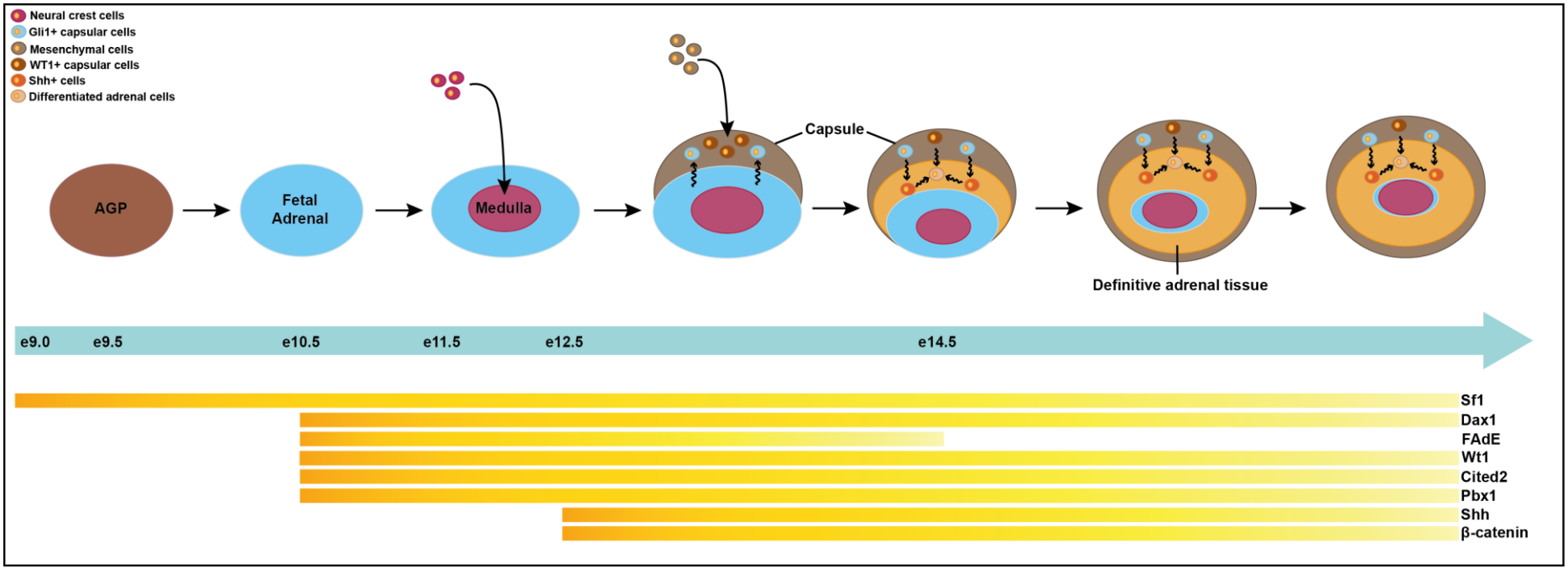

Figure 1.5 – Adrenal gland development in mice. Schematic diagram illustrating the developmental process leading to adrenal gland formation in mice, showing the main events including AGP and DZ formation, and FZ regression. Additionally it highlights the time and duration of expression of key factors involved in mouse and human adrenal gland development such as Sf1, Dax1, FAdE, Wt1, Cited2, Pbx1, Shh and β-catenin.

1.3 Key factors and signalling pathways involved in adrenal development

1.3.1 Steroidogenic Factor 1 (SF1)

SF1 is a nuclear receptor encoded by the *NR5A1* gene. It has emerged as a master regulator of AGP formation and a key factor in the determination of the steroidogenic cell fate[37, 41, 43-46]. In mouse models of *Sf1* haploinsufficiency ($Sf1^{+/-}$) a delayed hypoplastic adrenal gland developed[47], while in *M33* knockout (KO) mice where *Sf1* expression is half compared to wild type (WT) a similar phenomenon was observed[48]. In addition, complete deletion of Sf1 *in vivo* leads to adrenal and gonadal agenesis with postnatal lethality[38]. In human studies it was shown that *SF1* mutations also have an effect on adrenal and gonadal development leading to adrenal insufficiency and developmental abnormalities, respectively. However, in the case of humans it seems that the gonads are more sensitive to *SF1* loss, compared to the adrenal gland where it is reported that primary adrenal insufficiency due to *SF1* loss is a rare event[49, 50]. On the other hand *SF1* over-expression leads to increased cell proliferation and neoplasia, which may lead to tumour development[51].

These findings suggest that *SF1* gene dosage is critical for normal adrenal and gonadal development, with suboptimal *SF1* levels leading to dose-dependent impairment and too high levels of *SF1* leading to aberrant proliferation and possibly tumourigenesis[52, 53]. Research into pathways responsible for regulating expression of *SF1*, has revealed important factors that help maintain the optimal levels of the protein. Current data indicate that Wilm's tumour 1 (*Wt1*) and Cbp/P300-Inreracting transactivator, with Glu/Asp-Rich carboxy-terminal domain, 2 (*Cited2*) regulate *Sf1* expression in the AGP and differentiation of the AP, respectively[54, 55]. In addition the fetal adrenal enhancer (*FAdE*) has been shown to be critical in *Sf1* modulation. *FAdE* expression begins at e10.5 in mice and is responsible for initiating *Sf1* expression in the AGP (Figure 1.5). *FAdE* acts in a two-

step mechanism involving an initial *FAdE* mediated *Sf1* expression controlled by the transcription complex containing homeobox protein PKNOX1 (Prep1), pre B-cell leukeumia factor 1 (Pbx1) and homeobox gene 9b (*Hox9b*). Following initial activation of *Sf1*, its expression is maintained by the establishment of an autoregulatory loop, where *Sf1* regulates itself by maintaining *FAdE* mediated *Sf1* expression[56]. In a study by Zubair et al., 2009, a *FAdE-Sf1* transgenic mouse was used to investigate the effect of *FAdE*-induced *Sf1* overexpression on adrenal development[52]. Their results showed an increase in adrenal size and formation of an ectopic adrenal, further supporting the role of *Sf1* in cell fate determination *in vivo*. In addition, it highlights the importance of the autoregulatory loop in preventing ectopic adrenals from forming[52, 57]. Following e14.5 in mice, *Sf1* expression regulation is no longer dependent on *FAdE* and therefore during DZ emergence, *Sf1* regulation is supported by a different definitive enhancer[57]. A similar mechanism however has not yet been observed in humans.

1.3.2 DAX1

DAX1 (dosage-sensitive sex-reversal, adrenal hypoplasia congenital, X chromosome; NR0B1) is an atypical orphan nuclear receptor and the gene responsible for X-linked adrenal hypoplasia congenital (AHC)[58, 59], as well as dosage-sensitive XY sex-reversal (DSS)[60]. In humans expression of DAX1/*DAX1* is restricted to the adrenal glands, hypothalamus, pituitary and testis[61].

In the adrenal glands, expression of *Dax1/DAX1* occurs in the developing urogenital ridge at e10.5 in mice and 33dpc in humans. It continues to be expressed in the adrenal primordium, as well as the fetal and adult adrenal cortex and it principally serves as a co-repressor of *Sf1*-mediated steroidogenesis [2]. Studies have shown that knockdown of *Dax1* results in premature differentiation of adrenocortical progenitors in mice, further supporting the role of DAX1 in the maintenance of the stem/progenitor cell population in the adrenal cortex. In addition, recent studies

have shown that *Dax1* and Sf1 SUMOylation both act as co-repressors of FAdE mediated Sf1 expression, which is crucial for fetal cortex regression and normal adrenal development and function[62]. Regulation of *Dax1* is hypothesized to be a tightly regulated process in order to maintain a balance between progenitor and differentiated cells. *Sf1* and Wnt signalling act as co-activators of *Dax1* transcription, while ACTH leads to *Dax1* inhibition and initiation of differentiation of Sf1+ progenitor cells[63]. Apart from regulating the stem/progenitor cell pool in the adrenal cortex, Dax1 is a key component of transcription factor networks that maintain mouse embryonic stem cells in a pluripotent state. This role was supported by Dax1 knockdown mouse studies in which embryonic stem cells spontaneously differentiate into all three germ layers[64].

1.3.3 ACTH and CRH

As mentioned earlier, both hormones are part of the HPA axis and have an effect on adrenal function. CRH release by the hypothalamus regulates production of proopiomelanocortin (POMC) by the anterior pituitary that is then converted to ACTH. ACTH in turn binds the MC2R receptor on adrenocortical cells to stimulate steroidogenesis and ultimately cortisol release[65]. In addition to its effects in adulthood, ACTH can play a role in the development and growth of the human fetal adrenal gland after 15 weeks of gestation, mainly through stimulation of other growth factors such as insulin-like growth factor 2 (IGF2) and fibroblast growth factor beta (FGFβ). In addition it is involved in the regulation of steroidogenesis during DZ formation[66-68].

CRH-homologous peptides (UCN1-3) and their respective receptors (CRF1/2) are found in both the adult and fetal adrenal gland however they have different expression patterns[69, 70]. In addition CRH is produced in vast amounts by the human placenta, particularly at the end of gestation. This leads to increased production of cortisol and DHEA/DHEA-S in human fetal adrenals and an enhanced

sensitivity of the adrenal gland to ACTH[71]. Furthermore, a study has shown that chromaffin cells in the medulla might be essential for the stimulatory action of CRH on cortisol production, suggesting a potential link between the adrenal cortex and the medulla[72].

1.3.4 Insulin-like growth factor 1 and 2

Insulin-like growth factor 1 (IGF1) and IGF2 are expressed in a variety of tissues and exert their biological functions by binding to their corresponding receptors, IGF-2R and insulin receptor, thus triggering receptor autphosphorylation. This in turn leads to the activation of the MAPK and AKT/PI3K pathways, which regulate cell metabolism, proliferation, differentiation and apoptosis[73, 74]. Both IGF1 and IGF2 are expressed in the adrenal glands, however at different spatial and temporal levels. In the developing fetal embryo, IGF2 is predominantly expressed throughout the adrenal cortex with minimal IGF1 expression in the capsule. Studies have shown that stimulated increase of ACTH secretion from the pituitary results in an increased expression of IGF2 and IGFR1 in the fetal adrenal gland. This in turn results in increased adrenal size, suggesting that these factors play a crucial role in adrenal growth[75]. In the adult human adrenal IGF1 is predominantly expressed, with only low levels of IGF2 expression in the peripheral cortex and capsule layer. The presence of IGFs stimulate basal and ACTH-induced steroidogenesis[74, 76]. IGF2 expression in the human adult adrenal is localised in the stem/progenitor cell compartments, suggesting a role of IGF2 in adrenal stem/progenitor cell maintenance. This is further supported by studies showing that both IGF2 and fibroblast growth factor (FGF) are also important in stem/progenitor cell maintenance of other organs[77, 78]. More recently a study showed that knocking down *Igfr1* in mice resulted in adrenal agenesis, decrease in Sf1 expression in the AGP and failure to form the AP, in addition to growth retardation, sex reversal and ovarian development[79]. These results suggest that the Igf pathway is essential in both adrenal and gonadal development as well as sex determination.

1.3.5 FGF signaling

FGF signalling is mediated by the FGF family of proteins and it regulates a number of developmental processes, such as anterior-posterior patterning, neurectoderm formation and organogenesis. FGFs comprise a large family of secreted glycoproteins that act by binding to FGF receptor tyrosine kinases (FGFR1-4) and activate a range of pathways, including Ras/MAPK, Akt and PKC activation[80]. Different isoforms of Fgf and Fgfr have been detected in adrenals of mouse embryos at e15.5, mainly in the capsule and in subcapsular regions of the cortex, suggesting a role of Fgf signaling in adrenal development, possibly after AGP development[1]. Mice harbouring a total KO of *Fgfr2* isoform IIIb had a hypoplastic adrenal with a disorganised capsule and decreased expression of side chain cleavage and Cyp11b1 at e16.5. Mice lacking all isoforms of *Fgfr2* (IIIb and IIIc) in the adrenal cortex exhibited severe hypoplastic adrenal glands at birth with a reduced number of cortical cells. However, cortical cells in these mice were able to differentiate into steroidogenic cells and achieve proper zonation[7].

1.3.6 Wnt/β-catenin signalling

Wnt/β-catenin signaling is one of the most important pathways in the regulation of tissue development and homeostasis of multiple organs including the adrenal glands. β-catenin is a bifunctional protein that regulates cell-to-cell interactions in the cytoskeleton, in addition to taking part in canonical Wnt signalling. In the absence of Wnt ligand, β-catenin becomes incorporated in the destruction complex (Axin/Apc/Gsk3β) where it gets phosphorylated and targeted for degradation[1, 81]. However, upon Wnt ligand binding to their respective frizzled receptor the degradation complex is prevented and active β-catenin translocates to the nucleus where it acts as a transcriptional coactivator for T-cell factor/ lymphoid enhancer-binding factor (TCF/LEF)[1, 81, 82].

Embryonically, active β-catenin is detected as early as e11.5 in the AGP and mesonephros of the mouse embryo and by e18.5 it is restricted to the subcapsular region of the cortex (ZG) and persists until adulthood, where it mostly but not exclusively co-localizes with Cyp11b2[36, 83]. In the human adult adrenal β-catenin is found to be expressed in the subcapsular region of the adrenal cortex. Multiple studies have identified a synergistic action between β-catenin and Sf1 in activating downstream genes important for adrenocortical development and function, such as *Dax1*, *Star*, *Inha*, *Hsd3b1* and *CYP19a1*, thus suggesting a crucial role of β-catenin in regulating adrenal development and homeostasis[84, 85]. The importance of β-catenin in adrenal gland development is supported by a study showing that ablation of *β-catenin* in mice results in embryonic lethality[86]. Disruption of *β-catenin* expression exclusively in steroidogenic cells using a highly penetrant *Sf1*:cre transgene also results in adrenal aplasia in mice at birth, further supporting a crucial role of canonical Wnt/β-catenin signalling in normal adrenal gland development[87]. The same study also showed that mice bearing the weakly penetrating *Sf1*:cre transgene (approximately 50% effective) have a normal adrenal gland at birth; however as the mice age the adrenal cortex decreases in size and steroidogenic function is compromised. This failure is possibly due to a loss of the adrenocortical progenitor cells in the cortex.

1.3.7 Shh signalling

Sonic hedgehog (Shh) is a secreted protein that belongs to the Hedgehog family of cell-fate regulators, comprised of two additional homologs, the Indian hedgehog (Ihh) and the Desert Hedgehog (Dhh). Hedgehog signaling pathway is key in organogenesis in the human embryo, as well as tissue homeostasis and regeneration in adulthood. Therefore, perturbation of this pathway, results in developmental abnormalities, disruption of homeostasis and in some cases tumourigenesis [88-91]. Each mammalian Hh homolog has distinct functions and different expression patterns. Shh in particular is expressed in the early stages of embryonic development

in multiple organs including the adrenal glands. The second homolog Dhh is mostly expressed in the gonads and neural sheaths, while Ihh expression is restricted to the primitive endoderm and pre-hypertrophic chondrocytes[92-94].

These Hh proteins act by binding to their main receptor, Patched 1 transmembrane binding protein (Ptch1), in addition to other more recently discovered co-receptors; Cdo (cell adhesion molecule-related/downregulated by oncogenes), Boc (brother of Cdo/bioregional Cdon-binding protein) and Gas1 (growth arrest specific 1) found on the target cells[95-97]. This releases the repressive action of Ptch1 on Smoothened (Smo), a 7-transmembrane G-protein coupled receptor, which leads to its phosphorylation and accumulation within the primary cilium. Phosphorylated Smo stimulates Gli1 expression by recruiting proteins to antagonize the repressive action of Sufu (Suppressor of Fused) on Gli. Finally, this results in the accumulation of Gli2 and Gli3 in their transcriptionally active forms which leads to subsequent initiation of transcription of target genes in the Hh pathway[94, 98-100]. In the absence of Hh proteins, Ptch1 inhibition of Smo remains, preventing association of Smo with cell membrane. In addition Hh negative regulator Sufu binds to Gli proteins, thus inhibiting their nuclear localization and transcription. As a result Gli2 is mostly proteolytically degraded, whereas Gli3 and remaining Gli2 are cleaved into a transcriptionally inactive form, repressing the expression of downstream Hh target genes.

In the developing adrenal gland, Shh expression is detected at e11.5 in the AP of the mouse embryo just after separation from the AGP (Figure 1.5) [98, 101]. Shh along with its downstream effectors (Gli1, Gli2 and Gli3) continue to be expressed throughout development and persist during adulthood. In the adult mouse adrenals, Shh is expressed in subcapsular non-steroidogenic cortical cells, co-localizing with Sf1 but not with any of the differentiation markers expressed in functional ZG or ZF cells (Cyp11b2 and Cyp11b1, respectively). Similarly, in the adult rat adrenal cortex, Shh

is expressed in a continuous manner in the ZU region, an area hypothesized to comprise of stem/progenitor cells suggesting a role of Shh in adrenocortical maintenance and homeostasis [101, 102].

Finally, multiple studies have shown that Shh is essential for normal adrenal gland development, as inactivation/deletion of *Shh* in Sf1-expressing cells of the mouse adrenal cortex, results in adrenal hypoplasia, decreased proliferation and a thinner capsule[103]. In addition, although conditional *Shh* knockouts in mice lead to significantly reduced adrenal size, adrenocortical zonation and differentiation of the medulla seem to be unaffected[101, 103, 104]. Collectively, these results support a significant role of Shh for proper adrenal development, but suggest that Shh doesn't have a role in initiation of differentiation into the different adrenocortical zones.

1.4 Mechanisms governing adrenocortical homeostasis and maintenance

1.4.1 Stem/progenitor cell populations

The presence of a stem/progenitor cell niche in the adrenal glands has been long hypothesized and there have been multiple studies focusing on the identification of such population. Initial studies in the rat have reported that removal of the inner content of one of the adrenal glands (ZF and medulla) leads to the complete restoration of that adrenal cortex six weeks later. These results suggest the presence of a progenitor population in the adrenal capsule and/or subcapsular region that is able to regenerate the adrenal cortex[105]. In addition transplantation studies in mice have supported the presence of a progenitor population in the adrenal cortex [106, 107]. It has also been demonstrated in multiple studies that newly formed adrenocortical cells are centripetally displaced to give rise to all 3 differentiated zones until they reach the cortico-medullary border where they become senescent and then apoptotic[108]. More recent lineage tracing studies have solidified the notion of centripetal migration of the outer cortical cells into cells of the inner zones of the adrenal cortex. [101, 109].

It is now well established that the adrenal gland has two main sites where stem or progenitor cells reside. The Gli1+/Sf1- stem cell population in the capsule and the of Shh+/Sf1+/Cyp11b2- adrenocortical progenitor cells in the subcapsular region of the adrenal cortex (Figure 1.6). Lineage tracing studies in mice used an inducible *Shh*-Cre recombinase with a fluorescent reporter to mark Shh+ cells and their progeny. These studies showed that marked cells were in clusters and restricted in the subcapsular region of the adrenal cortex. Longer tracing periods showed that these cells and their descendants migrate centripetally to form radial stripes giving rise to cells of all cortical zones of the adrenal cortex. While Shh+ cells give rise to steroidogenic cells in the adrenal cortex, studies have also shown that Cyp11b2+ cells (ZG) can also give rise to Cyp11b1+ cells (ZF) through lineage conversion (Figure 1.6) [101, 110].

In addition to giving rise to differentiated cells of the adrenal cortex, Shh+ progenitor cells can communicate with stem cells residing in the capsule. It has been shown that Shh+ cells target the overlying Gli1+ capsular cells. Genetic lineage tracing experiments have demonstrated that Gli+ cells in the capsule respond to Shh signal by delaminating into the cortex, while losing their responsiveness to Shh. They first become Gli1-/Sf1+/Shh+ cells, and later differentiate fully into cells of either the ZG or ZF (Figure 1.6)[98, 101, 109]. Indeed, both Gli1 and Shh cells can give rise to steroidogenic cells during adrenal development and in the adult gland. However, in the absence of Shh signaling functional adrenal glands can still be formed, suggesting that a founder population of adrenocortical cells must exist to overcome the loss of Shh signaling. This founder population is thought to be the original Sf1+ cells from the AGP[57].

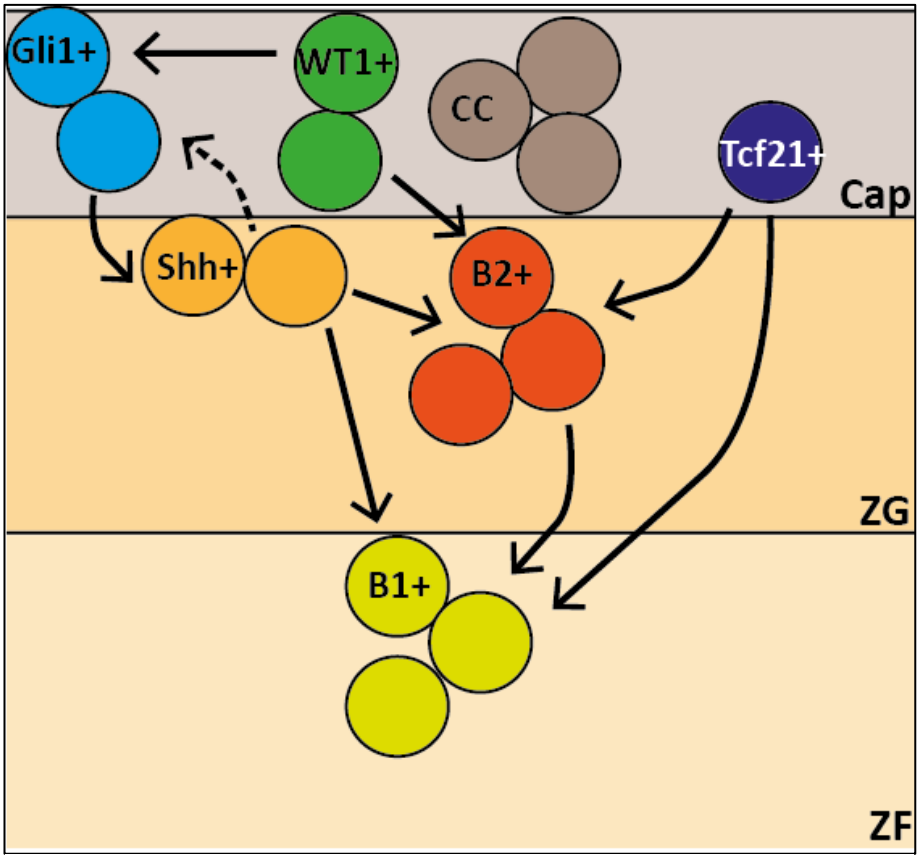

Figure 1.6 – Stem and/or progenitor cell populations in the adult adrenal gland. Schematic diagram illustrating stem cell populations (Gli1+, Wt1+ and Tcf21+ cells) found in the capsule and their progeny, as well as highlighting the interaction between cortical progenitor cells (Shh+) with capsular stem cells (Gli1+). Solid arrows show progeny, while dashed arrow shows signalling. CC=Capsular cells; Cap=Capsule, ZG=Zona glomerulosa; ZF=Zona fasciculata.

Over the years additional capsular cell populations have been identified as regulators of adrenocortical maintenance and homeostasis apart from the Gli1+ stem cells. These include cells expressing Wilms tumour protein homolog (Wt1) or cells expressing transcription factor 21 (Tcf21) [55, 111]. Lineage tracing experiments following capsular Wt1+ cells and their descendants have provided evidence that these cells can also give rise to steroidogenic cells as well as Gli1+ cells of the capsule,

suggesting a role of Wt1 in the activation of Gli1 transcription (Figure 1.6). Studies following the fate of Tcf21+ cells have shown that these cells begin to express Tcf21 at E9.5 and by E14.5 Tcf21+ cells are restricted to the capsule. Lineage tracing studies have shown that during development Tcf21+ cells and their descendants could give rise to Sf1- capsular cells as well as steroidogenic cells in the cortex. However, in the adult Tcf21+ cells only give rise to steroidogenic cortical cells (Figure 1.6) [111]. Collectively these data show that the capsule consists of multiple stem cell populations and suggests a role of these in the maintenance and regeneration of stem/progenitor or differentiated adrenocortical cells.

1.4.2 Signaling pathways and key factors

Several factors and signalling pathways that play a role in adrenal gland development are also responsible in maintaining a proper balance between adrenocortical progenitor maintenance, cell proliferation and differentiation. These factors are present in specific areas within the adrenal gland, where stem/progenitor cells reside and act as protective microenvironments that regulate stem cell proliferation and differentiation. This is a crucial regulatory mechanism to ensure a normal functioning adrenal gland throughout life. Components that have been identified within the stem/progenitor cell niche include Wnt ligands and growth factors (such as epidermal growth factor (EGF) and FGF). In addition, the extracellular matrix (ECM) has proven very important in providing additional structural and zone-specific support.

Wnt/β-catenin pathway has been described earlier as an important modulator of adrenal gland development (Section 1.3.6). In addition to its role during embryonic development it also has a crucial role in adrenocortical maintenance and zonation [112-114]. In fact Wnt4, a transcriptional target of Wnt/β-catenin signaling has been found to be expressed in the ZG of the adult mouse adrenal cortex. During development Wnt4 is required for proper ZG differentiation and aldosterone

production[115]. In the adult, mouse studies have shown that inhibition of Wnt4 expression and subsequent inactivation of the canonical Wnt pathway, by PKA, leads to ZG-to-ZF lineage conversion [116]. Therefore, Wnt4 acts as an autocrine activator of Wnt/β-catenin signaling and is essential for proper adrenocortical zonation. Alternatively, Wnt/β-catenin constitutive activation leads to an expansion of the capsular stem cell and subcapuslar progenitor cell populations leading to tumour formation (Discussed further in Section 1.6)[4, 117].

In addition, R-spondins (Rspo) are secreted proteins, which play an important role in modulating Wnt/β-catenin signalling pathway[118]. Functionally, Rspo can interact with members of the Lgr family of GPCRs, known markers of stem/progenitor cells. Binding of Rspo to Lgr receptors results in the inactivation of Rnf43 and Znrf3 ubiquitin ligases (negative regulators of Wnt), preventing internalization of Frizzled receptors and promoting Wnt signaling [119, 120]. Rspo1 and Rspo3 were found to be expressed in the adrenal capsule in mice at e12.5 and their expression was maintained throughout adulthood. In the adult, Rspo1 and Rspo3 expression in the capsule is restricted to Wt1+ and Gli1+ cells, respectively, suggesting a role of the two in the regulation of stem/progenitor cell niche. Knockout studies have shown that Rspo1 loss leads to no observable effects on the adrenal glands. However, genetic loss of Rspo3 resulted in major defects, including cortical atrophy, loss of canonical Wnt target genes (Axin2, Wnt4), loss of functional ZG (along with loss of ZG specific markers), a decrease in Shh+ (cortical progenitors) or Gli1+ cells (capsular stem cells) and a marked decrease in mitotic activity. The results from this study show that Rspo3 is a crucial regulator of Wnt and Shh pathways in the adrenal gland, thus supporting a role of Rspo3 in stem/progenitor cell maintenance and functional zonation[110, 121].

Moreover, growth factors such as FGFs are also proven to be essential for tissue homeostasis by regulating cell proliferation, differentiation, migration and

metabolism[122]. *In vivo*, different FGF ligands and their respective receptors are present in the adrenal cortex and overlying capsule, coinciding with the stem/progenitor cell niches. In the mouse embryo, Fgf1 is expressed in the adrenal cortex at E15.5, while Fgf2 and Fgf9 are expressed in the capsule region along with their respective receptors. Adrenocortical cells expressing Fgf2 also express Shh, suggesting that Fgf2 is an important regulator of adrenocortical progenitor cells[7, 102]. *In vivo* studies have shown that Fgf2 significantly enhances cell growth of adrenocortical cells that have been implanted under the kidney capsule, supporting the role of Fgf signaling in adrenal maintenance[123]. In addition as mentioned earlier knockout of *Fgfr2-IIIb* only or both *Fgfr2-IIIb* and *Fgfr2-IIIc* results in embryonic lethality. Evaluation of the embryonic adrenal glands following total *Fgfr2-IIIb* knockout has shown significant defects in the adrenal capsule, with an increased number of Gli1-positive cells, in addition to a hypoplastic cortex. The adrenal cortex had a reduced steroidogenic differentiation activity, as well as a markedly reduced capsular Dlk1-expression [7, 110]. All together these data support the importance of Fgf in adrenocortical homeostasis and maintenance and introduce Dlk1 as a mediator of a proposed homeostatic cross-talk between the capsular and adrenocortical cells.

1.4.3 The Extracellular Matrix

The ECM is a three-dimensional cellular network consisting of extracellular proteins including collagens, laminin, fibronectin, as well as bioactive compounds (growth factors, morphogens). It is responsible for providing structural and biochemical support for the surrounding cells within a tissue. Cells interact with the ECM, by binding on membrane-bound adhesion molecules, called integrins[110, 124]. Depending on the interaction between cells with these integrins, as well as the different factors that make up the ECM, different transcriptional programs can be triggered leading to proliferation, differentiation or stem cell maintenance [125, 126]. Therefore, the ECM has proven to be crucial in determining cell fate within organ

systems, with the adrenal gland being no exception. Within the human fetal adrenal, ECM components are differentially expressed between the different zones with laminin, collagen IV and fibronectin being found in the definitive, transitional and fetal zone[110, 127]. *In vitro* experiments have shown the influence that each of these components has on differentiation or stem cell maintenance of the adrenal gland, which reflects the phenotype of the zone they are present in. For example, collagen IV and laminin were shown to inhibit differentiation and promote proliferation [128]. In conclusion, the ECM is not only a support structure for the cells, but also a major determinant of cell fate regulating stem cell maintenance and differentiation.

1.5 Delta like protein homologue 1 (DLK1)

1.5.1 Structure and function

Dlk1/DLK1 gene, found on mouse chromosome 12 and human chromosome 14, is a maternally imprinted gene, coding for a 65kDa transmembrane glycoprotein and belongs to the family of EGF-like homeotic proteins[129, 130]. It consists of six EGF-like repeats at the extracellular N-terminus, a juxtamembrane region, a single transmembrane domain and a short cyoplasmic tail [131-133]. Therefore, it is structurally very similar to other EGF-like repeat containing proteins, such as EGF and transforming growth factor-α (TGF-α), which act through either the EGF or Notch receptor to regulate cell fate and differentiation, particularly during embryogenesis[132].

Various DLK1 splice variants have been identified in different species, as a result of alternative splicing. Six isoforms have been identified in the mouse (DLK1-A, -B, -C, -C2, -D, -D2), while four isoforms have been identified in humans, as shown in Figure 1.7[133-135]. Proteolytic cleavage of DLK1 by TNF-α-converting enzyme (TACE) at the juxtamembrane region, results in the release of a 50kDa soluble and active protein with potential paracrine targets[132]. The larger splice forms of DLK1 (DLK1-

A and DLK1-B) contain two proteolytic cleavage sites resulting in 25kDa and 50kDa proteins while the remaining shorter forms (DLK1-C, -C2, -D, -D2), lack the cleavage at the juxtamembrane region, giving rise to the 25kDa secreted form only, which is biologically inactive[134, 136, 137].

Most of what we know about DLK1 comes from studies in the adipose tissue. Several studies have shown that Dlk1 is highly expressed in preadipocytes, and absent in mature adipocytes making it a suitable preadipocyte marker[131]. It has been demonstrated that Dlk1 is a strong inhibitor of adipogenesis both *in vitro* and *in vivo*, and acts by preventing Sox9 downregulation through upstream activation of the Mitogen activated protein kinase (MAPK) pathway [131, 138-141]. Following expression of Sox9, it then directly binds to the promoter region and inhibits the expression of pro-adipogenic transcription factors CCAAT-enhancer-binding protein β (C/EBPβ) and CCAAT-enhancer binding protein δ (C/EBPδ), thus having a negative effect on adipogenesis[131, 142]. In order for adipocyte differentiation to occur, downregulation of Dlk1 was necessary, establishing Dlk1 as not only a preadipocyte marker, but also a key regulator of differentiation. It is important to note that only the cleaved 50kDa Dlk1 protein (Dlk1-A and Dlk1-B), was found to inhibit adipogenesis, while the remaining forms (Dlk1-C and Dlk1-D), as well as the membrane bound Dlk1 had no effect on adipogenesis.

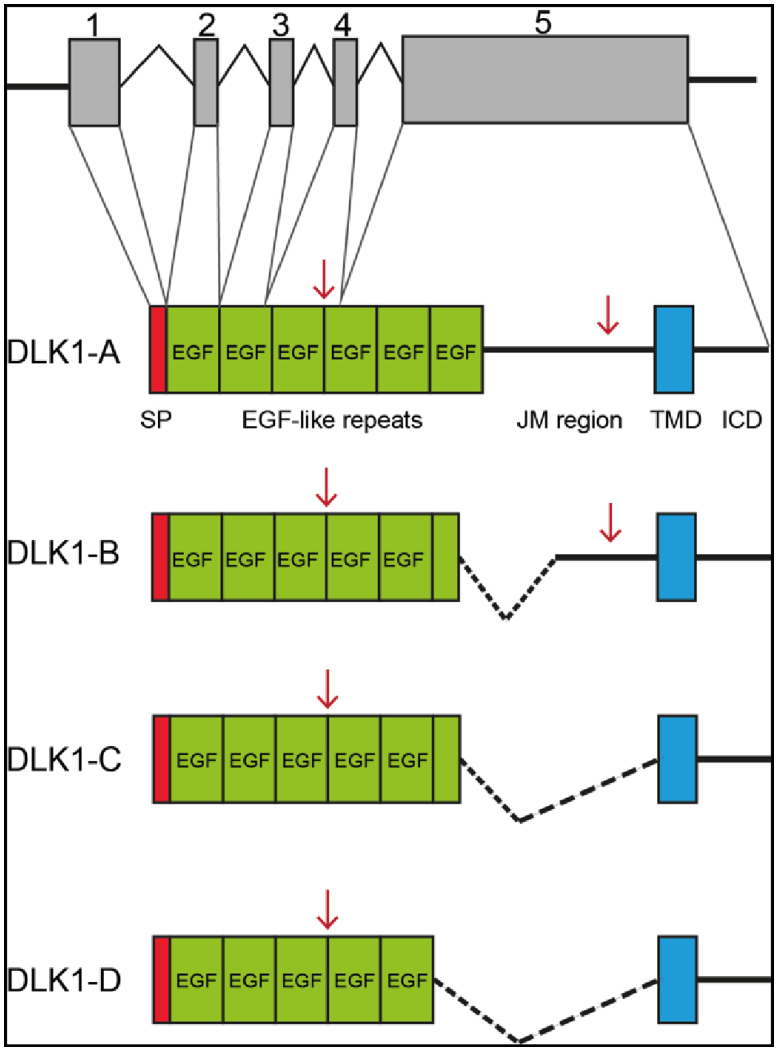

Figure 1.7 – Human DLK1 splice variants. Schematic diagram showing the structure of the different DLK1 splice variants and their proteolytic cleavage sites (red arrows). DLK1-A and DLK1-B contain two proteolytic cleavage sites and following proteolysis, two different proteins can be generated, including the 50kDa soluble and bioactive protein. DLK1-C and DLK1-D only contain one cleavage site resulting in the inactive form of the protein (25kDa).

1.5.2 Potential DLK1 – associated signaling pathways and interactions

Even though DLK1 has been established as a potent inhibitor of adipocyte differentiation, not much is known about its expression and function in other organ systems. In fact, studies aimed at elucidating the mechanism of action of DLK1, mainly in adipogenesis, have yielded contradictory results. While some studies support the notion that DLK1 acts via activation of the MAPK pathway (mentioned above), others state that DLK1 possibly acts by interacting with the Notch signaling pathway or fibronectin.

Notch signalling is an evolutionary conserved pathway with an important role in the regulation of cell-fate, cell proliferation and cell death during development. In mammals there are four different Notch receptors (NOTCH1-4) and ligands for these receptors include delta like (DLL1, DLL3, DLL4) and Jagged (JAG1, JAG2). Both the receptor and its ligands are transmembrane proteins containing a large extracellular domain mainly composed of EGF-like repeats. Notch ligands also include a Delta, Serrate and LAG-2 (DSL) domain, essential for ligand-receptor interaction[143, 144]. Given the structural similarity of DLK1 and Notch ligands, in their EGF-like extracellular domain, it was suggested that DLK1 could potentially exert its effects by interacting with the Notch receptor. However, DLK1 does not contain a DSL domain, and conflicting results regarding DLK1 and Notch receptor interaction have emerged in the literature with some studies favouring such interactions and others not[138, 145, 146]. Taking into account the potential inhibitory action of DLK1 on Notch signaling, it might be that DLK1 has a role in regulating Notch signaling by competing with the canonical ligands and thus preventing premature Notch dependent differentiation.

Finally, some studies have revealed an interaction between DLK1 and fibronectin, resulting in inhibition of adipocyte differentiation (REF: PMID:201457810). Fibronectin is a major regulator of the ECM and interacts with different types of

integrin receptors, thereby initiating a cascade of phosphorylation events of downstream kinases, as well as activating the MAPK signaling. As a result fibronectin can affect cell shape and growth, cell migration and cell differentiation. In a study by Sul and colleagues, it was shown that fibronectin is a DLK1 interacting protein following a yeast two hybrid assay. They further confirmed that the inhibitory effect of DLK1 on adipocyte differentiation is partly due to this DLK1-Fibronectin interaction. They described that DLK1 binds to the C-terminal region of fibronectin, which then activates integrin signaling and downstream MEK/ERK activation (MAPK pathway activation), eventually resulting in inhibition of adipocyte differentiation.

1.5.3 Role of DLK1 in the adrenal gland of rodents

DLK1 is abundantly expressed in the embryo, while its expression significantly decreases in the adult. In the mouse embryo, Dlk1 is expressed in the fat, liver, lung, pancreas, vertebrae, muscle, pituitary gland and the adrenal gland both at an mRNA and protein level[141, 147-150]. *Dlk1* KO studies performed in mice display a relatively mild phenotype including growth retardation, excess fat accumulation and skeletal malformation[151]. On the other end, *Dlk1* overexpression in mice results in reduced adipocity and decreased expression of adipocyte markers and adipocyte-secreted factors, with mice suffering from hypertriglyceridemia, decreased insulin sensitivity and reduced tolerance to glucose[139, 152]. In the adult mouse, Dlk1 expression is mainly restricted to the pituitary and adrenal glands (especially medulla) with expression in the liver being limited to progenitor cells[153]. In adulthood, Dlk1 is thought to have a role in cell-renewal and homeostasis, possibly by regulating the differentiation potential of stem cells. DLK1 is also expressed in relatively undifferentiated tumour cells, thus possibly having a role in tumour formation and differentiation[154, 155]. Dlk1 is expressed in the subcapsular region in the rat adrenal, specifically in the outer ZU[8]. As mentioned earlier, it is hypothesized that this subcapsular ZU region consists of progenitor/relatively undifferentiated cells, which are also expressing Shh, and only partially expressing

Cyp11b2. It was also demonstrated that Dlk1 could induce *Gli1* expression in a β1-integrin and ERK1/2 – dependent mechanism and that Dlk1 (and Shh) expression is inversely correlated to the size of the ZG in remodeling experiments (low Na+ diet vs captopril) [8]. This is in keeping with the notion that Dlk1 could maintain adrenocortical progenitor cells in an undifferentiated state, as it does in preadipocytes[156].

1.5.4 Association with tumourigenesis

Given the role of DLK1 in stem cell regulation and tissue homeostasis, some research was focused in identifying whether DLK1 has a role in tumourigenesis. In fact, studies reported enhanced DLK1 expression in different types of tumours; namely neuroblastomas, gliomas, breast cancer, colon cancer, pancreatic cancer as well as in pituitary tumours and some neuroendocrine tumours[154, 157, 158]. A study by Yun et al., (2012), investigating the role of DLK1 in regulating cancer cell differentiation *in vivo* using neuroblastoma xenograft models, suggested a role of DLK1 in maintaining the undifferentiated cancer stem cell-like character[155]. Another study focusing on hepatocellular carcinoma, has identified DLK1 expression in 17 liver cancer cell lines ranging from 0.18%-10.22% of the total population and showed that DLK1+ hepatocellular carcinoma cells are more resistant to chemotherapy.

1.6 Signaling pathways and key factors involved in adrenal tumourigenesis

Research aimed at unveiling the molecular mechanisms of tumour initiation and progression has identified that dysregulation of signalling pathways involved in normal adrenal development and adrenocortical homeostasis plays a crucial role in human adrenal disease and ACC. Factors like SF1, SHH, β-catenin and growth factors are some key proteins most commonly associated with tumourigenesis and will be discussed here.

Sf1's role in adrenocortical growth and differentiation, as well as findings showing an enhanced adrenocortical proliferation in Sf1 overexpressing mice, suggest that dysregulation of Sf1 could play a role in tumour initiation and progression[51]. In fact studies have found SF1 to be significantly upregulated in ACCs and its involvement in tumourigenesis is further supported by mouse studies in which Sf1 overexpression led to highly proliferating capsular cells and eventually tumour formation [51, 159, 160]. Sf1 expression is currently used to determine the adrenocortical origin of the tumour and can act as a prognostic marker in patients with ACC[161].

One of the most commonly mutated genes associated with multiple cancers is *CTNNB1* (β-catenin). In addition to tumourigenesis, dysregulation of the Wnt/β-catenin pathway leads to developmental abnormalities in the fetus. Mutations in the Wnt/β-catenin pathway have been associated with multiple cancers in different tissues. For example in familial adenomatous polyposis, a disease characterized by cancer in the large intestine and rectum, inactivating mutations in the *APC* gene leading to β-catenin accumulation in the nucleus, have been shown to be the molecular basis of the disease[162, 163]. Multiple studies investigating the involvement of Wnt/β-catenin in adrenocortical tumourigenesis have revealed that nuclear β-catenin accumulation and activating β-catenin *CTNNB1* point mutations were present in both adrenocortical adenomas (ACAs) and ACCs[164-166]. In addition, inactivating Axin2 mutations (part of β-catenin destruction complex) have also been described in adrenocortical tumours[167]. Mouse studies with adrenal specific APC inactivation, have shown that these mice develop adrenal hyperplasia and adenomas at 30 weeks of age. These studies confirm that Wnt activation has an important role in early adrenal tumourigenesis that can lead to malignant transformation[168].

The IGF pathway, in particular IGF2 has been shown to be involved in tumourigenesis, with overexpression of IGF2 and modification of the IGF2/H19 locus being identified in sporadic ACC. In fact, studies have shown that 80-90% of these ACCs have almost 100-fold increased expression of IGF2 compared to normal or ACAs[169-171]. In addition high levels of IGF2 expression in both benign and malignant adrenal tumours have been associated with a 5-fold increased risk of recurrence and a shorter survival (184,191). IGF2 is a maternally imprinted gene and therefore only expressed from the paternal gene. However, loss of imprinting results in upregulation of IGF2, a phenomenon often observed in Beckwith-Wiedemann syndrome (BWS)[172, 173]. BWS is a genetic disease that increases the risk of childhood cancers including ACC. In addition IGF2 is found to be upregulated in both pediatric and sporadic adult ACC

Finally, mutations in Shh signaling pathway have been identified in many cancers such as glioblastomas, pancreatic cancer and medulloblastomas [4, 174]. As mentioned earlier Shh is involved in the development and maintenance of the adrenal gland, however a link between Shh+ or Gli1+ cells and ACC formation and/or maintenance is not clear. Interestingly, profiling studies of ACCs do not show any upregulation of Gli and Shh compared to ACA and normal adrenals[175].

1.7 Adrenocortical tumours

Cancer development occurs following accumulation of multiple genetic changes at the DNA level that lead to the dysregulation of genes controlling cell cycle or cell proliferation. Mutations in specific genes can be common amongst different types of tumours, however there are also mutational events that are unique for specific cancers. Identification of these genes is important in providing a better understanding of the molecular mechanisms and signalling pathways that are critical in tumour development. This will lead in the development of better and more effective biomarkers and therapeutic strategies.

In most tissues, tumours formed can be classified as either benign or malignant depending on their invasiveness and ability to metastasize. In the case of the adrenal glands, benign tumours or ACAs are mostly incidentalomas that are commonly found in the general population. On the other hand, ACCs are rare malignant tumours with a poor clinical outcome (Discussed in Section 1.7.2). The frequency of ACAs is significantly higher than that of ACCs, suggesting that a greater number of mutations need to accumulate for a lesion to develop into a carcinoma as opposed to an adenoma. This is also in agreement with the hypothesis that an adenoma is part of the process of tumour progression, whereby accumulation of additional mutations leads to malignant tumour or carcinoma formation (multistage tumourigenesis). However, a different theory suggests that adenomas and carcinomas are completely different entities[176].

1.7.1 Adrenocortical adenoma

Adrenocortical adenomas are benign tumours of the adrenal cortex, are often asymptomatic and diagnosed incidentally (80%). However, in approximately 20% of cases they can present with Cushing's syndrome or primary aldosteronism[177, 178]. Recent efforts have been made to identify key signalling pathways mutated in adrenocortical adenomas. In the case of cortisol-producing adenomas, the PKA signalling pathway is often affected, with mutations in PRKAR1A (cAMP-dependent protein kinase type I-alpha regulatory subunit) and GNAS1 (stimulatory G-protein alpha subunit) identified in a small percentage of these adenomas so far [178, 179]. Genome-wide profiling of 22 ACAs also showed an upregulation of genes involved in cortisol secretion and steroidogenesis, as well as cholesterol metabolism[178, 180]

Primary aldosteronism on the other hand results in excess aldosterone secretion as the name suggests and can be subdivided into eight subtypes including Familial hyperaldosteronism Type I (FH-I), FH-II and FH-III[181]. FH-I is an autosomal dominant inherited disorder, caused by the genetic defect leading to unequal

recombination of *CYP11B1* and *CYP11B2*, thus resulting in a hybrid *CYP11B* gene (5'region of *CYP11B1* and 3'end *CYP11B2*). This results in aldosterone synthesis under ACTH stimulation[182].FH-II is another inherited form of primary aldosteronism, which is caused by either an aldosterone producing adenoma (APA) or bilateral adrenal hyperplasia. Genetic cause of FH-II is yet to be identified[183]. In the case of FH-III however, the underlying cause of the disease has been found to be an inactivating mutation in *KCNJ5*, a gene encoding a G-protein activated inward rectifier K+ channel 4[183, 184]. This results in increased adrenal cell proliferation and aldosterone production.

In addition to KCNJ5, which accounts for approximately 40% of all sporadic APAs, exome sequencing has identified additional somatic mutations present in APAs[185]. These include *ATP1A1*, encoding Na^+/K^+ ATPase alpha subunit, and *ATP2B3*, encoding the plasma membrane Ca^{2+} ATPase, which account for a total of 8% of cases[186]. Perturbation of the function of these two ATPases due to the somatic mutations in *ATP1A1* and *ATP2B3*, eventually leads to higher levels of cell depolarization, resulting in increased aldosterone secretion[178, 186]. As mentioned earlier, Nishimoto et al., (2015) has shown that these mutations are not only found in APAs, but are also found in aldosterone producing cell clusters (APCCs), but not adjacent cortical cells, in healthy human adrenal tissue. This finding is of particular interest as it suggests that APCCs appearing in healthy individuals are likely to be precursors of APAs[187].

1.7.2 Adrenocortical carcinoma

1.7.2.1 Epidemiology and key features

ACCs are rare but aggressive tumours of the adrenal cortex, with an annual incidence of 0.7-2 per million and a poor prognosis[188, 189]. A highest relative incidence has been observed in children compared to adults, with 1.3% of all childhood cancers and only 0.02-0.2% of adult cancers being ACCs[190-192]. In addition in both childhood and adult cancers the ratio of female to male patients with ACC ranges from 1.5-

2.5:1[192, 193]. Evidence of genetic predisposition has been reported, with ACCs often being associated to Li-Fraumeni syndrome and BWS arising from mutations in *TP53* and *IGF2*, respectively[188].

ACCs are usually large, heterogeneous tumours measuring more than 6cm in diameter at diagnosis. Their surface ranges from brown to orange/yellow depending on their lipid content and tissue necrosis is almost always present. Expression markers such as SF1 and KI67 have proven useful in the identification and determination of ACCs. A key histological feature that discriminates an ACC from an ACA is the presence of tumoural invasion in ACCs. This can occur in different forms, either direct invasion of the tumour capsule, invasion of the tumour capsule into the extra-adrenal soft tissue or direct invasion of the lymph nodes and blood vessels [188, 194].

1.7.2.2 Diagnosis and Prognosis

Initial diagnosis to determine the presence of an ACC, includes biochemical and imaging analysis. Biochemical tests are performed to measure steroid hormones produced by the tumour and this is dependent upon clinical symptoms of the patient. For example, patients with cortisol secreting tumours will have suppressed ACTH and elevated levels of cortisol, following an 8am blood test. Diagnosis of hypercortisolism is established mainly following a dexamethasone suppression test[195]. Additional biochemistry tests to screen for aldosterone, DHEAS and testosterone levels are also used in practise. However, in some cases signs and symptoms of steroid excess can be absent, and instead elevated levels of a number of hormone precursors are observed. In these cases a urine steroid analysis is the most sensitive method to diagnose ACCs[188].

In addition to biochemical tests, imaging techniques provide useful information regarding the appearance, invasiveness and origin of tumours, further confirming

ACC appearance. Contrast enhanced computer tomography (CT) and magnetic resonance imaging (MRI) scans are the most commonly used diagnostic imaging tools for initial imaging, staging and follow up analysis of the tumours[195]. As mentioned earlier, ACCs are usually large and heterogeneous, with signs of internal haemorrhage, necrosis and calcification in some cases. These are all features that distinguish an ACC from an ACA. In addition, following CT or MRI scans some ACCs also show signs of metastases to the liver, lungs or lymph nodes in addition to invasion into adjacent organs; characteristics that are absent in ACAs. Finally, after initial diagnosis a positron emission tomography (PET) scan is usually performed to confirm the diagnosis of a malignant lesion and/or establish the origin of the tumour[188].

ACC prognosis is poor and as mentioned earlier usually has a maximum of 5 year disease survival. However, prognosis is dependent on the stage of the cancer, the resection status (R0,R1,R2,Rx) and the proliferation index. Survival is greatly dependent on the staging of the ACC, where chance of 5 year survival being 66-82% for stage I, 64% for stage II, 24-50% for stage III and 0-17% for stage IV[194, 196-198]. Following surgery to remove the tumour in ACC, complete resection (R0) is associated with better prognosis, while macroscopic (R2) or unknown (Rx) resection are correlated with the worst prognosis[189]. Finally, measuring the proliferation index with Ki67 and mitotic count has proven an important factor of predicting recurrence in patients following surgery and a critical prognostic marker of survival[197, 199].

1.7.2.3 Current treatment options

Currently, the only approach to treating ACC is complete tumour resection and adjuvant therapy with/without the adrenolytic agent mitotane chemotherapy to decrease the chance of recurrence[188, 194]. Treatment is dependent on the stage of ACC as summarised in Figure 1.7, where Stage I and Stage II tumours are

considered organ specific or localised, while Stage III and Stage IV tumours are invasive and/or metastatic, respectively with a poor prognosis[194]. In the case of localised ACC, complete surgical resection is the first line of treatment, followed by adjuvant mitotane treatment to decrease the risk of recurrence. Patients with Stage I/II ACC undergoing surgery that have a Ki67 index <10% can be enrolled in ADIUVO, a randomised mitotane trial. In Stage III ACC, where cancer can be more invasive, and surgery leads to incomplete resection of the tumour, patients also undergo treatment with the adrenolytic agent mitotane and in some cases also undergo radiation therapy to reduce the risk of local recurrence[188, 194]. In patients with Stage IV metastatic ACC treatment options are considered palliative and are restricted to chemotherapy or radiotherapy with/without mitotane administration. Depending on the extent of tumour metastases, surgery can also be performed in some cases. Continuous surveillance to monitor disease progression is essential and depending on whether disease is stable or not different treatment options are suggested as shown in Figure 1.8. Finally, a study showed that response rate of patients with metastatic ACC to mitotane was 24% at best, suggesting that current treatments are not ideal and highlighting the need for better and more targeted treatment options[200].

To this end, attempts at identifying new potential drug therapies for ACC have been directed to targeting EGFR, vascular endothelial growth factor (VEGF) and IGF2 pathways. Both EGFR and VEGF were targeted in clinical trials of ACC, as they represent important mediators of cell proliferation and angiogenesis, thus supporting tumour growth and metastasis. Additionally, these two factors have been long established as being involved in tumorigenesis and therefore have been a target for various chemotherapeutic treatments for multiple cancers[201]. EGFR is a tyrosine kinase receptor belonging to the ErbB family of receptors, which play an important role in multiple biologic responses via activation of intracellular signalling pathways (MAPK and PI3K-Akt pathways in the case of EGFR). Mutations in EGFR

result in its constitutive active and leads to tumour growth, metastasis, inhibition of apoptosis and angiogenesis[202]. EGFR overexpression has been described in numerous cancer tissues including pancreatic cancer, breast cancer, non-small-cell lung cancer as well as in over 50% of ACCs[203-205]. Moreover, *in vitro* studies have demonstrated that EGFR levels in ACC tissues have been positively correlated with tumour growth and metastasis. Additionally, EGFR overexpression in tumour cells results in increased synthesis of angiogenic and anti-apoptotic factors including VEGF[201]. VEGF is expressed in many cell types including the adrenal glands and plays a role in haematopoiesis, wound healing, and organ development. VEGF is found to be overexpressed in tumour tissues and functions to support tumour growth, proliferation and angiogenesis[206]. Therefore, cancer therapies targeting VEGF can have a negative effect its pro-angiogenic and anti-apoptotic properties, therefore affecting tumour microenvironment and restricting tumour growth. Unfortunately, in the case of ACC treatment, results from trials using drugs targeting either EGFR or VEGF were not very successful, despite promising *in vitro* data[207, 208]. In the case of the IGF2 pathway, when using IMCA12 (cixutumumab), a fully humanized IGF-1R antibody alone there was no observable effect on disease progression in patients with ACC[178, 209]. However, when the same drug (cixutumumab) was combined with temsirolimus, an inhibitor of IGF-1R targets, this resulted in maintaining a stable disease in 42% of the patients in the trial[209]. These results suggest that new agents identified to treat ACC, will possibly have beneficial effects in combination therapies rather than single agent therapies. Thorough investigation of molecular pathways leading to ACC would also be beneficial for the discovery of new and more effective treatment options.

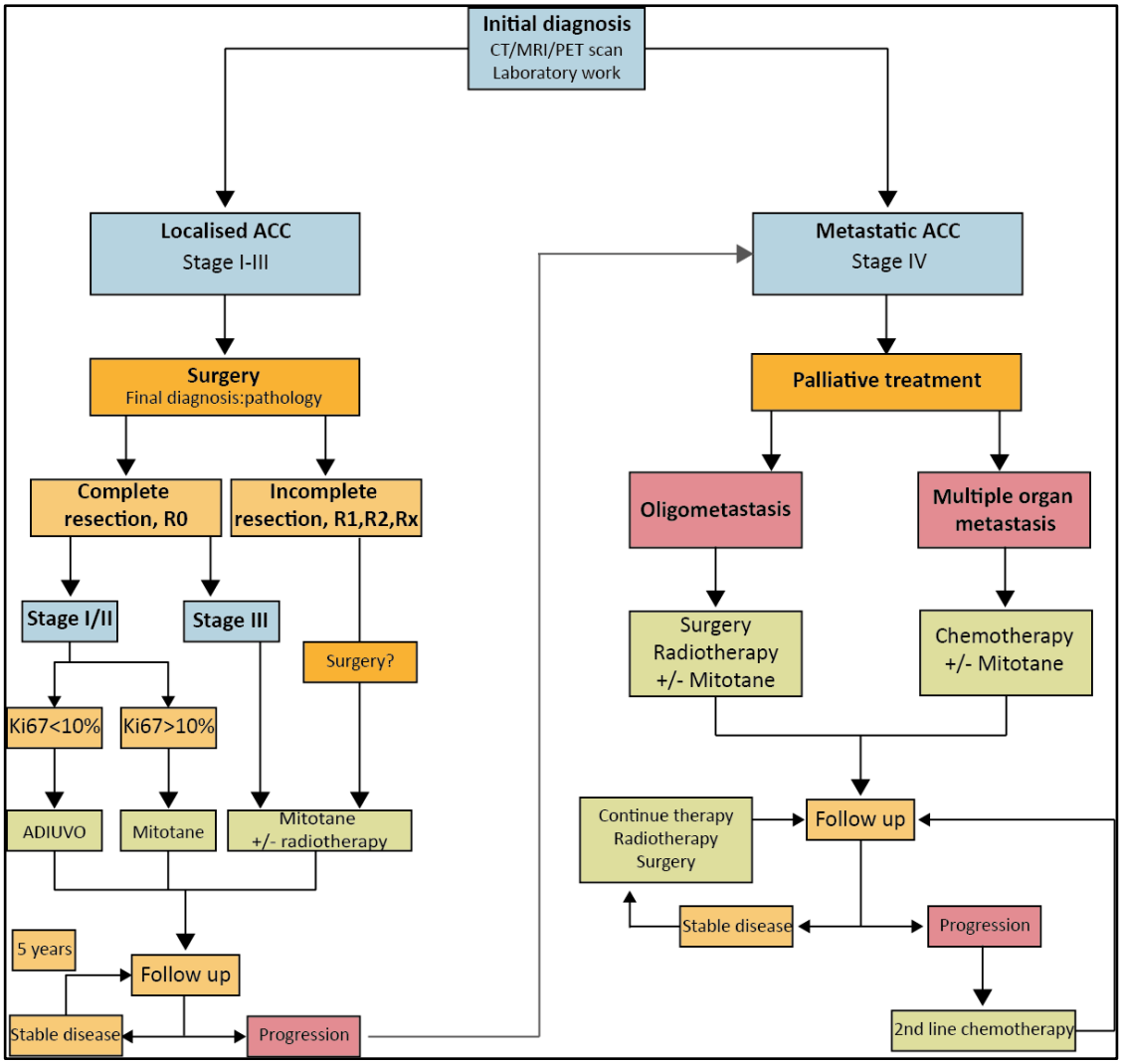

Figure 1.8- Therapy strategies for ACC management. Flow chart summarising the different treatment options based on type, severity and recurrence of ACCs.

1.7.2.4 Genomic analysis of ACCs

In recent years, genome-wide expression profile studies, microRNA and methylation profiling of ACCs in patient cohorts, has identified frequently mutated genes and other molecular interactions in ACCs, thus providing a better molecular characterisation of the disease. Exome-sequencing and single nucleotide polymorphism analysis, as well as studies employing next generation sequencing have also identified a number of mutations in genes driving ACC (Summarised in Table 1.1)[199, 210-213]. The main drivers identified are involved in Wnt/β-catenin

pathways and/or cell cycle regulation. More specifically the most common mutations, each accounting for 15-20% of ACCs investigated are inactivating mutations in *ZNRF3* (Wnt/β-catenin), *CTNNB1* (Wnt/β-catenin) and *TP53* (cell cycle). Both *ZNRF3* and *CTNNB1* are involved in the regulation and/or activation of Wnt/β-catenin signaling. Wnt signaling pathway is involved in cell growth, proliferation and differentiation both during embryogenesis and in adulthood. Mutations in these two genes lead to aberrant activation of the Wnt pathway, which results in tumorigenesis. Both these genes are known to be commonly mutated in ACCs as well as multiple other cancers. ZNRF3 is a cell-surface transmembrane E3 ubiquitin protein ligase, and along with RNF43 acts as a negative regulator of Wnt signal. It associates with the Wnt receptor complex and targets the receptor components Frizzled and LRP6 for degradation, thus inhibiting Wnt signalling[120]. Rspo1 and Rspo3 are natural antagonists of this action, thus restoring Wnt signalling (Section 1.4.2). Genetic mutations in *ZNRF3/RNF43* and *RSPO1/RSPO3* have been associated with multiple cancers and hold great promise as predictive biomarkers and potential downstream therapeutic cancer targets[214]. In the case of ACC, *ZNRF3* has been recently identified as one of the most commonly mutated genes, with inactivating mutations occurring in approximately 20% of cases (Table 1.1). *CTNNB1* encodes for β-catenin, an important component of the Wnt-signaling. Briefly, in the canonical Wnt pathway and upon activation, free β-catenin in the cytoplasm translocates to the nucleus where it binds TCF, displacing co-receptors and enabling downstream target genes to be expressed (previously discussed in Section 1.6). Similar to *TP53*, mutations in *CTNNB1* have also been identified in multiple cancers. More specifically, in the case of ACCs, activating somatic mutations in *CTNNB1* have been found in more than 10% of cases (Table 1.1). *TP53* is a tumour suppressor gene encoding a 393aa transcription factor, which in response to cellular stress can exert antiproliferative functions including cell cycle arrest, DNA repair or apoptosis[215]. Somatic *TP53* mutations have been found in multiple types of cancers, while germline mutations in *TP53* have been associated with a predisposition to early onset cancers such as Li Fraumeni syndrome[216]. In

the adrenal glands, inactivating TP53 mutations account for approximately 23% of ACCs, usually as a result of missense substitution. This leads to a significant loss of DNA binding and transactivation capacity resulting in an altered cell cycle[216]. In addition to inactivating mutations, high-level amplifications, homozygous deletions as well as somatic copy number alterations have also been identified in various studies and summarised in Table 1.1 below. In addition to Wnt/β-catenin pathway and cell cycle regulation, mutations in genes involved in histone modification and regulation of telomere length have also been identified[210].

Despite an overall poor prognosis, the outcome of patients with ACC is heterogeneous. Genomic and transcriptomic analysis have identified two molecular subgroups predictive of distinct ACC outcomes and survival on patients. These were termed C1A and C1B groups, corresponding to poor and good prognosis, respectively. It was shown that the C1A group displayed multiple mutations and DNA methylation alterations whereas the C1B group only showed specific deregulation of two microRNA clusters[199]. However, more recently Zheng et al., introduced a new more detailed classification of ACCs based on molecular and methylation signatures (Table 1.2). They divided ACCs into three groups namely CoCI, CoCII and CoCIII; where the majority of CoCI were classified as C1B and most of CoCII and CoCIII were classified as aggressive C1A. ACCs are classified into the three groups based on different properties, including methylation phenotype, disease progression, proliferation as highlighted in Table 1.2[210].

In conclusion, these studies have led to the identification of genomic alterations commonly observed in ACCs, paving the way for the discovery of specific markers of ACC as well as markers that can be associated to the different ACC outcomes and therefore more accurate prognosis. In addition, identifying these alterations and the pathways they are affecting might be crucial in the discovery of new therapeutic targets of ACC.

Table 1.1 Most common mutations in ACC

Gene	Role	Mutation type	Somatic/ Germline	Effect	Average Occurrence	Reference
ZNRF3	Negative regulator of Wnt/β-catenin pathway	Inactivating mutations/ Homozygous deletions	Somatic	Activation of Wnt/β-catenin pathway	17.5%	[199, 210, 213]
CTNNB1	Gene encoding β-catenin	Activating mutations	Somatic	Activation of Wnt/β-catenin pathway	13%	[199, 210, 211, 213]
APC	Negative regulator of Wnt/β-catenin pathway	Inactivating mutations	Germline	Activation of Wnt/β-catenin pathway	4.1%	[199, 210, 211]
KREMEN1	Wnt repressor	Homozygous deletion	Somatic	Activation of Wnt/ β-catenin pathway	7.3%	[213]
MED12	Encodes mediator complex subunit 12; interacts with β-catenin	Inactivating mutations	Somatic	Disturb transcription of β-catenin target genes	5%	[199]
TP53	Encodes p53, positive regulator of apoptosis, cell cycle arrest, DNA repair	Inactivating mutations	Somatic (Germline)	Altered cell cycle	22.7%	[199, 210, 211, 213]
CDKN2A	Tumour suppressor gene, acts via p53, pRB	Inactivating mutations/ Homozygous deletions	Somatic	Altered cell cycle	13.6%	[199, 210, 211]
RB1	Encodes pRB; negative regulator of cell cycle	Inactivating mutations/ Homozygous deletions	Somatic	Altered cell cycle	7%	[199, 210, 211]

Gene	Role	Mutation type	Somatic/ Germline	Effect	Average Occurrence	Reference
MDM2	E3 ubiquitin ligase; negative regulator of p53	High level amplification	Somatic	Altered cell cycle	4%	[199, 210, 211]
CCNE1	Encodes G1/S specific cyclin-E1; Important for G1 to S-phase transition	High level amplification	Somatic	Altered cell cycle	5.7%	[210]
CCND2	Encodes cyclin D2; required for G1/S	High level amplification	Somatic	Altered cell cycle	7%	[211]
CDK4	Oncogene; Inhibits pRB	High level amplification	Somatic	Altered cell cycle	5.3%	[199, 210, 211]
MEN1	Chromatin remodelling; Transcriptional regulator	Inactivating mutations	Somatic (Germline)	Chromatin remodelling	9.3%	[199, 210, 211]
DAXX	Chromatin remodelling; Telomere lengthening; apoptosis	Inactivating mutations	Somatic	Abnormal chromatin remodelling & telomere length	6.5%	[199, 211]
ATRX	Chromatin remodelling; Telomere lengthening;	Inactivating mutations	Somatic	Abnormal chromatin remodelling & telomere length	4%	[199]
TERT	Reverse transcriptase of telomerase complex	High level amplification	Somatic	Abnormal chromosome telomere length	9.6%	[199, 210]
TERF2	Maintains telomere length	High level amplification	Somatic	Abnormal chromosome telomere length	6.6%	[210]

Gene	Role	Mutation type	Somatic/ Germline	Effect	Average Occurrence	Reference
PPKAR1A	Negative regulator subunit of PKA	Inactivating mutations/ Homozygous deletions	Somatic (Germline)	Activation of PKA	11%	[210]
RPL22	Encodes 60S ribosomal protein L22	Inactivating mutations/ Homozygous deletions	Somatic	Unknown	7.7%	[210]
NF1	Encodes neurofibromin; Tumour suppressor gene	Inactivating mutations/ Homozygous deletions	Somatic	Abnormal cell growth	10.9%	[210, 211]
NF2	Tumour suppressor gene	Inactivating mutation	Somatic	Abnormal cell growth	5%	[213]

Table 1.2 - Classification of ACCs

Description	CoCI	CoCII	CoCIII
Disease progression	7%	56%	96%
Tumour stage	75% I/II	47% III/IV	52% III/IV
CIMP	Low	Intermediate	High
Proliferation rate (Ki67)	Low	Intermediate	High
Steroid phenotype	Mostly low	Mostly high	High
Whole Genome Doubling Score	0-1	0-2	0-2
IGF2 Expression	High	High	High
***CTNNB1* mutation rate**	Low	Intermediate	High

1.8 Project hypotheses

We believe that a better characterisation of the human adrenal cortex and identification of different cell populations that exist within the adrenocortical region will provide a better understanding of human adrenal development, function, and tumorigenesis.

Previous work in rodents has identified an undifferentiated zone in the adrenal cortex expressing Dlk1 and Shh (See section 1.1). However, this ZU has not yet been characterised in humans. Given the similarities between rodents and human adrenocortical zonation, we hypothesise that an ZU might also exist in human adrenal glands.

DLK1 is involved in maintaining cells in an undifferentiated state in human adipose tissue (See section 1.5), we therefore hypothesise that DLK1 could potentially act as a marker of adrenal progenitor cells in the ZU of humans. Finally, DLK1 is involved in tumorigenesis in other human tissues (See section 1.5), and may also be involved in adrenal tumorigenesis in humans.

1.9 Aims and Objectives

1. Characterise human adrenocortical zonation to provide a better understanding of structural organisation of cells and their function.

2. Identify whether a ZU exists in the subcapsular region of the human adrenal glands, by looking at the expression of DLK1 and other known steroidogenic markers (CYP11B1, CYP11B2, CYP17).

3. Study the expression and localisation patterns of DLK1 in normal and tumorigenic adrenal glands, and explore the potential of DLK1 as a biomarker of human ACCs.

4. Evaluate whether DLK1+ cells could represent cancer stem cells in H295R human adrenal cancer cell lines.

5. Investigate the involvement of capsular Dlk1+ cells in adrenocortical homeostasis and tumorigenesis in mice, using adrenocortical tumour mouse models and the $Dlk1^{CreERT2/+}$; $Rosa^{Tm/Tm}$ transgenic mouse model.

Chapter 2: Materials and Methods

2.1 Human adrenal collection ethics

All human adrenal collections and studies performed and presented as part of this project were approved under the "Genetics of endocrine tumours" ethics (reference: 06/Q0104/133).

2.2 Paraffin embedding of adult adrenals

Adrenal glands collected were fixed in 4% paraformaldehyde (PFA) (Acros Organics, 416780010) overnight at 4°C and then washed with phosphate buffered saline (PBS) solution (Oxoid, BR100) for 1 hour. Following PBS washes the adrenals were dehydrated in a series of ethanol washes, 50%, 70%, 90% and 100% (Fischer Scientific, E/0650/17) for 1 hour each, on a rotating plate (Stuart, analogue tube roller SRT6). Adrenals were then incubated in xylene (Fischer Scientific, X/0250/17) twice for 5 minutes, and 10 minutes incubation before being placed in a container with melted paraffin (VWR, 361077E) for overnight incubation at 56°C. The following day adrenals were placed in the embedding cassettes (VWR, 18000-244) filled with melted paraffin and were allowed to set at room temperature. Frontal sections of paraffin embedded adrenals were cut at 6-8µm using a rotary microtome (Thermo scientific, 902100A) and serial sections were transferred onto superfrost plus glass slides (VWR, 48311-703) covered with ddH_2O, and heated at 56°C on a hotplate (Thermo scientific, E181SL) for 30-60 minutes or until sections were flat. Finally, excess water was removed; sections were allowed to dry at 37°C and stored at room temperature.

2.3 Sucrose-cryopreserved and OCT-embedded adrenals

Human and mouse adult adrenals collected were fixed in 4% PFA overnight at 4°C, followed by a PBS wash for 1 hour. They were then incubated in filtered 30% sucrose solution (Fisher Scientific, S/8560/60) overnight or until tissue sunk to the bottom of the tube. Finally, specimens were transferred in a container filled with liquid optimal cutting temperature compound (OCT) (VWR, 361603E), orientated and placed on dry ice until the OCT solidified. Embedded specimens were stored at -80°C. Frontal sections of OCT embedded adrenals were cut at 14-18µm using a cryostat (Leica GM1510S) and serial sections were mounted on superfrost plus glass slides. Sections

were incubated at room temperature overnight and then stored at -80°C.

2.4 Snap frozen and OCT embedded adrenals

Mouse and human adrenals were snap-frozen on dry ice or in liquid nitrogen, immediately after collection. Frozen tissues were then transferred into a container with OCT medium, orientated and placed on dry ice until OCT solidified. Once frozen embedded adrenals were stored at -80°C until sectioned. Sections were cut at 14-18µm using a cryostat and serial sections were mounted on superfrost plus glass slides and stored at -80°C immediately after cutting.

2.5 Fluorescent Immunohistochemistry on fresh frozen sections

Sections previously stored at -80°C, were immediately fixed in 4% PFA for 15 minutes on ice, followed by three washes in PBS-0.1% Triton X-100 (PBS-Triton) for 10 minutes each. If antibody used required antigen unmasking, slides were incubated in 10mM Citrate Buffer pH 6.0 (see Section 2.19.5) for 30 minutes in a water bath at 95°C and then allowed to cool for 20 minutes at room temperature before blocking for non-specific binding. If no antigen unmasking was required slides were directly blocked for non-specific binding by incubating slides in blocking solution consisting of 10% goat serum (Sigma-Aldrich, G9023) in PBS-Triton for 1 hour. Following blocking, slides were incubated with primary antibody diluted in PBS-Triton (Table 2.1) overnight at room temperature. The following day, slides were washed three times in PBS-Triton for 10 minutes each and incubated with secondary antibodies diluted in PBS-Triton (Table 2.2) for 1 hour at room temperature. Additional 10-minute washes were performed and slides were finally incubated with 4,6-Diamidino-2-phenylindole (DAPI) (Sigma-Aldrich, D9542) diluted 1:1000 in PBS-Triton for 1 minute at room temperature. Finally, slides were washed with PBS-Triton three times for 10 minutes each and mounted with glass cover slips (VWR, 631-0137) using PBS:Glycerol (Sigma-Aldrich, G5516) solution at a ratio of 1:3. Fluorescent antibody staining of the tissues was visualised using a Leica DM5500B automated upright microscope. Tissue sections were stored at 4°C.

2.6 Fluorescent Immunohistochemistry on paraffin sections

Sections were initially de-paraffinised with three xylene incubations for 10 minutes each at room temperature, followed by rehydration steps of 10 minutes each from 100% ethanol to H_2O (100%, 90%, 70%, 50% and H_2O). Sections were then washed in PBS-Triton three times for 10 minutes each. At this point if the antibody used required antigen unmasking, slides were incubated in 10mM Citrate Buffer pH 6.0 for 30 minutes in water bath at 95^oC and then allowed to cool for 20 minutes at room temperature before blocking for non-specific binding. Following unmasking, slides were incubated in blocking solution consisting of 10% goat serum in PBS-Triton for 1 hour, to prevent non-specific binding. Following blocking, slides were incubated with the primary antibody diluted in PBS-Triton (Table 2.1) overnight at room temperature. The following day, slides were washed three times in PBS-Triton for 10 minutes each and incubated with the secondary antibody diluted in PBS-Triton (Table 2.2) for 1 hour at room temperature. Additional 10-minute washes were performed and slides were finally incubated for 1 minute with DAPI diluted 1:1000 in PBS-Triton at room temperature. Finally, slides were washed with PBS-Triton three times for 10 minutes each and mounted with glass cover slips using PBS:Glycerol (1:3) solution. Fluorescent antibody staining of the tissues was visualised using a Leica DM5500B automated upright microscope. Tissue sections were stored at 4^oC.

2.7 Chromogenic Immunohistochemistry with DAB on paraffin sections

Sections were de-paraffinised in xylene incubations, washed in 100% ethanol and incubated in 3% H_2O_2 (Sigma Aldrich, 21,676-3) diluted in methanol (Fischer Scientific, M/4000/PC17) for 30 minutes at room temperature to block endogenous peroxidase activity. Following peroxidase treatment sections were rehydrated in decreasing concentrations of ethanol (100%, 90%, 70% and 50%) for 10 minutes each, followed by incubation in H_2O for 10 minutes and washes in PBS-Triton. At this point if the antibody used required antigen unmasking, slides were incubated in 10mM Citrate Buffer pH 6.0 for 30 minutes in water bath at 95^oC and then allowed to cool for 20 minutes at room temperature before blocking for non-specific binding. Following unmasking, slides were incubated in blocking solution consisting of 10% goat serum in PBS-Triton for 1 hour, to prevent non-specific binding. Following blocking, slides

were incubated overnight with the primary antibody diluted in PBS-Triton (Table 2.1) at room temperature. Slides were then washed with PBS-Triton and incubated with the biotinylated secondary antibody (Table 2.3) diluted in PBS-Triton for 2 hours at room temperature. Following secondary antibody incubation, slides were washed in PBS-Triton three times for 10 minutes each and at the same time Avidin-Biotin Complex (ABC) was prepared according to manufacturer's instructions (Vector labs, PK-6100) and allowed to incubate at room temperature for at least 30 minutes before use. Following washes slides were incubated with ABC for 1 hour and then washed three times with PBS-Triton. Finally, sections were developed with 3,3'-diaminobenzidine substrate according to manufacturer's instructions (Vector labs, SK-4105). Once staining developed, reaction was stopped by placing slides in diethyl pyrocarbonate (DEPC)-H_2O. Slides were finally dehydrated in increasing concentrations of ethanol (50%, 70%, 90% and 100%) and then xylene incubations three times for 5 minutes each and mounted using Vectamount mounting medium (Vector labs, H-5000). Chromogenic antibody staining was visualised using a Leica DM5500B microscope.

Table 2.1 - Primary Antibodies for fluorescent and chromogenic IHC

Antibody	Species Reactivity	Host	Supplier	Catalogue Number	Dilution	Requires AUM
CYP11B1	Human	Rat	Gomez-Sanchez	N/A	1:100	Yes
CYP11B2	Human	Mouse	Gomez-Sanchez	N/A	1:100	Yes
CYP11B2	Mouse/Rat	Rabbit	Gomez-Sanchez	N/A	1:100	Yes
CYP17A1	Human/Mouse/Bovine	Rabbit	Gift	N/A	1:500	No
DLK1 (H-118)	Human/Mouse/Rat	Rabbit	Santa-Cruz	sc-25437	1:500	No
DAB2 (H-110)	Human/Mouse/Rat	Rabbit	Santa-Cruz	sc-13982	1:200	No
GFP	Human/Mouse/Rat/Rabbit	Chicken	Abcam	ab13970	1:100	No
SF1 (A-1)	Human/Mouse	Mouse	Santa-Cruz	sc-393592	1:200	Yes
VILIP1	Human/Mouse/Rat	Rabbit	Abcam	ab151741	1:100	No
β-catenin	Human/Mouse/Chicken/ Canine/Bovine	Mouse	Sigma-Aldrich	C7082	1:200	No

Table 2.2 - Secondary Antibodies for fluorescent IHC

Antibody	Species Reactivity	Host	Supplier	Catalogue Number	Dilution
Alexa Fluor 488	Mouse IgG	Goat	Invitrogen	A11029	1:1000
Alexa Fluor 568	Mouse IgG	Goat	Invitrogen	A11004	1:1000
Alexa Fluor 488	Rabbit IgG	Goat	Invitrogen	A11008	1:1000
Alexa Fluor 568	Rabbit IgG	Goat	Invitrogen	A11036	1:1000
Alexa Fluor 488	Rat IgG	Goat	Invitrogen	A11006	1:1000

Table 2.3 – Secondary Antibodies for chromogenic IHC

Antibody	Species Reactivity	Host	Supplier	Catalogue Number	Dilution
Biotinylated	Mouse IgG	Goat	Vector	BA-9200	1:500
Biotinylated	Goat IgG	Horse	Vector	BA-9500	1:500
Biotinylated	Rabbit IgG	Goat	Vector	BA-1000	1:500
Biotinylated	Rat IgG	Goat	Vector	BA-9401	1:500

2.8 Hematoxylin and Eosin staining

Sections were incubated with Hematoxylin Solution Gill No.3 (Sigma, GHS332) for 2 minutes and then washed under running water for 2 minutes. Following washes sections were incubated in 1% acid alcohol (1% hydrochloric acid (Fisher Scientific, A481-212) in 70% ethanol) for 1 minute and washed in water for an additional minute. Sections were then dipped in 0.2% ammonia solution (concentrated ammonium hydroxide (Sigma-Aldrich, 320145) diluted in distilled water) 10 times and washed for 5 minutes under running water. Slides were then incubated in 80% ethanol for 1 minute followed by eosin (National diagnostics, HS 402) incubation for 30-45 seconds. Sections were further dehydrated in 95% ethanol twice and 100% ethanol for 1 minute each followed by 2 xylene incubations for 3 minutes each. Following staining and dehydration steps, sections were mounted with Vectamount (Vector, H-5000).

2.9 Human DLK1 probe preparation for in situ hybridization

2.9.1 Amplification and isolation of gene of interest

Primers for the human *DLK1* gene were designed and ordered from Sigma Aldrich (FW:5'-AAATGGATTCTGCGAGGATG-3'; REV:5'-CAGGCCCGAACATCTCTATC-3'). The human *DLK1* gene was amplified by Polymerase chain reaction (PCR) using human adrenal cDNA as a template. PCR master mix for this reaction was prepared as shown in Table 2.4. PCR cycle included an initial 2-minute hot start, followed by 35 cycles of 94^{o}C for 30 seconds, 52^{o}C for 30 seconds, 68^{o}C for 90 seconds with final extension at 68^{o}C for 10 minutes. PCR products were then run on a 1% agarose gel and bands corresponding to the gene of interest were extracted using the QIAGEN Gel Extraction Kit (QIAGEN, 28706).

Table 2.4 –PCR Master Mix

Reagent	Volume, µl
Taq Buffer (New England Biolabs, M0273X)	2.5
dNTPs (New England Biolabs, N0447S)	0.5
Primers (F+R)	1
Taq Polymerase (New England Biolabs, M0273X)	0.5
ddH_2O	19.5
Sample (added individually)	1
Total	**25**

2.9.2 Gel Extraction

Following gel electrophoresis, appropriate bands were excised from the gel for DNA extraction using QIAquick Gel Extraction Kit (QIAGEN, 28706). Excised bands were placed in an eppendorf, weighed (max. 400mg) and 3 volumes of Buffer QG were added to 1 volume of gel (100mg gel corresponds to 100µl). Samples were incubated at 50^{o}C for 10 minutes (or until gel was completely dissolved). Then 1 volume of 100% isopropanol (Fisher Scientific, 67-63-0) was added to the sample, mixed and the sample was transferred to a QIAquick spin column placed in 2ml collection tube (both provided in the Kit) and centrifuged for 1 minute at high speed. Following this, 500µl of Buffer QG were added to each column and centrifuged for another minute (flow-through discarded). Columns were washed with 750µl Buffer PE allowed to stand for 2-5 minutes and centrifuged for another minute discarding the flow-through. Columns were re-centrifuged for a second time to remove any residual buffer. To elute DNA, columns were transferred into a clean 1.5ml microcentrifuge tube and 30µl of Buffer EB or DNAse/RNAse free H_2O (Sigma, W4502) were added to each column, allowed to stand for 1 minute, and then centrifuged for another minute. Concentration of DNA collected was measured using a nanodrop (Thermo Fisher, Nanodrop ND-1000) and samples were stored at -20^{o}C until use.

2.9.3 Ligation and Transformation

The DNA band extracted and purified above was then ligated in the PGEM T-Easy vector (Promega, A1360) (Appendix I). 3µl of the insert, 1µl of the vector, 5µl of 2X ligation buffer and 1µl of T4 ligase were mixed together and incubated on ice at 4^{o}C overnight. The next day transformation was performed, where 2µl of ligation product was added to 65µl of competent bacterial cells and incubated on ice for 20 minutes, followed by 1-minute incubation at 42^{o}C and a further 2-minute incubation on ice. Then 900µl of Super Optimal broth with Catabolite repression (SOC) medium (Sigma-Aldrich, S1797) were added to the bacteria-ligation mix followed by a further 1-hour incubation at 37^{o}C. Following the incubation period, the tube was centrifuged at high speed for 20 seconds and 600µl of the supernatant were removed. The remaining 300µl were mixed and plated on agar plates coated with Ampicillin (Sigma, A0166), IPTG (Sigma-Aldrich, I6758) and X-gal (Thermo Fisher, B-1690) and incubated upside down at 37^{o}C overnight in a bacterial incubator. The next day colonies were picked for a mini- or midi-prep. A mini-prep was initially performed when cloning a new gene of interest for DNA sequencing, while a midi-prep was performed for DNA extraction.

2.9.4 Mini-prep for Sanger Sequencing

Mini-prep was performed on bacterial colonies collected and grown overnight at 37^{o}C in 5ml LB media using the QIAprep Spin miniprep Kit and following manufacturer's instructions (Qiagen, 27106). Overnight grown bacterial cells were harvested by centrifugation at 8,000rpm for 3 minutes, re-suspended in 250µl Buffer P1 and transferred to a microcentrifuge tube. 250µl Buffer P2 (lysis buffer) were added and tubes were mixed thoroughly by inverting 4-6 times. Then 350µl of Buffer N3 (neutralization buffer) were added to each sample, mixed by inverting the tube 4-6 times and centrifuged for 10 minutes at 13,000rpm. Following centrifugation 800µl of supernatant were added to the provided QIAprep spin columns and centrifuged for 60 seconds discarding flow-through. Columns were then washed with 750µl Buffer PE and centrifuged for a further 60 seconds discarding flow-through. Columns were re-centrifuged for an additional minute to remove excess buffer. Finally, columns were transferred into a clean 1.5ml microcentrifuge tube, 50µl of ddH2O were added and tubes were allowed to stand for 1 minute before being

centrifuged for another minute to elute DNA. Following mini-prep, samples were digested with a suitable enzyme, EcoRI in this case, to linearize the vector and DNA was sent for sequencing. Once the reagents were added (Table 2.5), the samples were incubated at 37°C for 3 hours. A negative control was also included by addition of 2µl of sample and 18µl of ddH2O. Following incubation both uncut (negative control) and cut vector were run on a 1% agarose gel and bands were gel extracted and purified (see Section 2.9.2). Concentration of DNA was measured for each sample using a nandrop and adjusted to 100ng/µl before being sent for Sanger sequencing.

Table 2.5 – Enzyme digestion with EcoRI

Reagent	**Volume, µl**
CutSmart Buffer (New England Biolabs, B7204S)	2
EcoRI-HF (New England Biolabs, R3101S)	1
DNA	5
ddH_2O	12
Total	**25**

2.9.5 Midi-prep for probe preparation

Midi-prep was performed using QIAGEN Plasmid Midi Kit (Qiagen, 12145), on bacterial colonies that have successfully incorporated the vector (and insert) transformed as confirmed by DNA sequencing (Section 2.9.4). Bacterial cells from overnight cultures at 37°C in 200ml LB medium, were harvested by centrifugation at 6000xg for 15 minutes at 4°C and the pellet was re-suspended in 4ml Buffer P1. Then 4ml Buffer P2 were added to each sample, mixed thoroughly by inverting the tube 4-6 times and incubated for 5 minutes at room temperature. 5ml of pre-chilled Buffer P3 were then added to each sample, mixed and incubated on ice for 15 minutes. Following incubation samples were centrifuged at 14,000-18,000xg for 30 minutes at 4°C, followed by a further centrifugation of the supernatant at 20,000g for 15 minutes at 4°C. At the same time, QIAGEN-tip (provided with the kit) were equilibrated by addition of 4ml Buffer QBT, which was allowed to flow through by

gravity. The supernatant of the second centrifugation was then added to the equilibrated tips and washed twice with 10ml of Buffer QC. Following the two washes, 5ml of Buffer QF were added to the tips and DNA was eluted in a new 15ml tube. Then DNA was precipitated following addition of 3.5ml isopropanol to the eluted mix and centrifugation at 15,000xg for 30 minutes at 4°C. The supernatant was removed and the DNA pellet washed with 2ml of 70% ethanol and centrifuged at 15,000xg for 10 minutes. Following centrifugation, the supernatant was removed and the pellet was air-dried for 5-10 minutes. Finally, DNA was re-dissolved in 200µl of RNAse/DNAse free water. DNA concentration was measured using a nanodrop and 5µg were used for the digestion to get the sense and antisense mRNA for in situ hybridization, using the appropriate restriction enzymes with their corresponding buffer (Table 2.6). The digestion mix was incubated at 37°C for 2.5-3 hours including a negative control (x µl sample + 20-x µl ddH2O). Finally, the samples were run on a 1% agarose gel and the bands excised for DNA purification (see Section 2.9.2).

Table 2.6 – Enzyme digestion for ISH probes

Reagent	**Volume, µl**
4-CORE Buffer C or B (Promega, R9921)	3
SacII or SpeI (Promega, R6221 or R6591)	1
DNA	X (5µg)
ddH_2O	16-x
Total	**20**

2.9.6 *In vitro* transcription

Following DNA purification of the sense and/or antisense, 1µg DNA (or maximum volume 16µl) was used for *in vitro* transcription to obtain the cRNA probes. DNA was mixed with 5X Transcription Buffer (TB) (Roche, 11465384001), RNA digoxigenin labeling mix (Roche, 11277073910), 1,4-dithiothreitol (Invitrogen, P/N y00147), RNAse inhibitor (New England Biolabs, M0314S) and T7 RNA polymerase (Roche, 10881767001) or Sp6 RNA polymerase (Roche, 10810274001) for either the sense or the antisense (Table 2.7) depending on the results from the sequencing, and

incubated at 37°C for 3 hours. Following incubation, 1.5µl were removed from the mix and collected as 'pre' in 10µl of ddH2O. DNAse mix was prepared as shown in Table 2.8 and 14µl were added to each sample and incubated at 37°C for 40 minutes. After incubation 1.5µl of DNAse treated sample was collected as 'post' and both 'pre' and 'post' (DNAse treatment) samples were run on a 1% agarose gel to ensure that there was no DNA contamination following treatment.

Table 2.7 - *In vitro* transcription

Reagent	**Volume, µl**
Sample (SacII or SpeI)	x (1µg, max 16µl)
5X TB	6
RNA Digoxigenin labeling mix	2
DTT	3
RNAse inhibitor	1
Enzyme	2
ddH_2O	(16-x)
Total	30

Table 2.8 - DNAse mix

Reagent	**Volume, µl**
DTT	1.5
5X TB	3
DNAse I	1.5
ddH_2O	8
Total	**14**

2.9.7 Precipitation and post-precipitation

Following DNAse treatment, samples were mixed with 46µl ddH2O, 3.2µl 0.5M Ethylenediaminetetraacetic acid (EDTA) (Sigma Aldrich, E9884), 2.5µl 4M lithium chloride (Sigma-Aldrich, 43,137-0) and 250µl ethanol and incubated overnight at -

20°C. The next day, samples were centrifuged for 20 minutes at 4°C and the supernatant was removed. The pellet was washed with 300µl of 70% ethanol and centrifuged for a further 20 minutes at 4°C. The supernatant was removed and the pellet was allowed to air dry before being re-suspended in 100µl of ddH2O. RNA concentration was measured using a nanodrop, aliquoted at 800ng/µl and stored at -80°C until use.

2.10 *In situ* hybridization (ISH) on paraffin embedded sections

Paraffin sections were de-paraffinised in xylene and then rehydrated in decreasing ethanol concentrations (100%, 90%, 79% and 50%) and final incubation in DEPC-H_2O. Sections were then fixed in 4% PFA on ice and washed in DEPC-PBS-Tween twice for 10 minutes. The slides were then treated with proteinase K (Section 2.20.8) for 16 minutes at 37°C in a water bath and washed twice with DEPC-PBS-Tween. Following washes slides were incubated again in 4% PFA and washed twice in DEPC-PBS-Tween for 10 minutes each. Sections were acetylated by incubating in solution containing 0.1% triethanolamine (Sigma-Aldrich, 90279), 0.25% acetate anhydride (Sigma-Aldrich, 320102) in DEPC-PBS-Tween for 10 minutes, followed by additional washes. Hybridization buffer (see Section 2.19.9) was then added on the slides, and slides were covered with parafilm (Sigma-Aldrich, P7793) and incubated at 56°C for 2 hours in the oven. Saturation solution (see Section 2.19.10) was added at the bottom of the tray to prevent evaporation. Following incubation with the buffer, probes targeting the desired gene were added on each slide and incubated in the oven at 56°C overnight. Probes were used at a concentration of 800ng/ml and were heated at 85-90°C for 3 minutes, vortexed and kept on ice for 1 minute before use. The following day saline sodium citrate buffer (SCC) washes of 2X, 1X, 0,2X and 0.05X (National Diagnostics, EC-873) were performed as described in Table 2.9. Following SCC incubations, slides were washed with RNAse A buffer for 10 minutes at room temperature, before being treated with RNAse A solution (Invitrogen, 12091-021) (25µl of RNAse A solution in 50ml RNAse Buffer) at 37°C for 30 minutes. Sections were then washed twice in Maleic acid buffer (see section 2.19.11) for 10 minutes and then incubated in blocking buffer (consisting of 10% blocking buffer at 1:200 and Anti-digoxigenin (Roche, 11093274910) at 1:2000, both diluted in Maleic acid buffer

overnight at 4°C. The next day slides were washed with PBS-Tween twice for 10 minutes and then incubated in alkaline phosphatase (NTMT) Buffer pH 9.0 for 10 minutes before being developed. Developing solution was prepared by adding 50µl of NBT/BCIP (Roche, 11681451001) and 1 drop of Levamisole (Vector, SP-5000) in every 5 ml of NTMT Buffer. Sections usually developed after a few hours and if not, developing solution was changed and slides were incubated at 4°C overnight.

Table 2.9 – SCC Washes

SCC wash	20X SCC	H_2O - Tween	Incubation
2X	5ml	45ml	20' at room temperature
2X	5ml	45ml	15' at 65°C oven
1X	2.5ml	47.5ml	15' at 65°C oven
0.2X	0.5ml	49.5ml	15' at 65°C oven
0.05X	125µl	50ml	15' at 65°C oven

2.11 *In situ* hybridization on fresh frozen sections

Same procedure was followed as described in Section 2.10 above but without de-paraffinisation and dehydration steps.

2.12 Cell Culture

2.12.1 Culture of HEK293 cell line

Cells were initially seeded at 3-6x10^3 cells/cm^2 in Dulbecco's Modified Eagle's medium (DMEM) (Sigma-Aldrich, D5796), supplemented with 10% Fetal bovine serum (FBS)(Sigma-Aldrich, F2442) and 1% Penicillin-streptomycin (Sigma-Aldrich, P4458). Cells were passaged when they reached 70-80% confluent. To split cells, medium was initially removed and cells were washed with PBS (Sigma-Aldrich, D8662) twice. Trypsin-EDTA (Sigma-Aldrich, T4174) was added to the flasks (0.5ml/T75) for 5 minutes at 37°C. Two volumes of medium were added to stop trypsin reaction and cells were collected in a 15ml tube and centrifuged at 1000g for 5 minutes. Supernatant was removed and pellet was re-suspended in 1ml medium.

At this stage cells were counted if needed to set up experiments otherwise they were replated in T75 flasks (ratio 1:5). Cell stocks were prepared by trypsinizing cells as described above and then re-suspending the pellet in 1ml of freezing medium (95% HEK293 medium and 5% DMSO (ChemCruz, 67-68-5)) instead of normal HEK293 medium, and transferred into a cryovial (Sigma-Aldrich, V7884). Cryovials were placed in a freezing container (Sigma-Aldrich, BCS-405) and stored at -80^{o}C to freeze down gradually before being transferred to liquid nitrogen for long-term storage.

2.12.2 Culture of H295R cell line

Cells were seeded at 1-1.5x10^{5}cells/cm^{2} in DMEM/F-12 HAM (1:1) + GlutaMAX (Gibco, 31331-028) supplemented with 2.5% NuSerum (Scientific lab, 355100), 1% Insulin-Transferrin-Selenium (Scientific lab, 354352) and 1% Penicillin-streptomycin. Cells were passaged when they reached 80-90% confluency. To split cells medium was initially removed and cells were washed with PBS twice. Trypsin was added to the flasks (0.5ml/T75) for 5 minutes at 37^{o}C. Two volumes of medium were added to stop the reaction and cells were collected in a 15ml tube and centrifuged at 1000g for 5 minutes. Supernatant was removed and pellet was re-suspended in 1ml medium. At this stage cells were counted if needed to set up experiments otherwise they were re-plated in T75 flasks (ratio 1:3). Cell stocks were prepared by trypsinizing cells as described above and then re-suspending pellet in freezing medium [95% H295R medium (+7.5% NuSerum) + 5% DMSO] and transferred into cryovials. Cryovials were placed in a freezing container and stored at -80^{o}C to freeze down gradually before being transferred to liquid nitrogen for long-term store.

2.12.3 H295R spheroid formation

H295R cells were plated at 4-5x10^{3} cells per well in ultra-low attachment 6 well plates (Corning, CLS3471-24EA) in spheroid medium (DMEM/Nutrient Mixture F-12 Ham (Sigma-Aldrich, D8062) supplemented with recombinant human basic fibroblast growth factor (20 ng/mL) (Sigma-Aldrich, HBFGF-RO), B-27 (ThermoFisher Scientific, 0080085-SA), N-2 supplements (ThermoFisher Scientific, 17502-048), and recombinant human epidermal growth factor (20 ng/mL) (Sigma-Aldrich, E9644)).

Medium was added twice a week and cells were passaged at two weeks. Briefly medium was collected in a 15ml Falcon tube and allowed to stand for 30 minutes for the spheroids to form a pellet at the bottom due to gravity. Supernatant was then removed and 2 drops of trypsin were added to dissociate cell clusters for 2-3 minutes. Then 1ml of medium was added to re-suspend the pellet. Cells were counted using a Neubauer improved hemocytometer (Sigma-Aldrich, BR717805) and re-plated in a new ultra-low adherence 6 well plate at 4-5x10^3 cells per well.

2.12.4 Generation of DLK1 over-expressing H295R cell line

2.12.4.1 Vector preparation

Primers to amplify human *DLK1* gene were designed and ordered from Sigma Aldrich to be used for cloning the gene into pCMVHA (Appendix II) and pCMVTag4 vectors (Appendix III)(Table 2.10). PCR amplification was performed using human adrenal cDNA as a template. General PCR cycle was used with an initial 2 minute hot start, followed by 35 cycles of 94°C for 30 seconds, 52°C for 30 seconds, 68°C for 90 seconds with final extension at 68°C for 10 minutes. PCR products were then run on a 1-1.5% agarose gel and bands corresponding to the gene of interest were extracted using the QIAGEN Gel Extraction Kit (See Section 2.9.2). Following gel extraction both the vector and the insert were incubated with restriction enzymes (REs) (Table 2.10) for 1 hour at 37°C and treated with alkaline phosphatase for 30 minutes prior to ligation (Negative controls were incubated with ddH2O only). Following RE digestion samples were run on a gel and desired bands gel extracted for the ligation process. The linearized plasmid vector DNA and DNA fragment were mixed at a ratio of 1:4 in a total volume of 10µl with 1 volume of ligase also added using the Takara DNA ligation Kit, Version2.1 (6022). Solution was incubated at 16°C for 1 hour. For transformation 100µl of supercompetent bacteria were added to the ligation reaction and incubated on ice for 30 minutes followed by 2-minute incubation at 42°C and further 2-minute incubation on ice. Then they were incubated for 1 hour at 37°C, plated on ampicillin plates and allowed to form colonies overnight at 37°C. Colonies from the overnight bacterial incubation were collected for a mini-prep (See Section 2.9.4) to test whether they contain the correct vector+insert, by cutting with the same REs that

were used for cloning. If the colony has taken up the vector with the insert then that colony will be used for the midi-prep (See Section 2.9.5) to collect high concentration of DNA.

Table 2.10 – Primer sequences and Restriction enzymes used for cloning

Vector	Primer Sequence	Restriction Enzymes
pCMVHA	FW-cggaattcagATGACCGCGACCGAAGCC	EcoRI
	RW-ccgctcgagTTAGATCTCCTCGTCGCC	XhoI
pCMVTag4	FW-cgcggatccACCATGTACCCATACGATG	BamHI
	RW- ccgctcgagGATCTCCTCGTCGCCGGC	XhoI
pHIV-EGFP	FW-gctctagaACCATGTACCCATACGAT	XbaI
	RW-cgcggatccCTACTTATCGTCGTCATCCTT	BamHI

2.12.4.2 Lentiviral preparation

To obtain lentiviral particles, the insert (HA-DLK1-FLAG) previously prepared (Section 2.12.4.1) was cloned into a pHIV-EGFP (Appendix IV) (Table 2.10). Then HEK293T cells were plated in separate 100mm dishes at a density of $3x10^6$ cells/dish and cells were transfected once they reached 70-80% confluency. One hour before transfection complete medium was changed to serum-free medium. Transfection samples were prepared by mixing 10µg of pHIV-EGFP with 3.2µg of psPAX2 (Addgene, 12260) and 1.8µg of pMD2.G (Addgene, 12259) (packaging and envelope expressing plasmids), as well as 100µl polyethylenimine (PEI) agent in 1ml serum-free medium/well. Samples were vortexed and incubated at room temperature for 10 minutes before being added to each dish dropwise. Medium was changed to complete medium 2 hours later. (Lentivirus containing empty vector was also used as a control). Medium from transfected cells was collected 24 and 48 hours later and kept in a 50ml Falcon tube. Following both collection time-points, medium collected was centrifuged at 50,000g (25,000rpm) in a Beckman Coulter Optima XL-70 Ultracentrifuge, for 2 hours at 16°C and pellet was re-suspended in 150µl of sterile PBS. This was then aliquoted and kept at -80°C until it was used.

2.12.4.3 Lentiviral infection of the H295R cell line

H295R cells were plated in a 6 well plate at a seeding density of $3x10^5$. Once they reached 80% confluency they were infected with the lentiviral particles prepared above and polybrene at 8µg/ml (Merck Millipore, TR-1003-G). Twelve hours later the medium was changed to complete H295R medium and 2 days later cells were checked for GFP expression indicating success of infection. GFP positive cells were sorted using the fluorescence activated cell sorter machine (FACS Calibur) and GFP positive cells were expanded. In addition cells were also infected with an empty vector as a negative control.

2.12.5 Cell preparation for fluorescence activated cell sorting (FACS)

Cells were initially trypsinized and collected in 1ml of medium. Cells were then counted using a hemocytometer and appropriate volumes (cell numbers) were separated to different tubes for subsequent staining ($5x10^5$ for the isotype control and at least $1x10^7$ for DLK1 antibody staining). Once separated, falcons were centrifuged at 1000rpm for 5 mins, re-suspended in 500µl of FACS Buffer (1.5% bovine serum albumin (Sigma-Aldrich, A2058), 5% FBS and 1% penicillin-streptomycin) and transferred to a new eppendorf. Cells were washed in FACS buffer twice, by aspirating supernatant, re-suspending in FACS buffer and centrifuging. Following washes, DLK1 conjugate and isotype control antibodies were added at a volume of 5µl for every $1x10^6$cells and added to the respective eppendorfs. DAPI was also added at 1µg/ml to stain live cells. Cells were incubated for 30 minutes on ice and vortexed at 10 minute intervals. Following incubation, cells were washed 3 times in FACS buffer and following final wash cells were resuspended in at least 500µl (1ml for every $1x10^6$cells) of FACS buffer and transferred into FACS tubes to be sorted. Following FAC-sorting, cells were collected for qPCR analysis or re-plated for further *in vitro* experiments.

2.12.6 Cell Survival Assays

Cells were plated in a 96 well plate at $4x10^3$ cells per well. Once they reached 70-80% confluency they were treated with chemotherapeutic drugs, mitotane (Sigma-Aldrich, 53-19-0), doxorubicin (Sigma-Aldrich, D2975000), cisplatin (Sigma-Aldrich,

C2210000), 5-Flurouracil (Sigma-Aldrich, F0250000)(Table 2.11) for 72 hours. Drugs were dissolved in DMSO or ethanol. Control wells included untreated cells and wells with medium or vehicle only (no cells). Following 72-hour drug treatment, 10µl of cell counting 8 solution (CC8, Sigma-Aldrich, 96992) were added in each well and plates were incubated for 1-2 hours or until a colour change was observed. Plate was read on a Multiskan FC Microplate Photometer (Thermo Scientific, 51119000) at a wavelength of 450nm. Percentage of cell survival for each drug concentration group was calculated by initially subtracting the average reading of medium- or vehicle-only wells from the reading of all other groups and then converting the new readings (after subtraction) of the concentration groups as a percentage of the untreated control (which was normalized to 100%). Graphs were plotted as % cell survival to log concentration of the drugs and LD_{50} for each drug was determined.

Table 2.11 – Drug concentrations for Cell survival Assays

Chemotherapeutic drug	Concentrations used, µM
Mitotane	5, 10, 15, 20, 22.5, 25, 30, 35, 40, 45
Doxorubicin	0.5, 1, 1.5, 2, 3, 4, 5, 6, 6.5, 7
Cisplatin	5, 10, 20, 25, 30, 40, 50, 60
5-Flurouracil	10, 30, 40, 60, 70, 100, 120

2.12.7 Drug treatment for flow cytometry analysis of H295R cells

H295R cells were plated in a 6 well plate at $0.3x10^6$ cells/well. Once they reached 70-80% confluency they were treated with chemotherapeutic drugs for 24 hours (short term) or 1 week (long term). Mitotane treatment was performed at 30µM (short term) and 15µM (long term), doxorubicin at 2µM (short term) and 1µM (long term), and 5-Flurouracil at 40µM (long term). Drugs were dissolved in DMSO or ethanol. Wells with untreated cells were used as a negative control. Following short or long term treatment cells were collected for flow cytometry analysis and stained with DLK1 conjugate or isotype control as described in Section 2.12.5. Flow cytometry analysis was performed using the BD LSRFortessa to determine the percentage of DLK1+ cells in the samples to be tested.

2.12.8 Cell proliferation assay

Initially, known numbers of H295R cells, ranging from 0-1.5x10^5 cells, were plated in separate wells in a 96 well plate, to produce a standard curve for cell proliferation experiments. Half a day after plating, cells were treated with cell counting 8 solution for an hour and OD value was measured on Multiskan FC Microplate Photometer. To create a standard curve, the OD value for each well was plotted against the known number of cells it corresponded to and an equation for the line of best fit was produced. This was used to determine unknown cell numbers in the cell proliferation assays performed. DLK1+ and DLK1- FAC-sorted H295R cells were immediately plated in 96 well-plates at a density of 3x10^3 cells/well. Cells were plated in triplicate. Each day different wells were treated with cell counting 8 solution for 1 hour and OD value was measured using a Multiskan FC Microplate Photometer. Line equation was used to derive the number of cells for each OD value measured. This was done for 7 days and a graph of cell numbers against time (Days) was plotted for each cell population (DLK1+ and DLK1-).

2.12.9 Colony formation assay

DLK1+ and DLK1- FAC-sorted H295R cells were immediately plated in 6 well-plates at a density of 3x10^3 cells/well. These were cultured for 3 weeks, after which the number of colonies in each plate was counted manually.

2.12.10 Immunocytochemistry

Cells were washed two times in PBS and fixed in 4%PFA for 15 minutes on ice. Following fixation cells were washed again with PBS 3 times for 10 minutes each and blocked with 10% goat serum in PBS-Triton for 1 hour at room temperature. Then they were incubated with primary antibody (Table 2.1) diluted in PBS-Triton overnight at room temperature. The next day cells were washed with PBS-Triton 3 times for 10 minutes and incubated with secondary antibody at a 1:1000 dilution (Table 2.2) for 2 hours at room temperature. Cells were washed again with PBS and incubated with DAPI for 1 minute, after which they were washed with PBS and viewed under the inverted microscope.

2.13 RNA Extraction

RNA from tissue or cell samples was extracted using the Qiagen RNeasy Mini Kit (Qiagen, 74106). Initially, 350µl or 600µl of buffer RLT were added to either cell or tissue samples respectively, after which the samples were scraped and collected in an eppendorf tube. If tissue samples were used, lysates were centrifuged for 3 minutes at high speed and supernatant was removed before adding 1 volume of 70% ethanol. If cell samples were used, 1 volume of 70% ethanol was added directly without centrifugation. Then 700µl of sample were transferred to an RNeasy Mini spin column in a 2ml collection tube and centrifuged for 15 seconds at 8000xg. After centrifugation 700µl buffer RW1 were added to each sample and centrifuged for 15 seconds at 8000xg. At this point samples were treated with RNase free DNase set (Qiagen, 79254). 10µl of DNase I and 70µl of RDD buffer were added to each sample and incubated for 15 minutes at room temperature. Following this treatment samples were washed with 700µl buffer RW1 for 15 seconds at 8000xg. Then 500µl buffer RPE were added to each sample in the columns and centrifuged for 2 minutes at 8000xg discarding the flow through. Columns were then transferred to a clean eppendorf tube and RNA was eluted by addition of 30µl RNase/DNase free water and RNA concentration was measured using a nanodrop.

2.14 RNA to cDNA conversion

For RNA to cDNA conversion, 1µg of RNA was used. The appropriate volume of RNA (to make 1µg) was mixed with 1µl/µg random primers (New England Biolabs, S1330S) and made up to 15µl total volume by addition of RNase/DNase free water. Samples were incubated at 70^{o}C for 5 minutes in a PCR machine. Following incubation 2µl of 10x M-MLV reaction buffer, 1µl 10mM dNTPs, 1µl M-MLV Reverse transcriptase (New England Biolabs, M0253S) and 1µl RNase inhibitor (New England Biolabs, M0314S) were added per sample and placed in a PCR machine. Retro-transcription cycle included 25-minute incubation at 25^{o}C, 90 minutes at 42^{o}C and 15 minutes at 70^{o}C. The cDNA was then stored at -20^{o}C until use.

2.15 Quantitative real time PCR (RT-qPCR)

For gene expression measurements cDNA (1µl) was used as template for quantitative real time PCR using a SYBR Green PCR Master Mix (Invitrogen, 4309155). A 1X reaction was made up of 1µl template, 5µl SYBR Green, 0.5µl forward and 0.5µl reverse primers, 3µl H_20. Each sample was amplified in triplicates. The reaction was initiated at 55 °C for 2 min followed by the activation and pre-denaturation step at 95 °C for 10 min. The run was made up of 40 cycles of 15s at 95 °C and 1 min at 60 °C. Following RT-qPCR, mRNA levels were measured using the ΔΔCt method, where GAPDH was used as the endogenous control gene for normalisation.

2.16 Protein Extraction

For protein extraction cells were plated in 6 well plates at a density of $3x10^5$ cells/ well. Once the cells reached 80% confluency they were used for protein extraction. Initially cells were washed with PBS two times and 200µl RIPA buffer (Sigma-Aldrich, R0278) with protease inhibitor (Roche, 04693159001) were added in each well. Cells were scraped off, collected in an eppendorf and incubated on ice for 20 minutes. Following incubation, they were centrifuged at high speed for 10 minutes, supernatant was collected and heated for 5 minutes at 95^{o}C. Finally, 1 volume of 2xLaemmli Buffer (Sigma-Aldrich, S3401-1VL) was added and samples were either used directly for further analysis or stored at -20^{o}C.

2.17 Western Blot Analysis

Both the resolving and the stacking gels were prepared manually and allowed to set (Table 2.12 and 2.13, respectively). Once the gels were prepared, 25µl to 40µl of each sample (described in section 2.16) were added per well along with a 3.5µl of a PageRuler Plus prestained protein ladder (ThermoScientific, 26619). Gels were placed in the tank filled with 1X running buffer [prepared from 10X stock including 10g sodium dodecyl sulfate (Sigma-Aldrich, L3771), 30.3g TRIS-Base (Fisher, BP152-5) and 144g glycine (VWR, 444495D) dissolved in 1L ddH2O] and allowed to run at 200V/400mA for 45-60 minutes. Proteins were then transferred on a nitrocellulose blotting membrane (GE Healthcare, 10600002). Gels along with the nitrocellulose blotting membrane and blotting paper (Bio-Rad, 1703965) were dipped in 1X transfer

buffer (prepared from 10X stock including 30g TRIS-Base and 144g glycine dissolved in 1L ddH2O), placed on the transfer machine and run at 15V/0.8A for 45 minutes (1gel) or 1 hour (2 gels). After the transfer, the nitrocellulose blotting membranes were soaked in ponceau red staining (0.1% ponceau S (VWR, IC19064410), 5% acetic acid (Fisher Scientific, 64-19-7) in ddH2O) to visualise the protein bands and then washed under running ddH2O. Membranes were incubated for 1 hour in 5% milk powder dissolved in PBS-Tween, after which they were washed with PBS-Tween 2 times for 10 minutes and incubated overnight with the primary antibodies diluted in blocking buffer at room temperature (Table 2.14). The next day membranes were washed 2 times with PBS-Tween for 10 minutes and incubated with secondary antibodies (Table 2.15) diluted in PBS-Tween for 1 hour at room temperature in the dark. Following incubation with secondary antibody the membranes were washed with PBS-Tween 2 times for 10 minutes and then viewed using Licor Odyssey Infrared Imager.

Table 2.12 – 10% Resolving gel preparation

Reagents	**Volume**
Acrylamide	6.7 ml
ddH_2O	8.3 ml
Resolving Buffer	5 ml
APS (Sigma-Aldrich, A3678)	150 µl
Temed (Sigma-Aldrich, T9281)	30 µl

Table 2.13 – Stacking gel preparation

Reagents	**Volume**
Acrylamide	800 µl
ddH_2O	3.8 ml
Stacking Buffer	325 µl
APS	50 µl
Temed	5 µl

Table 2.14 – Primary antibodies for Western Blot

Antibody	Species Reactivity	Host	Supplier	Catalogue Number	Dilution
HA	Human	Mouse	Sigma-Aldrich	H3663	1:1000
Flag	Human	Mouse	Sigma-Aldrich	F1804	1:1000
DLK1 (H-118)	Human/Mouse/Rat	Rabbit	Santa-Cruz	sc-25437	1:500
DLK1 (N-18)	Human	Goat	Santa-Cruz	Sc-8623	1:500

Table 2.15 – Secondary antibodies for Western Blot

Antibody	Supplier	Catalogue Number	Dilution
IRDye 680RD donkey anti-goat	LI-COR	926-68074	1:10000
IRDye 680RD goat anti-mouse	LI-COR	926-68070	1:10000
IRDye 680RD goat anti-rabbit	LI-COR	926-68071	1:10000
IRDye 800CW goat anti-rabbit	LI-COR	926-3211	1:10000

2.18 In vivo mouse work

2.18.1 Animal maintenance

All animal procedures were carried out in accordance to the regulations and recommendations provided in the Animals (Scientific procedures) Act 1986 of the UK Government (PPL:70/8597; PIL: IC636FF3C). Mice were maintained on a 12 hour light: dark cycle with constant access to water and food. $Axin2^{Cre:ERT2/+}$ mice and $Rosa^{YFP/YFP}$ mice were purchased from Jackson laboratories. These mice were crossed to produce $Axin2^{CreERT2/+}$;$Rosa^{YFP/YFP}$ mice for lineage tracing studies.

2.18.2 Genotyping

Litters following breeding of the two mouse lines, were genotyped between P10-P20. Tissue samples from the ears of the mice to be genotyped were collected at P10 for DNA extraction. This was performed by addition of 20µl of ddH_2O and 5µl of DNAreleasy solution (Anachem, LS02) into the Eppendorf tube containing the sample. DNA extraction of each sample was performed using a PCR machine. DNA extraction program included initial incubation at 95°C for 2 minutes, followed by 65°C for 1 hour, 96°C for 2 minutes, 65°C for 1 minute, 96°C for 30 seconds and final incubation at 72°C for 5 minutes. Samples were then used for further PCR analysis to identify which ones had the required $Axin2^{CreERT2/+}$; $Rosa^{YFP/YFP}$ genotype using 2 different PCR protocols (Cre PCR and Rosa26-YFP PCR). Specific primer sequences were designed to either recognize Cre gene transcript or differentiate between Wild type ($Rosa^{+/+}$), heterozygous ($Rosa^{YFP/+}$) and homozygous mutant ($Rosa^{YFP/YFP}$) Rosa locus (Table 2.16).

Table 2.16 – Primer sequences for genotyping

Primer name	Sequence
Cre A	GATGCAACGAGTGATGAGGTTCGC
Cre B	ACCCTGATCCTGGCAATTTCGGC
Rosa-Wt	GGAGCGGGAGAAATGGATATG
Rosa-Com	AAAGTCGCTCTGAGTTGTTAT
Rosa-Mut	AAGACCGCGAAGAGTTTGTC

For Cre PCR, a DNA master mix and an enzyme mix were prepared separately (Table 2.17). Initially 12µl of DNA master mix, 1µl of DNA sample and 1 drop of mineral oil were added in 0.5ml microcentrifuge tubes and placed in PCR machine. PCR program included initial denaturation step at 94°C for 2 minutes, followed by 1 minute at 85°C (at which point reaction was paused and 8µl of the enzyme mix were added), followed by 30 cycles of 94°C for 30 seconds, 63°C for 30 seconds and 72°C for 45 seconds; with a final step of 72°C for 5 minutes. Samples were then run on a 2% agarose gel at 120V for 40 minutes and PCR products were viewed using a UV Transilluminator (Uvitec). Samples from mice that have the Cre allele (Cre+) produced a single product at approximately 400bp while samples from mice that did not have the Cre allele (Cre-) produced no product. For the Rosa-YFP PCR, a single DNA master mix was prepared (Table 2.18) and tubes were placed in the PCR machine. PCR program included an initial denaturation step at 94°C for 3 minutes followed by 35 cycles of 94°C for 30 seconds, 58°C for 30 seconds and 72°C for 1 minute with a final step at 72°C for 2 minutes. Samples were then run on a 3% agarose gel at 120V for 40 minutes and PCR products were viewed using a UV Transilluminator. Positive YFP/YFP samples produced a single product of approximately 320bp while heterozygote YFP/+ samples produced two products of 320bp and 600bp. Wild type samples with no YFP expression produced a single product at 600bp. Negative controls were also used for both PCR containing Master Mix and water but no sample. Positive adult mice as well as some of the negative mice were embedded, sectioned and analysed by IHC as described in Sections 2.2-2.7.

Table 2.17 – Cre PCR Master Mix reagents per sample

Reagent	DNA mix/µl	Enzyme mix/µl
Taq polymerase Buffer	1.2	0.8
$MgCl_2$	0.72	0.48
CreA	1	-
CreB	1	-
dNTPs	-	0.16
Taq polymerase	-	0.16
ddH_2O	8.08	6.4
Sample DNA (added individually)	1.0	-
Total	13	8

Table 2.18 – Rosa-YFP PCR Master Mix reagents per sample

Reagent	Volume/µl
Taq polymerase Buffer	2.5
Rosa-WT	0.5
Rosa-Com	0.5
Rosa-Mut	0.5
dNTPs	0.5
Taq polymerase	0.125
ddH_2O	18.375
Sample DNA (added individually)	2.0
Total	25

2.18.3 Lineage tracing experiments in adult mice

Adult mice were injected with 0.2mg/g tamoxifen (Sigma-Aldrich, T5648) in 3 consecutive doses and then culled 2 weeks later for adrenal collection. Adult mice were genotyped as described in section 2.18.1 and only the ones with the desired

genotype were used for subsequent experiments, while some of the remaining were kept as negative controls.

2.19 Solutions

2.19.1 4% Paraformaldehyde solution (PFA)

Solution was prepared by dissolving 40g of PFA (Acros Organics, 416780010) in 1L ddH_2O in fume hood. Once dissolved 10 tablets of PBS (Oxoid, BR100) were added (1tablet per 100ml ddH_2O) and Sodium hydroxide (NaOH) pellets (Sigma-Aldrich, 221465) were added until solution was clear. This was aliquoted in 50ml tubes and stored at -20^oC until further use.

2.19.2 PBS Solution

PBS was prepared by dissolving 10 PBS tablets (Oxoid, BR100) in 1L dd H_2O. The solution was autoclaved before use. Following autoclaving 1ml of either Triton X-100 (Sigma-Aldrich, T8787) or Tween20 (Sigma-Aldrich, P9416) was added to 1L of autoclaved PBS to make up PBS-Triton or PBS-Tween, respectively.

2.19.3 DEPC-H_2O

To prepare DEPC-H_2O, 1ml of DEPC (Sigma-Aldrich, D5758) was added in 1L of ddH2O and incubated at 37^oC for 2-3 hours. Following incubation, solution was autoclaved. Finally, 1ml of either Triton X-100 or Tween20 was added to 1L of autoclaved DEPC H_2O to make up DEPC H_2O -Triton or DEPC H_2O-Tween, respectively.

2.19.4 DEPC-PBS

To prepare DEPC-PBS, normal PBS was prepared as in Section 2.19.2. Once tablets were fully dissolved, 1ml of DEPC was added in 1L of PBS solution and incubated at 37^oC for 2-3 hours. Following incubation, solution was autoclaved and then 1ml of either Triton X-100 or Tween20 was added to 1L of autoclaved DEPC-PBS to make up DEPC-PBS-Triton or DEPC-PBS-Tween, respectively.

2.19.5 Citrate Buffer

For antigen unmasking 1.05g of Citric acid monohydrate (Fisher Scientific, 10345410) was weighed and dissolved in 500ml ddH2O to make up 10mM Citrate buffer. Once dissolved the pH was adjusted to 6.0 following addition of NaOH.

2.19.6 LB Media preparation

For LB media preparation 25g of LB Broth (Sigma-Aldrich, L3022) were dissolved in 1L ddH_2O and autoclaved immediately.

2.19.7 LB Agar plate preparation with Ampicillin

For LB Agar plate preparation 25g of LB Broth (Sigma Aldrich, L3022) and 12g of LB Agar (Sigma Aldrich, A9915) were dissolved in 1L ddH_2O and autoclaved immediately. Once autoclaved solution was allowed to cool down before adding Ampicillin (Sigma Aldrich, A5354) at 100µg/ml. This was then poured into plates working close to a flame and allowed to set.

2.19.8 Proteinase K treatment

Proteinase K treatment included 5ml 0.5M EDTA pH8.0, 5ml TRIS pH 7.5, 40ml DEPC H2O and 50µl Tween.

2.19.9 Hybridization Buffer

50ml hybridization buffer were prepared by adding 25ml formamide (Sigma-Aldrich, F9035), 5ml 3M DEPC NaCl, 100µl 0.5M EDTA pH 8.0, 100µl 10%SDS, 2.5g 5% Dextran Sulfate (Sigma-Aldrich, D8906), 1ml Denhardt's 1X (Sigma Aldrich, D2532) and 125µl Salmon sperm DNA (Thermo Fisher, 15632-011).

2.19.10 Saturation solution

Saturation solution included Formamide, DEPC H2O and DEPC SCC 20X at a ratio of 2:1:1.

2.19.11 Maleic Acid Buffer

To prepare this buffer, 11.61g of Maleic Acid (Sigma-Aldrich, M0375) along with 8.7g of NaCl were dissolved in 1L ddH2O and the pH was adjusted to 7.5. Solution was autoclaved and 1% Tween was then added.

2.19.12 Tamoxifen preparation

For the injections 40g of Tamoxifen (Sigma-Aldrich, T5648) powder were dissolved in 1800µl Corn oil (Sigma-Aldrich,C8267) and 200µl of 100% pure Ethanol to make up 20mg/ml stock solution. The solution was vortexed and kept on the roller for at least 30 minutes before use. For adult mice 0.2mg tamoxifen were injected per gram of mouse body weight. Aliquots were stored at -20^{o}C.

Chapter 3: Appearance and characterisation of DLK1 Cell clusters in the human adrenal cortex

3.1 Introduction

Adrenal glands are vital endocrine organs composed of the capsule, adrenal cortex and adrenal medulla. The cortex is the largest part of the adrenal gland and is subdivided in at least three distinct zones responsible for synthesizing and secreting hormones and steroids. These hormones have significant effects on metabolic homeostasis, blood pressure regulation as well as other aspects involved in controlling normal development and homeostasis. It is therefore important that the process of hormone synthesis is tightly regulated, since dysregulation of this process may lead to adrenal insufficiency or tumour formation.

Through studies in rodents we have gained insight into adrenocortical zonation, homeostasis and maintenance, including the more recently identified ZU in rat adrenals[102]. The ZU of rats is located between the ZG and the ZF, with cells in that region expressing both Shh and Dlk1. Studies have confirmed the presence of stem cell populations in the adrenal capsule in rodents and have established a cross talk between Shh+ cells in the cortex and Gli1+ capsular cells during adrenal regeneration of cortical zones[8, 102]. Although multiple studies have uncovered important cell/stem cell populations and unveiled homeostatic mechanisms in rodents, little is known about what happens in the human adult adrenal gland. Most of what is known about human adrenocortical zonation revolves around enzymes involved in the synthesis and secretion of mineralocorticoids and glucocorticoids; the main function of the adrenal glands. As such we know that the various members of the cytochrome p450 family involved in steroid synthesis will be expressed in the adrenal gland in their respective adrenocortical zones, including *CYP11B1, CYP11B2, CYP11A1, CYP17* and *StAR* (as previously described in Section 1.1.2, Figure1.3). In addition, SF1 is known to be expressed in all steroidogenic cells of the adrenal cortex, while *SOAT1* and *DAX1* have been found to be expressed in some areas of the human adrenal cortex. However, additional studies in the human adrenal gland are required in order to provide a better understanding of human adrenocortical zonation and identify

genes/proteins that are expressed in adrenocortical cell populations.

In our study, we hypothesize that like rodents, a progenitor cell population also exists in the human adrenal cortex. Therefore the main aim of this chapter is to better characterize the subcapsular region of the human adrenal cortex and possibly identify a progenitor cell population in the human adrenal glands.

Tools available to use in order to mark and identify known cell populations include the use of antibodies targeting proteins solely expressed by specific types of cells in the adrenal gland. Two of these antibodies include those targeting the enzymes CYP11B1 and CYP11B2, the development of which has significantly improved human adrenal gland research. CYP11B1 and CYP11B2 represent the terminal enzymes in the synthesis of cortisol in the ZF and aldosterone in the ZG, respectively, and are the best markers to distinguish functional ZF and ZG in adrenal tissue sections. Given their high homology in amino acid sequence (93%) (Figure 3.1), it has been historically difficult to produce specific and reliable antibodies against the two proteins. Recently, two independent groups have successfully developed antibodies (polyclonal and monoclonal) targeting these proteins individually[9, 217]. Preparation of these antibodies is key to achieve the aim of the first part of the project, as it would allow us to accurately and efficiently mark cell populations in the human adrenal cortex expressing either CYP11B2 or CYP11B1. In addition, this would enable us to identify cell populations that express neither protein and thus might represent a novel cellular compartment within the adrenal cortex.

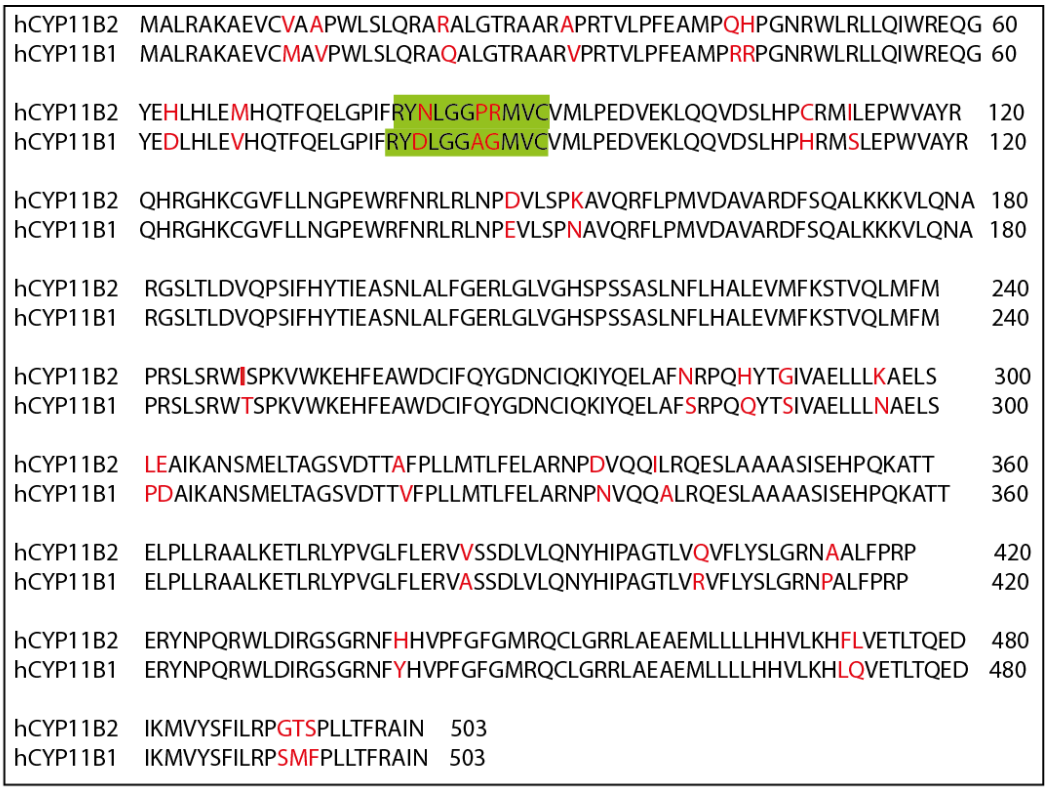

Figure 3.1 – Alignment of human CYP11B2 and CYP11B1 amino acid sequences. Protein sequences for hCYP11B2 (NCB1 accession: NP_000489.3) and hCYP11B1 (NCBI accession: NP_000488.3) were obtained and aligned on NCBI. Letters in black represent fully conserved residues between the two proteins, while residues in red represent the ones that are different between the two proteins. Highlighted residues in green show the ones used for immunisation to develop respective antibodies.

In addition, other enzymes involved in steroidogenesis, including CYP17, could represent useful tools in identifying and confirming the presence of specific adrenocortical cell populations. Multiple research studies have also identified Visinin-like protein 1 (VILIP1) and Disabled 2 (DAB2) as markers of the ZG in rodents[218, 219].

VILIP1 is a calcium-sensor protein encoded by *VSNL1.* It is involved in the regulation of intracellular calcium-dependent signalling pathway, including cAMP-, cGMP- and MAPK signalling[218, 220, 221]. Changes in intracellular calcium concentration by the mitochondria, has a number physiological and pathological effects on multiple organ systems including the ZG cells of the adrenal cortex[222-224]. Aldosterone secretion by the ZG can be modulated by a number of activators, including Angiotensin II, ACTH, potassium levels and intracellular calcium concentration [23, 24, 225]. In fact studies have shown that increased calcium concentration in the mitochondria positively correlates with the rate of aldosterone synthesis[221, 226, 227]. The link between VILIP1 – calcium regulation and calcium concentration – aldosterone synthesis, along with the fact that VILIP1 was found to be expressed in the ZG of rat and developing mouse adrenal glands, makes it an interesting factor to study in humans. In fact it was suggested that VILIP1 does not only represent ZG cells in the rat, but rather a mixed population of ZG and ZU cells [220]. DAB2 is a mitogen-responsive phosphoprotein, with a potential role as a tumour suppressor. Previous studies have demonstrated the presence of DAB2 in the ZG of rodents and more recently in normal human adrenals and suggested a link between DAB2 and CYP11B2 expression[219, 228]. These results are suggestive of a role of DAB2 in aldosterone biosynthesis, as well as DAB2 being a marker of ZG.

3.1.1 Hypothesis

We hypothesise that characterising the human adrenal cortex will provide a better understanding of human adrenal development, function, and tumorigenesis. Previous work in rodents has identified an ZU in the adrenal cortex and we hypothesise that an ZU might also exist in human adrenal glands.

3.1.2 Aims

1. Develop and test antibodies targeting human CYP11B1 and CYP11B2 to mark the human ZF and ZG, respectively.
2. Study the subcapsular region of the human adrenal cortex and identify potential cell populations that could represent the ZU, by co-staining of CYP11B2 with DLK1, DAB2, or VILIP1.
3. Investigate the expression pattern of DLK1 in the human adrenal cortex according to age and gender, using IHC staining.

3.2 Developing antibodies for zonal specific markers

For the purpose of our project we initially aimed at developing our own antibodies to target human CYP11B2 and CYP11B1 proteins expressed in the ZG and ZF, respectively. Antibodies were designed following the method used by Nishimoto *et al.,* [217]. Briefly, peptides corresponding to amino acid residues 80-90 of each protein (RYNLGGPRMVC for CYP11B2 and RYDLGGAGMVC for CYP11B1) were used for immunization (Figure 3.1). Peptide synthesis and injection in two rabbits, as well as sera collection and purification were done at Thermofisher. Extensive testing of various bleeds and purified fractions by Western Blot on cells transfected with vectors encoding CYP11B1 and CYP11B2 (Appendix I) and immunohistochemistry on human adrenal sections (with different antigen unmasking procedures) showed that the antibodies produced were not recognizing either protein. These experiments were always performed in parallel with monoclonal antibodies to CYP11B1 and CYP11B2, which were provided by our collaborator Prof. Gomez- Sanchez (University of Mississipi, USA). These antibodies show great specificity and successfully mark the ZG (CYP11B2) and ZF (CYP11B1) of the human adrenal cortex as shown in Figure 3.2b and also in previous reports [9]. Therefore, these antibodies were subsequently used for the current project.

Following CYP11B2 staining on human adrenals, we observed two different organization types of ZG cells in the subcapsular region; the classical layered-continuous, with large portions of subcapsular and adjacent rosettes uninterruptedly stained with CYP11B2 (Figure 3.2d), and random bigger clusters, known as aldosterone producing cell clusters, APCCs (Figure 3.2c)[187, 217]. In addition, when double-staining with either CYP11B1/CYP11B2 (Figure 3.2b) or CYP17/CYP11B2 (Figure 3.2a), we observe a clear area of cells that are negative for both ZG (CYP11B2) and ZF (CYP17/CYP11B1) markers (Figure 3.2a/b). Therefore, our results confirm the presence of a subpopulation of cells in the subcapsular region of the adrenal gland, which does not express any steroidogenic enzymes. This is also in line with our hypothesis that an undifferentiated zone exists in the human adrenal glands, since the identified subpopulation does not express differentiation markers and therefore, might consist of undifferentiated adrenocortical progenitor cells. The next step was

to characterize the subcapsular region of the adrenal cortex with the purpose of classifying these distinct cell clusters.

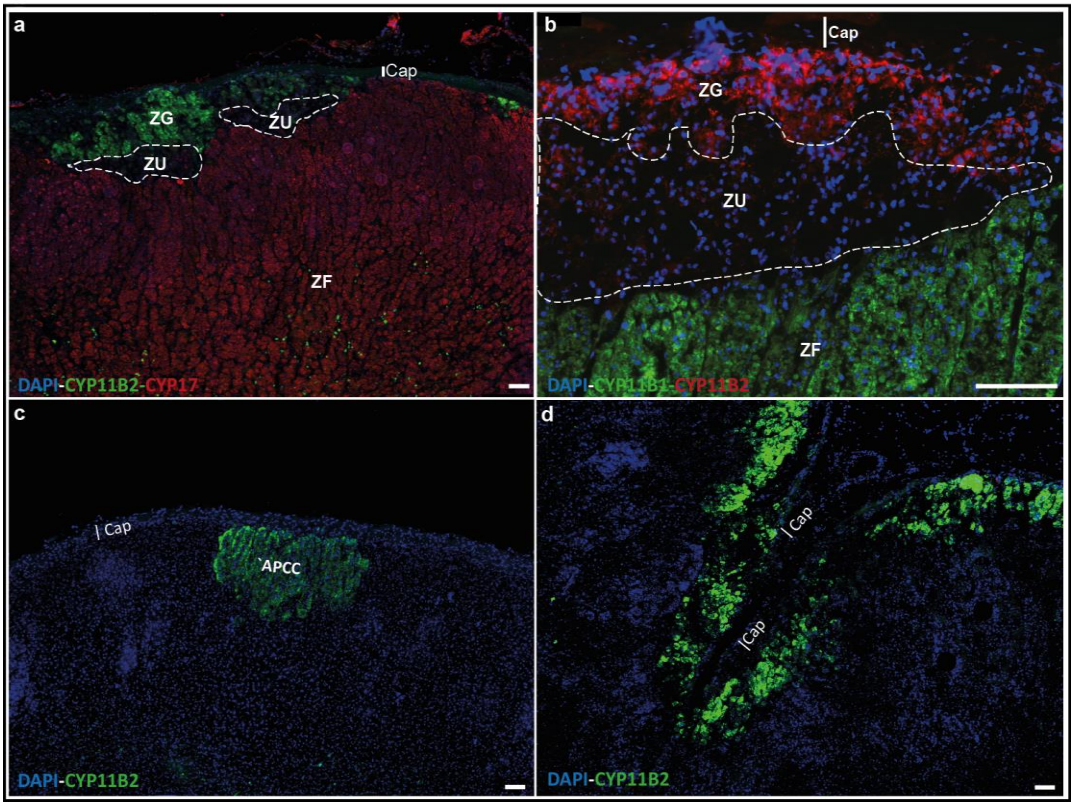

Figure 3.2 – Expression of zonal specific markers. Immunofluorescence analysis of zonation markers staining for ZG and ZF with either CYP11B2 and CYP17 (a) or CYP11B2 and CYP11B1 (b) on human adult adrenals (age range of samples analysed: 40-56 years old). Representative images of the samples are shown. Double negative area marked here as ZU appears in both (a) and (b). The bottom panels show the two different patterns of CYP11B2 expression appearing as either clustered cells/APCCs (c) or as a continuous layer of cells (d). n=3. Scale bars:100µm. Cap=Capsule; APCC=Aldosterone producing cell clusters.

3.3 Investigating the subcapsular region of the human adrenal cortex

3.3.1 Expression pattern of VILIP1 and DAB2 in the human adrenal cortex

Following immunohistochemical analysis for DAB2 and VILIP1 on normal human adrenal sections, we observed a layered-continuous expression of the two proteins in the subcapsular region of the adrenal gland (Figure 3.3). The two proteins were

selected as they were previously found to be expressed in the subcapsular/ZG region of rodents[219, 220, 229].

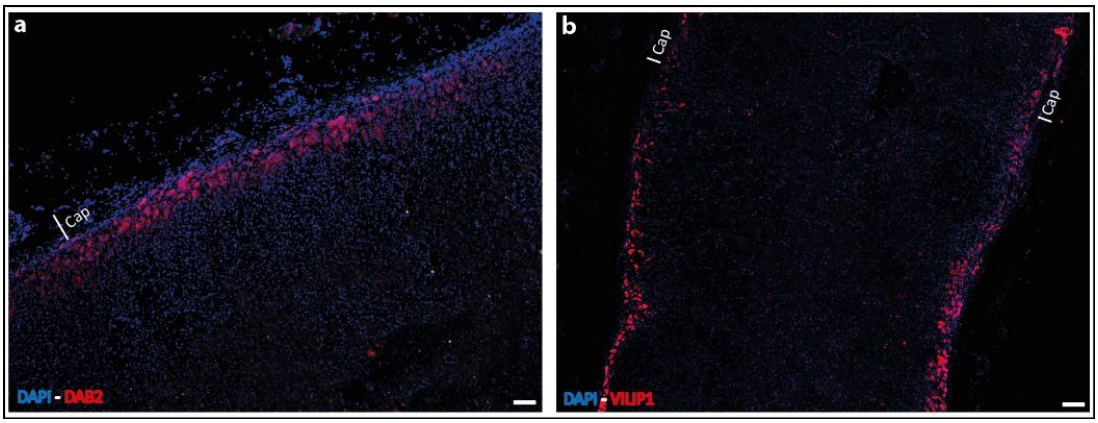

Figure 3.3 – Subcapsular localisation of DAB2 and VILIP1 in the human adrenal cortex. Immunofluorescence analysis of DAB2 (a) and VILIP1 (b) on human adrenal sections (age range of samples analysed: 40-56 years old) showing subcapsular expression of the two proteins. n=3. Scale bars: 100µm. Cap=capsule.

Double staining of DAB2 and CYP11B2 (Figure 3.4a-e), showed that all the cells that where positive for CYP11B2 were also DAB2 positive, however approximately 60% of DAB2+ cells were negative for CYP11B2 (Figure 3.4e). Finally, immunostaining for CYP11B2 and VILIP1 (Figure 3.4f-j), showed that most of the cells where either CYP11B2+ or VILIP1+ with only minimal co-localisation of the two proteins which accounted for approximately 10% and 25%, respectively (Figure 3.4j).

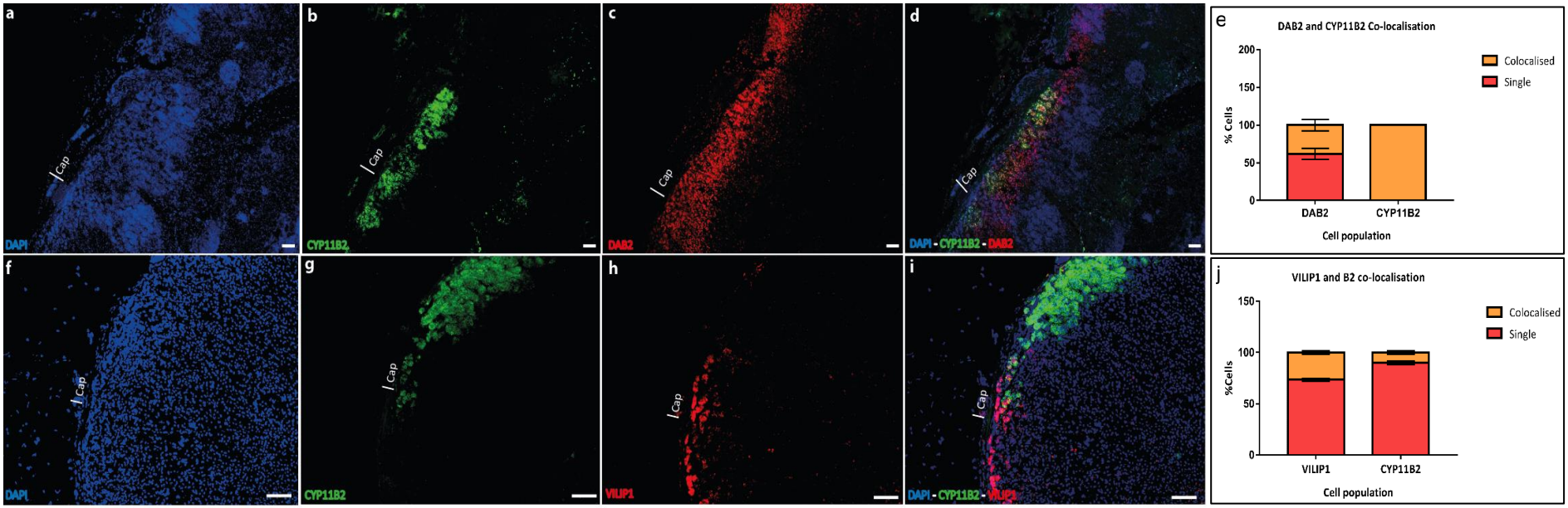

Figure 3.4 – CYP11B2 co-localisation with DAB2 and VILIP1. Double immunofluorescence analysis of CYP11B2 with DAB2 (a-d) and CYP11B2 with VILIP1 (f-i) on human adrenal glands (age range: 40-56 years old), showing full and partial co-localisation with CYP11B2, respectively. Graphs on the right, are showing the stained area (%) of either single or double positive cells immunostained with CYP11B2 and DAB2 (e) or CYP11B2 and VILIP1 (j). Error bars represent standard error of the mean. For each double staining, n=3. Scale bars: 100µm. Cap=capsule.

However, since both proteins (VILIP1 and DAB2) displayed continuous subcapsular expression with some co-localisation with CYP11B2, we assumed that cells expressing these proteins could not solely represent the undifferentiated (double negative) cell population observed in Section 3.2.

3.3.2 Appearance of DLK1 cell clusters

Given expression of DLK1 in the ZU of rat adrenal glands, we thought that it could be a promising candidate that could mark progenitor cells in the human adrenal gland[8].

Here we showed that *DLK1* was expressed in the subcapsular region of both human adult adrenals and human fetal adrenals (HFA) at the mRNA level (Figure 3.5). However, expression pattern of *DLK1* differs between adult and fetal adrenals. We observed a uniform and continuous subcapsular *DLK1* mRNA expression in the HFA in all embryonic stages investigated (10-33 weeks). In contrast, in the adult adrenal *DLK1* expression was mainly clustered and islets of *DLK1*+ cells were seen throughout the adrenal cortex (Figure 3.5a). This data was supported by IHC analysis for DLK1 on human adult adrenal glands, which also show that DLK1 was expressed in clusters throughout the cortex (Figure 3.6). Given the similarity in the expression pattern of DLK1 to that of CYP11B2, we performed a double immunofluorescent analysis to confirm whether the two proteins are expressed in the same cell populations. Results following double IHC, clearly show that the two proteins are in fact never co-expressed throughout the human adrenal cortex (Figure 3.6). Therefore, we have shown that clusters of DLK1 expression are not the same as APCCs and have termed these as DLK1 Cell clusters (DCCs).

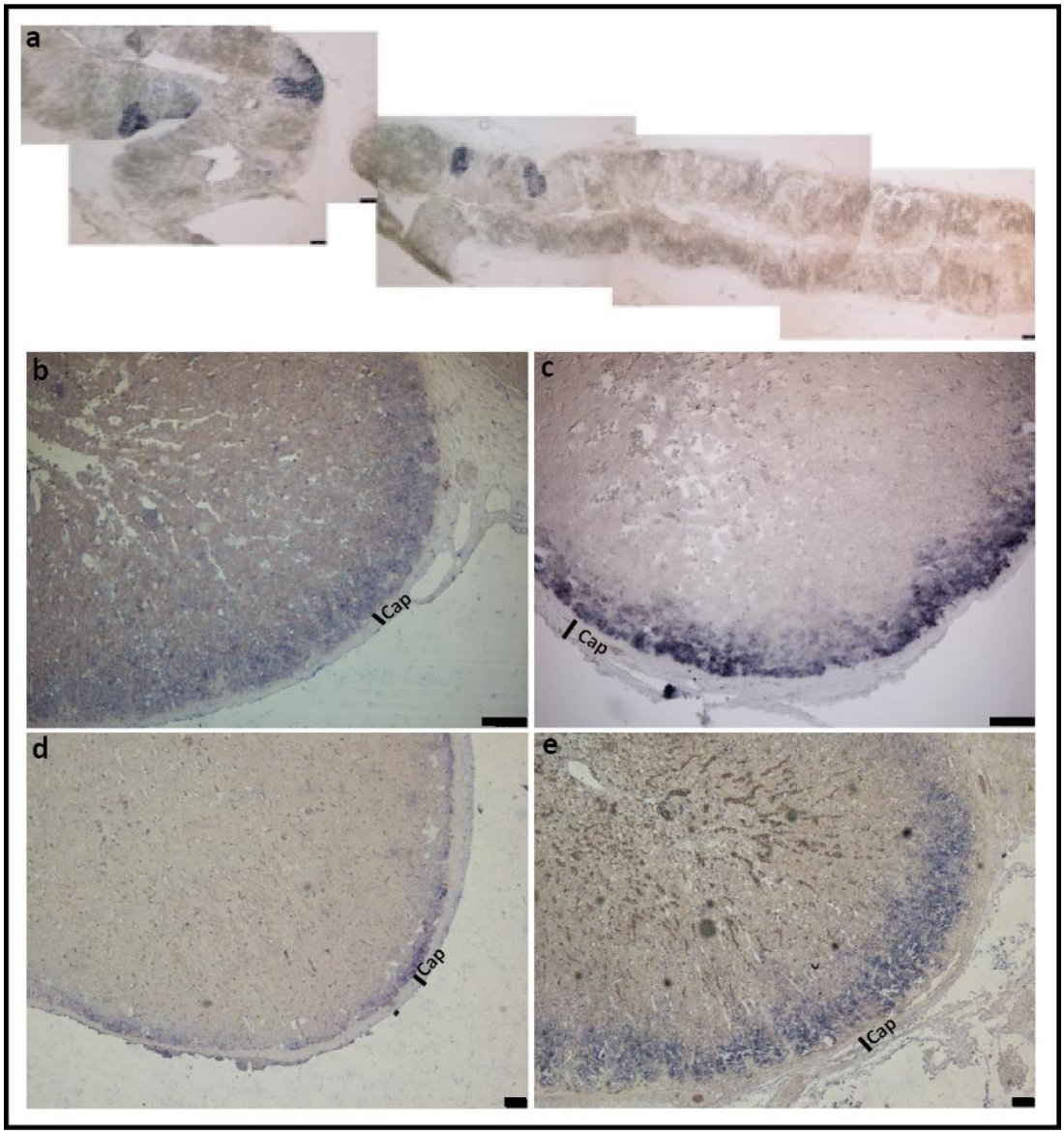

Figure 3.5 – *DLK1* localisation in the human and fetal adrenal cortex. Results following *in situ* hybridization targeting *DLK1* mRNA expression in the human adult adrenal (50 years old) (a) and the HFA at 10 weeks (b), 16 weeks (c), 20 weeks(d) and 33 weeks (e) of gestation showing subcapsular *DLK1* expression in both human adult and fetal adrenal, albeit with different expression patterns. n=3. Scale bars: 100µm. Cap=capsule.

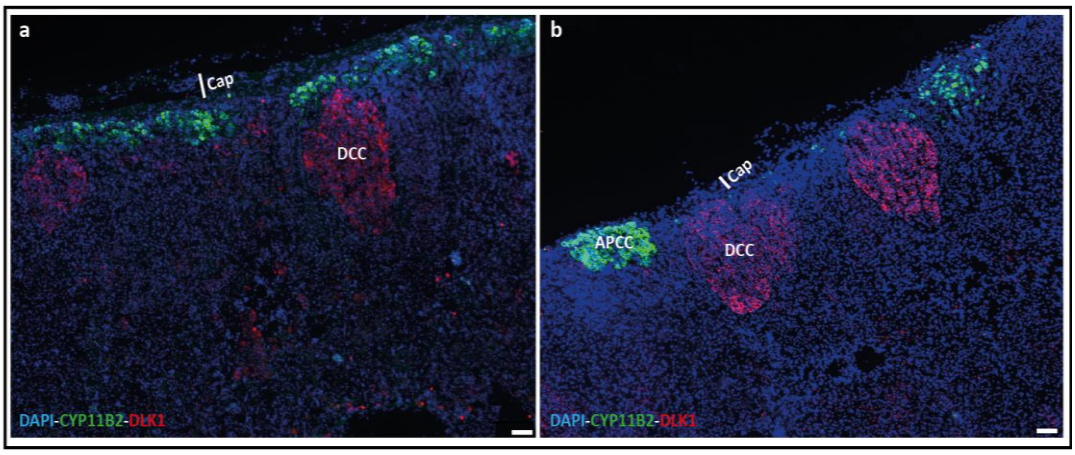

Figure 3.6 – DLK1 and CYP11B2 represent distinct cell populations in the adrenal cortex. Results following double immunofluorescent analysis for DLK1 and CYP11B2 (a,b) in human adult adrenals (age range: 40-56 years old) showing that the two proteins are never co-localised. n=3. Scale bar=100µm. Cap= Capsule; APCC=Aldosterone producing cell clusters; DCC=DLK1 cell clusters.

We next investigated the expression pattern of DLK1 across a number of normal human samples from donors of different ages (ranging from newborn babies to 70 year olds). For this purpose we collected a number of normal human adrenal samples from different biobanks. Following adrenal collection we wanted to investigate whether there are any differences in DLK1 expression between different samples based on age and gender. We used a total number of 23 adrenal glands and separated them into different age classes. We determined age classes based on two factors; the number of samples we had per age group and ages with known adrenal differences. For example one known adrenal difference is the change in CYP11B2 expression pattern in individuals with 40 or more years of age [230]. Details of the normal adrenal samples collected and the age group they belong to are shown in Table 3.1.

Table 3.1 – List of adrenal samples collected for analysis

Sample name	Gender	Age Group	Adrenal description	Cause of death/Reason for surgery	Biobank
33160413	Female	0-2	Normal	Pneumonia	IMIB
33160409	Male	0-2	Normal	Pulmonary haemorrhage	IMIB
33160407	Female	0-2	Normal	Macrosomia, aspiration of amniotic fluid	IMIB
33160411	Male	0-2	Normal	Diaphragmatic hernia	IMIB
15P3200885	Male	16-25	Normal	Arrhythmia secondary to congenital heart disease	IDIS
A2-C15016_049	Male	16-25	Normal	Cirrhosis	BioBANC
A2-C15016_057	Female	26-40	Normal	Retroperitoneal undiferenciated neoplasia	BioBANC
A2-C15016_060	Male	26-40	Normal	Renal carcinoma	BioBANC
A2-C15016_064	Male	26-40	Normal	Renal carcinoma	BioBANC
A2-C15016_065	Female	26-40	Normal	Pheochromocytoma	BioBANC
A2-C15016_050	Female	26-40	Normal	Surgery due to traumatism	BioBANC
A2-C15016_075	Male	41-50	Normal	N/A	BioBANC
A2-C15016_073	Male	41-50	Normal	Renal carcinoma	BioBANC
A2-C15016_072	Female	41-50	Normal	Neurofibroma	BioBANC
A2-C15016_066	Male	41-50	Normal	Cystic Kidney Disease	BioBANC

Sample name	Gender	Age Group	Adrenal description	Cause of death/Reason for surgery	Biobank
A2-C15016_085	Female	51-60	Normal	Renal carcinoma	BioBANC
A2-C15016_077	Male	51-60	Normal	Renal carcinoma	BioBANC
A2-C15016_076	Male	51-60	Normal	Myelolipoma	BioBANC
A2-C15016_089	Male	61-70	Normal	Renal carcinoma	BioBANC
A2-C15016_093	Male	61-70	Normal	Renal carcinoma	BioBANC
A2-C15016_090	Male	61-70	Normal	Renal pelvic urothelial carcinoma	BioBANC
A2-C15016_086	Male	61-70	Normal	Renal carcinoma	BioBANC
A2-C15016_094	Female	61-70	Normal	Acquired renal cystic disease and renal carcinoma	BioBANC

Following classification of the normal adrenal samples we performed IHC staining for DLK1 on each sample. We observed that staining with DLK1 resulted in two different expression patterns, a subcapsular continuous expression and a clustered expression (DCCs). We were also able to see a correlation between different expression patterns and age, with individuals of a younger age (Age group:0-2 and 16-25) having a continuous subcapsular DLK1 expression pattern (Figure 3.7a,b), while older individuals (Ages: 41-70) had a more clustered DLK1 expression pattern across the adrenal cortex, with some signs of a continuous pattern in some cases (Figure 3.7d-f). Finally, individuals belonging to age group 26-40 had a mixed pattern of mostly continuous DLK1 expression with some DCCs as well (Figure 3.7c, DCCs not shown), suggesting that DCCs start appearing between the age of 26 and 40.

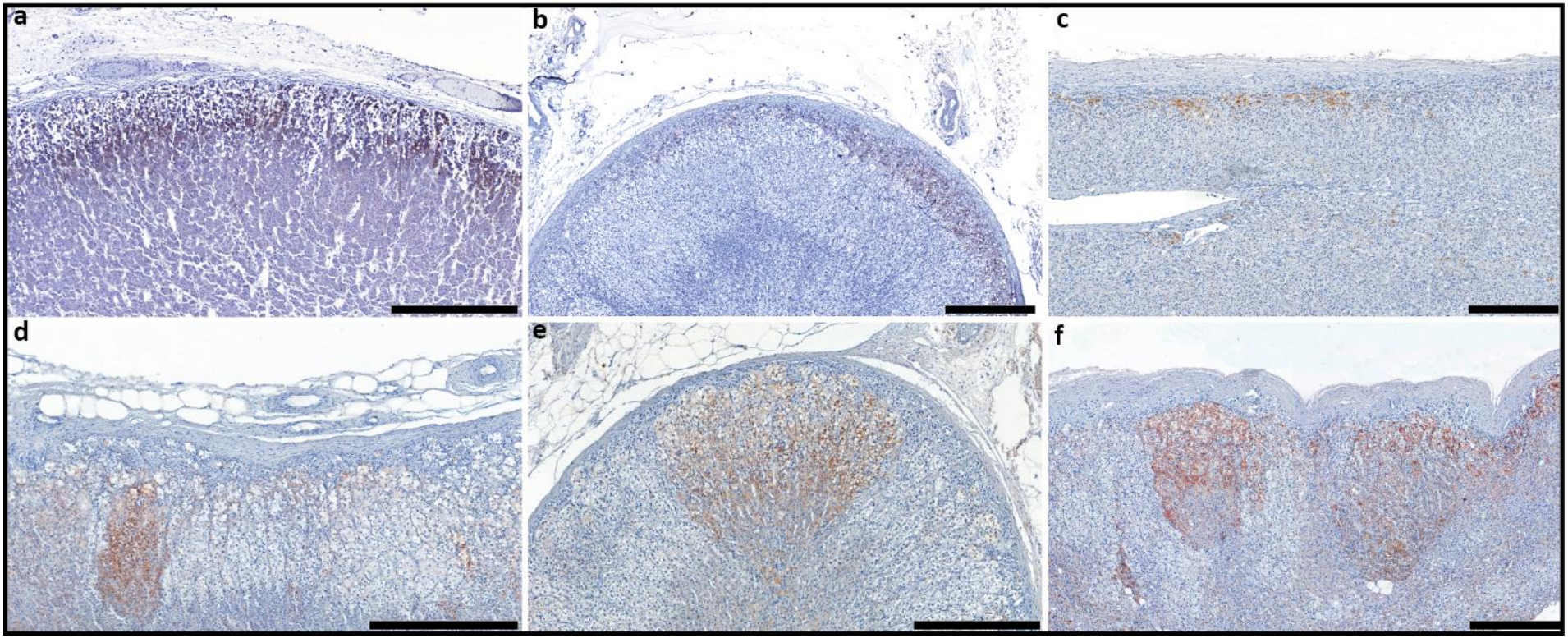

Figure 3.7 – DLK1 expression pattern changes with age. Results following IHC analysis for DLK1 expression in human adrenals of patients with different ages, showing a change in DLK1 expression pattern with increasing age, from a continuous to a patchy expression. Images above are representative of the cohort in their respective age group with (a) 0-2, (b) 16-25, (c) 26-40, (d) 41-50, (e) 51-60 and (f) 61-70 years old. For each age group n=2-5. Scale bars: 500µm.

Following our initial observation suggesting that the cortex remodels to generate DCCs as we age, we wanted to further analyse and confirm whether this change or transformation was significant, taking into consideration all the samples. This was done by comparing DLK1 staining, expression pattern changes and DCC size between all age groups. Initially, panoramic images of all samples stained with DLK1 were taken and further analysed either using panoramic viewer software or Halo image analysis software to determine DLK1 staining levels and size of DCCs. We initially measured the DLK1+ cells that are found in a continuous layer against those found in a clustered manner, using Halo image analysis software as shown in Figure 3.8. Briefly, we selected 10 random equal areas to be analysed per sample. Halo analysis would calculate the number of cells stained in each square and produce a report with the raw data. To interpret the data we determined whether cells that were counted were part of a cluster or continuous pattern and added the totals of those numbers to a table as shown in Figure 3.8. Finally, the total number of cells stained was calculated to determine the percentage of cells in continuous versus clustered pattern for each sample. For example, calculations showed that for Sample A2-C15016_057 (36 year old female) 82.6% of DLK1+ cells were arranged in a continuous manner, while the remaining 17.4% were arranged in clusters. The percentages corresponding to the remaining samples are summarised in Table 3.2 and presented in Figure 3.9.

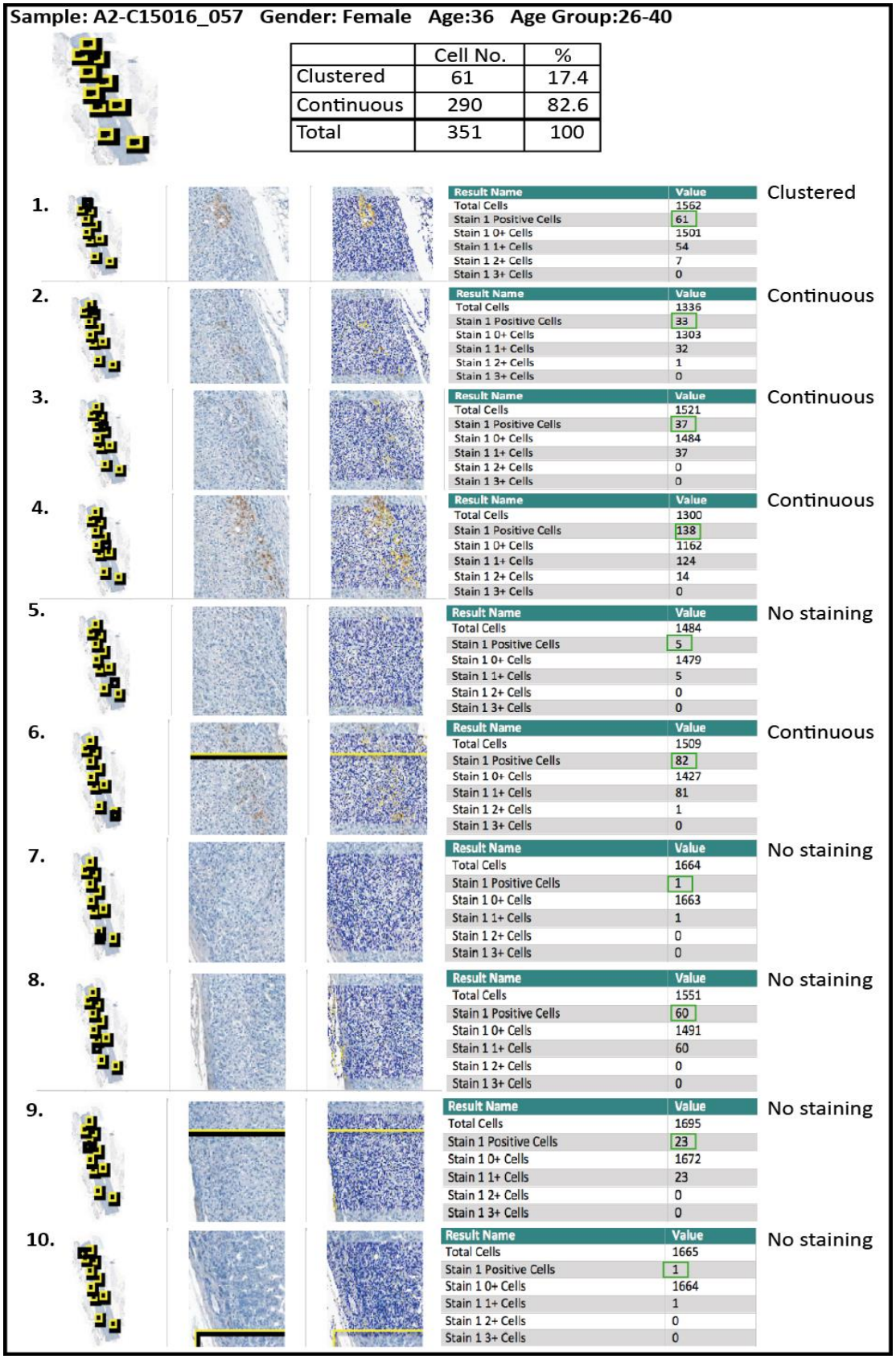

Figure 3.8 – Halo Image Analysis and Interpretation of sample A2-C15016_057. Figure showing results following Halo image analysis for one sample and the process used to interpret the results to determine %patchy and %continuous DLK1 expression.

Table 3.2 – Details of analysis of DLK1+ cells arranged in either clusters or continuous pattern in normal human adrenal samples.

Age Group	%DLK1 in clusters	%DLK1 continuous
0-2	0, 0, 0, 0	100, 100, 100, 100
3-15	N/A	N/A
16-25	0, 0	100, 100
26-40	69.8, 17.4, 0, 58.5, 71.2, 0	30.1, 82.6, 100, 41.5, 28.8, 100
41-50	100, 88.5, 66.6, 49.7	0, 11.5, 33.5, 50.3
51-60	100, 100, 73.7	0, 0, 26.3
61-70	100, 100, 93, 50.5, 76.3	0, 0, 7, 49.5, 23.7

Figure 3.9 shows a summary of the results following analysis, which confirms a strong correlation between clustered DLK1 expression and increased age. From the graph it is evident that younger age groups (Age:0-2 and Age:16-25) only show a continuous DLK1 expression pattern throughout the adrenal cortex, with the expression transforming to a clustered pattern in the older age groups. In age group 26-40 DCCs start appearing, accounting for a mean of 36% (ranging from 0-71% as shown in Table 3.2) of total DLK1 staining. A peak increase in DCC appearance was seen in the succeeding age group of 41-50 year olds, where an average of 70% (range of 50-100% shown in Table 3.2) DLK1+ cells were arranged in clusters. This increase was statistically significant when compared to the two youngest age groups of 0-2 and 16-25 years old. In the remaining age groups of 51-60 and 61-70 years of age, DCC appearance was significantly higher, compared to the three younger age groups of 0-2, 16-25 and 26-40 year olds, accounting for approximately 80-95% of total DLK1 staining (Table 3.2). In addition in some of the samples from donors of age between 41-70, the continuous pattern of DLK1 expression was completely lost and we could only observe DCCs throughout the adrenal cortex.

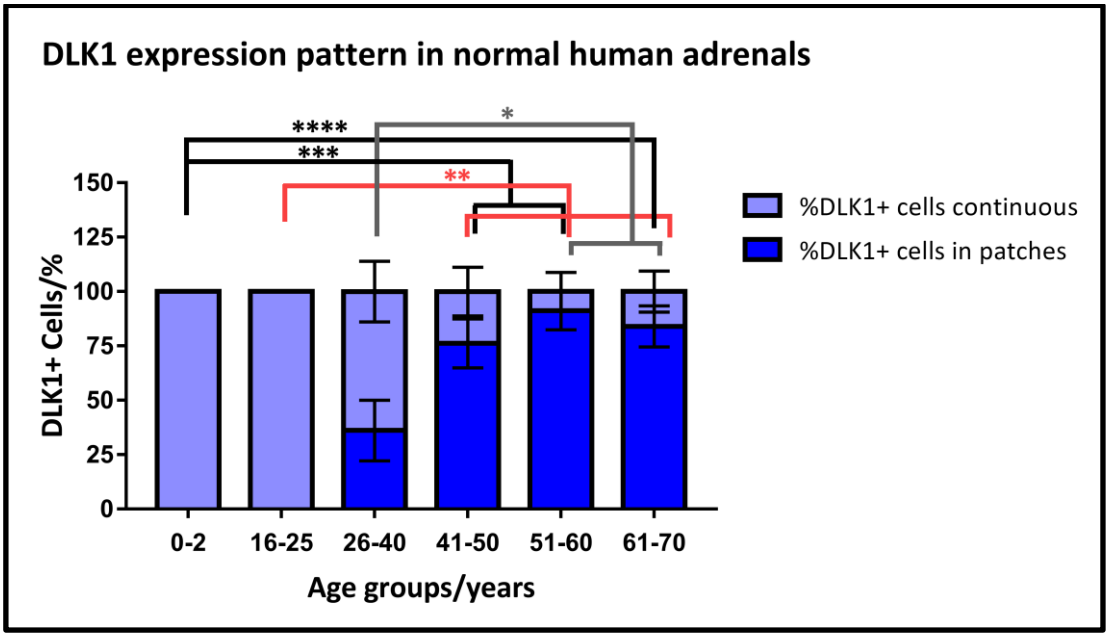

Figure 3.9 – DLK1 expression pattern changes with increasing age. Graph showing results following DLK1 expression analysis on human samples from donors of different ages. The above results highlight the appearance of DCCs at around 26-40 years of age. Most importantly these results show a significant increase in the percentage of DLK1+ cells appearing in clusters with increasing age, confirming that DLK1 expression pattern transforms from a layered continuous to a clustered expression with increasing age. Error bars represent standard error of the mean. Statistical analysis was performed using a two-way ANOVA on graphpad Prism and statistical significance is denoted as * ($p<0.05$), ** ($p<0.01$), *** ($p<0.001$) and **** ($p<0.0001$). For each age group n=2-5.

However, there was no observable difference in DCC appearance from 40 years onwards, neither in the % of DLK1+ cells appearing in clusters nor in the actual average number of DCCs appearing per adrenal gland (Figure 3.9 and Figure 3.10a). In addition, even though there are no DCCs appearing in age group 16-25 years old (as opposed to the older age groups), this was not statistically significant when comparing the number of DCCs to the older age groups. This is probably due to having a lower n number in the 16-25 year old group (n=2). I believe that is solely the reason, as in the case of age group 0-2 (higher n number), DCC number was significantly lower when compared to the older age groups of 41-70 years old (even

though the number of DCCs appearing in each adrenal in age group 0-2 is exactly the same as in 16-25). We then measured the area of DCC from each sample and plotted this against the age of individuals to which the DCCs belong to, as shown in Figure 3.10b. The dot plot in Figure 3.10b shows a significant positive correlation between DCC area and age, with a Pearson's correlation coefficient of r=0.5852, meaning that DCC area increases with increased age. Additionally, even though the DCC area increases with increasing age it seems that there is a trend that the overall DLK1+ area (clustered and continuous) decreases slightly with increasing age, however not significantly (Figure 3.10c).

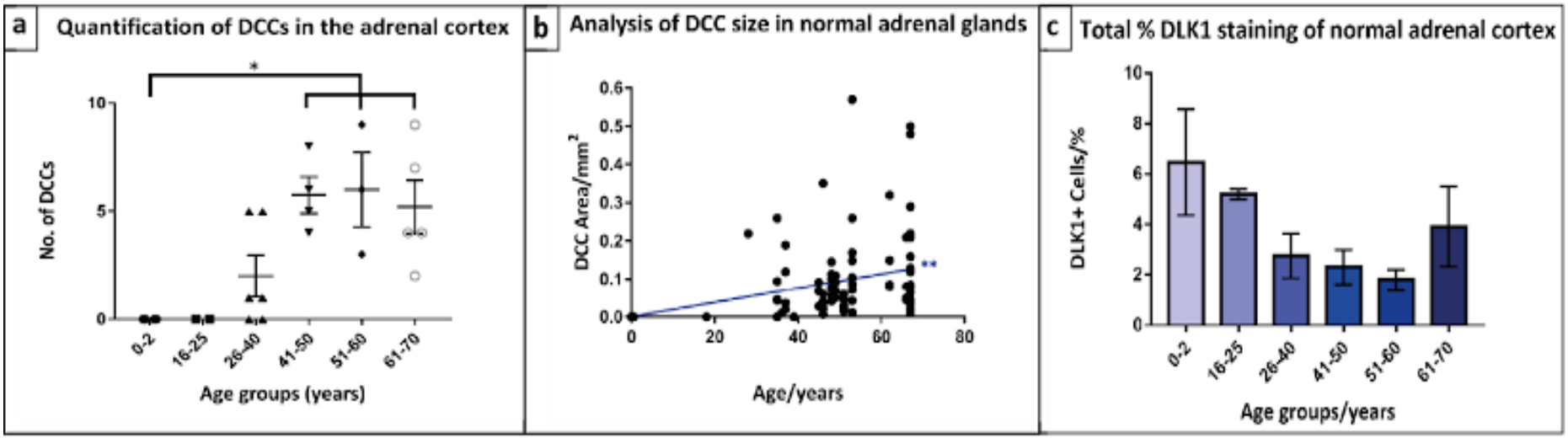

Figure 3.10 – DLK1 quantification in normal human adrenal cortex reveals differences between age groups. Figure showing results following quantitative analysis of the number of DCC appearance (a), DCC size (b) as well as percentage of total DLK1 staining (c) on normal human adrenal samples of varying ages. DCC size is shown in dotplot b, with each dot representing the area of one DCC measured, where more than one dot can correspond to the same sample. Error bars represent standard error of the mean. Statistical analysis was performed using one way anova (a), Pearson correlation test (b) and Kruskal Wallis test (c) where significance is denoted as * ($p<0.05$) and ** ($p<0.01$). For each age group n=2-5.

Finally, we examined whether there were any differences in gender within the different age groups with respect to DLK1 expression pattern. Instead of organising our samples in 6 different age groups, we now pooled some of the groups together and ended up comparing DLK1 expression pattern differences between males and females in 3 age groups (0-25$^{!}$, 26-40 and 41-70). The reason we pooled 0-2, 16-25 as 0-25 and 41-50, 51-60, 61-70 as 41-70 was to increase the n number for males and females within one group to make the analysis more accurate. Of note is that 0-25$^{!}$, only represents ages that fall between 0-2 and 16-25, but not ages between 3-15. We pooled those specific groups because as shown in Figure 3.9 there were no significant differences in DLK1 expression pattern between them (with respect to age). Therefore, we know that if we observe differences between males and females within the group it will be an accurate observation and difference of age will not have affected the results.

Following the comparative analysis between males and females within the age groups (Figure 3.11), there was no observable difference in DLK1 expression pattern between males and females in age groups 0-25$^{!}$ and 41-70. All adrenals in the former had a continuous-layered expression of DLK1 in all males and females tested, while in the latter an average of 79.6% DLK1+ cells in males and 93.6% DLK1+ cells in females, were arranged in clusters. In both cases, there was no stastistical difference between males and females. In age group 26-40 even though it seems that in females a lower percentage of DLK1+ cells is arranged in clusters (average of 8.7%) as compared to males (average of 50.04%), there was still no significant difference between the two following statistical analysis. Therefore, it seems that there are no differences in DLK1 expression pattern with respect to gender.

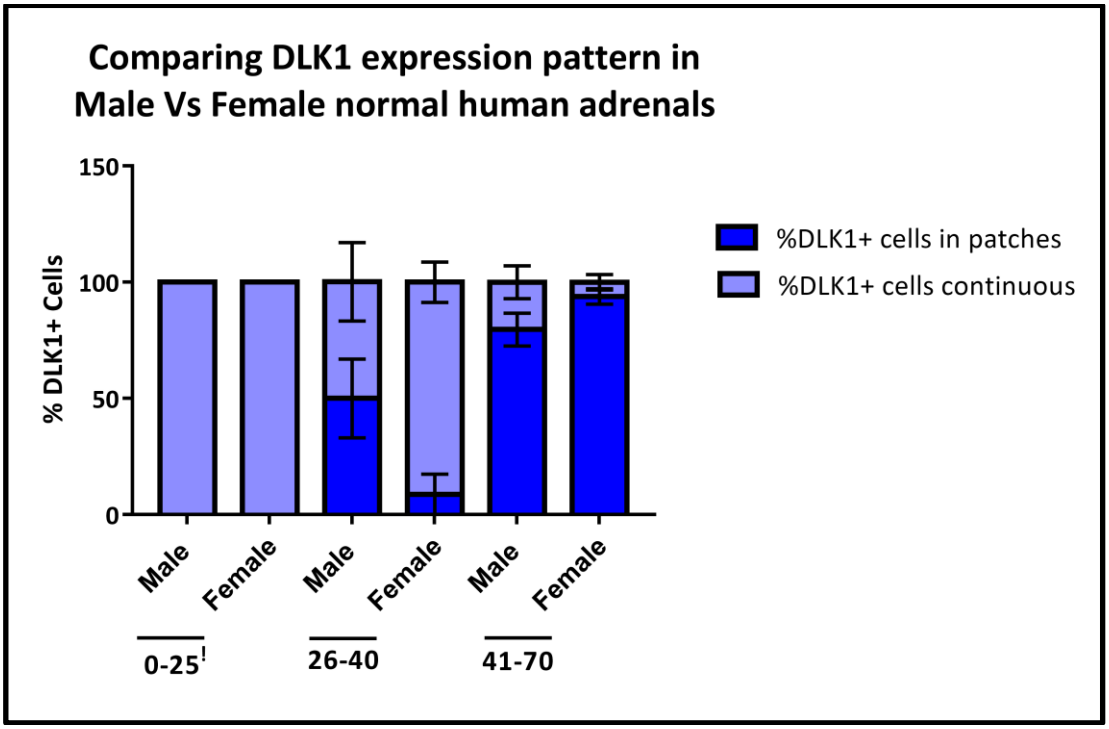

Figure 3.11 – Comparing DLK1 expression pattern between males and females in the same age group. Graph showing results following comparative analysis of DLK1 expression in males and females within the age groups (0-25!,26-40 and 41-70). The above results show that there seems to be a difference in DLK1 expression pattern, females bearing less patchy expression as compared to males, however the other two groups seem to have similar expression patterns between males and females. Error bars represent standard error of the mean. Statistical analysis was performed using an unpaired t-test on graphpad prism and showed no statistical significance. For each group n=2-9.

3.4 Discussion

In this first part of my project, I aimed to better characterise zonation in the human adrenal cortex. In doing so I have confirmed the presence of two staining patterns for CYP11B2 previously reported: the layered continuous as well as the clustered expression of CYP11B2 (APCCs) [187]. These clusters, but not adjacent adrenocortical cells, were previously found to harbour mutations that are commonly found in aldosterone producing adenomas (APAs) and therefore it was hypothesized that APCCs might represent precursors of APAs[187].

We have also shown that although both VILIP1 and DAB2 are expressed in the subcapsular ZG of the human adrenal cortex, only DAB2 is expressed in 100% of CYP11B2+ cells; with VILIP1 and CYP11B2 almost never being co-expressed. These results are in accordance with previous studies reporting the expression and role of these two proteins with respect to adrenal function in rodents. In the case of Vilip1, it could play an indirect role on aldosterone synthesis, in that it is involved in calcium regulation, which then has an effect on aldosterone synthesis, rather than regulating aldosterone synthesis directly. Additionally, previous studies have suggested that cells expressing Vilip1 could represent a mixed population of ZG and ZU cells in rodents, supporting our finding that VILIP1 and CYP11B2 are rarely co-expressed in the ZG, but are rather found in close proximity[220]. In the case of DAB2, we observed that all CYP11B2+ cells in the adrenal cortex are also positive for DAB2. This finding could suggest a direct role of DAB2 in aldosterone biosynthesis. Previous studies have also shown a positive correlation between the expression of the DAB2 and CYP11B2[219]. In a study looking at human adrenals with aldosterone producing adenomas it was shown that DAB2 expression was more heterogeneous as opposed to normal adrenals, with DAB2 overexpression significantly correlating to increased *CYP11B2* mRNA expression in these patients, thus further supporting our findings[228].

Most importantly, we have identified a new cell population within the human adrenal cortex, expressing the Notch atypical ligand DLK1. Similar to CYP11B2, DLK1 was

expressed in the subcapsular region of the human adrenal cortex, both in a layered continuous and/or clustered manner. However, although the two proteins had a similar expression pattern, they were never co-localised. Therefore, we concluded that these two proteins represent distinct cell populations within the human adrenal cortex. In addition, if we take into consideration the role of DLK1 in adipocytes, the expression of Dlk1 in the rat ZU[8, 131], as well as the fact that DLK1+ cells do not express CYP11B2 (steroidogenic marker), it is possible that the DLK1+ cell population might represent adrenocortical progenitor cells and hence the ZU in the human adrenal cortex. However, in order to confirm this, we would need to perform immunofluorescent studies to confirm that DLK1+ areas in the adrenal cortex are not co-expressing any steroidogenic markers (CYP11B1 and CYP11B2).

Assessment of DLK1 expression in a series of physiologically normal human adrenal glands confirmed the subcapsular expression of DLK1, as either layered continuous expression, clustered expression or a combination of the two patterns. Finally, we aimed to identify whether there was a pattern that could explain the two different expression forms. We investigated, whether there was any correlation of DLK1 expression pattern with either age and/or gender. Interestingly, this difference in DLK1 expression pattern across different adrenals was significantly correlated with age but not gender. We showed that in adrenals from younger donors (0-30 years old), DLK1 expression appears layered continuous, while this continuous expression slowly transformed into a clustered DLK1 expression (DCCs) with increasing age. Therefore, in human adrenals of 30+ years of age we observed increasing numbers of DCCs as compared to samples from younger donors. It is important to note that the peak of DCC occurrence in the samples analysed was in the 41-50 age range. This age range correlates with the second peak occurrence of ACCs (the first being in the first decade of life) [231, 232]. This correlation is of significance, as it might suggest a link between appearance of DCCs and ACC occurrence. The finding that clustered DLK1 expression was not correlated with gender, is also in line with the lack of significant difference in the prevalence of ACCs in males and females in previous studies. As mentioned previously, mutations in genes encoding for ion channels/pumps commonly found in APAs are also present in APCCs, implying that

APCCs might be precursor cells of APAs[187]. In addition, similar to our observations on DLK1 expression, other researchers have shown that CYP11B2 expression also changes with age from a subcapsular layered continuous expression to a more clustered expression pattern (APCC) [233].

Taking into account the similarities between DLK1 and CYP11B2 in their expression pattern in human adrenal glands, their expression pattern changes with age, in addition to the correlation of DCC appearance with ACC second peak occurrence in humans and the role of DLK1 in pre-adipocytes; has led us to speculate whether there is indeed a link between DCC appearance and ACC incidence in humans.

Chapter 4: DLK1 as a potential marker of cancer stem cells in the adrenal gland

4.1 Introduction

4.1.1 Adrenocortical carcinoma and correlation to DLK1

Adrenocortical carcinoma is a rare neoplasm with an incident rate of approximately 1-2 cases/1 million/year[231, 234, 235]. ACC can occur at any age, but has a bimodal peak incidence, with the first peak occurring at childhood (first decade) and the second peak occurring in the fourth to fifth decade in life [236, 237]. ACC has an overall poor prognosis and at the moment prognostic factors are based on tumour stage at the time of diagnosis. Treatment of ACC is dependent on tumour stage and type as described earlier in section 1.7.2.3, with surgical resection and adjuvant chemotherapy (ADIUVO or mitotane) being the most common line of treatment. However, it is reported that most of the ACC patients undergoing even complete resection, still present with local or distant recurrence [231]. Recent efforts have been made to identify germline/somatic mutations that are most common in ACCs and might aid diagnostic and treatment procedures in the future. These include mutations in *CTNNB1, TP53* and *ZNRF3* among others as previously highlighted in Table 1.1 (Section 1.7.2.4).

DLK1 has been previously reported to play a role in numerous cancer types including some neuroendocrine tumours (previously described in Section 1.5.4). However, it is not yet known whether DLK1 is involved in adrenocortical carcinoma. Although little is known about DLK1 expression in human adrenal, it has been shown to have a role in maintaining the undifferentiated state of adipocytes[238]. In addition, our group reported that i) Dlk1 is expressed in rat cortical non-steroidogenic cells (Shh-secreting and possibly Wnt receiving cells), ii) its expression is modulated by remodelling of the gland triggered by the activation/inactivation of the renin-angiotensin-aldosterone axis, a process likely involving the recruitment of stem/progenitor cells, and iii) Dlk1 itself functionally interacts with Shh in activating Gli1 cells in the capsule of rat adrenals in a β1 integrin-dependent fashion [8].

In the previous chapter, I have clearly shown that the human adrenal cortex remodels itself to generate clusters of DLK1+ cells (DCCs) as we age, in a similar manner to APCCs. As stated earlier, it is possible that DCCs might be precursors of ACCs, although this still needs to be proven[187]. Considering all the above, we hypothesize that DLK1 might have a direct or indirect role in ACC development and/or maintenance.

4.1.2 Common chemotherapeutic agents

4.1.2.1 Mitotane

Mitotane [1,1 dichloro-2(o-chlorophenyl)-2-(p-chloro-phenyl)ethane or o,p'-DDD] is an adrenal-specific cytotoxic agent and the only approved drug for the treatment of ACC both in adjuvant chemotherapy and in metastatic ACC [239] [231]. Mitotane is not the active compound, however it is metabolised in the liver to produce the therapeutic metabolites leading to adrenolysis. Briefly, mitotane is hydroxylated in the mitochondria and transformed into the active compound acyl chloride, which will either act on target cells and cause cell lysis or be converted into an acetic acid derivated for renal excretion[235]. Evidence for its efficiency comes from retrospective data of patients with ACC undergoing mitotane treatment, showing that response rates vary between 13-31%. Overall survival following mitotane treatment remains controversial, with some studies showing an increase in survival rate in specific patient groups while others show no difference [193, 196, 240, 241]. However, even though mitotane treatment might not increase survival rate, it may delay recurrence[242]. The reason that the response rates are so variable and relatively low might stem from the fact that mitotane requires metabolic activation to act and therefore response rates are dependent on the ability of each individual to metabolise mitotane within the given therapeutic window for mitotane. Dosing regimens for mitotane are largely unknown, however it was shown that mitotane plasma levels of 14-20mg/l have produced a significant response in patients. Plasma levels that exceed 20mg/l have been associated with significant toxicities (such as nausea, vomiting, memory loss and dizziness), while plasma levels below 14mg/l show limited therapeutic potential. Mitotane can have a significant impact on drug

metabolism and affect drug-drug interactions, as well as glucocorticoid metabolism due to induction of hepatic cytochrome P450 enzyme 3A4 (CYP3A4) [231, 235].

Recent efforts focusing on the mechanism of action of mitotane have identified Sterol-O-Acyl Transferase 1 (SOAT1) as the main target of mitotane in adrenocortical cells [239]. SOAT1 or ACAT1 is mainly expressed in the endoplasmic reticulum and plays an important role in cellular cholesterol homeostasis [243]. Sbiera et al., have shown that mitotane treatment inhibits SOAT1 activity with an IC_{50} of 21µm (7mg/L). The blockage of SOAT1 leads to the accumulation of fatty acids, oxysterols and free cholesterol in cells with high steroidogenic activity. This in turn causes a buildup of toxic steroids activating the stress response in the endoplasmic reticulum and subsequent cell death[239].

4.1.2.2 Doxorubicin

Doxorubicin is an anthracycline, antineoplastic drug, commonly used in the treatment of multiple cancers including lung, ovarian, breast, thyroid and gastric cancers as well as non-Hodgkin and Hodgkin's lymphoma, sarcoma, multiple myeloma and paediatric cancers [244, 245]. It can act either by DNA intercalation and disruption of DNA repair or by damaging cell membranes via accumulation of free radicals. However, limitations associated with doxorubicin treatment include cardiotoxicity and high drug resistance in patients[246-248], thus limiting its use. The fact that the mechanism of action of cardiotoxicity and the anticancer action are thought to be different, give hope for the development of better treatments with reduced adverse effects[246].

4.1.2.3 5-Fluorouracil

5-FU is an antimetabolite drug, widely used for the treatment of breast cancer, colorectal cancer and head/neck cancers [249]. It is most effective for the treatment of colorectal cancers, specifically when used in combination with other chemotherapeutic agents such as irinotecan and oxaliplatin [250, 251]. 5-FU is an analog of uracil and therefore is taken up by the cells via facilitated transport, where it is converted into its active metabolites (fluorodeoxyuridine monophosphate,

fluorodeoxyuridine triphosphate and fluorouridine triphosphate), which disrupt RNA synthesis and inhibit thymidylate synthase activity [251]. However, similar to other chemotherapeutic agents limitations include adverse side effects and chemoresistance.

4.1.2.4 Cisplatin

Cisplatin is a well-known chemotherapeutic drug clinically proven to be effective against multiple types of cancers including breast, testicular, ovarian, prostate, head and neck, bladder gastric cancers and leukaemia [252-254]. It is also used for recurrent childhood brain tumours [255]. It exerts its effects by targeting DNA repair mechanisms leading to DNA damage and apoptosis in cancer cells. However, like other chemotherapeutic agents, cisplatin's limitations include high levels of toxicity and in some cases resistance. To overcome these problems cisplatin is mostly used in combination therapies and efforts have been made to synthesize similar compounds that would be less toxic and more effective [253].

All three chemotherapeutic agents mentioned above, have been and/or are currently tested as chemotherapeutic agents for the treatment of ACC alone or as part of a combination regimen, in clinical trials.

4.1.3 Cancer and cancer stem cells

Over the years and with the aid of cancer research and advanced molecular techniques (whole genome sequencing and RNA sequencing) we have gained valuable insight into the development of different types of cancers [256, 257]. A cancer appears when a significant amount of mutations occurs, leading to aberrant cell growth and function. Research aimed at dissecting the key mutations that drive cancer development, has revealed a number of mutations that are most commonly associated with a particular type of cancer (eg. *CTNNB1*, *TP53* and *ZNRF3* in ACC [199]) or known to increase the risk of cancer (eg. *BRCA1* and *BRCA2* in breast cancer). However, due to the heterogenic nature of cancer, it has proven difficult to pinpoint

or distinguish the specific driving mutations that have an impact on cancer development and progression.

Tumour initiation, progression and maintenance are very complex and diverse processes and can vary between individuals. This variability results in cancer treatment outcome, recurrence rates and survival being different between patients with the same type and stage of cancer. It is important to note that despite clinical advances in cancer treatments, a number of patients still fails to respond to therapy, leading to disease progression or recurrence and overall decreased survival [258, 259]. The fact that cancer is not a homogeneous mixture but rather composed of a heterogeneous combination of distinct subclones arising through branching evolution, is an important aspect to consider when looking at tumour resistance and recurrence [260, 261]. In fact when individual cell clones, taken from a metastatic melanoma mouse model, were injected into syngeneic hosts, varying degrees of metastasis were observed, with only a fraction of the cells being able to form a metastasis in the hosts [262]. This shows the great functional variability that exists between subclones of the same tumour, supporting their heterogenic nature. In addition to tumour heterogeneity, the tumour microenvironment (TME) plays an indispensable role in the development and maintenance of cancer as well as drug resistance. Strong evidence also suggests that non-genetic determinants, including developmental pathways and epigenetic modifications can also contribute to cancer heterogeneity [263-265].

4.1.4 Cancer stem cell models and chemotherapy

Cancer stem cells arise from normal stem cells whose function becomes impaired, resulting in these cells to divide and differentiate uncontrollably leading to tumour formation. For this to occur it is thought that stem cells need to undergo at least two of the following changes: (i) Stem cell microenvironment disturbance, (ii) mutations in genes that control cell metabolism, cell cycle, key signalling pathways (e.g., Wnt, Shh) (iii) amplification of cell populations that have acquired advantageous altered molecular phenotypes which give rise to tumour heterogeneity and metastasis[266]

(Klonisch et al., 2008). Recent evidence suggests that high mutation rates in cancer stem cells contribute to tumour heterogeneity and represent the main cell population responsible for chemotherapeutic resistance, leading to therapy failure, cancer recurrence and metastasis in patients[267-269].

Advancements in identifying key stem cell populations within the tumour is key to understanding how chemoresistance, tumour development and tumour recurrence occurs in patients. There are currently two standing stem cell model hypotheses; the hierarchical and the dynamic CSC model. The initial hypothesis of the hierarchical cancer stem cell model, states that within a tumour exists a small population of cells (termed cancer stem cells) that has the ability to self-renew and differentiate into mature tumour cells. In this model CSCs follow the function of normal stem cells in normal tissues, meaning that they both display multi-lineage potential and also have the ability to self-renew (Figure 4.1) [267]. Alternatively the dynamic stem cell model suggests that the interchange of cancer stem cells to tumour cells can occur both ways. This means that the tumour microenvironment can influence both cancer stem cells to become mature tumour cells, as well as tumour cells to dedifferentiate to cancer stem cells (Figure 4.1) [270-273].

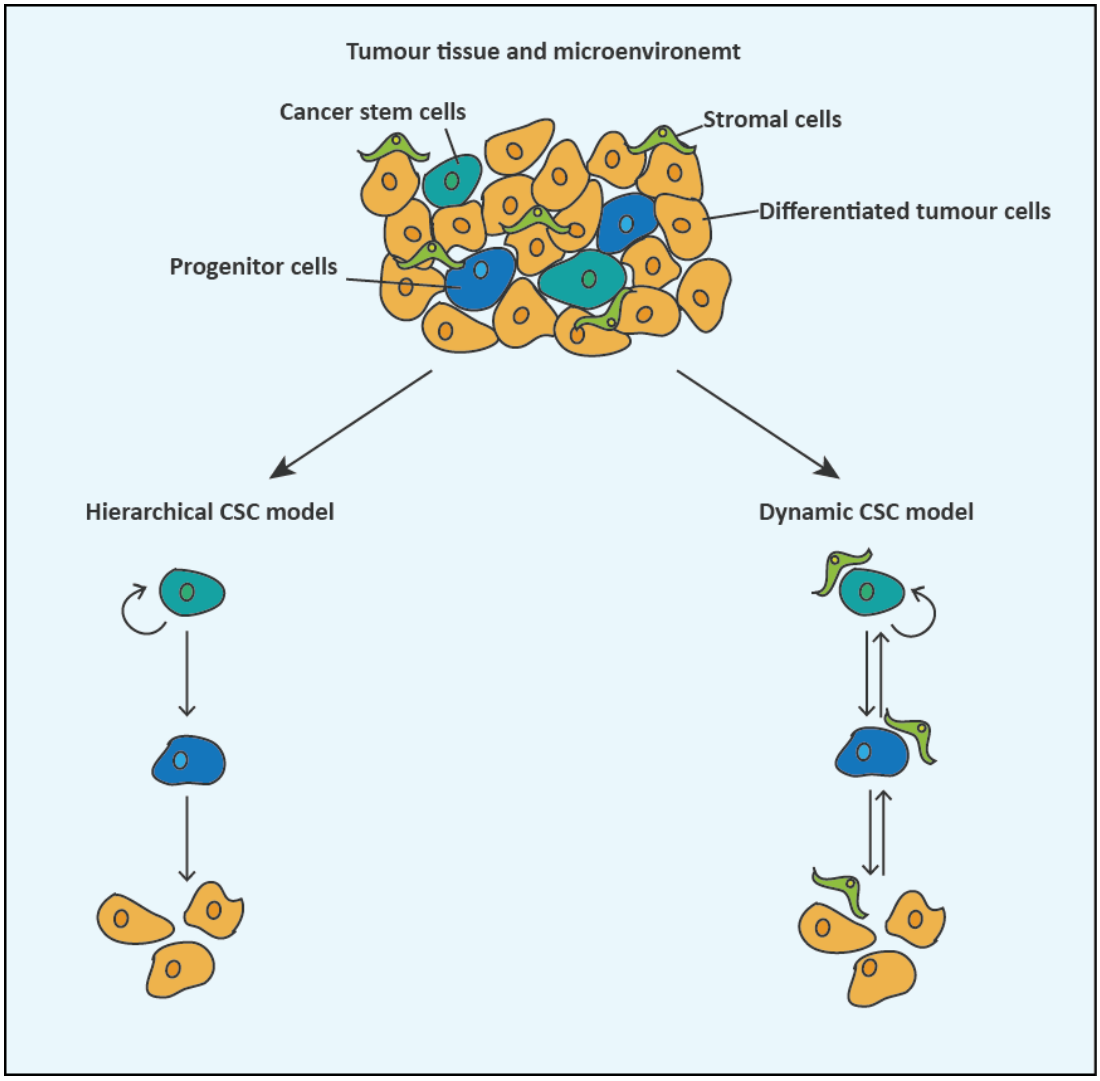

Figure 4.1 – Cancer stem cell models. Schematic diagram showing the heterogenic nature of cancer tissue (top) and the two main cancer stem cell models. The original hierarchical CSC model (left) shows that CSCs differentiate into progenitor cells which then give rise to terminally differentiated cells in a unidirectional fashion. The dynamic CSC model (right) shows that CSCs differentiate to progenitor cells and then differentiated tumour cells. However, in this model differentiated tumour cells can de-differentiate into progenitor and then stem cells, after receiving specific signals from the microenvironment. In the latter model, differentiation and de-differentiation of cells is highly dependent on tumour microenvironment.

The hierarchical stem cell model is widely accepted, and multiple studies confirm the existence and isolation of such populations within different types of tumours[266,

274-277]. These subpopulations of cancer stem cells have a tumourigenic capacity *in vivo* in mice and *in vitro* and exhibit a high expression of stem/progenitor cell genes/markers such as *β-catenin, NOTCH, OCT3/4 AND SHH* [266, 267, 278]. For example in pancreatic cancer, cells expressing surface markers CD44+, CD24+ and epithelial specific antigen, have been shown to have tumourigenic abilities *in vivo* in contrast to the remaining cancer cells. In human hepatocellular carcinoma and colorectal cancer CD133+ cells, but not CD133- cells have been shown to self-renew and differentiate and in the case of colorectal cancer generate tumours when injected in mice *in vivo,* thus representing cancer stem cells[274, 278]. These are just some examples of stem cells identified and isolated in cancers and additional researchers have identified markers expressed solely in stem cell populations[266].

4.1.5 Hypothesis

In humans, DLK1 plays a role in maintaining pre-adipocytes in their undifferentiated state and DLK1 expression levels are also implicated in tumorigenesis in other human tissues (See Section 1.5). Combined with our finding that clustered DLK1 expression in the cortex of human adrenal glands correlates with second-peak incidence of ACC (See Chapter 3), we hypothesize that DLK1 could potentially be involved in the formation and/or maintenance of ACCs.

4.1.6 Aims

1. Determine the expression levels of DLK1 in tissue samples of patients with ACCs, ACAs, and normal adrenal glands.
2. Explore whether DLK1 could be involved in the formation and/or maintenance of ACCs by evaluating whether DLK1+ cells display characteristics similar to cancer stem cells *in vitro*.

4.2 DLK1 expression in human adrenocortical carcinoma

To address the first aim of this chapter, we collected ACC samples from biobanks, details of which can be found in Table 4.1. Following DLK1 immunostaining on the samples, we observed a heterogeneous pattern of DLK1 expression (Figure 4.2). Unlike in normal tissues where DLK1 expression pattern was subcapsular continuous and/or patchy (see chapter 3.3.2); in ACCs there was no particular pattern within the samples. It is worth stating at this point, that the normal zonation and cell organisation normally observed in physiologically normal adrenal cortices was generally absent or difficult to observe in ACCs. As can be seen in Figure 4.2 some of the samples show subcapsular expression of DLK1 (Figure 4.2b-d), while in others expression occurs throughout the tissue (Figure 4.2a,e-i). In addition, unlike in normal adrenal glands, (see Chapter 3.3.2) in ACCs there didn't seem to be any correlation of DLK1 expression pattern with age, in the samples analysed (Figure 4.2).

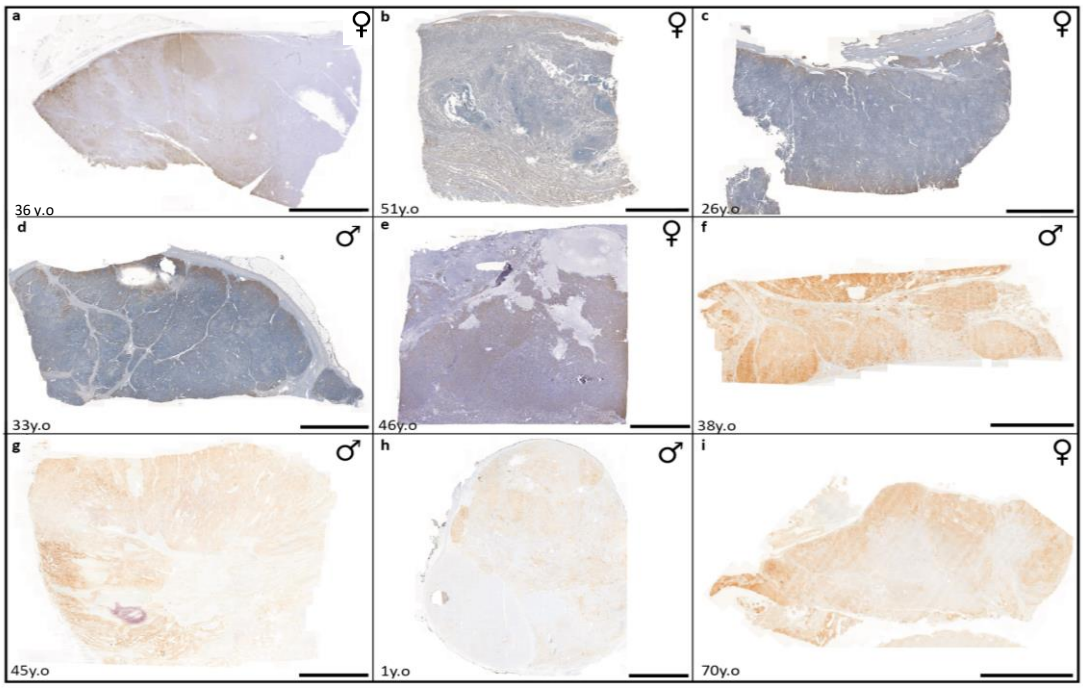

Figure 4.2 – DLK1 is highly expressed in adrenal glands of ACC patients. Results following immunostaining for DLK1 on human ACC samples from patients aged 1-70 years old, showing a heterogeneous expression of DLK1 in all samples analysed. n=9. Scale bars: 5000µm.

Table 4.1 – List of human adrenocortical carcinoma samples collected for analysis

Sample name	Gender	Age	Sample type	Diagnosis/Surgery	Biobank
A2-C15016_014	Female	46	Carinoma	Adrenocortical carcinoma	Biobanc
A2-C15016_012	Female	26	Carinoma	Adrenocortical carcinoma	Biobanc
A2-C15016_013	Male	33	Carinoma	Adrenocortical carcinoma	Biobanc
A2-C15016_011	Female	51	Carinoma	Adrenocortical carcinoma	Biobanc
33160763	Female	36	Carinoma	Adrenocortical carcinoma	N/A
33150007	Male	1	Carinoma	Adrenocortical carcinoma	N/A
Sample 1	Female	70	Carinoma	Adrenocortical carcinoma	IRBleida
Sample 2	Male	38	Carinoma	Adrenocortical carcinoma	IRBleida
Sample 3	Male	45	Carinoma	Adrenocortical carcinoma	IRBleida

In order to ensure that this observation was specific to carcinoma tissue, we collected adrenocortical adenoma (ACA) samples from biobanks (details shown in Table 4.2). Following DLK1 immunostaining of the adenoma tissues we observed minimal DLK1 staining (Figure 4.3), similar to or less than what we observed in normal human adrenals.

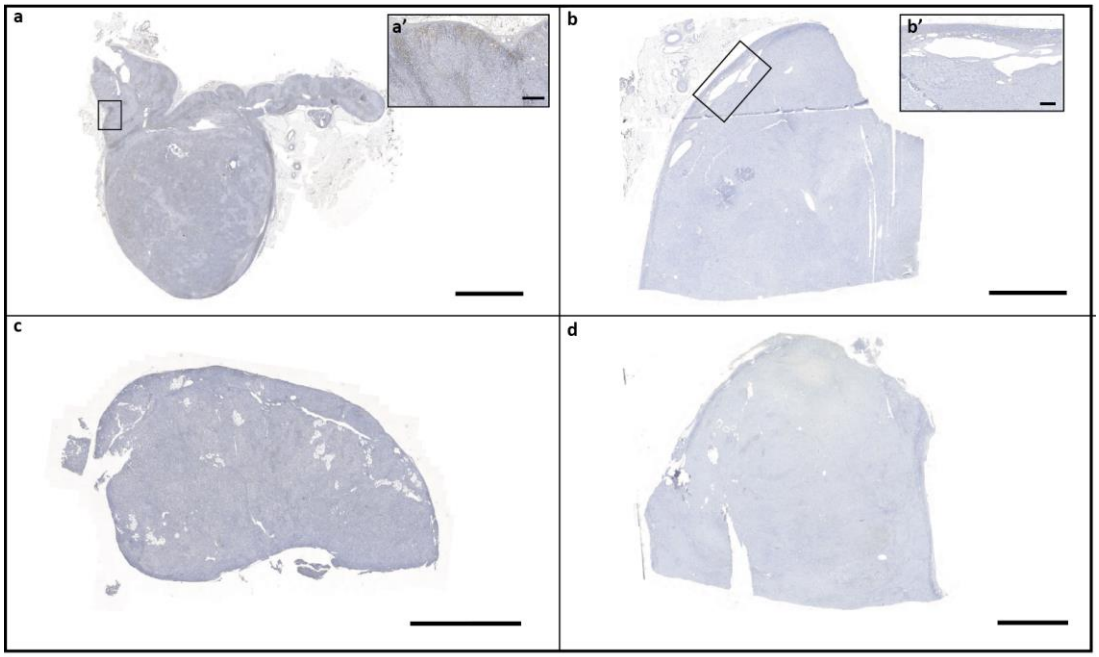

Figure 4.3 – DLK1 expression is minimal in adrenal glands from patients with ACA. Results following immunostaining for DLK1 on human ACA samples from patients aged 24-75 years old, showing low levels of DLK1 expression in all samples analysed. Images shown are representative of all samples analysed. n=10. Scale bars: 5000µm (a-d) and 500µm (a',b').

Table 4.2 List of human adrenocortical adenoma samples collected for analysis

Sample name	Gender	Age	Sample type	Diagnosis/Surgery	Biobank
A2-C15016_017	Female	59	Aldosterone adenoma	Cortical adenoma	Biobanc
A2-C15016_018	Female	75	Non-secreting adenoma	Cortical adenoma	Biobanc
A2-C15016_019	Female	67	Aldosterone adenoma	Cortical adenoma	Biobanc
A2-C15016_024	Male	46	Aldosterone adenoma	Cortical adenoma	Biobanc
A2-C15016_026	Female	48	Aldosterone adenoma	Cortical adenoma	Biobanc
A2-C15016_030	Female	24	Aldosterone adenoma	Cortical adenoma	Biobanc
A2-C15016_031	Female	42	Aldosterone adenoma	Cortical adenoma	Biobanc
A2-C15016_034	Male	67	Adenoma	Cortical adenoma	Biobanc
A2-C15016_035	Female	55	Aldosterone adenoma	Cortical adenoma	Biobanc
A2-C15016_037	Female	44	Aldosterone adenoma	Cortical adenoma	Biobanc

Finally, we performed quantitative analysis of DLK1 staining where we measured the area of DLK1 staining as a percentage of the total adrenal cortex area for all conditions (normal adrenal glands, ACA and ACC) as illustrated in Figure 4.4. The analysis showed a significant overexpression of DLK1 in ACC samples as compared to both normal and ACA tissue. No significant difference in DLK1 expression was observed in ACA as compared to normal adrenal glands.

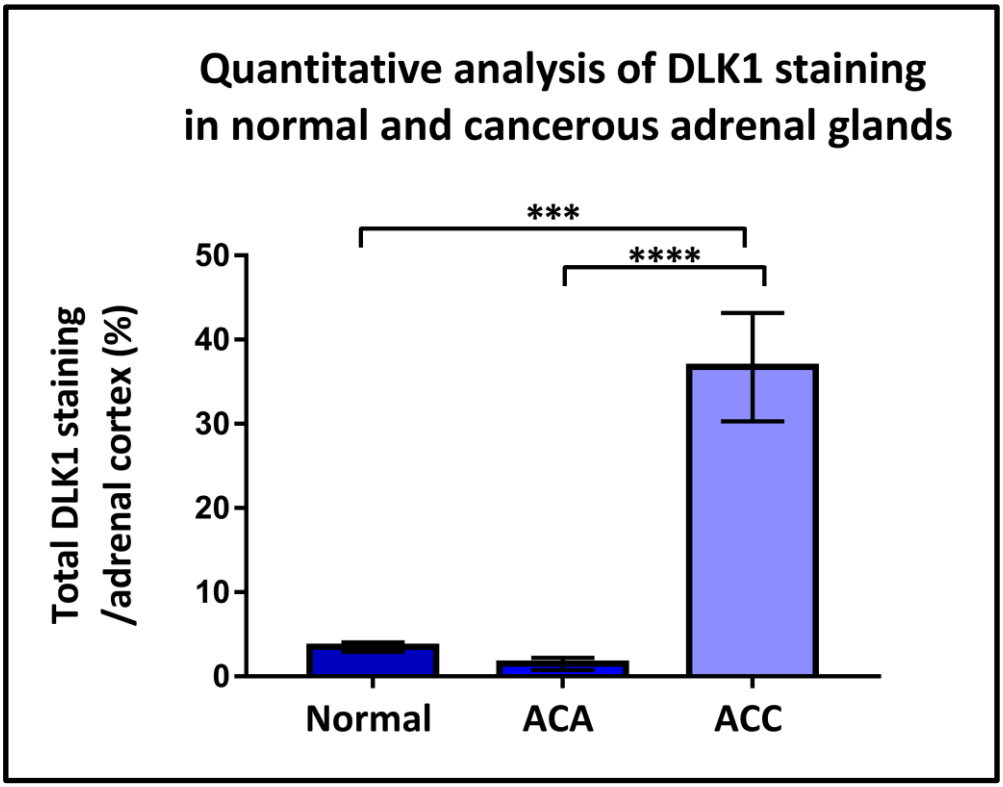

Figure 4.4 – DLK1 is overexpressed in ACCs. Results following quantitative analysis to measure DLK1+ area as a percentage of total adrenal cortex area in normal (n=23), ACA (n=10) and ACC (n=9) samples showed a significant overexpression of DLK1 in ACCs as compared to both normal and ACA. Error bars represent standard error of the mean. Statistical analysis was performed using one-way ANOVA and statistical significance is denoted as ***($p<0.001$) and ****($p<0.0001$).

4.3 Do DLK1+ cells possess cancer stem cell-like characteristics?

DLK1 is not only expressed in adrenal glands of patients with ACC, but is also expressed at a higher degree than both normal and adenoma tissue. Therefore, it is possible that DLK1 or DLK1+ cells might play a role in carcinoma formation and/or maintenance. To study the role of DLK1 in ACCs further, we used the H295R cell line, which is a human adrenocortical carcinoma cell line.

First, we showed that immunofluorescence analysis of DLK1 expression in H295R showed small clusters of positive cells, representing roughly 3-5% of the total cell population. In addition, DLK1+ cells were always arranged in clusters, surrounded by a majority of DLK1- cells, as can be seen in Figure 4.5.

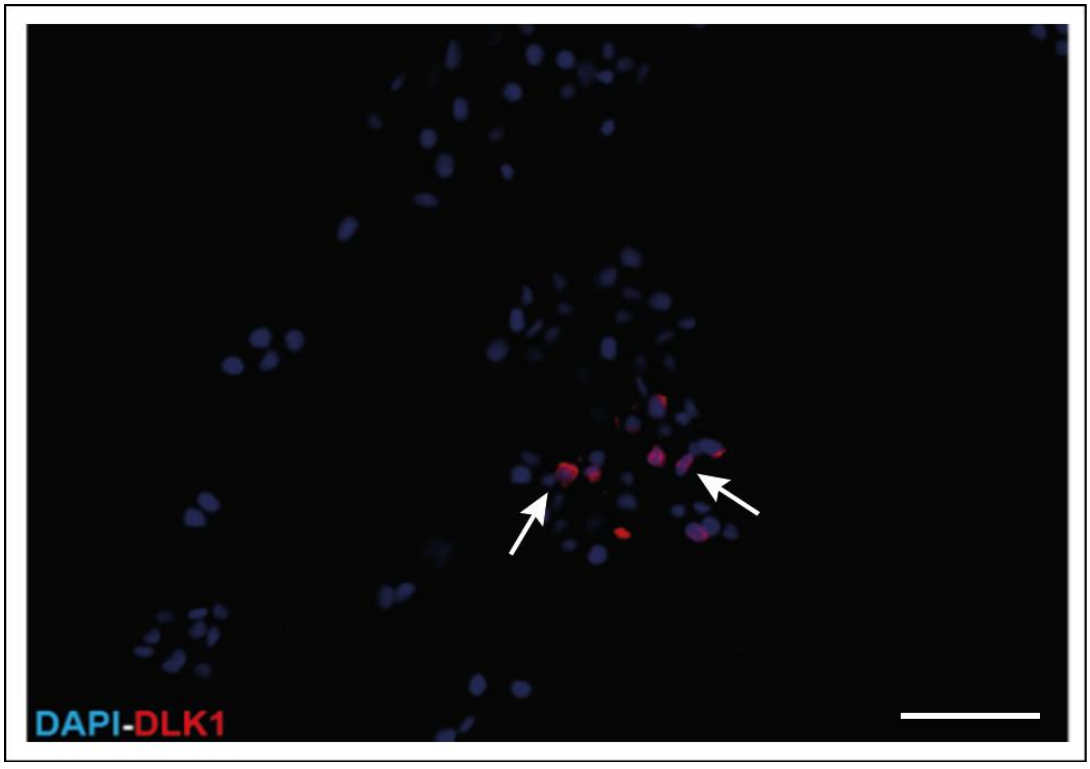

Figure 4.5 – DLK1 is expressed in the H295R cell line. Representative image taken after immunostaining of H295R cells for DLK1, showing that only small population of cells expresses DLK1. n=3. Scale bar=100µm.

Given DLK1's potential role in ACCs, and its known function in preventing cell differentiation in pre-adipocytes, we hypothesised that DLK1+ cells could act as cancer stem cells in ACCs.

Spheroids are described as unique 3D culture systems developed to more accurately mimic tumour microenvironment *in vitro,* as compared to 2D culture, greatly aiding cancer research [279]. Spheroids are a commonly used model to study cancer development and progression, with several studies showing that spheroids also exhibit an increased expression of specific cancer cell biomarkers (depending on cell origin), higher proportion of cancer stem cells, and higher survival rates following chemotherapeutic treatment. These studies have also highlighted spheroids as an accepted model for studying cancer stem cells *in vitro* [280, 281, 282, 283, 284].

We investigated whether the percentage of DLK1+ cells changed when H295R cells were cultured as spheroids. We established spheroid colonies from H295R cells, as shown in Figure 4.6a. Two-week old spheroids expressed DLK1 widely as observed with immunofluorescence (Figure 4.6b), in contrast to the adherent (2D) state (Figure 4.5). To quantify the expression of plasma membrane DLK1, flow cytometry analysis for DLK1, showed a significant increase in the percentage of DLK1+ cells in the spheroid state as compared to adherent (2D) state (Figure 4.6c,d) from 7.5% (2D) to 35% (spheroids), confirming immunofluorescent data.

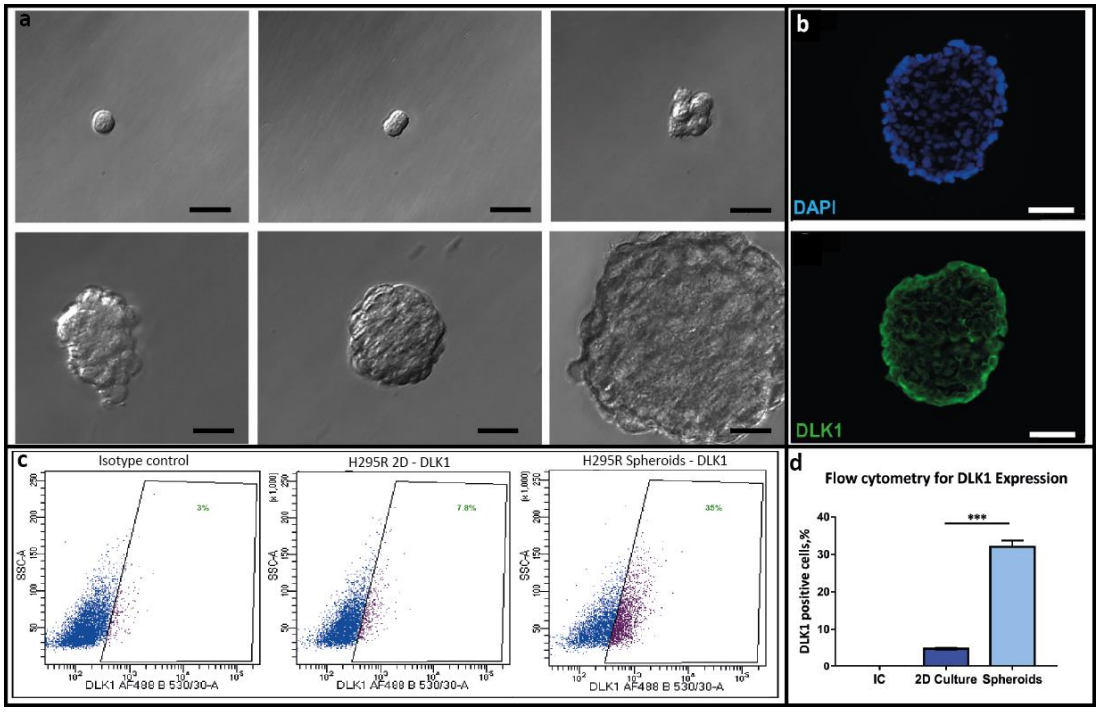

Figure 4.6 – DLK1 is enriched in a cancer stem cell model. H295R cells were cultured in suspension in low adherent plates for 2 weeks to form spheroids (a). Results following immunofluorescence analysis on cultured spheroids show an increased DLK1 expression (b). Flow cytometry analysis on H295R adherent (2D) culture and H295R spheroid culture shows significant upregulation of DLK1 in the latter (c, d). Error bars represent standard error of the mean. n=3. Statistical analysis was performed using unpaired t-test with statistical significance denoted as ***($p<0.001$).

The number of cells expressing DLK1 was found to be increased in the spheroid model, suggesting that DLK1 could be a marker of cancer stem cells. To further determine whether DLK1+ cells possessed stem cell-like characteristics, we assessed whether DLK1+ cells express other known stem cell markers. To do this we generated H295R cells over-expressing DLK1 (H295R-DLK1) through lentiviral infection. Control cells were infected with an empty vector (H295R-Control) (Appendix IV). H295R-DLK1 significantly over-expressed *DLK1* (Figure 4.7.a), confirming success of infection. We performed a gene expression analysis to evaluate expression levels *of NANOG, CTNNB1, DAX1* and *CYP17* in DLK1+ against DLK1- cells. *NANOG* is a known embryonic

stem cell marker and in the adult, is expressed in the skin, lung and testis. Additionally, it was also found to be expressed in human endometrial adrenocarcinoma samples at the protein level[285]. CTNNB1 is expressed in all tissues, including the adrenal gland and encodes the β-catenin gene, which is responsible for stem cell maintenance and cell-renewal. Finally, *DAX1* (*NR0B1*) is expressed throughout the hypothalamic pituitary gonadal axis, mainly in the adrenal glands and testis, and has a pivotal role in the normal development and function of steroidogenic tissues[286].

Following gene expression analysis we showed that stem cell/progenitor markers *NANOG* (Figure 4.7b) and *CTNNB1* (Figure 4.7c) were significantly upregulated in H295R-DLK1 by approximately 15-fold and 30-fold, respectively, as compared to H295R-Control. Expression of *DAX1* (another potential specific marker of adrenocortical progenitor cells), was increased by 5-fold in H295R-DLK1 compared to H295R-Control (Figure 4.7d), while expression of *CYP17* (an adrenal differentiation marker) was halved in H295R-DLK1 as compared to H295R-Control (Figure 4.7e). This shows that DLK1+ cells have an increased expression of stem cell markers and a decreased expression of differentiation markers, compared to the remaining H295R population and could possibly represent cancer stem cells. We could have also performed a protein expression analysis of stem cell and differentiation markers *in vivo* in ACC patient samples with respect to DLK1 staining, to confirm results. However as opposed to the gene expression analysis, this approach was not possible due to the limited availability of suitable, functioning antibodies.

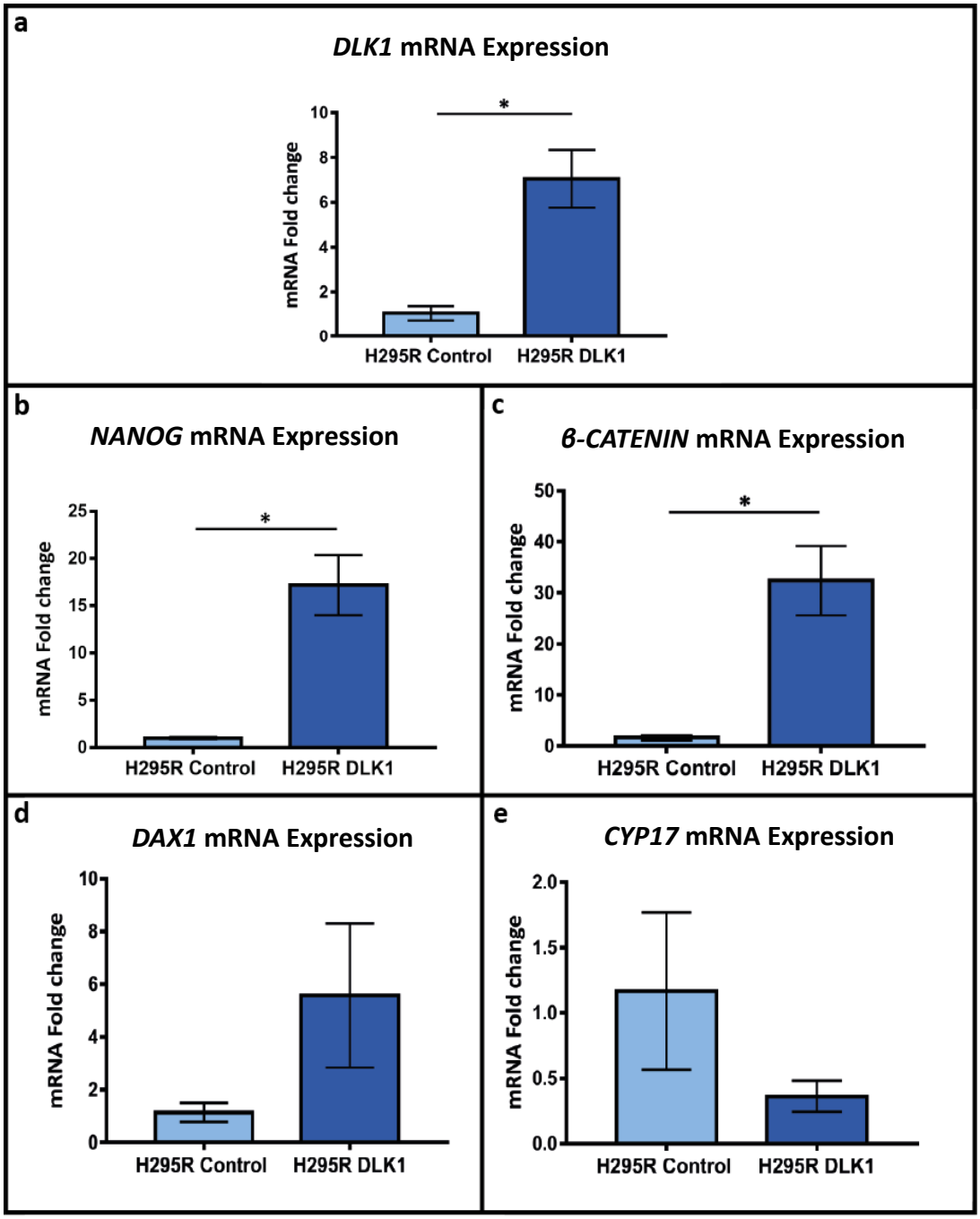

Figure 4.7 - H295R cells overexpressing DLK1 exhibit increased gene expression of stem cell markers. Results following RT-qPCR analysis of H295R-Control cells and H295R-DLK1 for SC (b-d) and differentiation markers (e) show that SC markers are upregulated in the H295R-DLK1 cell line while CYP17 (e) is downregulated as compared to control cell line. Error bars represent standard error of the mean. n=3. Statistical analysis was performed using unpaired t-test with statistical significance denoted as *($p<0.05$).

Additionally, we assessed whether DLK1+ cells possess any stem cell characteristics, such as high proliferation rates and clonogenicity. To do this we collected H295R cells and FAC-sorted them based on DLK1 expression. Details of the FAC-sorting, including gates used and percentages of cells collected are shown in Figure 4.8 below.

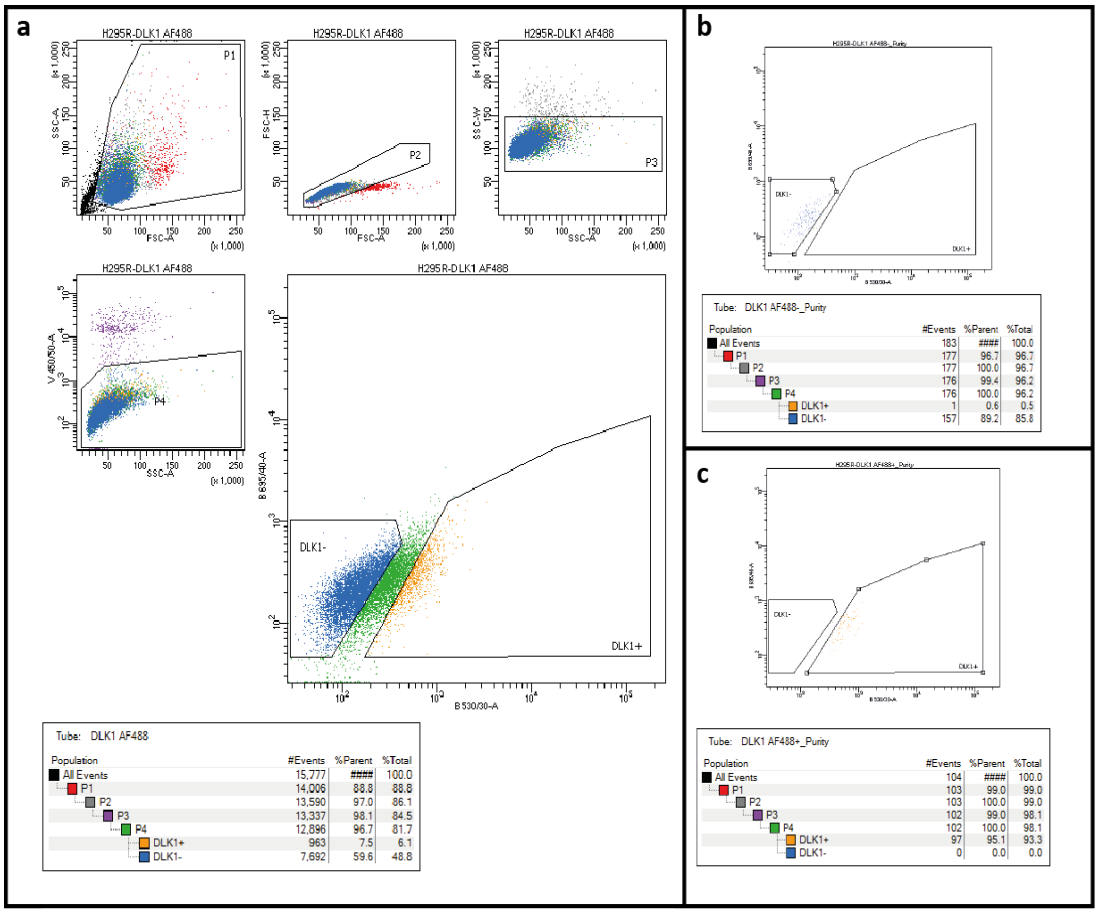

Figure 4.8 – Fluorescence activated cell sorter settings and purity controls. Figure shows the settings and gates assigned to sort H295R cells into DLK1+ and DLK1- (a) as well as quality controls to check purity of DLK1- (b) and DLK1+ (c) cells collected after sorting.

Following FAC-sorting of the H295R DLK1+ and DLK1- cells, collected cells were plated for the colony formation and cell proliferation assays. Colony formation assays showed that DLK1+ cells had a significantly increased clonogenic capacity as compare to DLK1- cells (Figure 4.9a). Following 3 weeks of culture DLK1+ cells formed an average of 500 colonies from single cells while DLK1-cells an average of

approximately 380 colonies. In addition, we showed that DLK1+ cells had a higher proliferation rate, which was evident on the 4^{th} to 5^{th} day of culture when compared to DLK1-. The difference in proliferation rate was clearer at later time points and in fact was significantly higher in DLK1+ when compared to DLK1- after 6 and 7 days of culture (Figure 4.9c). Based on our observations we can conclude that DLK1+ cells show an increased expression of stem cell genes and exhibit increased clonogenic and proliferative capacity compared to DLK1- cells. These results suggest that DLK1+ cells could possess stem cell-like characteristics, highlighting DLK1 as a potential future marker of cancer stem cells in ACCs. However, additional studies would be required to validate this hypothesis.

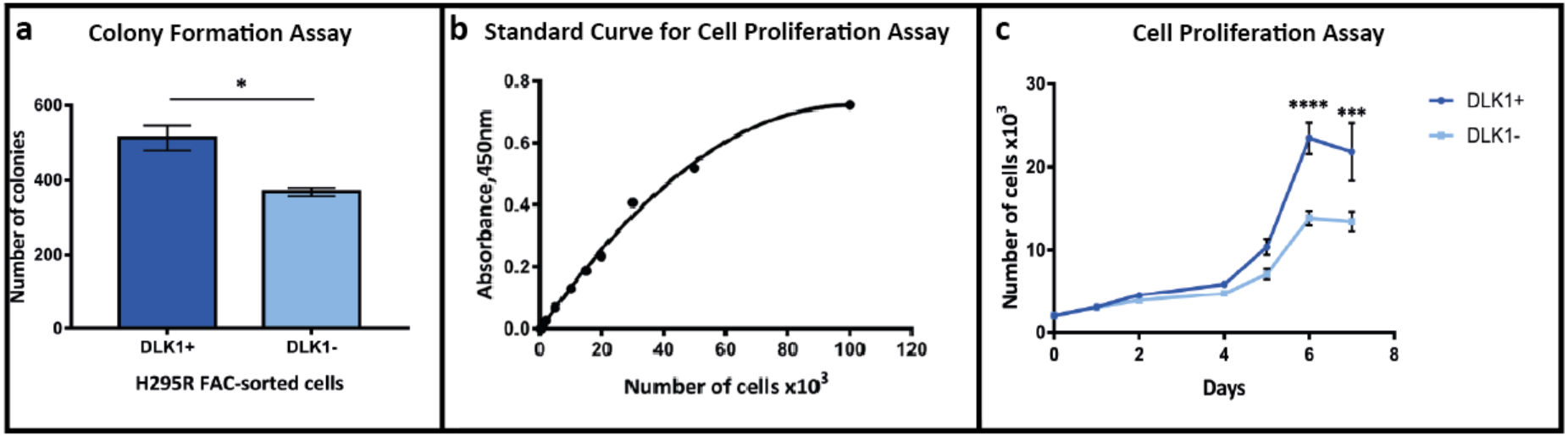

Figure 4.9 – DLK1+ H295R sorted cells display increased proliferation and colony formation compared to DLK1- H295R sorted cells. Results following colony formation assays (a) and cell proliferation assays(c) on DLK1+ and DLK1- cells depicting differences between the two populations with the former being more proliferative and having a significantly higher capacity of forming colonies from single cells. For the cell proliferation assays a standard curve(b) was constructed by plating known number of cells and measuring their OD values. These values were then plotted on the graph b shown above to form a standard curve from which we derived the approximate cell numbers corresponding to the OD values measured in the cell proliferation assays. Error bars represent standard error of the mean. For each assay n=3 Statistical analysis was performed using unpaired t-test (a) and a two way ANOVA (c), with statistical significance denoted as *($p<0.05$), ***($p<0.001$) and ****($p<0.0001$).

4.4 DLK1+ cells are less responsive to chemotherapeutic treatments *in vitro*

Another key characteristic of cancer stem cells is their inherent resistance to common chemotherapeutic drugs in some cases. Chemotherapeutic resistance is described as the ability of cancer cells to withstand the chemotherapeutic effects including apoptosis or growth inhibition [287, 288]. Here, we investigated whether there was any relationship between DLK1 expression and chemoresistance in H295R cells. This could highlight DLK1 as a possible prognostic marker of ACCs and also suggest DLK1+ cells could potentially be isolated to further study chemoresistance in ACCs, aiding drug development.

Initially we treated H295R cells with increasing concentrations of mitotane, doxorubicin, 5-FU and cisplatin to derive the LD_{50} of each drug as shown in Figure 4.10 and 4.11. Mitotane and doxorubicin showed an LD_{50} of 29µM (Figure 4.10a) and 3.7µM (Figure 4.10c), respectively. The remaining two drugs were not as effective and an LD_{50} could not be calculated (Figure 4.11a,c). Comparing individual drug concentrations of mitotane we observed that with the lower concentrations (5-20 µM) there was no significant difference in cell viability compared to vehicle, however significant decrease in cell viability was observed at higher mitotane concentrations (Figure 4.10b). In the case of doxorubicin, we observed a significant decrease in cell viability even at the lowest concentrations used, with the exception of 0.5µM compared to vehicle treatment (Figure 4.10d).

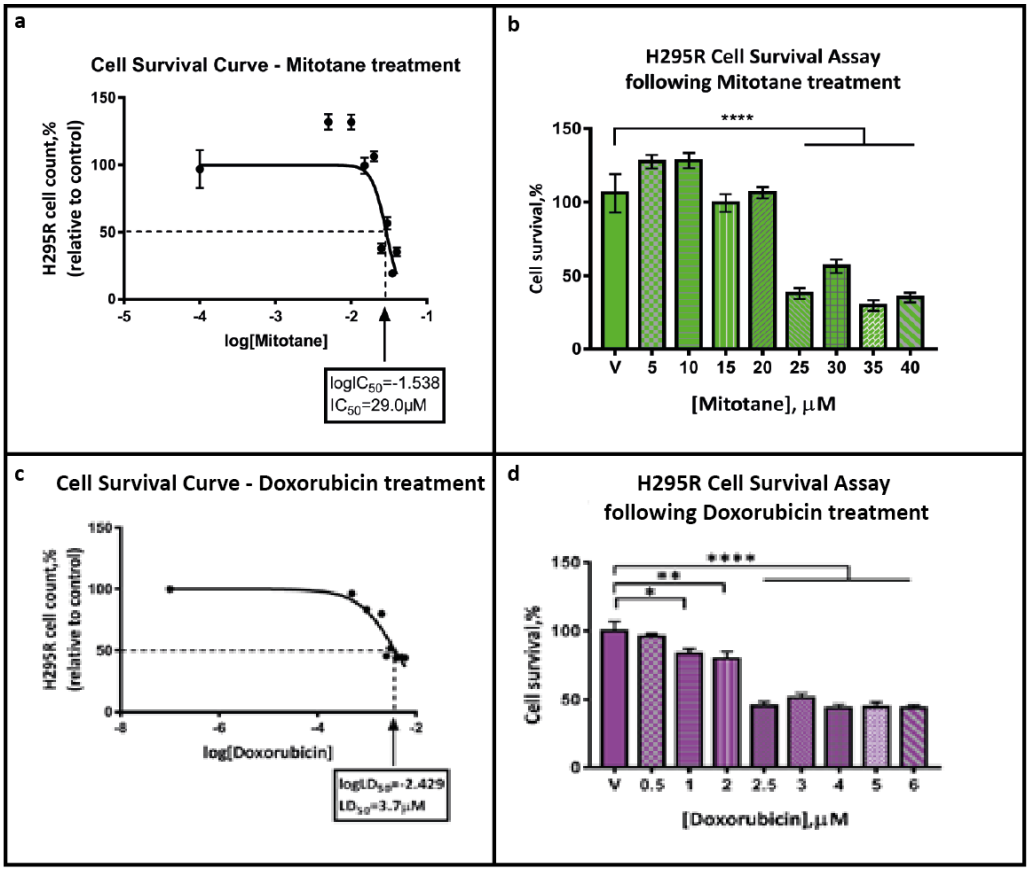

Figure 4.10 – H295R cell line response to 72-hour chemotherapeutic treatment with mitotane or doxorubicin. Figure showing results following chemotherapeutic treatment of H295R with increasing concentrations of either mitotane (a,b) or doxorubicin (c,d). Cell viability was measured after 72 hours and LD_{50} values where calculated; LD_{50} =29.0µm for Mitotane (a) and an LD_{50}=3.7µm for doxorubicin. Graphs (b) and (d) show % cell survival normalized to either vehicle for each concentration of drug used. Error bars represent standard error of the mean. For each drug n=3. Statistical analysis was performed using a one way ANOVA with significant difference being denoted as * ($p<0.05$), ** ($p<0.01$) and ****($p<0.0001$).

As shown in Figure 4.11a even at the highest concentration of 140 µM of 5-FU, more than 50% of cells were still viable. Despite the fact that LD_{50} was not reached, we still observed a significant decrease in cell viability in all treatment groups as compared to vehicle (Figure 4.11b). In the case of cisplatin H295R cells appeared to be non-responsive (Figure 4.11c), therefore we did not include this drug in future experiments.

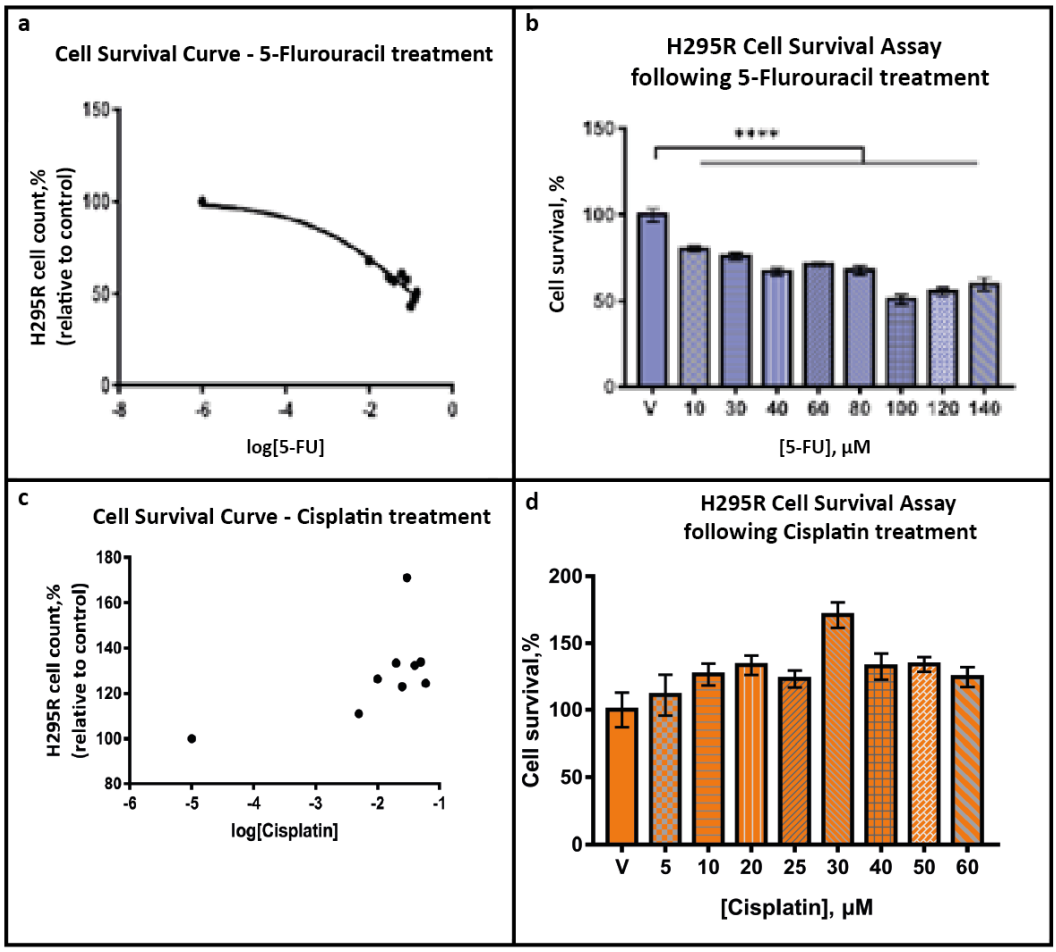

Figure 4.11 – H295R cell line response to 72-hour chemotherapeutic treatment with 5-Fluorouracil or cisplatin. Figure showing results following chemotherapeutic treatment of H295R with increasing concentrations of either 5-FU (a,b) or cisplatin (c,d). Cell viability was measured after 72 hours, however LD_{50} values could not be calculated due to lack of sufficient cell death even with the highest concentrations of 5-FU (a) and cisplatin (c). Graphs (b) and (d) show % cell survival normalized to vehicle for each concentration of drug used. Error bars represent standard error of the mean.

For each drug n=3. Statistical analysis was performed using a one way ANOVA with significant difference being denoted as ** ($p<0.01$) and ****($p<0.0001$).

After establishing the LD_{50} values we investigated whether surviving cells were enriched in DLK1 expression. We treated cells with mitotane and doxorubicin for 24 hours (short term) and 1 week (long term), in addition to 5-FU treatment for 1 week only. Following treatment, we performed flow cytometry analysis to evaluate the number of viable cells that were expressing DLK1 (DLK1+ cells). Following mitotane treatment we observed no difference in the % of cells that were DLK1+ after 24 hours, but we did observe a 5-fold increase in the % DLK1+ cells following 1-week mitotane treatment as compared to vehicle control (Figure 4.12). This increase however was not statistically significant. In the case of doxorubicin there was a significant 6-fold and 40-fold increase in the % of DLK1+ cells compared to vehicle following short and long-term treatment, respectively (Figure 4.12). Finally, long term treatment with 5-FU also resulted in a significant increase in the % of DLK1+ cells by approximately 20-times compared to the vehicle control (Figure 4.12).

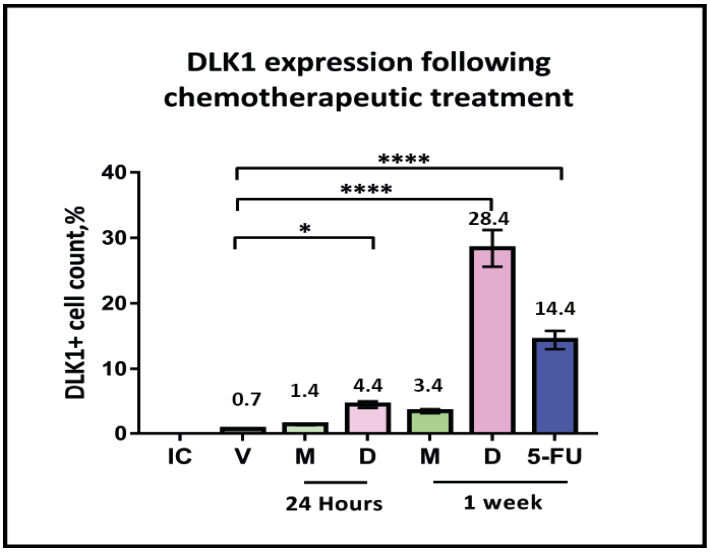

Figure 4.12 – Percentage of DLK1+ cells increases following chemotherapeutic treatment with Mitotane (M), Doxorubicin (D) and 5-Fluorouracil (5-FU). Flow cytometry results following short term (24 Hours) and/or long term (1 week) chemotherapeutic treatment with 30µM (24 hours) and 15µM (1 week) mitotane, 2µM (24 Hours) and 1µM (1 week) doxorubicin and 40µM (1 week) 5-FU, showed an

increase in the number of DLK1+ cells in all treatment groups as compared to the vehicle control. Error bars represent standard error of the mean. For each group n=3. IC=Isotype control; V=Vehicle. Statistical analysis was performed using one way ANOVA to compare treatment groups to control group and significance is denoted as **($p<0.01$) and ****($p<0.0001$).

The increase in the percentage of DLK1+ cells following chemotherapeutic treatment suggests that cells expressing DLK1 are more likely to survive chemotherapeutic treatment, evading their cytotoxic effects. In order to further study the effect of chemotherapy on DLK1+/DLK1- cells, we FAC-sorted DLK1+ and DLK1- H295R cells, as described previously in Figure 4.8. Collected cells were treated with increasing concentrations of mitotane for 24, 48 and 72 hours. Following treatment, cell viability of the cells was measured, and a cell-survival curve was constructed. We observed that in all 3 times points the LD_{50} values of DLK1+ cells were always significantly higher than those of DLK1- cells (Figure 4.13), meaning that a higher concentration of mitotane was required to kill 50% of DLK1+ cells compared to DLK1- cells. For example, following 24 hours of treatment DLK1+ cells showed an LD_{50} value of 30.76µM, while DLK1- cells had a significantly lower LD_{50} value of 24.47µM.

Finally, comparing cell survival of DLK1+ and DLK1- cells for individual concentrations of mitotane, we observed that there was a significant difference in cell survival between the two at lower concentrations of mitotane (5,10,20µM) after 24-hour treatment (Figure 4.14a). No significant difference was observed at higher mitotane concentrations. In addition, the significant difference in cell survival between DLK1+ and DLK1- cells seems to not only be concentration dependent but also time dependent. As can be seen in Figure 4.14b and 4.14c, which show cell survival after 48 and 72 hours treatment, there doesn't seem to be a significant difference in cell survival for mitotane concentrations of 10µM and 20µM. However, significant increase in DLK1+ cell survival following 5µM mitotane compared to DLK1- remains for all time points analysed (Figure 4.14). This suggests that DLK1+ cells are less

sensitive to chemotherapy compared to DLK1- cells, resulting in an increased ability to survive following treatment.

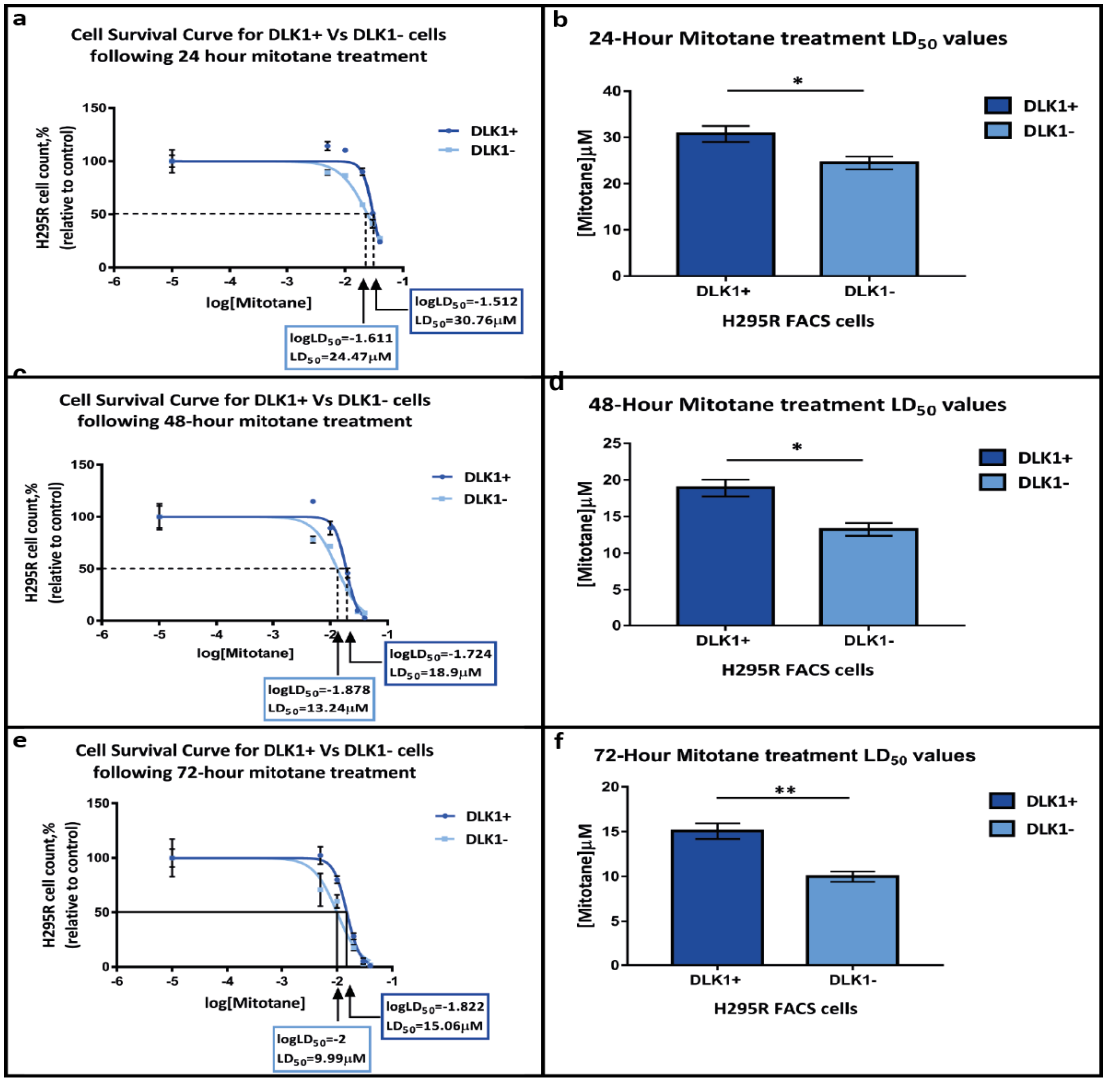

Figure 4.13 – DLK1+ H295R sorted cells display increased resistance to mitotane compared DLK1- sorted H295R cells. Figure showing comparative results following chemotherapeutic treatment of H295R FAC-sorted cells (DLK1+ Vs DLK1-) with increasing concentrations of mitotane. Cell viability was measured after 24 (a), 48 (c) and 72 (e) hours and LD_{50} values where calculated as shown in the respective graphs. Figures b,d and f display the LD_{50} value of each cell population (DLK1+ and DLK1-) for each time period and show a significant increase in the LD_{50} values for DLK1+ cells, as compared to DLK1- cells. Error bars represent standard error of the mean. For each time-point n=3. Statistical analysis was performed using an unpaired t-test and significance is denoted as *($p<0.05$) and **($p<0.01$).

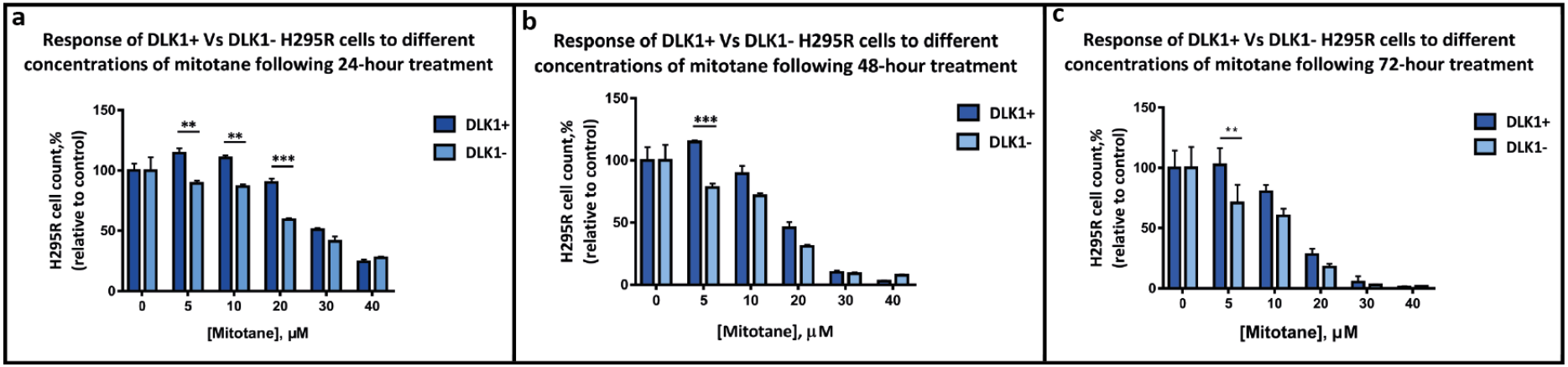

Figure 4.14 – DLK1+ H295R sorted cells show partial resistance to mitotane in a time and dose dependent fashion . Results following mitotane treatment of DLK1+ and DLK1- cells at 24 (a), 48(b) and 72(c) hours of treatment, show significantly increased cell survival of DLK1+ at lower mitotane concentrations as compared to DLK1- cells. Error bars represent standard error of the mean. For each time point n=3. Statistical analysis was performed using a two-way ANOVA with additional multiple comparisons tests. Statistical significance is denoted as **($p<0.01$) and ***($p<0.001$).

4.5 Discussion

Following the correlation of peak incidence of DCC occurrence and the second peak incidence of ACCs in humans at the age of 40-50 years old, we have now looked at the association between DLK1 expression and ACCs. In ACC sample tissues from human patients, expression pattern of DLK1 was heterogeneous, sometimes being clustered throughout the adrenal cortex and other times being expressed subcapsularly in a continuous manner. However, there was no observable pattern of DLK1 expression correlating to age or gender in the ACC samples analysed (unlike previously observed in normal adrenals). It has been demonstrated that in specific cancers like hepatoblastomas or gastrointestinal stromal tumours, DLK1 expression levels are associated with the disease outcome, making DLK1 a prognostic marker for those types of cancers [289, 290]. However, due to the lack of pre and post-operative patient details or pathological and/or histological reports of the tumour tissue, we were unable to study any potential correlation with disease outcome in the ACC samples.

Overall, DLK1 expression was significantly higher in ACC tissue as compared to control and ACA tissues, indicating that DLK1 expression level increase is specific to carcinoma only. This observation suggests that DLK1 could serve as a potential biomarker of ACC. However, to validate this hypothesis, more human ACC samples and patient histories would need to be gathered and analysed. Moreover, it would be valuable to look into the correlation of DCCs and ACC, and establish whether there is indeed a functional link between the two. We could investigate this by analysing the expression pattern of DLK1 in a greater number of samples, and performing a mutational analysis (for common ACC mutations) in DCCs and adjacent tissue in normal samples.

When culturing the H295R cells in a 3D environment to create spheroids, these spheroids were found to be enriched in DLK1+ cells, compared to adherent H295R cells. As spheroids are commonly used as a cancer stem cell model, we postulate that DLK1 could potentially be expressed in cancer stem cells in ACCs. Furthermore, DLK1

overexpressing/DLK1+ H295R cells showed increased expression of stem cell markers compared to DLK1 control cells, as well as higher clonogenic and proliferation abilities *in vitro.* Interestingly, DLK1 has been shown to be a marker of cells with cancer stem cell properties in different tumours, such as hepatocellular carcinoma and neuroblastoma, thus highlighting a potential role for DLK1 in tumour initiation and progression [291].

Cancer stem cells are also thought to be chemo-resistant, with the ability to evade the effects of chemotherapeutic agents. Therefore, we performed chemotherapeutic drug treatment to evaluate the response of H295R cells. Focusing on mitotane (gold standard of ACC treatment) and doxorubicin treatment, as these were the two drugs that H295R cells responded to, we showed that surviving cells were enriched in DLK1+ cells with % of DLK1+ cells increasing from 0.7% in control/ vehicle to 3.4% and 28.6% in mitotane- and doxorubicin- treated cells, respectively. This observation is further supported by cell survival curves following mitotane treatment of H295R DLK1+ and DLK1- cells for 24, 48 and 72 hours. We showed that LD_{50} values of DLK1+ were significantly higher compared to DLK1-, with actual values being 30.76µM (24hours), 18.9µM (48 hours), 15.06µM (72 hours) for DLK1+ and 24.47µM (24 hours), 13.24µM (48 hours), 9.94µM (72 hours) for DLK1-. This indicates that a higher concentration of mitotane is required to kill 50% of H295R DLK1+ cells as opposed to DLK1- cells, suggesting that DLK1+ cells are more resistant/less responsive to chemotherapy.

In this chapter we have shown that a population of DLK1-expressing cells exists in ACCs, and DLK1+ cells from a cancer cell line exhibit increased stem cell gene expression, higher clonogenicity, increased proliferative abilities, and reduced sensitivity to chemotherapy *in vitro*. These characteristics are in line with stem cell-like properties, and suggest that DLK1+ cells might represent cancer stem cells in ACCs. However, further studies would be required to validate this hypothesis, such as DLK1 knockout studies demonstrating a causative link between DLK1 expression and chemoresistance.

Chapter 5: Is Dlk1 involved in mouse adrenocortical regeneration and adrenocortical tumours?

5.1 Introduction

5.1.1 Mouse models of adrenocortical tumours

Mouse models have been extensively used in research to recapitulate human body functions and pathogenesis in order to aid the understanding of how different organ systems work and unveil the molecular mechanisms involved in their development and dysregulation, leading to normal function and tumourigenesis, respectively.

Multiple studies have indicated that there are several mouse models that can generate adrenocortical tumours and thus can be used to explore the molecular and cellular mechanisms leading to the development of these tumours. These models can occur naturally (either rare spontaneous forms or gonadectomy-induced) in certain mouse strains or by developing genetically engineered mice[292]. In susceptible mouse strains (DBA/2J, CE/J, C3H, NU/J, BALB/c and B6D2F1) prepubertal gonadectomy (GDX) has been shown to induce ACTs, which are hypothesized to arise from progenitor cell compartments within the adrenal glands[292-294]. However, not all strains are susceptible to GDX, with C57BL/6 being one of them. In GDX-sensitive strains or genetically modified GDX models the signalling between the gonads and the hypothalamic-pituitary axis is disrupted, resulting in an increase in gonadotropin hormones (LH and FSH), a decrease in inhibin production and adrenal gland activation of gonadal specific transcription factors (*Gata4*)[294-296].

Combined GDX with genetic manipulation of inhibin-α (Inha), which is either whole body Inha KO or transgenic expression of oncogenic SV40 from the Inha promoter (Inha/TAg), can lead to adrenal tumour formation[297](Table 5.1). Inhibin is a member of the TGFβ superfamily of cell signaling proteins, responsible for cell growth, differentiation and apoptosis. Loss of adrenal inhibin results in constitutive activation of downstream TGFβ effector proteins leading to tumourigenesis[292]. Different variations similar to the Inhα KO mouse model have been developed since, including Inhibin/TAg (Inhα /TAg) and Inhα/TAg; LHβ-CTP transgenic mice [298, 299],

which develop adrenocortical tumours, as well as Inhα/TAg; hpg (also lacking the GnRH receptor) which do not develop any tumours following GDX[300] (Table 5.1).

The 21-hydroxylase GATA4 (21-OH-Gata4) mouse model is a transgenic model with ectopic *Gata4* expression in the ZG, driven by 21-hydroxylase, and represents an additional ACT model. The GATA family of transcription factors, including GATA 4 and GATA 6, are important in the development, cellular reprogramming and differentiation pathways; with GATA 4 and GATA 6 expression driving gonadal and adrenal differentiation, respectively [292, 301]. In this ACT mouse model, adrenal neoplasia occurs both in intact and GDX mice[302](Table 5.1).

Table 5.1 – GDX induced ACT mouse models

Mouse model	Gene	Promoter	Phenotype
Inhα KO	*Inhibin-α*	Whole-body	Intact: Ovarian & testicular tumours GDX: Adrenal tumours
Inhα/TAg	*SV40*	6kb *Inhibin-α*	Intact: Granulosa & Leydic tumours GDX: Adrenocortical tumours
Inhα/Tag;LHβ-CTP	*SV40* *LH-β & hCG-β chimeric protein*	6kb *Inhibin-α* *LH-α*	Intact: Granulosa & ACT in females. Leydic cell tumours in males. GDX: ACAs
Inhα/Tag;hpg	*SV40* *GnRH*	6kb *Inhibin-α*	Intact: No tumours GDX: No tumours
21-OH-Gata4	*Gata4*	6.4kb Cyp21a1	Intact: Adrenal neoplasia GDX: Adrenal neoplasia

5.1.2 Lineage tracing techniques to study progenitor cell compartments in mice

Lineage tracing tools like the Cre-lox mouse model have been developed whereby specific cells of genetically engineered mice can be traced both spatially and temporally. The Cre-lox mouse is a genetically engineered mouse with a Cre or a tamoxifen-inducible CreERT2 gene incorporated after a cell-specific promoter. For the purpose of this project we will be using the Tg(Dlk1-cre/ERT2)26.10Ics

(DLK1$^{CreERT2/+}$) mouse model; meaning that CreERT2 will only be expressed in cell types that express Dlk1. CreERT2 is a fusion protein that consists of Cre recombinase and a mutant form of the human oestrogen receptor (ERT2). This receptor allows for temporal cytoplasmic expression of Cre recombinase, which upon tamoxifen administration becomes active and translocates to the nucleus. Without tamoxifen administration Cre recombinase is expressed in cells and remains in its inactive state in the cytoplasm (Figure 5.1).

The Cre-lox system can be used for lineage tracing when a Cre-lox mouse is crossed with a genetically modified mouse that contains a reporter gene, after a stop codon that is flanked by loxP sites. For the purpose of this project we will be using the DLK1$^{CreERT2/+}$;Rosa$^{Tm/Tm}$, developed by crossing the DLK1$^{CreERT2/+}$ mouse with the *B6.Cg-Gt(ROSA)26Sortm14(CAG-tdTomato)Hze/J (* Rosa$^{Tm/Tm}$)(kindly provided by Prof. Fiona Watt, King's College London) to perform lineage tracing of Dlk1+ progenitor cells and their progeny over a specific period of time. As shown in Figure 5.1, once Cre recombinase is activated, it translocates to the nucleus where it binds loxP sites and excises the stop codon allowing for the reporter gene to be expressed. In this way all cells that express the active Cre, as well as all their progeny from that point onward will be expressing the red fluorescent.

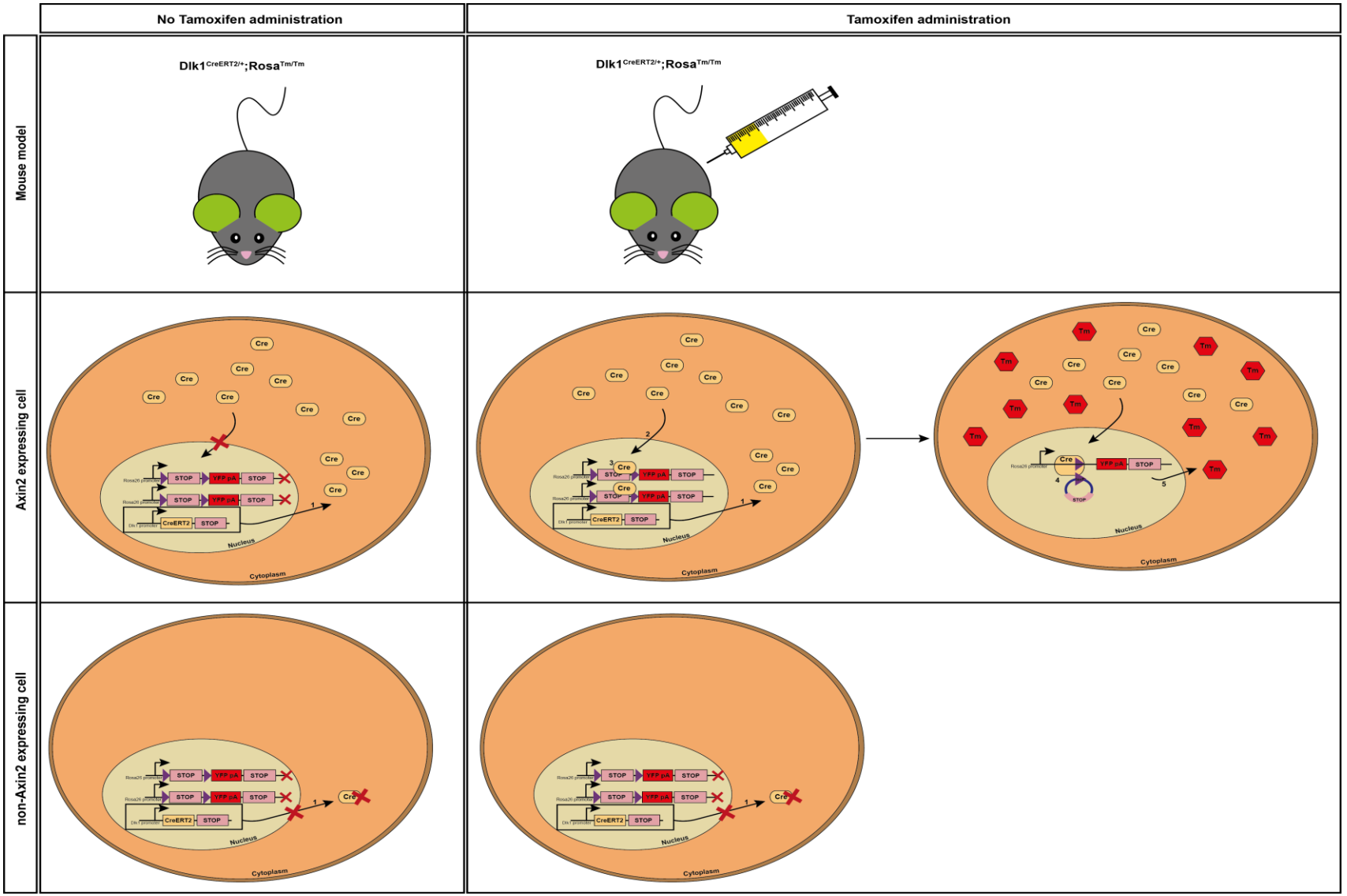
No Tamoxifen administration
Tamoxifen administration
Mouse model
Axin2 expressing cell
non-Axin2 expressing cell
Dlk1CreERT2/+;RosaTm/Tm
Dlk1CreERT2/+;RosaTm/Tm
Cre
Tm
STOP
YFP pA
CreERT2
Nucleus
Cytoplasm

Figure 5.1 – Inducible Cre-lox system. Schematic diagram illustrating the series of events occurring following tamoxifen injection in Dlk1 expressing (middle panel) and non-Dlk1 expressing (bottom panel) cells of $Dlk1^{CreERT2/+}$;$Rosa^{Tm/Tm}$ mouse.

The Gt(ROSA)26Sor$^{tm1(CAG-Brainbow2.1)Cle}$/J (R26R-Confetti) mouse model is a more complex version of the Rosa26$^{Tm/Tm}$, which allows for ubiquitous expression of more than one fluorescent protein. When Dlk1$^{CreERT2/+}$ transgenic mouse is crossed with the R26R-Confetti mouse to generate the Dlk1$^{CreERT2/+}$;R26R-Confetti transgenic mouse model (kindly provided by Prof. Fiona Watt, King's College London), the active Cre recombinase can now bind to a number of different loxP sites to perform either excision or inversion of the flanked DNA, resulting in a number of different outcomes as shown in Figure 5.2. In this case Dlk1+ cells can either express green, blue, red or yellow fluorescent protein depending on the type of Cre recombination. The progeny of each cell will retain the colour of the parent and the fact that different parent cells can express different fluorescent proteins allows for clonal analysis of the cell population.

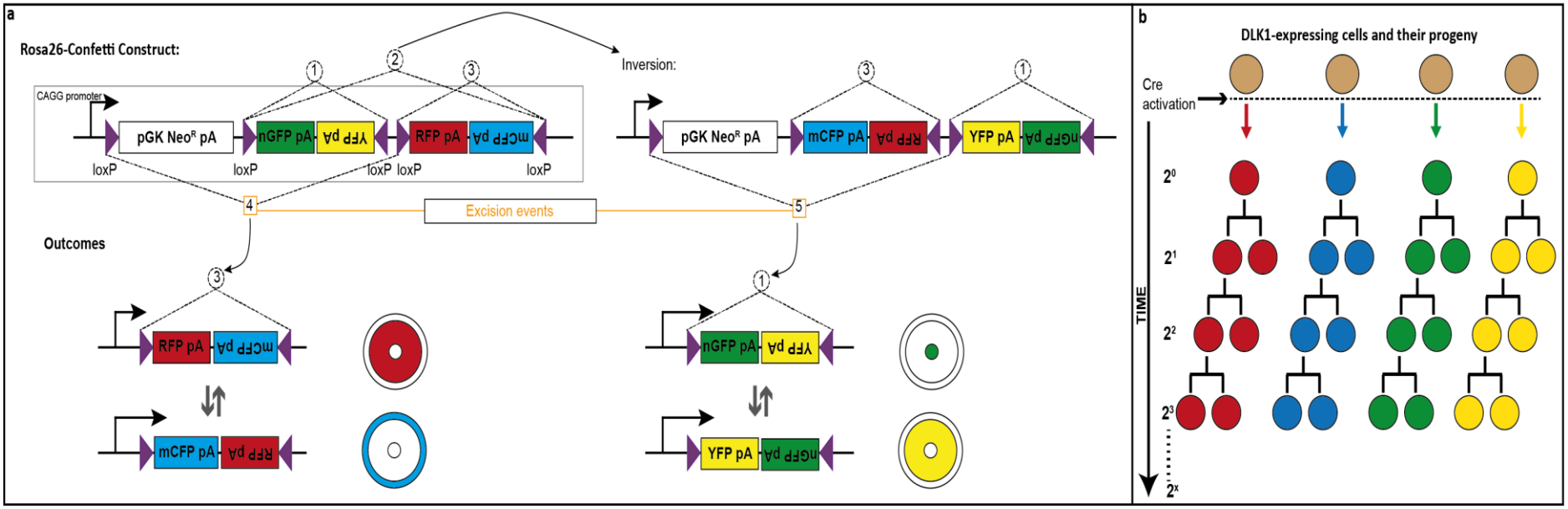

Figure 5.2 – R26R-Confetti transgenic mouse model. Schematic diagram showing inversion(1-3) and excision (4,5) recombination events of DNA segments flanked by loxP sites following Cre activation resulting in four different outcomes (expression of either RFP, CFP, GFP and YFP). Schematic diagram (b) illustrates the events following Cre activation, where Dlk1+ cells can express 1 of 4 colours, resulting in all their progeny expressing the same colour as the parent. Over time the number of cells arising from the same parent cell and thus expressing the same FP will increase exponentially and allow for clonal analysis of different cell populations.

5.1.3 Hypothesis

We hypothesise that Dlk1+ capsular cells might be involved in adrenocortical maintenance in mice, and could potentially lead to the generation of adrenocortical tumours.

5.1.4 Aims

1. Evaluate whether Dlk1 expression is localised in the region of adrenocortical hyperplasia in mouse models of ACTs, using IHC.
2. Investigate the involvement of Dlk1+ cells in adrenocortical cell maintenance, using the $Dlk1^{CreERT2/+}$;$Rosa^{Tm/Tm}$ lineage tracing mouse model.

5.2 Dlk1 expression in mouse models of ACT

Adrenocortical tumorigenesis in mice is thought to begin with hypertrophy of capsular cells, generating capsular/subscapular hyperplasia, which over time extends into the cortex altering the cytoarchitecture and zonation, and forming tumours. Therefore, we aimed to study the expression of Dlk1 in mouse models of ACT. For this purpose, we used the DBA and Inha/Tag mouse models (sections were kindly provided by Dr. Rahman alongside their controls), both of which are models of ACT and exhibit subcapsular hyperplasia (Figure 5.3). Immunohistochemical analysis of Dlk1 in control (Wild type) mice resulted in abundant Dlk1 expression in the adrenal medulla and capsule (as expected) (Figure 5.3a, a'). In both ACT mouse models, Dlk1 was again mainly localised in the adrenal medulla and capsule only and not expressed in regions of adrenocortical hyperplasia/tumours (Figure 5.3b, b', c, c'). In the DBA model we could observe a few cells within the adrenal hyperplasia, that possibly express low levels of Dlk1, however the vast majority of the cells were negative (Figure 5.3b').

These results might initially suggest that Dlk1 cells are not the cells of origin in these models of ACTs. However, it might still be possible that cells found in the areas of adrenal hyperplasia could derive from Dlk1+ cells in the capsule that migrate in the cortex, and act as tumour initiating cells, while losing expression of Dlk1. In order, to prove this hypothesis we first sought to investigate the fate of Dlk1 capsular cells in normal physiological and pathological conditions to show whether these cells can act as adrenocortical precursors.

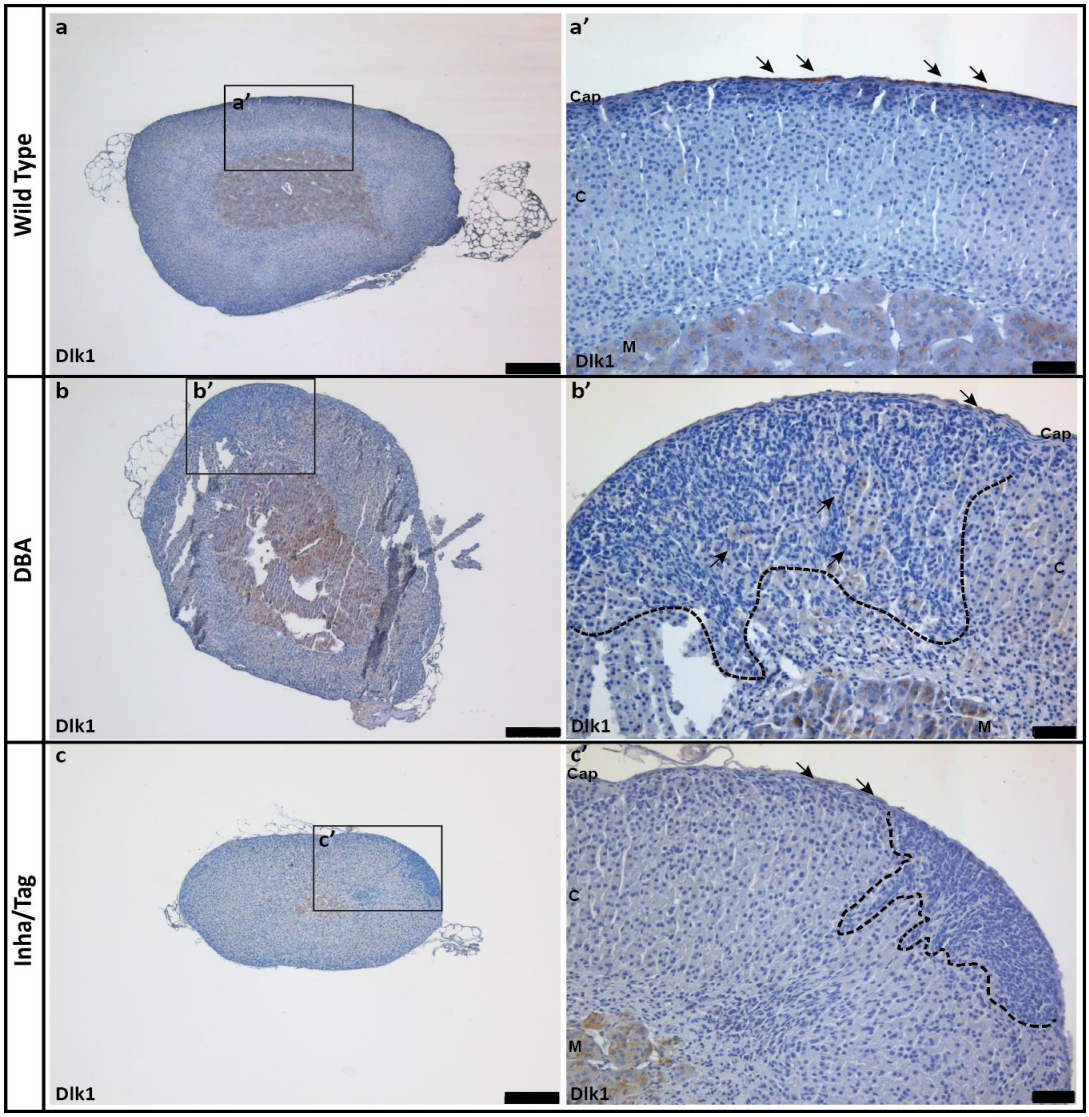

Figure 5.3 – Dlk1 expression in mouse models of adrenocortical tumours. Immunohistochemical analysis of Dlk1 expression in normal adrenal of wild type mice (a,a') and two ACT mouse models, the DBA (b,b') and Inha/Tag (c,c'), exhibiting adrenocortical hyperplasia (b,b',c,c'). Black arrows are showing areas of Dlk1 expression. n=3, Scale bars 250µm (left panels) and 50µm (right panels).

5.3 Lineage tracing of DLK1 capsular cells in the mouse adrenal gland

To investigate whether capsular Dlk1 cells are able to delaminate from the capsule and migrate into the cortex to become steroid-producing cells, we used the Dlk1$^{CreERT2/+}$;Rosa$^{Tm/Tm}$ to trace these progenitors over time. This model was generated at King's College London in Fiona Watt's group, by crossing the Tg(Dlk1-DLK1$^{CreERT2/+}$ mouse with the Rosa$^{Tm/Tm}$ mouse, as shown in Figure 5.4.

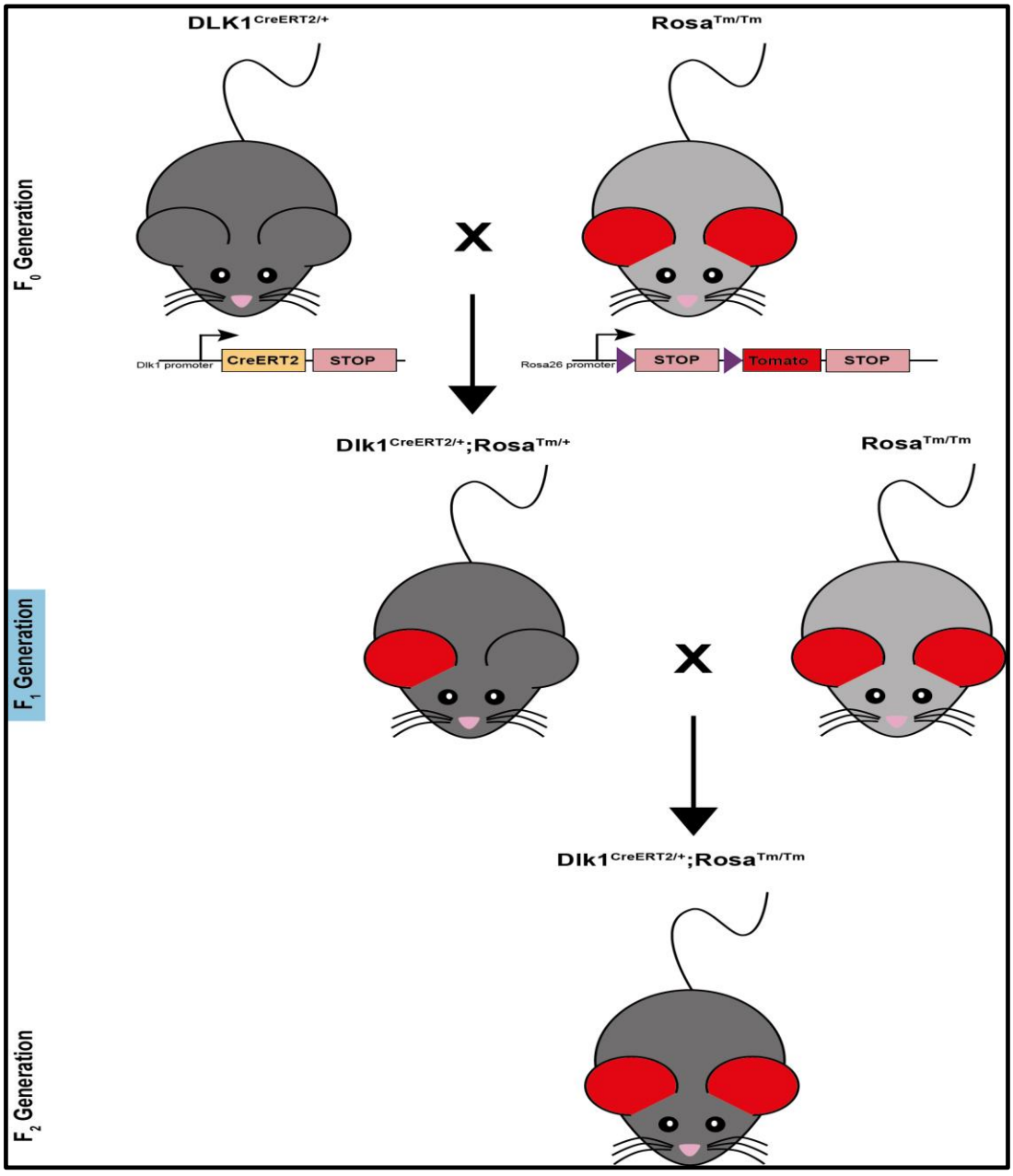

Figure 5.4 – Generation of the Dlk1$^{CreERT2/+}$; Rosa$^{Tm/Tm}$ transgenic mouse model. Schematic diagram depicting the individual mouse models used and crosses performed to generate the final transgenic mouse model for the lineage tracing experiments of Dlk1+ cells.

Mice were injected at P0 and the adrenals were collected when the mice were 2 years old as shown in Figure 5.5a. We collected the mouse adrenals and performed immunostaining for tomato expression to mark all Dlk1+ cells at time of injection as well as their progeny. Following immunohistochemistry, we observed that patches of cells in the cortex were positive for the staining (Figure 5.5 c,e,f), confirming that Dlk1+ cells originally found in the capsule can indeed give rise to Dlk1- cells in the cortex under normal physiological condition. In addition, the adrenal medulla was also stained, as expected. However, even after a two-year chase, there were still vast areas of the adrenal cortex that were negative, which shows that they did not descend from Dlk1+ capsular cells in the adult mouse. This suggests that additional stem/progenitor cell populations are responsible for adrenocortical self-renewal.

Additionally we wanted to use the DLK1$^{CreERT2/+}$;R26R-Confetti transgenic mouse, to investigate the migration of individually marked DLK1+ cells in the cortex. As explained earlier this mouse model will allow for clonal analysis and tracing of DLK1+ cells from the capsule. Following three months chase (performed at KCL), we obtained the adrenals of the DLK1$^{CreERT2/+}$;R26R-Confetti mice for analysis. As shown in Figure 5.6 only a few medullary cells were fluorescent. We could not observe any fluorescent cells in the capsule or cortex of these adrenals. This result is probably due to the low recombination efficiency, as indicated by low number of cells expressing the fluorescent proteins in the medulla (region of high Dlk1 expression). However, optimization of this technique will provide with a very useful lineage tracing mouse model.

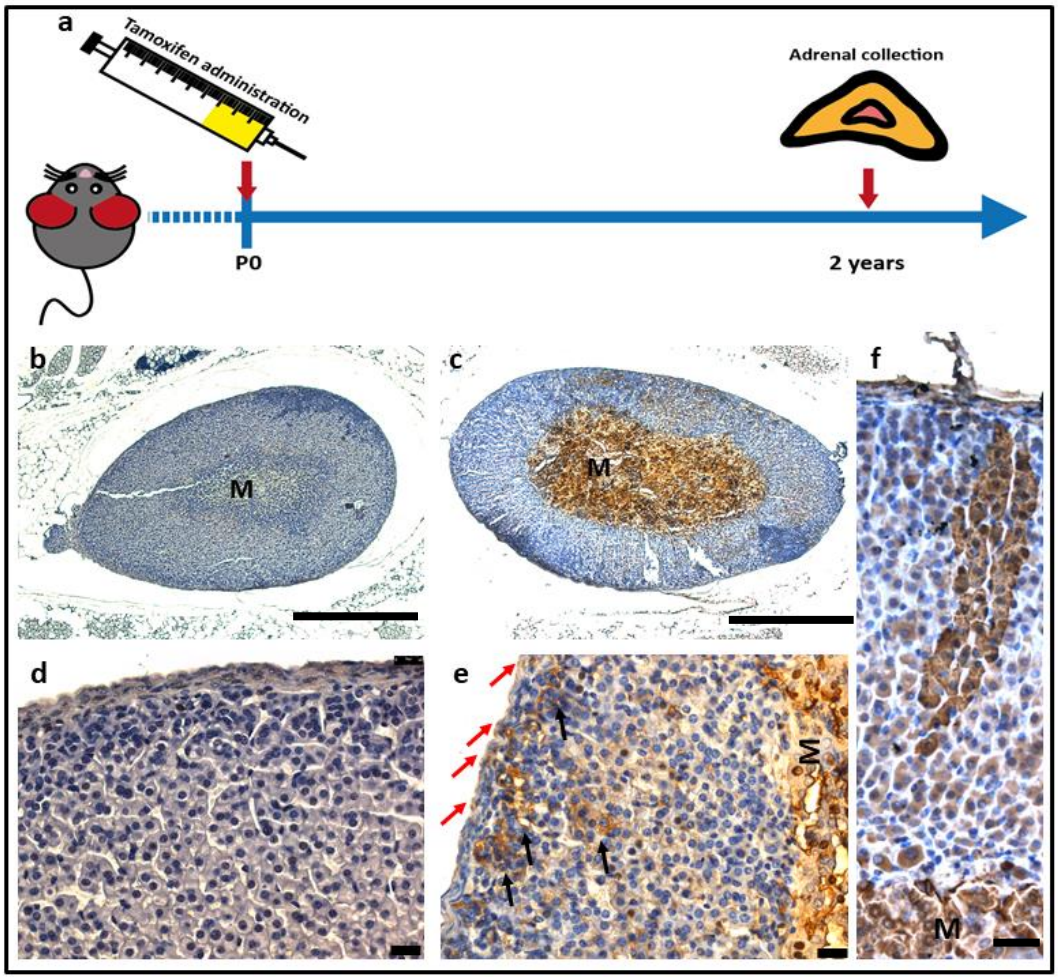

Figure 5.5 - Lineage tracing of Dlk1+ cells in the mouse adrenal gland. Schematic diagram (a) showing a timeline of tamoxifen injection at P21 and mouse adrenal collection 2 years later. Results following 2 years of chase show expression of tomato marking capsular Dlk1 cells (red arrows) and cortical descendants (black arrows) (c,e,f). Negative controls (b,d) show no tomato expression. n=3. Scale bars: 500Mμ (b,c) and 75μM (d,e,f). M=medulla.

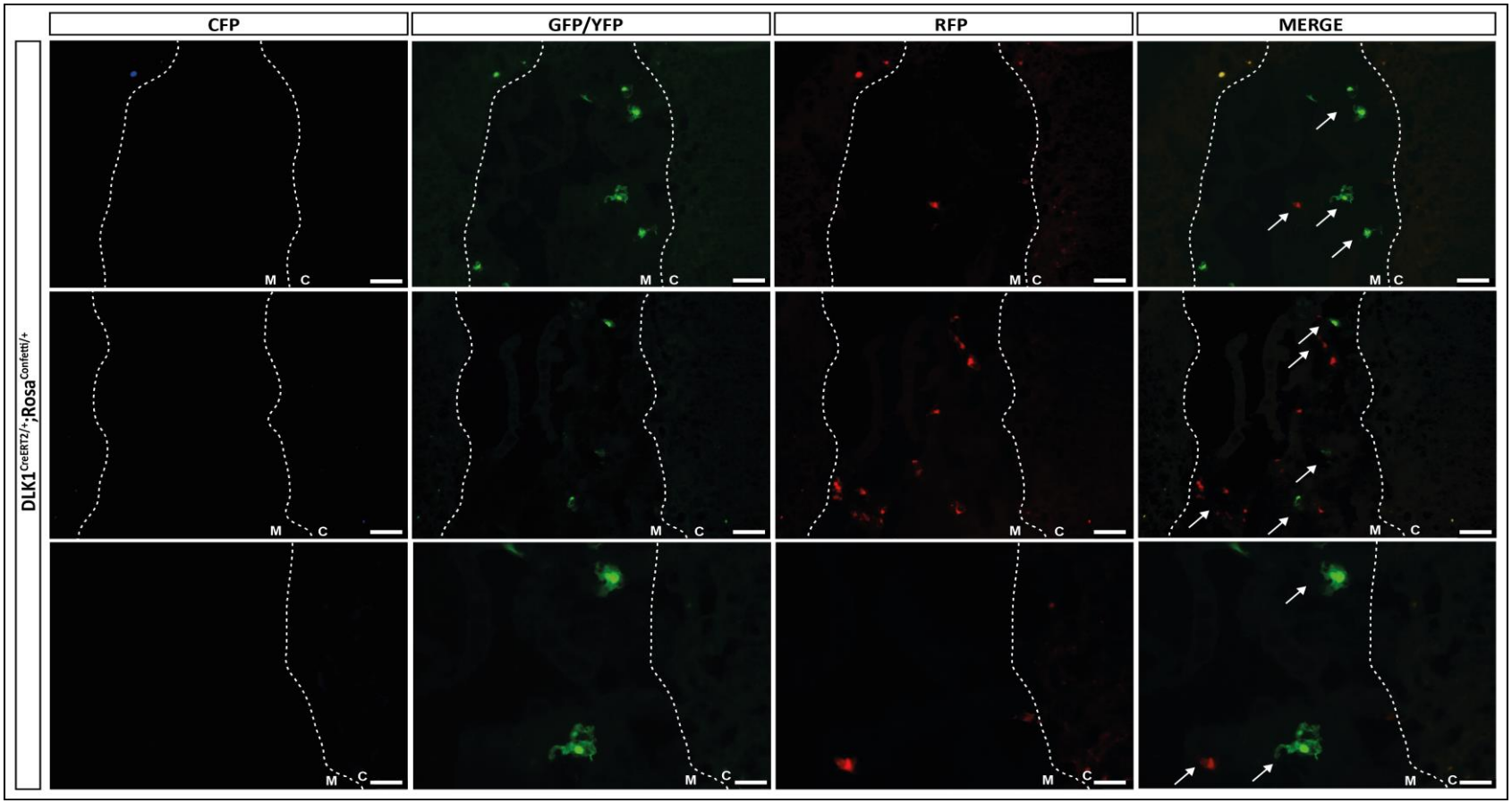
CFP
GFP/YFP
RFP
MERGE
DLK1CreERT2/+;RosaConfetti/+
M
C

Figure 5.6 - DLK1$^{CreERT2/+}$;R26R-Confetti transgenic mouse model as a promising adrenal progenitor cell tracing tool. Results following 3 months chase of the DLK1$^{CreERT2/+}$;Rosa26-Confetti mouse showing a few cells expressing either GFP/YFP or RFP in the adrenal medulla (indicated by white arrows). It is clear from the figure that poor FP expression is due to very low percentage of recombination events. n=3. Scale bar:50µM. M=medulla; C=cortex.

5.4 Discussion

In mouse models of ACC, we did not observe Dlk1 expression in the adrenocortical hyperplasia region of the cortex (representing pre-cancerous lesions). This suggests that the proliferating capsular cells leading to hyperplasia are not Dlk1+. However, based on these results we cannot rule out the possibility that capsular Dlk1+ cells delaminate into the cortex, lose Dlk1+ expression, and give rise to Dlk1- cells that are involved in the adrenal hyperplasia in ACT mouse models. To assess this possibility, we could trace Dlk1+ progenitors in ACT mouse model strains that are sensitive to gonadectomy-induced adrenal tumours (used here) and crossing them with a lineage-tracing mouse model (also used here). This would allow us to trace Dlk1+ cells and their progeny following gonadectomy, and investigate whether the capsular Dlk1+ cells would be involved in the formation of adrenal hyperplasia.

We could not obtain a lineage tracing ACT mouse model due to project license and time restrictions. Therefore, we used the $DLK1^{CreERT2/+}$;$Rosa^{Tm/Tm}$ mouse model to investigate whether Dlk1+ capsular cells migrate into the cortex. Following 2 years of chase, we observed stained cells in the cortex, supporting our hypothesis that Dlk1+ cells might give rise to adrenal tumours (even though we could not observe Dlk1 staining in the hyperplastic region). The importance of this finding is two-fold. Firstly, the fact that Dlk1+ cells can give rise to different types of cortical cells suggests that it could be possible for the cells that form part of the adrenocortical hyperplasia, to have risen from Dlk1+ cells in the capsule. Secondly, we have potentially identified a previously unreported capsular stem cell population able to give rise to adrenocortical progenitor cells in the mouse. However, it should be noted that these experiments are limited to long-term traces only, as these were the only mice available when they were obtained from King's College. While Dlk1 is not expressed in the cortex under normal physiological conditions, we could perform additional shorter traces (as a negative control) to verify the origin of the cells stained in the cortex.

The molecular mechanisms underlying adrenal gland regeneration and maintenance in the mouse are not fully characterised. Identifying the molecular pathways and key elements involved in adrenocortical maintenance will provide a better understanding of adrenal gland pathogenesis and tumour formation. The current model of adrenocortical regeneration suggests that Gli1+ cells in the capsule receive signals from Shh+ cells in the subcapsular region, to delaminate into the capsule and become Shh+/Gli1- adrenocortical progenitor cells. These progenitor cells then differentiate into ZG and then ZF cells by centripetal unidirectional differentiation to repopulate the adrenal cortex upon demand [101, 109] (Figure 5.9). The exact mechanism that causes these Dlk1+ cells to delaminate in the cortex is not known, yet it would be interesting to evaluate whether capsular Dlk1+ cells represent the same population of cells as Gli1+ cells. Unfortunately, we were unable to verify this hypothesis due to the lack of reliable antibodies targeting Gli1.

In conclusion, we show that Dlk1+ capsular cells could represent progenitors of adrenocortical steroidogenic cells in mice, building on the current model of Gli1+ cells being the main stem cell population involved in adrenal regeneration.

Chapter 6 – Conclusion and Future work

6.1 Characterisation of DCCs in human adrenal glands

Adrenal glands are vital endocrine organs essential for survival. Research providing insights into the function and disease of these organs is crucial for understanding how adrenal glands work, what mechanisms are involved in adrenal pathogenesis, and how to restore adrenal functionality. Adrenocortical carcinoma is one of the most serious, yet rare adrenal diseases with an incidence rate of 1-2 per million per year, and a median overall survival of 5 years. Given that human adrenal research is limited, the aim of this project was two-fold:

- To better characterise the human subcapsular region of the adrenal cortex, focusing on the identification of progenitor cell populations.
- To evaluate DLK1 expression in the adrenal cortex and potential involvement in ACC formation and maintenance.

We have shown here that in contrast to rodents, human adrenocortical zonation is more complex. We have confirmed the presence of CYP11B2+ cells in the ZG as either clustered APCCs or continuous, as previously described by Nishimoto and colleagues; and confirmed the expression of CYP11B1 and CYP17 in the ZF [187, 303] (Figure 6.1). Furthermore, we have identified a unique region in the subcapsular region of the human adrenal cortex that does not express steroidogenic enzymes CYP11B2 and CYP11B1, and hypothesised that this cell population could represent the human ZU.

In an attempt to characterise the ZU, we have shown that aldosterone producing cells (CYP11B2+) cells also express DAB2 (Figure 6.1). In addition, we demonstrated that VILIP1 is expressed in the subcapsular region, predominantly in cells that do not express CYP11B2 (Figure 6.1). We were unable to evaluate the presence of cell populations expressing both VILIP1 and DAB2, since both antibodies for VILIP1 and DAB2 were from the same host. Given that CYP11B2+ cells also express DAB2, we hypothesise that the minority of cells expressing both VILIP1 and CYP11B2 will also express DAB2. However, VILIP1 or DAB2 do not represent suitable markers of the ZU due to their partial co-expression with CYP11B2 (which is expressed in the ZG). This

does not exclude the possibility that some ZU cells might be positive for either of the two proteins, but it concludes that VILIP1 and DAB2 are not exclusively present in the ZU.

We also showed that DLK1 is also expressed in the subcapsular region of the human adrenal cortex either in a continuous-layered manner or clustered (DCCs), similar to CYP11B2 expression. However, following double immunostaining of CYP11B2 and DLK1, we demonstrated that the two proteins are not co-expressed and thus represent distinct cell populations in the subcapsular region (Figure 6.1). DLK1 expression in the subcapsular region of the human adrenal cortex has not been described previously.

Studies in rodents have identified DLK1 expression in the adrenal capsule in mice and the ZU region in rats (located between the ZG and the ZF). DLK1+ cells in rodents have been shown to represent stem or adrenocortical progenitor cells in the adrenal glands of mice and rats, respectively. Other than this, little is known about the function of DLK1 in the adrenal gland. Research in adipose tissue has identified DLK1 as a pre-adipogenic marker, that acts to maintain progenitor cells in an undifferentiated state[131]. Combined with the finding that DLK1 is not co-expressed with steroidogenic enzyme CYP11B2 (marking ZG cells) in the human adrenal cortex, we speculate that the novel DLK1+ cell population we have identified here in the subcapsular region, could potentially represent the adrenocortical progenitor cells of the ZU in humans.

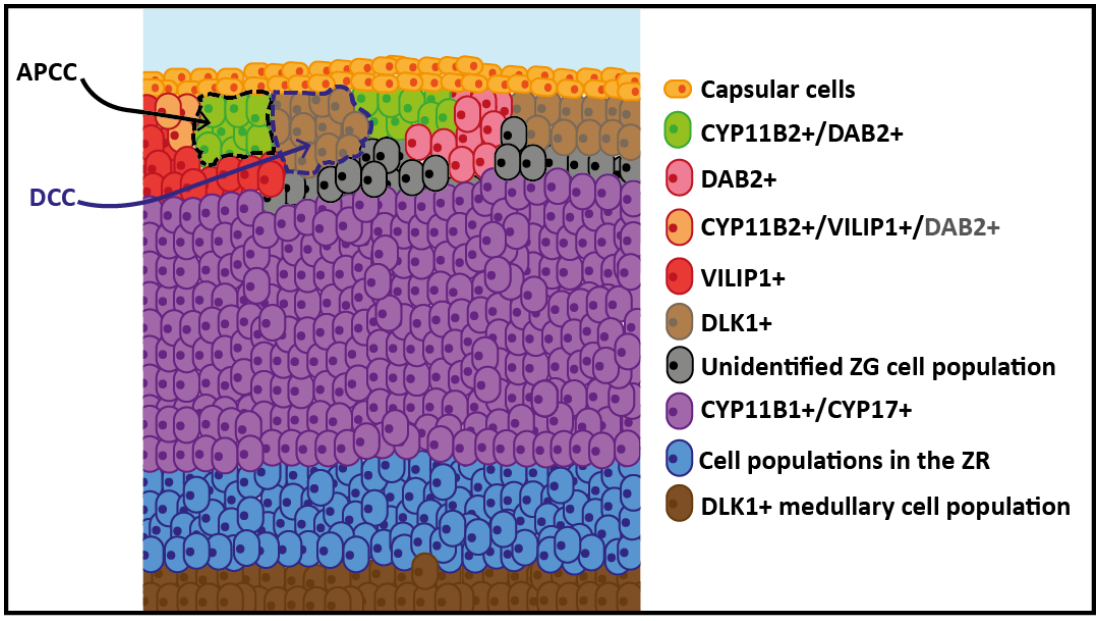

Figure 6.1 – Characterisation of subcapsular region in the human adrenal gland showing presence of DCCs. Schematic diagram illustrating the cell organisation and cell populations identified in the subcapsular region of the adrenal gland. The figure shows the presence and location of known cell populations including CYP11B2+, CYP11B1+ and CYP17+ and APCCs, in addition to the newly identified cell populations we present here including DAB2+, VILIP1+, CYP11B2/DAB2+, CYP11B2+/VILIP1+, DLK1+ cells and DCCs.

Additional analysis on DLK1 expression revealed that the expression pattern of DLK1 was age-dependent. Specifically, younger individuals showed a continuous expression of DLK1 until the age of 25, after which a transition from layered continuous to clustered expression was observed. Individuals of 40 years of age or more were found to have a statistically significant higher number of DCCs as opposed to younger individuals (Figure 6.2). DCC formation occurrence showed no significant correlation with gender. Notably, this increase in DCC appearance in individuals over 40 years of age correlated to the second peak incidence of ACC, which occurs in individuals aged 40-50 years. This was an interesting finding and we wanted to investigate whether there was any relationship between DCC appearance in the adrenal glands and ACC formation.

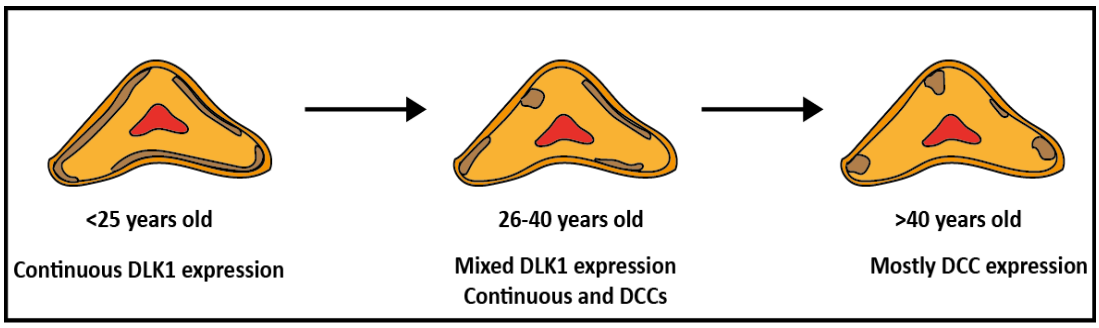

Figure 6.2 – DLK1 expression transitions from continuous to clustered expression with increasing age in human adrenal glands. Schematic diagram showing DLK1 expression change from continuous expression in young individuals (left) to a mixed DLK1 expression (continuous and clustered) in 26-40 year olds (middle) and a predominant clustered expression, with formation of DCCs in aged individuals (40+ years old).

6.2 DLK1 as a potential biomarker for ACC formation

In addition to the correlation between DCC appearance and ACC second peak incidence, we showed that DLK1 expression is significantly higher in ACC (approx. 40%) as compared to normal adrenals (approx. 5%) and adrenals from patients with ACA (approx. 2%). This shows that DLK1 is specifically overexpressed in ACCs, which suggests that DLK1 expression might have a direct or indirect role in carcinoma formation and/or maintenance. We hypothesised that DLK1 might be a potential biomarker for ACC and that DLK1+ cells might represent cancer stem cells. DLK1 represents a prognostic biomarker in other types of cancer such as hepatocellular carcinoma and offers a promising candidate for the development of novel therapies aiming to target cancer stem cells[157, 158, 304].

Our *in vitro* studies show that DLK1 is enriched in spheroids, an accepted cancer stem cell model (see Section 4.3 for details on spheroids). Moreover, increased colony formation and cell proliferation are also in line with the hypothesis that DLK1+ cells have cancer stem cell-like properties *in vitro*. This was in accordance with previous studies by Xu and colleagues, focusing on hepatocellular carcinoma, which also use spheroid models and colony formation and proliferation assays, to conclude that

DLK1+ cells do indeed possess cancer stem cell properties[157]. Additionally, gene expression profiling of the H295R cell line overexpressing DLK1 showed an increased expression of stem cell markers and a decrease in the expression of steroidogenic markers. A potential future experiment to confirm that DLK1+ cells represent a population of cancer stem cells, could include mouse studies looking at the tumorigenic ability of isolated human adrenal DLK1+ and DLK1- cells *in vivo*.

We also showed that treatment of H295R (an adrenocortical carcinoma cell line) with chemotherapy shows an enrichment in DLK1 following treatment. This suggests that cells expressing DLK1 are more likely to survive treatment and are more resistant to the effects of chemotherapy compared to cells that do not express DLK1. In addition, comparative analysis of DLK1+ and DLK1- H295R sorted cells showed a significant increase in the LD_{50} values of the drugs when treating DLK1+ H295R cells as opposed to DLK1-. Importantly, our observations do not directly show a causal link between DLK1+ cells and the effect of chemotherapy, but rather a correlation between the two. In order to demonstrate whether DLK1 plays a direct role in chemoresistance, future work could involve generating a DLK1-knockout H295R cell line and investigate to what extent this cell line remains resistant to chemotherapy.

6.3 Potential role of DCCs in ACC formation

In the previous sections we have described the appearance of DCCs in normal human adrenals, predominantly in individuals of 40 years of age or more. The timing of this transition corresponds to the second peak incidence of ACCs in humans. Notably, the transition from a continuous expression pattern to a clustered pattern with increasing age, was similar to the CYP11B2 expression pattern change observed in human adrenals previously described by Aiba and Fujibayashi[230]. Moreover, research focusing on these CYP11B2 clusters (APCCs) in normal human adrenals has shown that these APCCs harbor mutations most commonly found in APAs. Therefore, APCCs are now considered as a potential pre-cursor population of APAs[187, 305] (Figure 6.3).

Given that DCC formation also correlates with second peak incidence of ACCs, and DLK1+ cells appear to possess some cancer stem-cell like characteristics *in vitro*; we postulate that DCCs in normal adrenal glands might accumulate mutations that are commonly found in ACCs, ultimately leading to ACCs (See Figure 6.3).

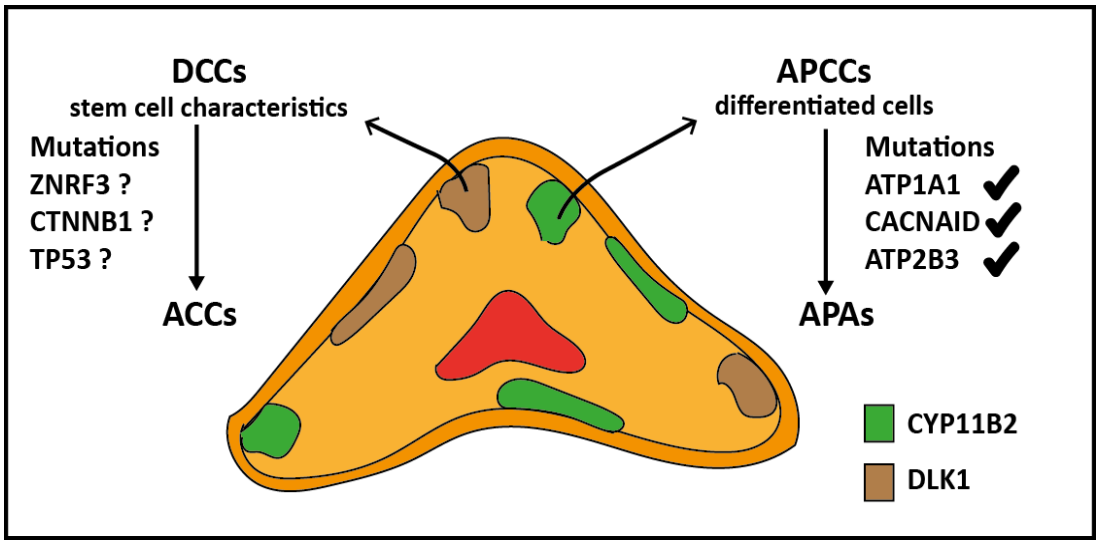

Figure 6.3 – Working model showing how DCCs could be precursors of ACCs in a similar way APCCs are suggested precursors of APAs. Schematic diagram showing the common APA mutations identified in APCCs of normal adrenals, making them a suggested APA precursor (right). In addition, this diagram shows our working hypothesis that DCCs in normal adrenals could be ACC precursors that over time accumulate mutations commonly found in ACCs (left).

To validate the hypothesis that DCCs could lead to ACCs, future work could include an analysis geared towards assessing the prevalence of genetic mutations in DCCs in genes commonly mutated in ACCs (e.g., *ZNRF3*, *CTNNB1*, *TP53*, *CDKN2A*, *MEN1*, *TERT*, *PPKAR1A* and *NF1*). A comparison of genomic DNA from DCCs and adjacent tissue from normal adrenals could indicate whether these mutations are more common in DCCs, which would be in line with the hypothesis that DCCs could be a precursor of ACCs.

Furthermore, it could prove useful to gain further insights on the gene expression profile of DLK1+ cells. Future experiments could include sorting DLK1+ and DLK1-

primary cells from normal and adrenocortical carcinoma tissue, for RNA sequencing analysis. If DLK1 is involved in tumour initiation/pathogenesis, a detailed analysis of the transcriptome could shed light on the mechanisms involved in this process and its potential role in chemoresistance.

6.4 *In vivo* mouse models of adrenal tumours

Finally, our *in vivo* research in mouse models was aimed at studying whether Dlk1 could be in involved in tumour initiation and/or progression. We used *in vivo* cancer models displaying adrenal hyperplasia, and showed that Dlk1 is not expressed in the hyperplastic region.

Notably, this finding did not exclude the possibility that capsular Dlk1-expressing cells migrate into the cortex to form the hyperplasia and cease to express Dlk1. In line with this potential scenario, we showed that Dlk1+ capsular stem cells do indeed give rise to differentiated steroidogenic cells of the adrenal cortex through lineage-tracing experiments. However, this only indicates that Dlk1-expressing cells give rise to cells in the adrenal cortex but not necessarily adrenal hyperplasia. To demonstrate whether Dlk1+ capsular cells give rise to adrenal hyperplasia in cancer mouse models, a potential future experiment could be to generate a Dlk1 lineage tracing cancer mouse model by crossing the cancer mouse models (e.g., DBA and Inha/Tag) with a $DLK1^{CreERT2/+}$;$Rosa^{TM/TM}$ transgenic mouse. This would allow Dlk1 tracing concurrently with cancer induction upon gonadectomising the mice. As a result, this would confirm whether Dlk1+ capsular cells and their progeny give rise to adrenal tumours in cancer mouse models.

Collectively, our data suggests that DLK1 could serve as a possible biomarker for ACC, while DLK1+ cells could act as a potentially novel target for ACC treatments. However, additional research is required to confirm our results and further elucidate the potential role of DLK1+ both in normal adrenals and ACCs.

Chapter 7 – *Sgpl1*$^{-/-}$ transgenic mouse as a disease model to study primary adrenal insufficiency

7.1 Introduction

Primary adrenal insufficiency (PAI) is a condition where the adrenal glands fail to produce adequate levels of hormones (aldosterone or cortisol), and is most commonly congenital in children. PAI can present alone or in combination with other comorbidities; it is associated with reduced life expectancy and can be life-threatening if undetected. The main mechanisms of the disease include ACTH resistance, adrenal dysgenesis, defects in steroid biosynthesis, cholesterol synthesis disorders, and metabolic disorders[306, 307].

The Metherell group's (our internal collaborator) main area of interest revolves around adrenal insufficiency syndromes and they have identified a number of genes responsible for these syndromes within their cohort of patients (n>350)[308-312]. However, even after thorough investigation, the underlying genetic cause of 38% of cases in this cohort remained unknown. In a recent project that formed part of our collaboration, they identified novel loss-of-function homozygous mutations in *SGPL1* as the cause of primary adrenal insufficiency and steroid-resistant nephrotic syndrome in a subset of their patient cohort (n=8, 5 different families) (Table 7.1)[313].

This study is the first report that identified *SGPL1* deficiency in humans as being involved in adrenal disease. *SGPL1* encodes sphingosine-1-phosphate lyase (SGPL1), an ER enzyme which plays an important role in sphingolipid catabolism by mediating the irreversible cleavage of the lipid-signaling molecule sphingosine-1phosphate (S1P), thus regulating the flow of sphingolipid biochemical intermediates. (Figure 7.1). S1P in turn regulates cell migration, differentiation and survival, as well as other complex physiological processes. Overall, sphingolipids play important roles as either structural cell components or signaling molecules[313].

Table 7.1 - *SGPL1* mutations identified in PAI patient cohort

Patient	Gender	Ethnicity	Age at last review	*SGPL1* mutation
1*	Male	Pakistani	5 years	c.665G>A; p.R222Q
2	Male	Pakistani	8 years	c.665G>A; p.R222Q
3	Male	Pakistani	3 years	c.665G>A; p.R222Q
4	Male	Saudi	3.6 years	c.665G>A; p.R222Q
5*	Female	Turkish	5.9 years	c.1633_1635delTTC; p.F545del
6*	Male	Peruvian	8.4 years	c.261+1G>A; p.S65Rfs*6
7*	Female	Peruvian	2.4 years	c.261+1G>A; p.S65Rfs*6
8*	Female	Spanish	17.5 years	c.7dupA; p.S3Kfs*11

* Patients also presented with steroid-resistant nephrotic syndrome.

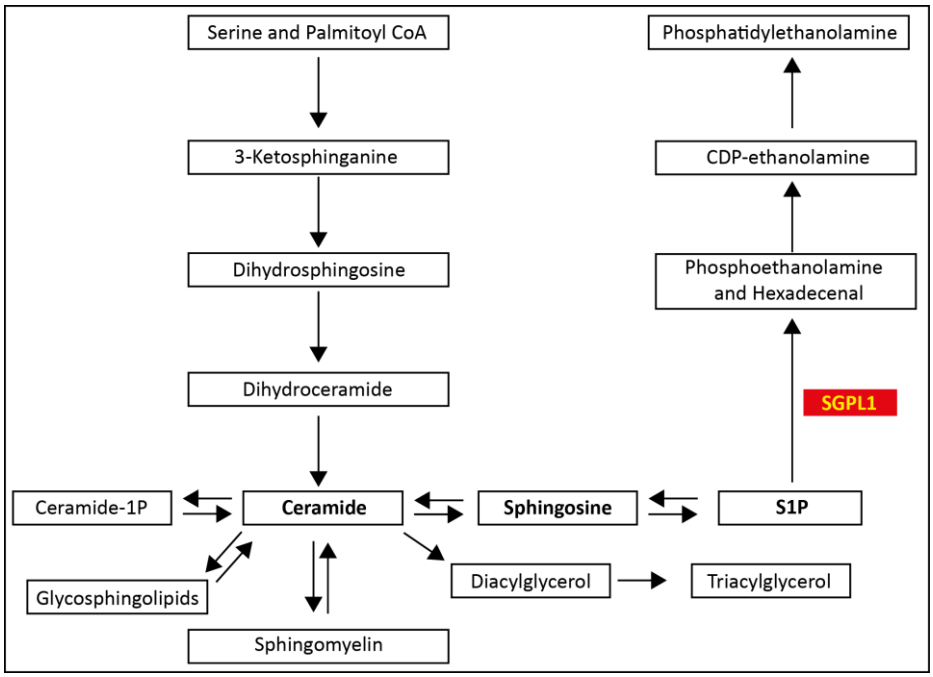

Figure 7.1 – Sphingolipid breakdown pathway highlighting the role of SGPL1. Schematic diagram showing that SGPL1 regulates the flow of the sphingolipid biochemical intermediates (in bold) and carries out the final irreversible degradation step in the pathway.

With regards to the adrenal gland, sphingolipids have been shown to control the steroid hormone biosynthesis within the gland. Specifically, sphingolipid intermediates ceramide and sphingosine were shown to reduce steroidogenesis *in vitro*[314-316], whereas S1P can induce expression of multiple steroidogenic factors[317]. However, it was also shown that abnormal accumulation of S1P in the cytosol can induce apoptosis[318].

Mutations in upstream components of the sphingolipid pathway can therefore lead to harmful accumulation of lysosomal sphingolipid species, associated with a number of conditions known as sphingolipidoses. In the case of SGPL1, mutations identified were loss-of function mutations. This resulted in the cytosolic accumulation of S1P and ceramide species in these patients supporting the notion that this disease alters sphingolipid metabolism. All patients in this cohort, harboring the *SGPL1* mutations, presented with PAI and focal segmental glomerulosclerosis and five of these patients also presented with steroid-resistant nephrotic syndrome. Additionally, extra-adrenal and -renal effects were described in most patients, while in 3 patients neurodegenerative disorders associated with accumulating sphingolipid metabolites were observed. In normal individuals SGPL1 is ubiquitously expressed in human tissues, with moderate expression in the adrenal cortex and the kidneys. A similar expression pattern is observed in rodents, making them a suitable *in vivo* model.

7.2 Hypothesis

SGPL1 is highly conserved between species, with human and mouse SGPL1 sharing 84% identity and 92% similarity. Since the mutations identified in our human cohort were loss-of function SGPL1 mutations, we hypothesize that *Sgpl1*$^{-/-}$ mice could provide a mouse model to study SGPL1 insufficiency-induced disorders in humans (e.g., adrenal insufficiency, steroid-resistant nephrotic syndrome).

7.3 Main Aims

1. Collect kidneys and adrenal glands from *Sgpl1*$^{-/-}$ transgenic mice and WT controls.
2. Analyse the histology and steroidogenic profile of the adrenal glands in *Sgpl1*$^{-/-}$ transgenic mice and WT controls.
3. Analyse the histology of the kidneys in *Sgpl1*$^{-/-}$ transgenic mice and WT controls.

7.4 Materials and Methods

7.4.1 Paraffin embedding of mouse kidneys and adrenals

Kidneys and adrenals from *Sgpl1*$^{+/+}$ and *Sgpl1*$^{-/-}$ mice were collected, fixed in 4% PFA overnight at 4^{o}C and then washed with PBS solution for 1 hour. Following PBS washes the adrenals were dehydrated in a series of ethanol washes, 50%, 70%, 90% and 100% for 1 hour each, on a rotating plate. Adrenals were then incubated in xylene twice for 5 minutes, and 10 minutes incubation before being placed in a container with melted paraffin for overnight incubation at 56^{o}C. The following day adrenals were placed in the embedding cassettes filled with melted paraffin and were allowed to set at room temperature. Frontal sections of paraffin embedded adrenals were cut at 6µm using a rotary microtome and serial sections were transferred onto superfrost plus glass slides covered with ddH_2O, and heated at 56^{o}C on a hotplate for 30-60 minutes or until sections were flat. Finally, excess water was removed; sections were allowed to dry at 37^{o}C and stored at room temperature.

7.4.2 Hematoxylin and Eosin staining

Mouse adrenal sections were incubated with Hematoxylin Solution Gill No.3 for 2 minutes and then washed under running water for 2 minutes. Following washes sections were incubated in 1% acid alcohol (1% hydrochloric acid in 70% ethanol) for 1 minute and washed in water for an additional minute. Sections were then dipped in 0.2% ammonia solution (concentrated ammonium hydroxide diluted in distilled water) 10 times and washed for 5 minutes under running water. Slides were then incubated in 80% ethanol for 1 minute followed by eosin incubation for 30-45 seconds. Sections were further dehydrated in 95% ethanol twice and 100% ethanol for 1 minute each followed by 2 xylene incubations for 3 minutes each. Following staining and dehydration steps, sections were mounted with Vectamount and visualised using a Leica DM5500B microscope.

.

7.4.3 Chromogenic immunohistochemistry of Sgpl1+/+ and Sgpl1-/- mouse adrenals

Sections were de-paraffinised in xylene incubations and washed in a series of 100% in decreasing ethanol concentrations (100%, 90%, 70% and 50%) for 10 minutes each, followed by incubation in H_2O for 10 minutes. Following the rehydration procedure, the sections were incubated in 3% H_2O_2 diluted in PBS for 30 minutes at room temperature to block endogenous peroxidase activity. Following peroxidase treatment sections washed in PBS-Triton. At this point if antigen unmasking was required, slides were incubated in 10mM Citrate Buffer pH 6.0 for 30 minutes in water bath at 95^{o}C and then allowed to cool for 20 minutes at room temperature before blocking for non-specific binding. Following unmasking, slides were incubated in blocking solution consisting of 10% goat serum in PBS-Triton for 1 hour, to prevent non-specific binding. Following blocking, slides were incubated overnight with the primary antibody diluted in PBS-Triton (Table 7.1) at room temperature. Slides were then washed with PBS-Triton and incubated with the biotinylated secondary antibody (Table 7.) diluted in PBS-Triton for 2 hours at room temperature. Following secondary antibody incubation, slides were washed in PBS-Triton three times for 10 minutes each and at the same time Avidin-Biotin Complex (ABC) was prepared according to manufacturer's instructions (Vector labs, PK-6100) and allowed to incubate at room temperature for at least 30 minutes before use. Following washes slides were incubated with ABC for 1 hour and then washed three times with PBS-Triton. Finally, sections were developed with 3,3'-diaminobenzidine substrate according to manufacturer's instructions (Vector labs, SK-4105). Once staining developed, reaction was stopped by placing slides in diethyl pyrocarbonate (DEPC)-H_2O. Slides were finally dehydrated in increasing concentrations of ethanol (50%, 70%, 90% and 100%) and then xylene incubations three times for 5 minutes each and mounted using Vectamount mounting medium (Vector labs, H-5000). Chromogenic antibody staining was visualised using a Leica DM5500B microscope

Table 7.2 - Primary Antibodies for chromogenic IHC

Antibody	Species Reactivity	Host	Supplier	Catalogue Number	Dilution	Requires AUM
CYP11B2	Mouse/Rat	Rabbit	Gomez-Sanchez	N/A	1:200	Yes
CYP11A1	Human/Mouse/Rat	Rabbit	Cell Signaling	D8F4F	1:200	No
SGPL1	Human/Mouse	Rabbit	Abcam	105183	1:200	No

Table 7.3 - Secondary Antibodies for chromogenic IHC

Antibody	Species Reactivity	Host	Supplier	Catalogue Number	Dilution
Biotinylated	Rabbit IgG	Goat	Vector	BA-1000	1:500

7.5 Results

We collected both *Sgpl1*$^{-/-}$ (n=3) and WT mice (n=3) and isolated both adrenal glands and kidneys, to investigate their phenotype. It is of note that *Sgpl1*$^{-/-}$ mice were born normally but most died within the first couple of weeks after weaning, for unknown reasons.

7.5.1 *Sgpl1*$^{-/-}$ mouse adrenal histology

Initially, we aimed to investigate whether there were any differences in the adrenal gland histology between the *Sgpl1*$^{-/-}$ mice and WT *Sgpl1*$^{+/+}$ mice (control), and if so whether these phenotypic differences resembled the adrenal disease observed in patients with SGPL1 mutations. Following histological investigation of the adrenal gland with H&E staining we showed that in the adrenal glands of *Sgpl1*$^{-/-}$ mice, cortical zonation was compromised and less defined, particularly between the ZG – ZF and ZF – X-zone regions (Figure 7.2b, c) as compared to WT *Sgpl1*$^{+/+}$ (Figure 7.2a). This observation was consistent in both male and female mice. Additionally, cells in the ZF of *Sgpl1*$^{-/-}$ mice appeared smaller and contained fewer lipid droplets with a higher degree of eosinophilia (Figure 7.2b', b'',c',c'') as compared to cells in the control WT *Sgpl1*$^{+/+}$ mice (Figure 7.2a',a'').

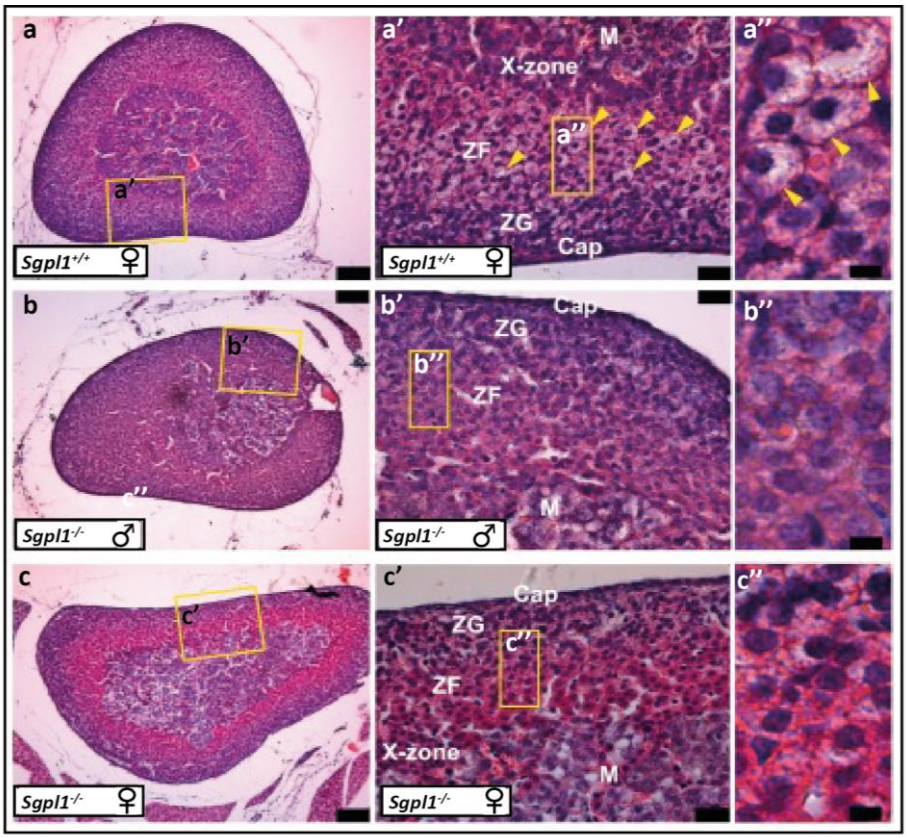

Figure 7.2 - Adrenals from *Sgpl1*$^{-/-}$ mice show histological abnormalities compared to WT mice. Results following H&E staining of *Sgpl1*$^{+/+}$ (a,a' and a'') and *Sgpl1*$^{-/-}$ (b,b',b'',c,c' and c'') mice show a less defined morphological zonation in the case of *Sgpl1*$^{-/-}$ mice (b,b',c and c') as compared to *Sgpl1*$^{+/+}$ mice (a,a'). Additionally the characteristic lipid droplets normally found in the ZF and visible here as large areas in the cytoplasm devoid of eosin staining (depicted by yellow arrows in a' and a'') are significantly reduced in *Sgpl1*$^{-/-}$ mouse adrenals (b',b'',c' and c''). n=3. Scale bars: 100µm (left panels); 25µm (middle panels); 5µm (right panels). Cap=Capsule.

Once we established that there were differences in the zonation and cell composition between the two mice, with *Sgpl1*$^{-/-}$ mice presenting an abnormal adrenocortical structure, we went on to investigate whether there were also differences in steroidogenesis. It is known that sphingolipid intermediates can have a negative effect in the expression of steroidogenic enzymes and this was indeed a pathological effect observed in our human cohort[313]. Additionally, following profile expression analysis of CYP11A1 and CYP11B2 we observed a clear difference in the expression pattern of the two proteins. IHC analysis of CYP11A1 showed a reduced expression

of CYP11A1 in *Sgpl1*$^{-/-}$ mice, which was mainly localised in the inner adrenal cortex (Figure 7.3b), in contrast to *Sgpl1*$^{+/+}$ mice that presented normal CYP11A1 expression throughout the adrenal cortex (Figure 7.3a). Additionally, in the case of CYP11B2 both mice showed a subcapsular expression of the protein, localised in the ZG region. However, in the case of *Sgpl1*$^{-/-}$ mice we observed a subcapsular continuous pattern of CYP11B2 (Figure 7.3d), rather than the classical pattern of subcapsular clusters of CYP11B2 found in WT *Sgpl1*$^{+/+}$ mice (Figure 7.3c). Therefore, our results suggest that steroidogenesis is indeed disrupted in the Sgpl1-deficient mouse models.

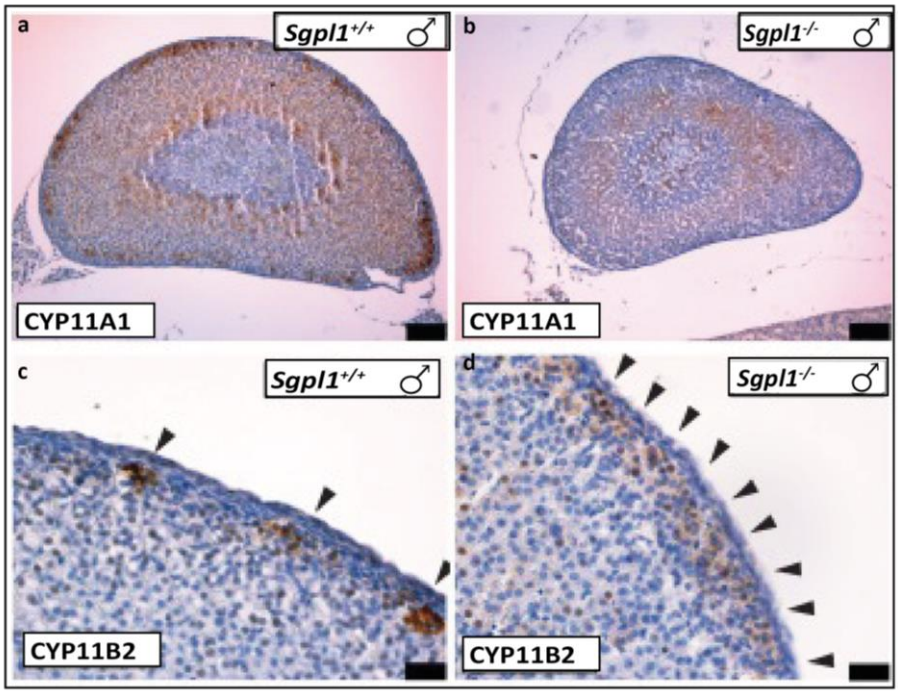

Figure 7.3 – Adrenals from *Sgpl1*$^{-/-}$ mice show abnormal steroidogenic expression compared to WT mice. Results following IHC analysis for CYP11A1 (a,b) AND CYP11B2 (c,d) expression in *Sgpl1*$^{-/-}$ (b,d) and *Sgpl1*$^{+/+}$ (a,c) show a different pattern of expression for the two enzymes. In *Sgpl1*$^{-/-}$ mice CYP11A1 expression is reduced (b) compared to *Sgpl1*$^{+/+}$ adrenals (a) and the characteristic patchy expression of CYP11B2 seen in normal *Sgpl1*$^{+/+}$ mice (c) is lost and appears in a continuous manner in *Sgpl1*$^{-/-}$ mouse adrenals (d). n=3. Scale bars: 100µm (top panels); 25µm (bottom panels).

7.5.2 *Sgpl1*$^{-/-}$ mouse kidney histology

Finally, we aimed to characterize the kidney histology of these mice to identify any phenotypic differences when compared to WT *Sgpl1*$^{+/+}$mice. Following H&E on kidney sections from both *Sgpl1*$^{-/-}$ and *Sgpl1*$^{+/+}$mice we observed a normal kidney histology *Sgpl1*$^{+/+}$mice (Figure 7.4a,b,b') in the case of and a pathological histology in the case of *Sgpl1*$^{-/-}$ mice (Figure 7.4c,d,d'). The latter showed mesangial hypercellularity and proteinaceous casts in the kidney tubules, with overall histological appearance supporting a glomerular phenotype.

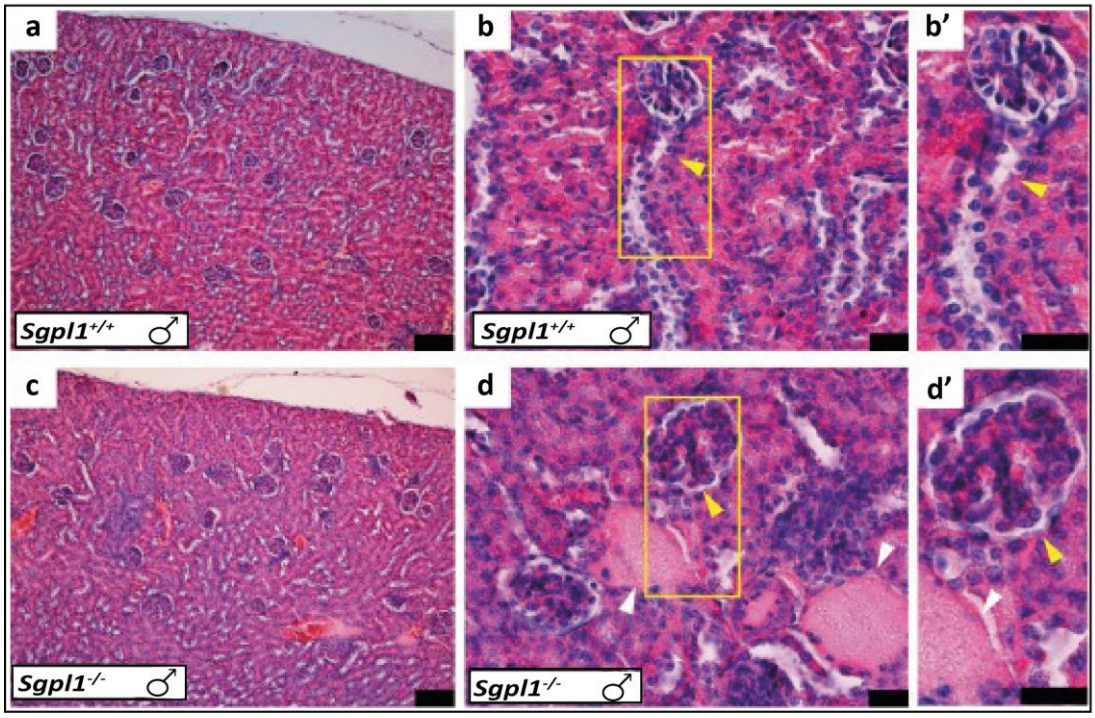

Figure 7.4 - Histological features of the kidneys differ in *Sgpl1*$^{-/-}$ and *Sgpl1*$^{+/+}$mice. Results following H&E staining of Sgpl1$^{+/+}$ (a, b, b') mice show normal cortical histology (a) and glomeruli with open capillary loops and normal cellular content, depicted here by yellow arrowheads (b and b'). H&E staining in kidneys of Sgpl1$^{-/-}$ mice (c, d, d') show mild hypercellularity with glomerular hypertrophy, depicted here by yellow arrowheads (d and d') with large protein casts in the tubules (white arrowheads in d and d').

7.6 Discussion

The scope of this chapter was to evaluate whether *Sgpl1*$^{-/-}$ mice could provide a mouse model to study the SGPL1 insufficiency induced disorders (PAI and steroid-resistant nephrotic syndrome)[313]. *SGPL1* mutations were identified in a cohort of eight patients with PAI and/or steroid-resistant nephrotic syndrome, with no other known mutations associated to PAI. Apart from adrenal pathology and nephrotic syndrome some of these patients also presented with other diseases including icthyosis, primary hypothyroidism, neurological symptoms and cryptorchidism as summarised in Table 7.4[313].

We have shown that unlike in humans, *Sgpl1* deficiency in mice leads to death within 2 weeks after birth. However, with regards to the adrenal glands we have shown that in the *Sgpl1*$^{-/-}$ mouse both adrenal gland zonation and steroidogenesis are impaired and have demonstrated a loss of vacuolization in the ZF. These findings are consistent with the biochemical finding of adrenal hormone insufficiency that occurs in humans with SGPL1 mutations described in Prasad *et al.,* 2017[313] Additionally, we demonstrated that *Sgpl1*$^{-/-}$ mice have renal defects with the histological changes in the kidney, in agreement with the human biopsy results presented in our paper and summarised in Table 7.4 below[313]. Therefore, we have demonstrated that both the adrenal and kidney phenotype observed in the *Sgpl1*$^{-/-}$ mice, is consistent with the pathological histology presented in PAI patients with *SGPL1* mutations. Table 7.4 shows the collective data of both our group and the collaborator summarising the clinical phenotype observed in these patients and the *Sgpl1*$^{-/-}$ mice.

Table 7.4 – Comparison of *Sgpl1*$^{-/-}$ mouse phenotype with clinical findings in the patients

	Adrenal pathology	Nephrotic disease	Ichthyosis*	Primary hypothyroidism*	Neurological disorder*	Lymphopenia*	Dyslipidemia*
Patient 1*	+	+	-	-	-	-	-
Patient 2*	+	-	-	-	-	-	-
Patient 3*	+	-	-	-	-	-	-
Patient 4*	+	-	-	-	-	+	-
Patient 5*	+	+	+	+	+	+	-
Patient 6*	+	+	+	+	+	-	+
Patient 7*	+	+	+	+	+	-	+
Patient 8*	+	+	+	+	-	-	+
***Sgpl1*$^{-/-}$ mice**	+	+	-	-	-	+	+

*Data supporting these findings was collected and analysed by other members of the collaboration and described in detail in Prasad *et al.,* 2017.

+, feature reported; -, feature not reported.

In conclusion, we have collectively shown that there are similarities in the clinical phenotypes of *Sgpl1*$^{-/-}$ mice and SGPL1-deficient patient cohort investigated in the Prasad *et al.,* 2017 paper. It was demonstrated that both the human cohort and the *Sgpl1*$^{-/-}$ mice presented with adrenal disease (PAI in humans), while nephrotic syndrome, icthyosis, disordered lipid metabolism and lymphodepletion occurred in all *Sgpl1*$^{-/-}$ mice and some of the patients. In contrast, the neurological defects and hypothyroidism presented in some patients were not observed in mice[313]. Finally, we have shown here that the *Sgpl1*$^{-/-}$ mouse model displays similar characteristics to the PAI and kidney resistant nephrotic syndrome occurring in *SGPL1* deficient patients, and could therefore potentially represent a suitable *in vivo* model to study some aspects of the disease.

References

1. Yates, R., et al., *Adrenocortical development, maintenance, and disease.* Curr Top Dev Biol, 2013. **106**: p. 239-312.
2. Xing, Y., et al., *Development of adrenal cortex zonation.* Endocrinol Metab Clin North Am, 2015. **44**(2): p. 243-74.
3. Gruenwald, P., *Embryonic and postnatal development of the adrenal cortex, particularly the zona glomerulosa and accessory nodules.* Anat Rec, 1946. **95**: p. 391-421.
4. Simon, D.P. and G.D. Hammer, *Adrenocortical stem and progenitor cells: implications for adrenocortical carcinoma.* Mol Cell Endocrinol, 2012. **351**(1): p. 2-11.
5. Hershkovitz, L., et al., *Adrenal 20alpha-hydroxysteroid dehydrogenase in the mouse catabolizes progesterone and 11-deoxycorticosterone and is restricted to the X-zone.* Endocrinology, 2007. **148**(3): p. 976-88.
6. Evelyn, H.-M., *A transitory zone in the adrenal cortex which shows age and sex relationships.* Developmental Dynamics, 1927. **40**(2): p. 251-293.
7. Guasti, L., et al., *FGF signalling through Fgfr2 isoform IIIb regulates adrenal cortex development.* Mol Cell Endocrinol, 2013. **371**(1-2): p. 182-8.
8. Guasti, L., et al., *Dlk1 up-regulates Gli1 expression in male rat adrenal capsule cells through the activation of beta1 integrin and ERK1/2.* Endocrinology, 2013. **154**(12): p. 4675-84.
9. Gomez-Sanchez, C.E., et al., *Development of monoclonal antibodies against human CYP11B1 and CYP11B2.* Mol Cell Endocrinol, 2014. **383**(1-2): p. 111-7.
10. Brown, M.S. and J.L. Goldstein, *A receptor-mediated pathway for cholesterol homeostasis.* Science, 1986. **232**(4746): p. 34-47.
11. Srivastava, R.A., *Scavenger receptor class B type I expression in murine brain and regulation by estrogen and dietary cholesterol.* J Neurol Sci, 2003. **210**(1-2): p. 11-8.
12. Clark, B.J., et al., *The purification, cloning, and expression of a novel luteinizing hormone-induced mitochondrial protein in MA-10 mouse Leydig tumor cells. Characterization of the steroidogenic acute regulatory protein (StAR).* J Biol Chem, 1994. **269**(45): p. 28314-22.
13. Stocco, D.M. and B.J. Clark, *Role of the steroidogenic acute regulatory protein (StAR) in steroidogenesis.* Biochem Pharmacol, 1996. **51**(3): p. 197-205.
14. Stocco, D.M., *The role of the StAR protein in steroidogenesis: challenges for the future.* J Endocrinol, 2000. **164**(3): p. 247-53.
15. Missaghian, E., et al., *Role of DNA methylation in the tissue-specific expression of the CYP17A1 gene for steroidogenesis in rodents.* J Endocrinol, 2009. **202**(1): p. 99-109.
16. Gallo-Payet, N. and M.-C. Battista, *Steroidogenesis - Adrenal Cell Signal Transduction.* Comprehensive Physiology, 2014. **4**: p. 889-962.
17. Payne, A.H. and D.B. Hales, *Overview of steroidogenic enzymes in the pathway from cholesterol to active steroid hormones.* Endocr Rev, 2004. **25**(6): p. 947-70.

18. Hu, J., et al., *Cellular cholesterol delivery, intracellular processing and utilization for biosynthesis of steroid hormones.* Nutr Metab (Lond), 2010. **7**: p. 47.
19. Johnson, J.A. and J.O. Davis, *Angiotensin. II. Important role in the maintenance of arterial blood pressure.* Science, 1973. **179**(4076): p. 906-7.
20. Tobian, L., A. Tomboulian, and J. Janecek, *The effect of high perfusion pressures on the granulation of juxtaglomerular cells in an isolated kidney.* J Clin Invest, 1959. **38**(4): p. 605-10.
21. Miller, E.D., *The role of the renin-angiotensin-aldosterone system in circulatory control and hypertension.* Br J Anaesth, 1981. **53**(7): p. 711-8.
22. Oparil, S., C.A. Sanders, and E. Haber, *In-vivo and in-vitro conversion of angiotensin I to angiotensin II in dog blood.* Circ Res, 1970. **26**(5): p. 591-9.
23. Nogueira, E.F., W.B. Bollag, and W.E. Rainey, *Angiotensin II regulation of adrenocortical gene transcription.* Mol Cell Endocrinol, 2009. **302**(2): p. 230-6.
24. Bird, I.M., et al., *Human NCI-H295 adrenocortical carcinoma cells: a model for angiotensin-II-responsive aldosterone secretion.* Endocrinology, 1993. **133**(4): p. 1555-61.
25. Ramalingam, L., et al., *The renin angiotensin system, oxidative stress and mitochondrial function in obesity and insulin resistance.* Biochim Biophys Acta, 2017. **1863**(5): p. 1106-1114.
26. Wehling, M., et al., *Rapid cardiovascular action of aldosterone in man.* J Clin Endocrinol Metab, 1998. **83**(10): p. 3517-22.
27. Fuller, P.J. and M.J. Young, *Mechanisms of mineralocorticoid action.* Hypertension, 2005. **46**(6): p. 1227-35.
28. Waterman, M.R. and L.J. Bischof, *Mechanisms of ACTH(cAMP)-dependent transcription of adrenal steroid hydroxylases.* Endocr Res, 1996. **22**(4): p. 615-20.
29. Sewer, M.B., E.B. Dammer, and S. Jagarlapudi, *Transcriptional regulation of adrenocortical steroidogenic gene expression.* Drug Metab Rev, 2007. **39**(2-3): p. 371-88.
30. Aumo, L., et al., *Functional roles of protein kinase A (PKA) and exchange protein directly activated by 3',5'-cyclic adenosine 5'-monophosphate (cAMP) 2 (EPAC2) in cAMP-mediated actions in adrenocortical cells.* Endocrinology, 2010. **151**(5): p. 2151-61.
31. Roberge, C., et al., *Adrenocortical dysregulation as a major player in insulin resistance and onset of obesity.* Am J Physiol Endocrinol Metab, 2007. **293**(6): p. E1465-78.
32. Dallman, M.F., et al., *Minireview: glucocorticoids--food intake, abdominal obesity, and wealthy nations in 2004.* Endocrinology, 2004. **145**(6): p. 2633-8.
33. Franchimont, D., *Overview of the actions of glucocorticoids on the immune response: a good model to characterize new pathways of immunosuppression for new treatment strategies.* Ann N Y Acad Sci, 2004. **1024**: p. 124-37.
34. Whitworth, J.A., et al., *Cardiovascular consequences of cortisol excess.* Vasc Health Risk Manag, 2005. **1**(4): p. 291-9.

35. Bird, I.M., *In the zone: understanding zona reticularis function and its transformation by adrenarche.* J Endocrinol, 2012. **214**(2): p. 109-11.
36. Ross, I.L. and G.J. Louw, *Embryological and molecular development of the adrenal glands.* Clinical Anatomy, 2015. **28**: p. 235-42.
37. Hatano, O., et al., *Identical origin of adrenal cortex and gonad revealed by expression profiles of Ad4BP/SF-1.* Genes Cells, 1996. **1**(7): p. 663-71.
38. Luo, X., Y. Ikeda, and K.L. Parker, *A cell-specific nuclear receptor is essential for adrenal and gonadal development and sexual differentiation.* Cell, 1994. **77**(4): p. 481-90.
39. Doupe, A.J., S.C. Landis, and P.H. Patterson, *Environmental influences in the development of neural crest derivatives: glucocorticoids, growth factors, and chromaffin cell plasticity.* J Neurosci, 1985. **5**(8): p. 2119-42.
40. Hillarp, N.A. and B. Hokfelt, *Evidence of adrenaline and noradrenaline in separate adrenal medullary cells.* Acta Physiol Scand, 1953. **30**(1): p. 55-68.
41. Keegan, C.E. and G.D. Hammer, *Recent insights into organogenesis of the adrenal cortex.* Trends Endocrinol Metab, 2002. **13**(5): p. 200-8.
42. C.Kim, A., et al., *In search of adrenocortical stem and progenitor cells.* Endocrine Reviews, 2009. **30**(3): p. 241-263.
43. Ikeda, Y., et al., *Developmental expression of mouse steroidogenic factor-1, an essential regulator of the steroid hydroxylases.* Mol Endocrinol, 1994. **8**(5): p. 654-62.
44. Crawford, P.A., Y. Sadovsky, and J. Milbrandt, *Nuclear receptor steroidogenic factor 1 directs embryonic stem cells toward the steroidogenic lineage.* Mol Cell Biol, 1997. **17**(7): p. 3997-4006.
45. Gondo, S., et al., *Adipose tissue-derived and bone marrow-derived mesenchymal cells develop into different lineage of steroidogenic cells by forced expression of steroidogenic factor 1.* Endocrinology, 2008. **149**(9): p. 4717-25.
46. Yazawa, T., et al., *Differentiation of adult stem cells derived from bone marrow stroma into Leydig or adrenocortical cells.* Endocrinology, 2006. **147**(9): p. 4104-11.
47. Bland, M.L., R.C. Fowkes, and H.A. Ingraham, *Differential requirement for steroidogenic factor-1 gene dosage in adrenal development versus endocrine function.* Mol Endocrinol, 2004. **18**(4): p. 941-52.
48. Katoh-Fukui, Y., et al., *Mouse Polycomb M33 is required for splenic vascular and adrenal gland formation through regulating Ad4BP/SF1 expression.* Blood, 2005. **106**(5): p. 1612-20.
49. Achermann, J.C., J.J. Meeks, and J.L. Jameson, *Phenotypic spectrum of mutations in DAX-1 and SF-1.* Mol Cell Endocrinol, 2001. **185**(1-2): p. 17-25.
50. El-Khairi, R., et al., *Role of DAX-1 (NR0B1) and steroidogenic factor-1 (NR5A1) in human adrenal function.* Endocr Dev, 2011. **20**: p. 38-46.
51. Doghman, M., et al., *Increased steroidogenic factor-1 dosage triggers adrenocortical cell proliferation and cancer.* Mol Endocrinol, 2007. **21**(12): p. 2968-87.
52. Zubair, M., et al., *Transgenic expression of Ad4BP/SF-1 in fetal adrenal progenitor cells leads to ectopic adrenal formation.* Mol Endocrinol, 2009. **23**(10): p. 1657-67.

53. Fatchiyah, et al., *Differential gene dosage effects of Ad4BP/SF-1 on target tissue development.* Biochem Biophys Res Commun, 2006. **341**(4): p. 1036-45.
54. Val, P., J.-P. Martinez-Barbera, and A. Swain, *Adrenal development is initiated by Cited2 and Wt1 through modulation of Sf-1 dosage.* Development, 2007. **134**(12): p. 2349-2358.
55. Bandiera, R., et al., *WT1 maintains adrenal-gonadal primordium identity and marks a population of AGP-like progenitors within the adrenal gland.* Dev Cell, 2013. **27**(1): p. 5-18.
56. Zubair, M., et al., *Two-step regulation of Ad4BP/SF-1 gene transcription during fetal adrenal development: initiation by a Hox-Pbx1-Prep1 complex and maintenance via autoregulation by Ad4BP/SF-1.* Mol Cell Biol, 2006. **26**(11): p. 4111-21.
57. Zubair, M., K.L. Parker, and K. Morohashi, *Developmental links between the fetal and adult zones of the adrenal cortex revealed by lineage tracing.* Mol Cell Biol, 2008. **28**(23): p. 7030-40.
58. Ahmad, I., et al., *A novel missense mutation in DAX-1 with an unusual presentation of X-linked adrenal hypoplasia congenita.* Horm Res, 2007. **68**(1): p. 32-7.
59. Mantovani, G., et al., *DAX1 and X-linked adrenal hypoplasia congenita: clinical and molecular analysis in five patients.* Eur J Endocrinol, 2006. **154**(5): p. 685-9.
60. Swain, A., et al., *Dax1 antagonizes Sry action in mammalian sex determination.* Nature, 1998. **391**(6669): p. 761-7.
61. Achermann, J.C., et al., *Missense mutations cluster within the carboxyl-terminal region of DAX-1 and impair transcriptional repression.* J Clin Endocrinol Metab, 2001. **86**(7): p. 3171-5.
62. Xing, Y., et al., *Timing of adrenal regression controlled by synergistic interaction between Sf1 SUMOylation and Dax1.* Development, 2017. **144**(20): p. 3798-3807.
63. Gummow, B.M., et al., *Reciprocal regulation of a glucocorticoid receptor-steroidogenic factor-1 transcription complex on the Dax-1 promoter by glucocorticoids and adrenocorticotropic hormone in the adrenal cortex.* Mol Endocrinol, 2006. **20**(11): p. 2711-23.
64. Khalfallah, O., et al., *Dax-1 knockdown in mouse embryonic stem cells induces loss of pluripotency and multilineage differentiation.* Stem Cells, 2009. **27**(7): p. 1529-37.
65. Feek, C.M., D.J. Marante, and C.R. Edwards, *The hypothalamic-pituitary-adrenal axis.* Clin Endocrinol Metab, 1983. **12**(3): p. 597-618.
66. Pepe, G.J. and E.D. Albrecht, *Regulation of the primate fetal adrenal cortex.* Endocr Rev, 1990. **11**(1): p. 151-76.
67. Beshay, V.E., B.R. Carr, and W.E. Rainey, *The human fetal adrenal gland, corticotropin-releasing hormone, and parturition.* Semin Reprod Med, 2007. **25**(1): p. 14-20.
68. Simpson, E.R. and M.R. Waterman, *Regulation by ACTH of steroid hormone biosynthesis in the adrenal cortex.* Can J Biochem Cell Biol, 1983. **61**(7): p. 692-707.
69. Takahashi, K., et al., *Expression of urocortin 3/stresscopin in human adrenal glands and adrenal tumors.* Peptides, 2006. **27**(1): p. 178-82.

70. Fukuda, T., et al., *Urocortin 1, urocortin 3/stresscopin, and corticotropin-releasing factor receptors in human adrenal and its disorders.* J Clin Endocrinol Metab, 2005. **90**(8): p. 4671-8.
71. Sirianni, R., et al., *Corticotropin-releasing hormone directly stimulates cortisol and the cortisol biosynthetic pathway in human fetal adrenal cells.* J Clin Endocrinol Metab, 2005. **90**(1): p. 279-85.
72. Willenberg, H.S., et al., *Effects of a novel corticotropin-releasing-hormone receptor type I antagonist on human adrenal function.* Mol Psychiatry, 2000. **5**(2): p. 137-41.
73. Schwartz, J., J.S. Huo, and G. Piwien-Pilipuk, *Growth hormone regulated gene expression.* Minerva Endocrinol, 2002. **27**(4): p. 231-41.
74. Backlin, C., et al., *Immunohistochemical expression of insulin-like growth factor 1 and its receptor in normal and neoplastic human adrenal cortex.* Anticancer Res, 1995. **15**(6b): p. 2453-9.
75. Coulter, C.L., et al., *Functional maturation of the primate fetal adrenal in vivo: I. Role of insulin-like growth factors (IGFs), IGF-I receptor, and IGF binding proteins in growth regulation.* Endocrinology, 1996. **137**(10): p. 4487-98.
76. Brice, A.L., et al., *Temporal changes in the expression of the insulin-like growth factor II gene associated with tissue maturation in the human fetus.* Development, 1989. **106**(3): p. 543-54.
77. Bendall, S.C., et al., *IGF and FGF cooperatively establish the regulatory stem cell niche of pluripotent human cells in vitro.* Nature, 2007. **448**(7157): p. 1015-21.
78. Jiang, F., T.J. Frederick, and T.L. Wood, *IGF-I synergizes with FGF-2 to stimulate oligodendrocyte progenitor entry into the cell cycle.* Dev Biol, 2001. **232**(2): p. 414-23.
79. Pitetti, J.L., et al., *Insulin and IGF1 receptors are essential for XX and XY gonadal differentiation and adrenal development in mice.* PLoS Genet, 2013. **9**(1): p. e1003160.
80. Bottcher, R.T. and C. Niehrs, *Fibroblast growth factor signaling during early vertebrate development.* Endocr Rev, 2005. **26**(1): p. 63-77.
81. Berthon, A., et al., *Wnt/beta-catenin signalling in adrenal physiology and tumour development.* Mol Cell Endocrinol, 2012. **351**(1): p. 87-95.
82. Drelon, C., et al., *Adrenal cortex tissue homeostasis and zonation: A WNT perspective.* Mol Cell Endocrinol, 2015. **408**: p. 156-164.
83. Kempna, P. and C.E. Fluck, *Adrenal gland development and defects.* Best Pract Res Clin Endocrinol Metab, 2008. **22**(1): p. 77-93.
84. Gummow, B.M., J.N. Winnay, and G.D. Hammer, *Convergence of Wnt signaling and steroidogenic factor-1 (SF-1) on transcription of the rat inhibin alpha gene.* J Biol Chem, 2003. **278**(29): p. 26572-9.
85. Mizusaki, H., et al., *Dax-1 (dosage-sensitive sex reversal-adrenal hypoplasia congenita critical region on the X chromosome, gene 1) gene transcription is regulated by wnt4 in the female developing gonad.* Mol Endocrinol, 2003. **17**(4): p. 507-19.
86. Haegel, H., et al., *Lack of beta-catenin affects mouse development at gastrulation.* Development, 1995. **121**(11): p. 3529-37.

87. Kim, A.C., et al., *Targeted disruption of beta-catenin in Sf1-expressing cells impairs development and maintenance of the adrenal cortex.* Development, 2008. **135**(15): p. 2593-602.
88. Chiang, C., et al., *Cyclopia and defective axial patterning in mice lacking Sonic hedgehog gene function.* Nature, 1996. **383**(6599): p. 407-13.
89. Litingtung, Y., et al., *Sonic hedgehog is essential to foregut development.* Nat Genet, 1998. **20**(1): p. 58-61.
90. Dosch, J.S., M. Pasca di Magliano, and D.M. Simeone, *Pancreatic cancer and hedgehog pathway signaling: new insights.* Pancreatology, 2010. **10**(2-3): p. 151-7.
91. Santini, R., et al., *Hedgehog-GLI signaling drives self-renewal and tumorigenicity of human melanoma-initiating cells.* Stem Cells, 2012. **30**(9): p. 1808-18.
92. Varjosalo, M. and J. Taipale, *Hedgehog: functions and mechanisms.* Genes Dev, 2008. **22**(18): p. 2454-72.
93. Ingham, P.W. and A.P. McMahon, *Hedgehog signaling in animal development: paradigms and principles.* Genes Dev, 2001. **15**(23): p. 3059-87.
94. Finco, I., et al., *Hedgehog signaling and steroidogenesis.* Annu Rev Physiol, 2015. **77**: p. 105-29.
95. Allen, B.L., T. Tenzen, and A.P. McMahon, *The Hedgehog-binding proteins Gas1 and Cdo cooperate to positively regulate Shh signaling during mouse development.* Genes Dev, 2007. **21**(10): p. 1244-57.
96. Izzi, L., et al., *Boc and Gas1 each form distinct Shh receptor complexes with Ptch1 and are required for Shh-mediated cell proliferation.* Dev Cell, 2011. **20**(6): p. 788-801.
97. Allen, B.L., et al., *Overlapping roles and collective requirement for the coreceptors GAS1, CDO, and BOC in SHH pathway function.* Dev Cell, 2011. **20**(6): p. 775-87.
98. Laufer, E., et al., *Sonic hedgehog signaling during adrenal development.* Mol Cell Endocrinol, 2012. **351**(1): p. 19-27.
99. Stone, D.M., et al., *The tumour-suppressor gene patched encodes a candidate receptor for Sonic hedgehog.* Nature, 1996. **384**(6605): p. 129-34.
100. Pan, Y., et al., *Sonic hedgehog signaling regulates Gli2 transcriptional activity by suppressing its processing and degradation.* Mol Cell Biol, 2006. **26**(9): p. 3365-77.
101. King, P., A. Paul, and E. Laufer, *Shh signaling regulates adrenocortical development and identifies progenitors of steroidogenic lineages.* Proc Natl Acad Sci U S A, 2009. **106**(50): p. 21185-90.
102. Guasti, L., et al., *Localization of Sonic hedgehog secreting and receiving cells in the developing and adult rat adrenal cortex.* Mol Cell Endocrinol, 2011. **336**(1-2): p. 117-22.
103. Ching, S. and E. Vilain, *Targeted disruption of Sonic Hedgehog in the mouse adrenal leads to adrenocortical hypoplasia.* Genesis, 2009. **47**(9): p. 628-37.
104. Huang, C.C., et al., *Progenitor cell expansion and organ size of mouse adrenal is regulated by sonic hedgehog.* Endocrinology, 2010. **151**(3): p. 1119-28.

105. Ingle, D.J. and G.M. Higgins, *Autotransplantation and regeneration of the adrenal gland.* Endocrinology, 1938. **22**(4): p. 458-464.
106. Thomas, M., S.R. Northrup, and P.J. Hornsby, *Adrenocortical tissue formed by transplantation of normal clones of bovine adrenocortical cells in scid mice replaces the essential functions of the animals' adrenal glands.* Nat Med, 1997. **3**(9): p. 978-83.
107. Thomas, M. and P.J. Hornsby, *Transplantation of primary bovine adrenocortical cells into scid mice.* Mol Cell Endocrinol, 1999. **153**(1-2): p. 125-36.
108. Chang, S.P., et al., *Cell proliferation, movement and differentiation during maintenance of the adult mouse adrenal cortex.* PLoS One, 2013. **8**(12): p. e81865.
109. Freedman, B.D., et al., *Adrenocortical zonation results from lineage conversion of differentiated zona glomerulosa cells.* Dev Cell, 2013. **26**(6): p. 666-73.
110. Lerario, A.M., et al., *Molecular Mechanisms of Stem/Progenitor Cell Maintenance in the Adrenal Cortex.* Front Endocrinol (Lausanne), 2017. **8**: p. 52.
111. Wood, M.A., et al., *Fetal adrenal capsular cells serve as progenitor cells for steroidogenic and stromal adrenocortical cell lineages in M. musculus.* Development, 2013. **140**(22): p. 4522-32.
112. Walczak, E.M., et al., *Wnt-signaling inhibits adrenal steroidogenesis by cell-autonomous and non-cell-autonomous mechanisms.* Mol Endocrinol, 2014. **28**(9): p. 1471-86.
113. Kim, A., et al., *Wnt/betacatenin signaling in adrenocortical stem/progenitor cells: implications for adrenocortical carcinoma.* Ann Endocrinol (Paris), 2009. **70**(3): p. 156.
114. Walczak, E.M. and G.D. Hammer, *Regulation of the adrenocortical stem cell niche: implications for disease.* Nat Rev Endocrinol, 2015. **11**(1): p. 14-28.
115. Heikkila, M., et al., *Wnt-4 deficiency alters mouse adrenal cortex function, reducing aldosterone production.* Endocrinology, 2002. **143**(11): p. 4358-65.
116. Drelon, C., et al., *PKA inhibits WNT signalling in adrenal cortex zonation and prevents malignant tumour development.* Nat Commun, 2016. **7**: p. 12751.
117. Berthon, A., et al., *WNT/beta-catenin signalling is activated in aldosterone-producing adenomas and controls aldosterone production.* Hum Mol Genet, 2014. **23**(4): p. 889-905.
118. Kim, K.A., et al., *R-Spondin proteins: a novel link to beta-catenin activation.* Cell Cycle, 2006. **5**(1): p. 23-6.
119. Barker, N., S. Tan, and H. Clevers, *Lgr proteins in epithelial stem cell biology.* Development, 2013. **140**(12): p. 2484-94.
120. Hao, H.X., et al., *ZNRF3 promotes Wnt receptor turnover in an R-spondin-sensitive manner.* Nature, 2012. **485**(7397): p. 195-200.
121. Vidal, V., et al., *The adrenal capsule is a signaling center controlling cell renewal and zonation through Rspo3.* Genes Dev, 2016. **30**(12): p. 1389-94.

122. Ornitz, D.M. and N. Itoh, *The Fibroblast Growth Factor signaling pathway.* Wiley Interdiscip Rev Dev Biol, 2015. **4**(3): p. 215-66.
123. Chu, Y., W.J. Ho, and J.C. Dunn, *Basic fibroblast growth factor delivery enhances adrenal cortical cellular regeneration.* Tissue Eng Part A, 2009. **15**(8): p. 2093-101.
124. Hynes, R.O., *The extracellular matrix: not just pretty fibrils.* Science, 2009. **326**(5957): p. 1216-9.
125. Ahmed, M. and C. Ffrench-Constant, *Extracellular Matrix Regulation of Stem Cell Behavior.* Curr Stem Cell Rep, 2016. **2**: p. 197-206.
126. Brizzi, M.F., G. Tarone, and P. Defilippi, *Extracellular matrix, integrins, and growth factors as tailors of the stem cell niche.* Curr Opin Cell Biol, 2012. **24**(5): p. 645-51.
127. Chamoux, E., et al., *Identification of extracellular matrix components and their integrin receptors in the human fetal adrenal gland.* J Clin Endocrinol Metab, 2001. **86**(5): p. 2090-8.
128. Chamoux, E., et al., *Fibronectin, laminin, and collagen IV interact with ACTH and angiotensin II to dictate specific cell behavior and secretion in human fetal adrenal cells in culture.* Endocr Res, 2002. **28**(4): p. 637-40.
129. Takada, S., et al., *Delta-like and gtl2 are reciprocally expressed, differentially methylated linked imprinted genes on mouse chromosome 12.* Curr Biol, 2000. **10**(18): p. 1135-8.
130. Schmidt, J.V., et al., *The Dlk1 and Gtl2 genes are linked and reciprocally imprinted.* Genes Dev, 2000. **14**(16): p. 1997-2002.
131. Sul, H.S., *Minireview: Pref-1: role in adipogenesis and mesenchymal cell fate.* Mol Endocrinol, 2009. **23**(11): p. 1717-25.
132. Wang, Y. and H.S. Sul, *Ectodomain shedding of preadipocyte factor 1 (Pref-1) by tumor necrosis factor alpha converting enzyme (TACE) and inhibition of adipocyte differentiation.* Mol Cell Biol, 2006. **26**(14): p. 5421-35.
133. Deiuliis, J.A., et al., *Alternative splicing of delta-like 1 homolog (DLK1) in the pig and human.* Comp Biochem Physiol B Biochem Mol Biol, 2006. **145**(1): p. 50-9.
134. Smas, C.M., L. Chen, and H.S. Sul, *Cleavage of membrane-associated pref-1 generates a soluble inhibitor of adipocyte differentiation.* Mol Cell Biol, 1997. **17**(2): p. 977-88.
135. Smas, C.M., D. Green, and H.S. Sul, *Structural characterization and alternate splicing of the gene encoding the preadipocyte EGF-like protein pref-1.* Biochemistry, 1994. **33**(31): p. 9257-65.
136. Mei, B., et al., *Only the large soluble form of preadipocyte factor-1 (Pref-1), but not the small soluble and membrane forms, inhibits adipocyte differentiation: role of alternative splicing.* Biochem J, 2002. **364**(Pt 1): p. 137-44.
137. Garces, C., et al., *Adipocyte differentiation is modulated by secreted delta-like (dlk) variants and requires the expression of membrane-associated dlk.* Differentiation, 1999. **64**(2): p. 103-14.
138. Wang, Y., et al., *Pref-1 interacts with fibronectin to inhibit adipocyte differentiation.* Mol Cell Biol, 2010. **30**(14): p. 3480-92.

139. Lee, K., et al., *Inhibition of adipogenesis and development of glucose intolerance by soluble preadipocyte factor-1 (Pref-1).* J Clin Invest, 2003. **111**(4): p. 453-61.
140. Smas, C.M., et al., *Transcriptional control of the pref-1 gene in 3T3-L1 adipocyte differentiation. Sequence requirement for differentiation-dependent suppression.* J Biol Chem, 1998. **273**(48): p. 31751-8.
141. Smas, C.M. and H.S. Sul, *Pref-1, a protein containing EGF-like repeats, inhibits adipocyte differentiation.* Cell, 1993. **73**(4): p. 725-34.
142. Wang, Y. and H.S. Sul, *Pref-1 regulates mesenchymal cell commitment and differentiation through Sox9.* Cell Metab, 2009. **9**(3): p. 287-302.
143. Bray, S.J., *Notch signalling: a simple pathway becomes complex.* Nat Rev Mol Cell Biol, 2006. **7**(9): p. 678-89.
144. Aster, J.C., *In brief: Notch signalling in health and disease.* J Pathol, 2014. **232**(1): p. 1-3.
145. Baladron, V., et al., *dlk acts as a negative regulator of Notch1 activation through interactions with specific EGF-like repeats.* Exp Cell Res, 2005. **303**(2): p. 343-59.
146. Komatsu, H., et al., *OSM-11 facilitates LIN-12 Notch signaling during Caenorhabditis elegans vulval development.* PLoS Biol, 2008. **6**(8): p. e196.
147. Tanimizu, N., et al., *Isolation of hepatoblasts based on the expression of Dlk/Pref-1.* J Cell Sci, 2003. **116**(Pt 9): p. 1775-86.
148. Jensen, C.H., et al., *Studies on the isolation, structural analysis and tissue localization of fetal antigen 1 and its relation to a human adrenal-specific cDNA, pG2.* Hum Reprod, 1993. **8**(4): p. 635-41.
149. Yevtodiyenko, A. and J.V. Schmidt, *Dlk1 expression marks developing endothelium and sites of branching morphogenesis in the mouse embryo and placenta.* Dev Dyn, 2006. **235**(4): p. 1115-23.
150. Falix, F.A., et al., *Possible roles of DLK1 in the Notch pathway during development and disease.* Biochim Biophys Acta, 2012. **1822**(6): p. 988-95.
151. Moon, Y.S., et al., *Mice lacking paternally expressed Pref-1/Dlk1 display growth retardation and accelerated adiposity.* Mol Cell Biol, 2002. **22**(15): p. 5585-92.
152. Villena, J.A., et al., *Resistance to high-fat diet-induced obesity but exacerbated insulin resistance in mice overexpressing preadipocyte factor-1 (Pref-1): a new model of partial lipodystrophy.* Diabetes, 2008. **57**(12): p. 3258-66.
153. Andersen, M., et al., *Fetal antigen 1 in healthy adults and patients with pituitary disease: relation to physiological, pathological, and pharmacological GH levels.* J Clin Endocrinol Metab, 2001. **86**(11): p. 5465-70.
154. Altenberger, T., et al., *Identification of DLK1 variants in pituitary- and neuroendocrine tumors.* Biochem Biophys Res Commun, 2006. **340**(3): p. 995-1005.
155. Begum, A., et al., *DLK1, delta-like 1 homolog (Drosophila), regulates tumor cell differentiation in vivo.* Cancer Lett, 2012. **318**(1): p. 26-33.

156. Nueda, M.L., et al., *dlk1 specifically interacts with insulin-like growth factor binding protein 1 to modulate adipogenesis of 3T3-L1 cells.* J Mol Biol, 2008. **379**(3): p. 428-42.
157. Xu, X., et al., *DLK1 as a potential target against cancer stem/progenitor cells of hepatocellular carcinoma.* Mol Cancer Ther, 2012. **11**(3): p. 629-38.
158. Yanai, H., et al., *Dlk-1, a cell surface antigen on foetal hepatic stem/progenitor cells, is expressed in hepatocellular, colon, pancreas and breast carcinomas at a high frequency.* J Biochem, 2010. **148**(1): p. 85-92.
159. Almeida, M.Q., et al., *Steroidogenic factor 1 overexpression and gene amplification are more frequent in adrenocortical tumors from children than from adults.* J Clin Endocrinol Metab, 2010. **95**(3): p. 1458-62.
160. Pianovski, M.A., et al., *SF-1 overexpression in childhood adrenocortical tumours.* Eur J Cancer, 2006. **42**(8): p. 1040-3.
161. Sbiera, S., et al., *High diagnostic and prognostic value of steroidogenic factor-1 expression in adrenal tumors.* J Clin Endocrinol Metab, 2010. **95**(10): p. E161-71.
162. Kinzler, K.W., et al., *Identification of FAP locus genes from chromosome 5q21.* Science, 1991. **253**(5020): p. 661-5.
163. Groden, J., et al., *Identification and characterization of the familial adenomatous polyposis coli gene.* Cell, 1991. **66**(3): p. 589-600.
164. Berthon, A., et al., *Constitutive beta-catenin activation induces adrenal hyperplasia and promotes adrenal cancer development.* Hum Mol Genet, 2010. **19**(8): p. 1561-76.
165. Gaujoux, S., et al., *Wnt/beta-catenin and 3',5'-cyclic adenosine 5'-monophosphate/protein kinase A signaling pathways alterations and somatic beta-catenin gene mutations in the progression of adrenocortical tumors.* J Clin Endocrinol Metab, 2008. **93**(10): p. 4135-40.
166. Tadjine, M., et al., *Frequent mutations of beta-catenin gene in sporadic secreting adrenocortical adenomas.* Clin Endocrinol (Oxf), 2008. **68**(2): p. 264-70.
167. Chapman, A., et al., *Identification of genetic alterations of AXIN2 gene in adrenocortical tumors.* J Clin Endocrinol Metab, 2011. **96**(9): p. E1477-81.
168. Heaton, J.H., et al., *Progression to adrenocortical tumorigenesis in mice and humans through insulin-like growth factor 2 and beta-catenin.* Am J Pathol, 2012. **181**(3): p. 1017-33.
169. de Fraipont, F., et al., *Gene expression profiling of human adrenocortical tumors using complementary deoxyribonucleic Acid microarrays identifies several candidate genes as markers of malignancy.* J Clin Endocrinol Metab, 2005. **90**(3): p. 1819-29.
170. Ilvesmaki, V., et al., *Insulin-like growth factors (IGFs) and their receptors in adrenal tumors: high IGF-II expression in functional adrenocortical carcinomas.* J Clin Endocrinol Metab, 1993. **77**(3): p. 852-8.
171. Erickson, L.A., et al., *Pathologic features and expression of insulin-like growth factor-2 in adrenocortical neoplasms.* Endocr Pathol, 2001. **12**(4): p. 429-35.

172. DeBaun, M.R., et al., *Epigenetic alterations of H19 and LIT1 distinguish patients with Beckwith-Wiedemann syndrome with cancer and birth defects.* Am J Hum Genet, 2002. **70**(3): p. 604-11.
173. Gicquel, C., et al., *Molecular markers and long-term recurrences in a large cohort of patients with sporadic adrenocortical tumors.* Cancer Res, 2001. **61**(18): p. 6762-7.
174. Ng, J.M. and T. Curran, *The Hedgehog's tale: developing strategies for targeting cancer.* Nat Rev Cancer, 2011. **11**(7): p. 493-501.
175. Giordano, T.J., et al., *Molecular classification and prognostication of adrenocortical tumors by transcriptome profiling.* Clin Cancer Res, 2009. **15**(2): p. 668-76.
176. Herbet, M., J.J. Feige, and M. Thomas, *Insights into the role of genetic alterations in adrenocortical tumorigenesis.* Mol Cell Endocrinol, 2009. **300**(1-2): p. 169-74.
177. Arnaldi, G. and M. Boscaro, *Adrenal incidentaloma.* Best Pract Res Clin Endocrinol Metab, 2012. **26**(4): p. 405-19.
178. Lerario, A.M., A. Moraitis, and G.D. Hammer, *Genetics and epigenetics of adrenocortical tumors.* Mol Cell Endocrinol, 2014. **386**(1-2): p. 67-84.
179. Bertherat, J., et al., *Molecular and functional analysis of PRKAR1A and its locus (17q22-24) in sporadic adrenocortical tumors: 17q losses, somatic mutations, and protein kinase A expression and activity.* Cancer Res, 2003. **63**(17): p. 5308-19.
180. Wilmot Roussel, H., et al., *Identification of gene expression profiles associated with cortisol secretion in adrenocortical adenomas.* J Clin Endocrinol Metab, 2013. **98**(6): p. E1109-21.
181. Quack, I., O. Vonend, and L.C. Rump, *Familial hyperaldosteronism I-III.* Horm Metab Res, 2010. **42**(6): p. 424-8.
182. Jackson, R.V., et al., *New genetic insights in familial hyperaldosteronism.* Ann N Y Acad Sci, 2002. **970**: p. 77-88.
183. Mulatero, P., et al., *KCNJ5 mutations in European families with nonglucocorticoid remediable familial hyperaldosteronism.* Hypertension, 2012. **59**(2): p. 235-40.
184. Choi, M., et al., *K+ channel mutations in adrenal aldosterone-producing adenomas and hereditary hypertension.* Science, 2011. **331**(6018): p. 768-72.
185. Azizan, E.A., et al., *Somatic mutations affecting the selectivity filter of KCNJ5 are frequent in 2 large unselected collections of adrenal aldosteronomas.* Hypertension, 2012. **59**(3): p. 587-91.
186. Beuschlein, F., et al., *Somatic mutations in ATP1A1 and ATP2B3 lead to aldosterone-producing adenomas and secondary hypertension.* Nat Genet, 2013. **45**(4): p. 440-4, 444e1-2.
187. Nishimoto, K., et al., *Aldosterone-stimulating somatic gene mutations are common in normal adrenal glands.* Proc Natl Acad Sci U S A, 2015. **112**(33): p. E4591-9.
188. Else, T., et al., *Adrenocortical carcinoma.* Endocr Rev, 2014. **35**(2): p. 282-326.
189. Bilimoria, K.Y., et al., *Adrenocortical carcinoma in the United States: treatment utilization and prognostic factors.* Cancer, 2008. **113**(11): p. 3130-6.

190. Wajchenberg, B.L., et al., *Adrenocortical carcinoma: clinical and laboratory observations.* Cancer, 2000. **88**(4): p. 711-36.
191. Schteingart, D.E., et al., *Management of patients with adrenal cancer: recommendations of an international consensus conference.* Endocr Relat Cancer, 2005. **12**(3): p. 667-80.
192. Michalkiewicz, E., et al., *Clinical and outcome characteristics of children with adrenocortical tumors: a report from the International Pediatric Adrenocortical Tumor Registry.* J Clin Oncol, 2004. **22**(5): p. 838-45.
193. Luton, J.P., et al., *Clinical features of adrenocortical carcinoma, prognostic factors, and the effect of mitotane therapy.* N Engl J Med, 1990. **322**(17): p. 1195-201.
194. Libe, R., *Adrenocortical carcinoma (ACC): diagnosis, prognosis, and treatment.* Front Cell Dev Biol, 2015. **3**: p. 45.
195. Nieman, L.K., et al., *The diagnosis of Cushing's syndrome: an Endocrine Society Clinical Practice Guideline.* J Clin Endocrinol Metab, 2008. **93**(5): p. 1526-40.
196. Icard, P., et al., *Adrenocortical carcinomas: surgical trends and results of a 253-patient series from the French Association of Endocrine Surgeons study group.* World J Surg, 2001. **25**(7): p. 891-7.
197. Libe, R., et al., *Prognostic factors in stage III-IV adrenocortical carcinomas (ACC): an European Network for the Study of Adrenal Tumor (ENSAT) study.* Ann Oncol, 2015. **26**(10): p. 2119-25.
198. Fassnacht, M., et al., *Limited prognostic value of the 2004 International Union Against Cancer staging classification for adrenocortical carcinoma: proposal for a Revised TNM Classification.* Cancer, 2009. **115**(2): p. 243-50.
199. Assie, G., et al., *Integrated genomic characterization of adrenocortical carcinoma.* Nat Genet, 2014. **46**(6): p. 607-12.
200. De Francia, S., et al., *Mitotane treatment for adrenocortical carcinoma: an overview.* Minerva Endocrinol, 2012. **37**(1): p. 9-23.
201. De Luca, A., et al., *The role of the EGFR signaling in tumor microenvironment.* J Cell Physiol, 2008. **214**(3): p. 559-67.
202. Angelousi, A., et al., *The role of epithelial growth factors and insulin growth factors in the adrenal neoplasms.* Ann Transl Med, 2018. **6**(12): p. 253.
203. Nagane, M., et al., *Aberrant receptor signaling in human malignant gliomas: mechanisms and therapeutic implications.* Cancer Lett, 2001. **162 Suppl**: p. S17-s21.
204. Ciardiello, F. and G. Tortora, *EGFR antagonists in cancer treatment.* N Engl J Med, 2008. **358**(11): p. 1160-74.
205. Furnari, F.B., et al., *Malignant astrocytic glioma: genetics, biology, and paths to treatment.* Genes Dev, 2007. **21**(21): p. 2683-710.
206. Duff, A.M., D.J. Bouchier-Hayes, and J.H. Harmay, *VEGF and Cancer*. Vascular Endothelial Growth Factor (VEGF) and its role in non-endothelial cells: Autocrine signaling by VEGF. 2004: Kluwer Academic/Plenum Publishers.
207. Wortmann, S., et al., *Bevacizumab plus capecitabine as a salvage therapy in advanced adrenocortical carcinoma.* Eur J Endocrinol, 2010. **162**(2): p. 349-56.

208. Quinkler, M., et al., *Treatment of advanced adrenocortical carcinoma with erlotinib plus gemcitabine.* J Clin Endocrinol Metab, 2008. **93**(6): p. 2057-62.
209. Naing, A., et al., *Insulin growth factor receptor (IGF-1R) antibody cixutumumab combined with the mTOR inhibitor temsirolimus in patients with metastatic adrenocortical carcinoma.* Br J Cancer, 2013. **108**(4): p. 826-30.
210. Zheng, S., et al., *Comprehensive Pan-Genomic Characterization of Adrenocortical Carcinoma.* Cancer Cell, 2016. **29**(5): p. 723-36.
211. Ross, J.S., et al., *Next-generation sequencing of adrenocortical carcinoma reveals new routes to targeted therapies.* J Clin Pathol, 2014. **67**(11): p. 968-73.
212. Faillot, S. and G. Assie, *ENDOCRINE TUMOURS: The genomics of adrenocortical tumors.* Eur J Endocrinol, 2016. **174**(6): p. R249-65.
213. Juhlin, C.C., et al., *Whole-exome sequencing characterizes the landscape of somatic mutations and copy number alterations in adrenocortical carcinoma.* J Clin Endocrinol Metab, 2015. **100**(3): p. E493-502.
214. Hao, H.X., X. Jiang, and F. Cong, *Control of Wnt Receptor Turnover by R-spondin-ZNRF3/RNF43 Signaling Module and Its Dysregulation in Cancer.* Cancers (Basel), 2016. **8**(6).
215. Kato, S., et al., *Understanding the function-structure and function-mutation relationships of p53 tumor suppressor protein by high-resolution missense mutation analysis.* Proc Natl Acad Sci U S A, 2003. **100**(14): p. 8424-9.
216. Petitjean, A., et al., *TP53 mutations in human cancers: functional selection and impact on cancer prognosis and outcomes.* Oncogene, 2007. **26**(15): p. 2157-65.
217. Nishimoto, K., et al., *Adrenocortical zonation in humans under normal and pathological conditions.* J Clin Endocrinol Metab, 2010. **95**(5): p. 2296-305.
218. Braunewell, K.H. and A.J. Klein-Szanto, *Visinin-like proteins (VSNLs): interaction partners and emerging functions in signal transduction of a subfamily of neuronal Ca2+ -sensor proteins.* Cell Tissue Res, 2009. **335**(2): p. 301-16.
219. Romero, D.G., et al., *Disabled-2 is expressed in adrenal zona glomerulosa and is involved in aldosterone secretion.* Endocrinology, 2007. **148**(6): p. 2644-52.
220. Trejter, M., et al., *Visinin-like peptide 1 in adrenal gland of the rat. Gene expression and its hormonal control.* Peptides, 2015. **63**: p. 22-9.
221. Spilker, C., E.D. Gundelfinger, and K.H. Braunewell, *Evidence for different functional properties of the neuronal calcium sensor proteins VILIP-1 and VILIP-3: from subcellular localization to cellular function.* Biochim Biophys Acta, 2002. **1600**(1-2): p. 118-27.
222. Bernardi, P. and A. Rasola, *Calcium and cell death: the mitochondrial connection.* Subcell Biochem, 2007. **45**: p. 481-506.
223. Duchen, M.R., *Ca(2+)-dependent changes in the mitochondrial energetics in single dissociated mouse sensory neurons.* Biochem J, 1992. **283 (Pt 1)**: p. 41-50.

224. Rohacs, T., et al., *Intracellular calcium release is more efficient than calcium influx in stimulating mitochondrial NAD(P)H formation in adrenal glomerulosa cells.* Biochem J, 1997. **328 (Pt 2)**: p. 525-8.
225. Spat, A. and L. Hunyady, *Control of aldosterone secretion: a model for convergence in cellular signaling pathways.* Physiol Rev, 2004. **84**(2): p. 489-539.
226. Szanda, G., A. Rajki, and A. Spat, *Control mechanisms of mitochondrial Ca(2+) uptake - feed-forward modulation of aldosterone secretion.* Mol Cell Endocrinol, 2012. **353**(1-2): p. 101-8.
227. Wiederkehr, A., et al., *Mitochondrial matrix calcium is an activating signal for hormone secretion.* Cell Metab, 2011. **13**(5): p. 601-11.
228. Li, P., et al., *Expression and Histopathological Significance of Disabled-2 in Aldosterone-Producing Adenoma.* Horm Metab Res, 2017. **49**(7): p. 520-526.
229. Ola, R., et al., *The expression of Visinin-like 1 during mouse embryonic development.* Gene Expr Patterns, 2012. **12**(1-2): p. 53-62.
230. Aiba, M. and M. Fujibayashi, *Alteration of subcapsular adrenocortical zonation in humans with aging: the progenitor zone predominates over the previously well-developed zona glomerulosa after 40 years of age.* J Histochem Cytochem, 2011. **59**(5): p. 557-64.
231. Fay, A.P., et al., *Adrenocortical carcinoma: the management of metastatic disease.* Crit Rev Oncol Hematol, 2014. **92**(2): p. 123-32.
232. Muttarak, M., et al., *Adrenal carcinoma.* Biomed Imaging Interv J, 2006. **2**(1): p. e9.
233. Nanba, K., et al., *Age-Related Autonomous Aldosteronism.* Circulation, 2017. **136**(4): p. 347-355.
234. Kebebew, E., et al., *Extent of disease at presentation and outcome for adrenocortical carcinoma: have we made progress?* World J Surg, 2006. **30**(5): p. 872-8.
235. Schteingart, D.E., *Adjuvant mitotane therapy of adrenal cancer - use and controversy.* N Engl J Med, 2007. **356**(23): p. 2415-8.
236. Ng, L. and J.M. Libertino, *Adrenocortical carcinoma: diagnosis, evaluation and treatment.* J Urol, 2003. **169**(1): p. 5-11.
237. Aparna, C., et al., *Adrenocortical carcinoma: Report of two cases.* Indian J Endocrinol Metab, 2011. **15**(3): p. 217-9.
238. Rakhshandehroo, M., A. Koppen, and E. Kalkhoven, *Pref-1 preferentially inhibits heat production in brown adipose tissue.* Biochem J, 2012. **443**(3): p. e3-5.
239. Sbiera, S., et al., *Mitotane Inhibits Sterol-O-Acyl Transferase 1 Triggering Lipid-Mediated Endoplasmic Reticulum Stress and Apoptosis in Adrenocortical Carcinoma Cells.* Endocrinology, 2015. **156**(11): p. 3895-908.
240. Vassilopoulou-Sellin, R., et al., *Impact of adjuvant mitotane on the clinical course of patients with adrenocortical cancer.* Cancer, 1993. **71**(10): p. 3119-23.
241. Haak, H.R., et al., *Optimal treatment of adrenocortical carcinoma with mitotane: results in a consecutive series of 96 patients.* Br J Cancer, 1994. **69**(5): p. 947-51.

242. Terzolo, M., et al., *Adjuvant mitotane treatment for adrenocortical carcinoma.* N Engl J Med, 2007. **356**(23): p. 2372-80.
243. Shibuya, Y., C.C. Chang, and T.Y. Chang, *ACAT1/SOAT1 as a therapeutic target for Alzheimer's disease.* Future Med Chem, 2015. **7**(18): p. 2451-67.
244. Cortes-Funes, H. and C. Coronado, *Role of anthracyclines in the era of targeted therapy.* Cardiovasc Toxicol, 2007. **7**(2): p. 56-60.
245. Thorn, C.F., et al., *Doxorubicin pathways: pharmacodynamics and adverse effects.* Pharmacogenet Genomics, 2011. **21**(7): p. 440-6.
246. Carvalho, C., et al., *Doxorubicin: the good, the bad and the ugly effect.* Curr Med Chem, 2009. **16**(25): p. 3267-85.
247. Swain, S.M., F.S. Whaley, and M.S. Ewer, *Congestive heart failure in patients treated with doxorubicin: a retrospective analysis of three trials.* Cancer, 2003. **97**(11): p. 2869-79.
248. Kaye, S. and S. Merry, *Tumour cell resistance to anthracyclines--a review.* Cancer Chemother Pharmacol, 1985. **14**(2): p. 96-103.
249. *Efficacy of adjuvant fluorouracil and folinic acid in colon cancer. International Multicentre Pooled Analysis of Colon Cancer Trials (IMPACT) investigators.* Lancet, 1995. **345**(8955): p. 939-44.
250. Giacchetti, S., et al., *Phase III multicenter randomized trial of oxaliplatin added to chronomodulated fluorouracil-leucovorin as first-line treatment of metastatic colorectal cancer.* J Clin Oncol, 2000. **18**(1): p. 136-47.
251. Douillard, J.Y., et al., *Irinotecan combined with fluorouracil compared with fluorouracil alone as first-line treatment for metastatic colorectal cancer: a multicentre randomised trial.* Lancet, 2000. **355**(9209): p. 1041-7.
252. Dhar, S., et al., *Targeted delivery of a cisplatin prodrug for safer and more effective prostate cancer therapy in vivo.* Proc Natl Acad Sci U S A, 2011. **108**(5): p. 1850-5.
253. Dasari, S. and P.B. Tchounwou, *Cisplatin in cancer therapy: molecular mechanisms of action.* Eur J Pharmacol, 2014. **740**: p. 364-78.
254. Previati, M., et al., *Cisplatin-induced apoptosis in human promyelocytic leukemia cells.* Int J Mol Med, 2006. **18**(3): p. 511-6.
255. Khan, A.B., et al., *Cisplatin therapy in recurrent childhood brain tumors.* Cancer Treat Rep, 1982. **66**(12): p. 2013-20.
256. Ma, X., et al., *Pan-cancer genome and transcriptome analyses of 1,699 paediatric leukaemias and solid tumours.* Nature, 2018.
257. Grobner, S.N., et al., *The landscape of genomic alterations across childhood cancers.* Nature, 2018.
258. Hanahan, D. and R.A. Weinberg, *Hallmarks of cancer: the next generation.* Cell, 2011. **144**(5): p. 646-74.
259. Kreso, A. and J.E. Dick, *Evolution of the cancer stem cell model.* Cell Stem Cell, 2014. **14**(3): p. 275-91.
260. Burrell, R.A., et al., *The causes and consequences of genetic heterogeneity in cancer evolution.* Nature, 2013. **501**(7467): p. 338-45.
261. Greaves, M. and C.C. Maley, *Clonal evolution in cancer.* Nature, 2012. **481**(7381): p. 306-13.
262. Fidler, I.J. and M.L. Kripke, *Metastasis results from preexisting variant cells within a malignant tumor.* Science, 1977. **197**(4306): p. 893-5.

263. Dick, J.E., *Stem cell concepts renew cancer research.* Blood, 2008. **112**(13): p. 4793-807.
264. Meacham, C.E. and S.J. Morrison, *Tumour heterogeneity and cancer cell plasticity.* Nature, 2013. **501**(7467): p. 328-37.
265. Nguyen, L.V., et al., *Cancer stem cells: an evolving concept.* Nat Rev Cancer, 2012. **12**(2): p. 133-43.
266. Klonisch, T., et al., *Cancer stem cell markers in common cancers - therapeutic implications.* Trends Mol Med, 2008. **14**(10): p. 450-60.
267. Vermeulen, L., et al., *The developing cancer stem-cell model: clinical challenges and opportunities.* Lancet Oncol, 2012. **13**(2): p. e83-9.
268. Bardsley, M.R., et al., *Kitlow stem cells cause resistance to Kit/platelet-derived growth factor alpha inhibitors in murine gastrointestinal stromal tumors.* Gastroenterology, 2010. **139**(3): p. 942-52.
269. Tanei, T., et al., *Association of breast cancer stem cells identified by aldehyde dehydrogenase 1 expression with resistance to sequential Paclitaxel and epirubicin-based chemotherapy for breast cancers.* Clin Cancer Res, 2009. **15**(12): p. 4234-41.
270. Chaffer, C.L., et al., *Normal and neoplastic nonstem cells can spontaneously convert to a stem-like state.* Proc Natl Acad Sci U S A, 2011. **108**(19): p. 7950-5.
271. Mani, S.A., et al., *The epithelial-mesenchymal transition generates cells with properties of stem cells.* Cell, 2008. **133**(4): p. 704-15.
272. Scheel, C., et al., *Paracrine and autocrine signals induce and maintain mesenchymal and stem cell states in the breast.* Cell, 2011. **145**(6): p. 926-40.
273. Vermeulen, L., et al., *Wnt activity defines colon cancer stem cells and is regulated by the microenvironment.* Nat Cell Biol, 2010. **12**(5): p. 468-76.
274. Ricci-Vitiani, L., et al., *Identification and expansion of human colon-cancer-initiating cells.* Nature, 2007. **445**(7123): p. 111-5.
275. Salcido, C.D., et al., *Molecular characterisation of side population cells with cancer stem cell-like characteristics in small-cell lung cancer.* Br J Cancer, 2010. **102**(11): p. 1636-44.
276. Mimeault, M., et al., *Recent advances in cancer stem/progenitor cell research: therapeutic implications for overcoming resistance to the most aggressive cancers.* J Cell Mol Med, 2007. **11**(5): p. 981-1011.
277. S, S.F., et al., *In vitro models of cancer stem cells and clinical applications.* BMC Cancer, 2016. **16**(Suppl 2): p. 738.
278. Ma, S., et al., *Identification and characterization of tumorigenic liver cancer stem/progenitor cells.* Gastroenterology, 2007. **132**(7): p. 2542-56.
279. Li, W., et al., *A novel tissue-engineered 3D tumor model for anti-cancer drug discovery.* Biofabrication, 2018. **11**(1): p. 015004.
280. Redondo-Castro, E., et al., *Generation of Human Mesenchymal Stem Cell 3D Spheroids Using Low-binding Plates.* Bio Protoc, 2018. **8**(16).
281. Sanchez-Maldonado, B., et al., *Spheroids Spontaneously Generated In Vitro from Sheep Ovarian Cortical Cells Contain Integrating Cells That Exhibit Hallmarks of Neural Stem/Progenitor Cells.* Stem Cells Dev, 2018. **27**(22): p. 1557-1576.

282. Yilmazer, A., *Evaluation of cancer stemness in breast cancer and glioblastoma spheroids in vitro.* 3 Biotech, 2018. **8**(9): p. 390.
283. Pandit, H., et al., *Enrichment of cancer stem cells via beta-catenin contributing to the tumorigenesis of hepatocellular carcinoma.* BMC Cancer, 2018. **18**(1): p. 783.
284. Weiswald, L.B., D. Bellet, and V. Dangles-Marie, *Spherical cancer models in tumor biology.* Neoplasia, 2015. **17**(1): p. 1-15.
285. Zhou, X., et al., *Expression of the stem cell marker, Nanog, in human endometrial adenocarcinoma.* Int J Gynecol Pathol, 2011. **30**(3): p. 262-70.
286. Lalli, E., *Role of Orphan Nuclear Receptro DAX-1/NR0B1 in Development, Physiology, and Disease.* Advances in Biology, 2014: p. 1-19.
287. Pommier, Y., et al., *Apoptosis defects and chemotherapy resistance: molecular interaction maps and networks.* Oncogene, 2004. **23**(16): p. 2934-49.
288. Alfarouk, K.O., et al., *Resistance to cancer chemotherapy: failure in drug response from ADME to P-gp.* Cancer Cell Int, 2015. **15**: p. 71.
289. Xu, J., et al., *Prognostic values of DLK1 for surgery and imatinib mesylate adjuvant therapy in gastrointestinal stromal tumors.* Am J Cancer Res, 2016. **6**(11): p. 2700-2712.
290. Dezso, K., et al., *Delta-like protein (DLK) is a novel immunohistochemical marker for human hepatoblastomas.* Virchows Arch, 2008. **452**(4): p. 443-8.
291. Cai, C.M., et al., *Targeting endogenous DLK1 exerts antitumor effect on hepatocellular carcinoma through initiating cell differentiation.* Oncotarget, 2016. **7**(44): p. 71466-71476.
292. Basham, K.J., et al., *Mouse models of adrenocortical tumors.* Mol Cell Endocrinol, 2016. **421**: p. 82-97.
293. Bielinska, M., et al., *Mouse strain susceptibility to gonadectomy-induced adrenocortical tumor formation correlates with the expression of GATA-4 and luteinizing hormone receptor.* Endocrinology, 2003. **144**(9): p. 4123-33.
294. Johnsen, I.K., et al., *Gonadectomy in mice of the inbred strain CE/J induces proliferation of sub-capsular adrenal cells expressing gonadal marker genes.* J Endocrinol, 2006. **190**(1): p. 47-57.
295. Krachulec, J., et al., *GATA4 is a critical regulator of gonadectomy-induced adrenocortical tumorigenesis in mice.* Endocrinology, 2012. **153**(6): p. 2599-611.
296. Looyenga, B.D. and G.D. Hammer, *Origin and identity of adrenocortical tumors in inhibin knockout mice: implications for cellular plasticity in the adrenal cortex.* Mol Endocrinol, 2006. **20**(11): p. 2848-63.
297. Matzuk, M.M., et al., *Development of cancer cachexia-like syndrome and adrenal tumors in inhibin-deficient mice.* Proc Natl Acad Sci U S A, 1994. **91**(19): p. 8817-21.
298. Kananen, K., et al., *Gonadectomy permits adrenocortical tumorigenesis in mice transgenic for the mouse inhibin alpha-subunit promoter/simian virus 40 T-antigen fusion gene: evidence for negative autoregulation of the inhibin alpha-subunit gene.* Mol Endocrinol, 1996. **10**(12): p. 1667-77.

299. Mikola, M., et al., *High levels of luteinizing hormone analog stimulate gonadal and adrenal tumorigenesis in mice transgenic for the mouse inhibin-alpha-subunit promoter/Simian virus 40 T-antigen fusion gene.* Oncogene, 2003. **22**(21): p. 3269-78.
300. Kananen, K., et al., *Suppression of gonadotropins inhibits gonadal tumorigenesis in mice transgenic for the mouse inhibin alpha-subunit promoter/simian virus 40 T-antigen fusion gene.* Endocrinology, 1997. **138**(8): p. 3521-31.
301. Shu, J., et al., *GATA family members as inducers for cellular reprogramming to pluripotency.* Cell Res, 2015. **25**(2): p. 169-80.
302. Chrusciel, M., et al., *Transgenic GATA-4 expression induces adrenocortical tumorigenesis in C57Bl/6 mice.* J Cell Sci, 2013. **126**(Pt 8): p. 1845-57.
303. Nishimoto, K., et al., *Human Adrenocortical Remodeling Leading to Aldosterone-Producing Cell Cluster Generation.* Int J Endocrinol, 2016. **2016**: p. 7834356.
304. Li, H., et al., *Serum DLK1 is a potential prognostic biomarker in patients with hepatocellular carcinoma.* Tumour Biol, 2015. **36**(11): p. 8399-404.
305. Omata, K., et al., *Aldosterone-Producing Cell Clusters Frequently Harbor Somatic Mutations and Accumulate With Age in Normal Adrenals.* J Endocr Soc, 2017. **1**(7): p. 787-799.
306. Charmandari, E., N.C. Nicolaides, and G.P. Chrousos, *Adrenal insufficiency.* Lancet, 2014. **383**(9935): p. 2152-67.
307. Malikova, J. and C.E. Fluck, *Novel insight into etiology, diagnosis and management of primary adrenal insufficiency.* Horm Res Paediatr, 2014. **82**(3): p. 145-57.
308. Chan, L.F., et al., *Whole-Exome Sequencing in the Differential Diagnosis of Primary Adrenal Insufficiency in Children.* Front Endocrinol (Lausanne), 2015. **6**: p. 113.
309. Hughes, C.R., et al., *MCM4 mutation causes adrenal failure, short stature, and natural killer cell deficiency in humans.* J Clin Invest, 2012. **122**(3): p. 814-20.
310. Meimaridou, E., et al., *Mutations in NNT encoding nicotinamide nucleotide transhydrogenase cause familial glucocorticoid deficiency.* Nat Genet, 2012. **44**(7): p. 740-2.
311. Metherell, L.A., et al., *Mutations in MRAP, encoding a new interacting partner of the ACTH receptor, cause familial glucocorticoid deficiency type 2.* Nat Genet, 2005. **37**(2): p. 166-70.
312. Prasad, R., et al., *Thioredoxin Reductase 2 (TXNRD2) mutation associated with familial glucocorticoid deficiency (FGD).* J Clin Endocrinol Metab, 2014. **99**(8): p. E1556-63.
313. Prasad, R., et al., *Sphingosine-1-phosphate lyase mutations cause primary adrenal insufficiency and steroid-resistant nephrotic syndrome.* J Clin Invest, 2017. **127**(3): p. 942-953.
314. Li, Q.L., et al., *Inhibition of steroidogenesis and induction of apoptosis in rat luteal cells by cell-permeable ceramide in vitro.* Sheng Li Xue Bao, 2001. **53**(2): p. 142-6.
315. Meroni, S.B., et al., *Possible involvement of ceramide in the regulation of rat Leydig cell function.* J Steroid Biochem Mol Biol, 2000. **75**(4-5): p. 307-13.

316. Urs, A.N., et al., *Steroidogenic factor-1 is a sphingolipid binding protein.* Mol Cell Endocrinol, 2007. **265-266**: p. 174-8.
317. Lucki, N.C., D. Li, and M.B. Sewer, *Sphingosine-1-phosphate rapidly increases cortisol biosynthesis and the expression of genes involved in cholesterol uptake and transport in H295R adrenocortical cells.* Mol Cell Endocrinol, 2012. **348**(1): p. 165-75.
318. Hagen, N., et al., *Sphingosine-1-phosphate links glycosphingolipid metabolism to neurodegeneration via a calpain-mediated mechanism.* Cell Death Differ, 2011. **18**(8): p. 1356-65.

Appendix I: PGEM T-Easy Vector Map

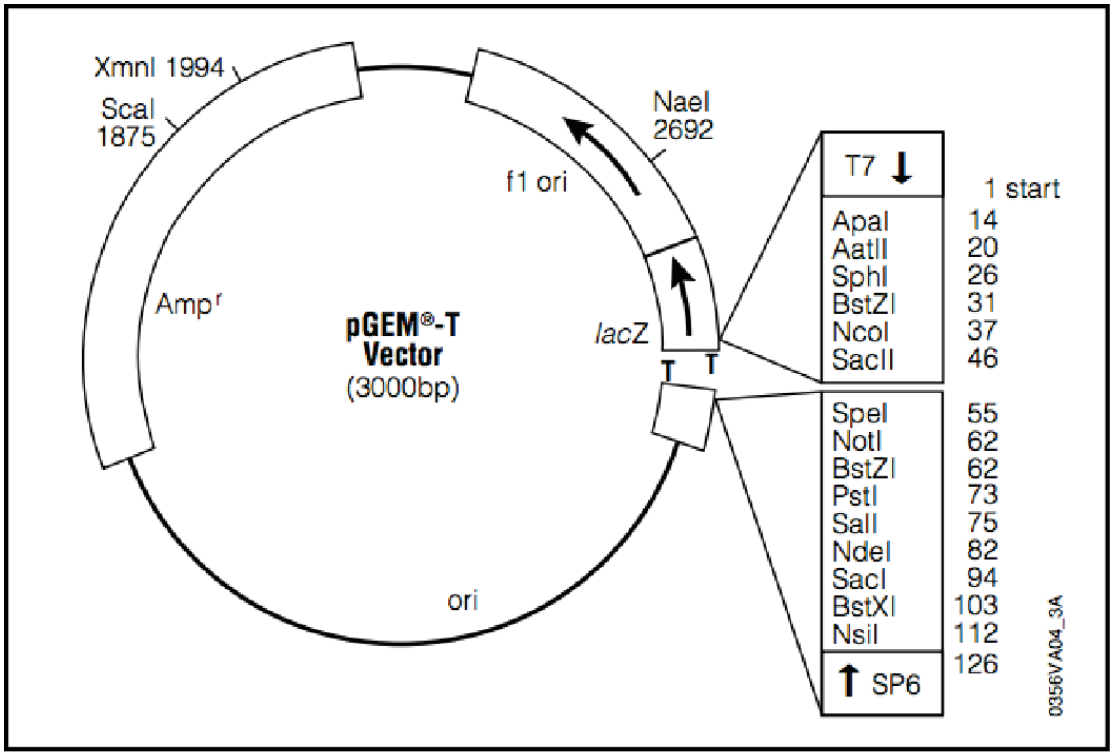

Appendix II: pCMVHA Vector Map

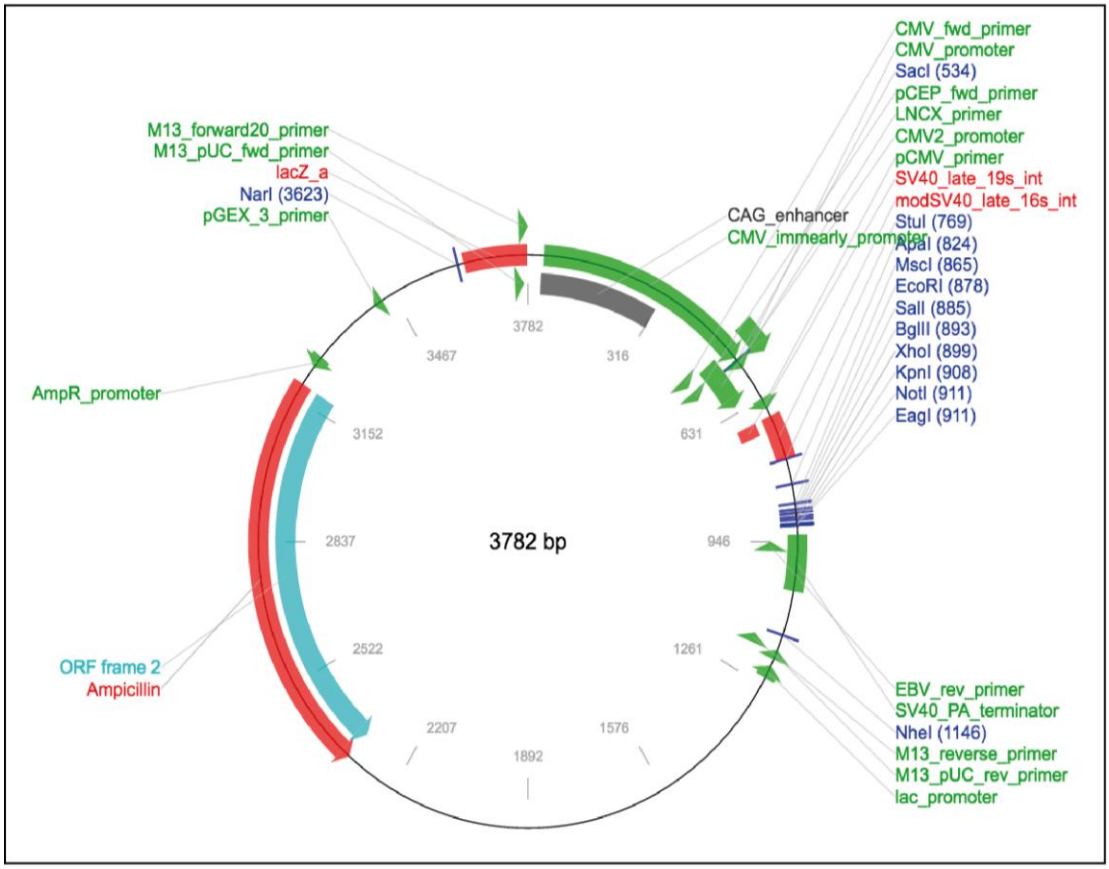

Appendix III: pCMVTag4 Vector Map

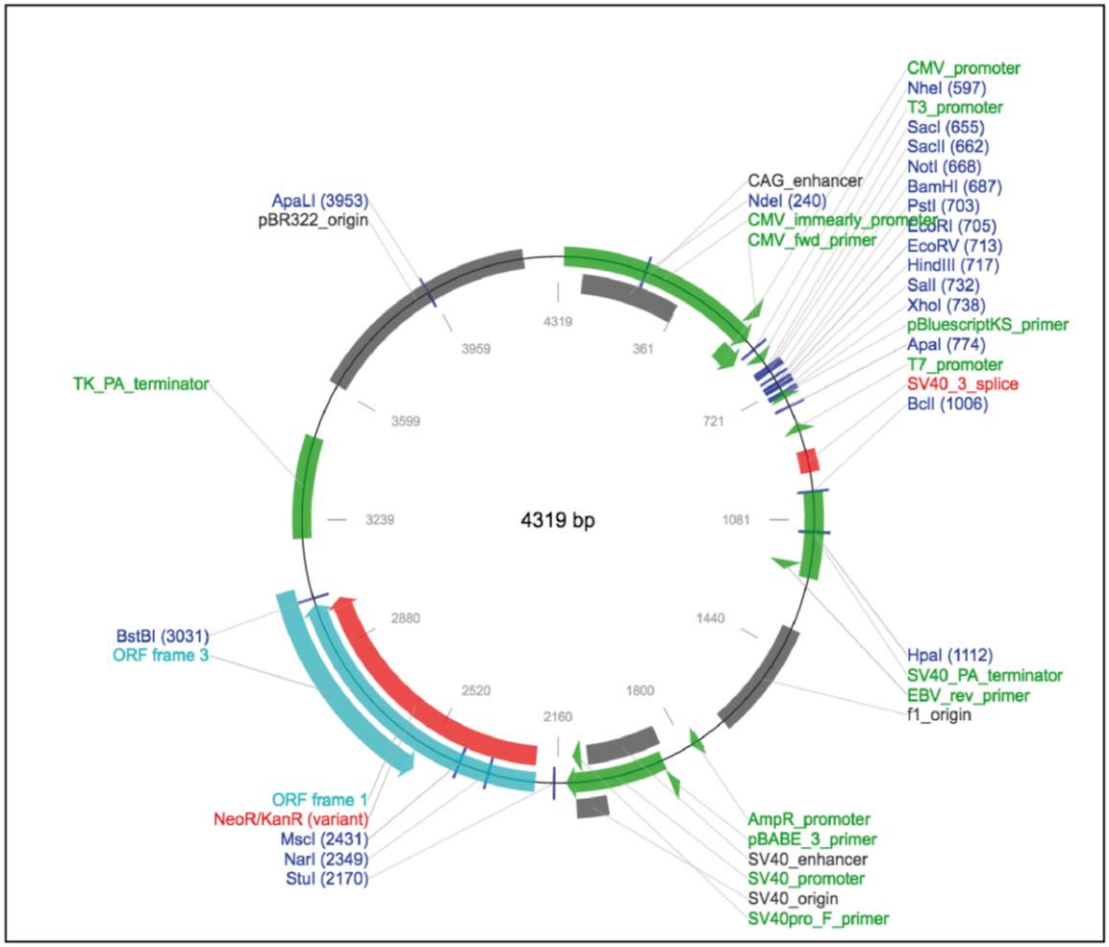

Appendix IV: pHIV-EGFP Vector Diagram

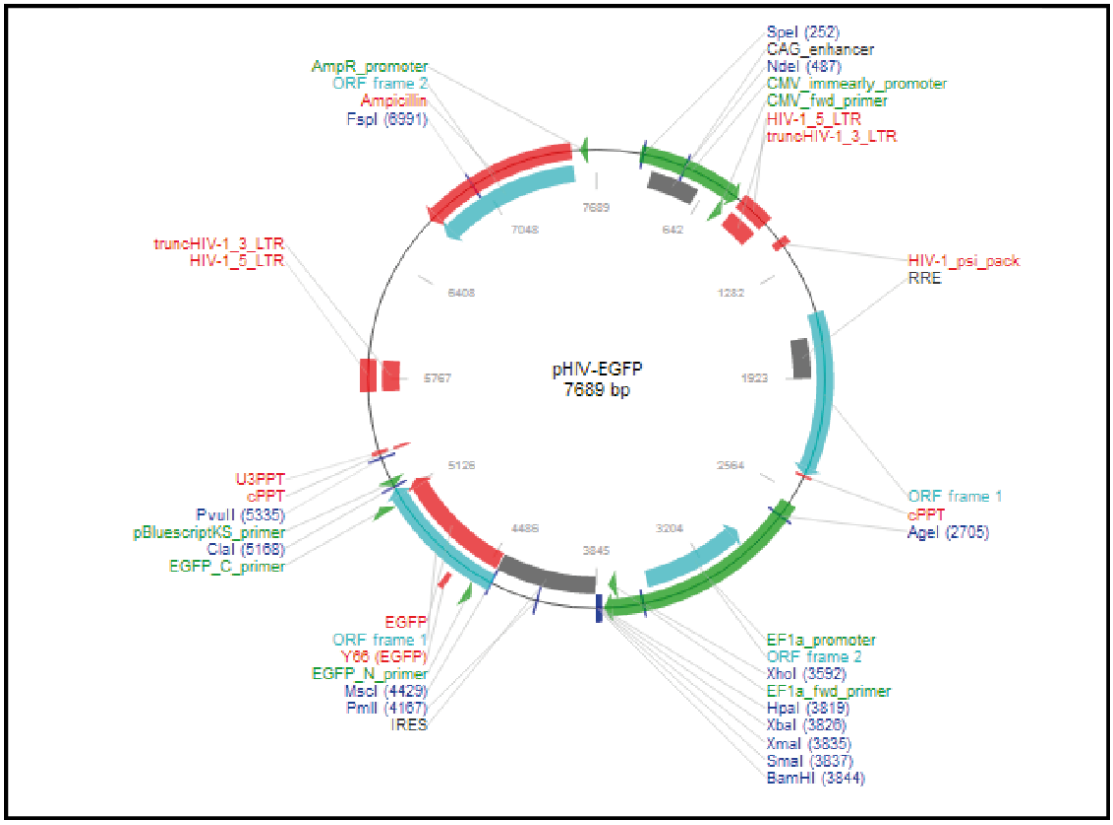

Appendix V: Western blots testing human CYP11B2 and CYP11B1 antibodies developed at Thermofisher.

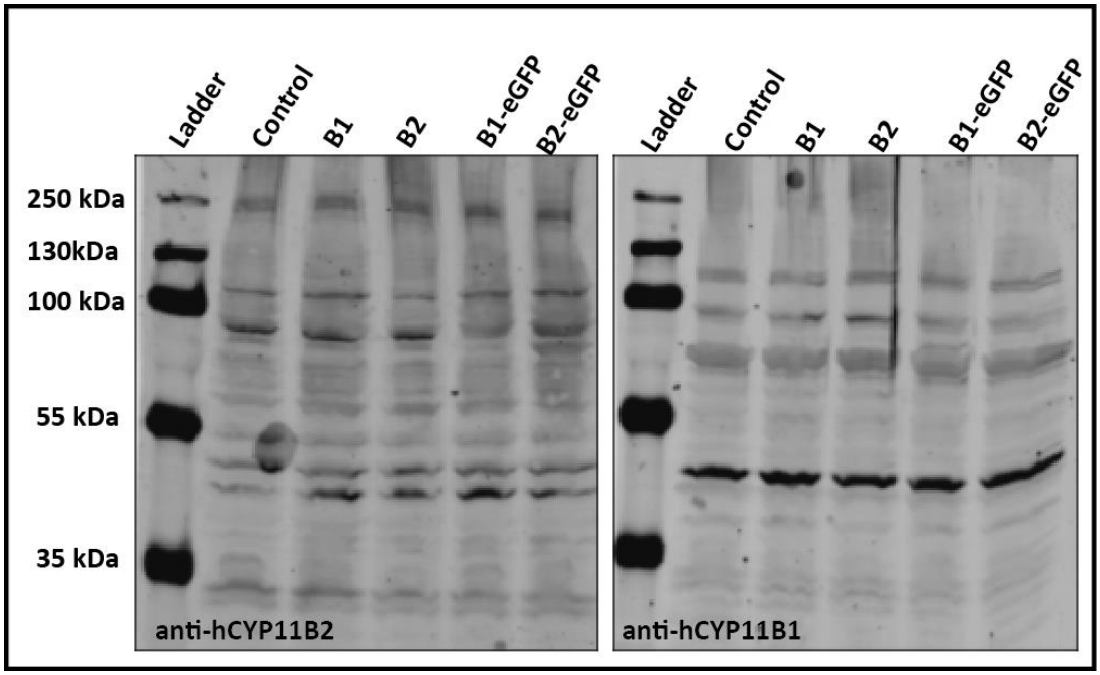

Figure V: Poor specificity of CYP11B2 (left) and CYP11B1 (right) antibodies developed. Western blots performed on HEK293 cells transfected with vectors encoding either CYP11B2 (left) or CYP11B1 (right), show that CYP11B2 and CYP11B1 antibodies developed are not specific in targeting their respective proteins.

Appendix VI: Western blots testing human lentiviral infected H295R over-expressing cell line.